

**RATE PROCESSES DURING GASIFICATION AND REDUCTION
OF BLACK LIQUOR CHAR**

by

Jian Li

A Thesis Submitted to the Faculty of Graduate Studies
and Research in Partial Fulfillment of the
Requirements for the Degree of
Doctor of Philosophy

Department of Chemical Engineering
McGill University
Montreal, Canada

October 1989

ABSTRACT

The rate processes during gasification and reduction of kraft black liquor char were investigated in a well characterized thermogravimetric analysis system below 800°C.

Both CO₂ and steam gasification rates are described by Langmuir-Hinshelwood type of kinetics, consistent with the redox mechanisms also proposed for gasification of other alkali-metal containing carbonaceous materials. The gasification rates of black liquor char, however, are one order of magnitude higher, because of its unique, very fine distribution of sodium in the bulk of the carbon matrix.

COS and H₂S are the major sulfur containing gaseous products formed during respectively CO₂ and steam gasification of reduced black liquor char. S₂ is suggested as another important product emitted under certain conditions during CO₂ gasification. COS emission from a char bed at relatively low CO₂ concentration and high temperature is limited by external mass transfer, while the COS concentration inside the bed is at thermodynamic equilibrium. The H₂S emission rate during steam gasification is controlled by the carbon gasification rate. The H₂S concentration inside a char bed is in thermodynamic equilibrium with the gasification product gases.

The kinetics of sodium sulfate reduction by both CO and carbon indicate that the reactions are auto catalytic. The major decelerating part of the sigmoid conversion-time curve of Na₂SO₄ reduction by CO is well described by product layer diffusion controlled or phase boundary reaction controlled kinetics depending on whether respectively CO₂ is present or not. The reduction rate by carbon is well described by second order nuclei growth controlled reaction kinetics. The production of an intermediate, possibly liquid poly-sulfide, from reaction between Na₂SO₄ and Na₂S is proposed as rate determining step in the mechanism of Na₂SO₄ reduction by both CO and carbon.

RESUME

On a étudié la cinétique de la gazéification et de la réduction de la liqueur noire Kraft solidifiée à l'aide d'un système d'analyse thermogravimétrique bien caractérisé, à des températures n'excédant pas 800°C.

On a décrit les taux de gazéification dans du CO₂ et de la vapeur d'eau par des expressions cinétiques du type Langmuir-Hinshelwood, ce qui est consistant avec les mécanismes d'oxydation-réduction également proposés pour la gazéification d'autres matières carbonées contenant des métaux alcalins. Cependant, les taux de gazéification de la liqueur noire solidifiée sont un ordre de grandeur plus élevés que ceux de ces autres matières, à cause de la distribution très fine du sodium dans la matrice de carbone.

Le COS et l'H₂S sont les deux produits sulfureux majeurs que l'on obtient lors de la gazéification de la liqueur noire solidifiée réduite dans des atmosphères de CO₂ et de vapeur d'eau, respectivement. On suggère que le soufre est un autre produit important de la gazéification dans du CO₂, sous certaines conditions particulières. L'émission du COS d'un lit peu profond, à une concentration en CO₂ relativement basse et à haute température, est limitée par le transfert de masse externe, et la concentration de COS dans le lit est celle de l'équilibre thermodynamique. Le taux d'émission du H₂S est contrôlé par le taux de gazéification du carbone lors de la gazéification dans de la vapeur d'eau. La concentration du H₂S est celle de l'équilibre thermodynamique avec les produits gazeux.

La cinétique de la réduction du sulfate de sodium par le CO et par le carbone démontre que cette réduction est auto-catalytique. La portion décélérante de la réduction du Na₂SO₄ par le CO est bien décrite par des expressions cinétiques représentant le contrôle de la diffusion dans la couche des produits, lorsque le CO₂ est présent, et par le contrôle des réactions aux limites de phase, lorsque le CO₂ est absent. Le taux de réduction par le carbone est bien décrit par une expression du deuxième ordre représentant le contrôle de la croissance des noyaux. On propose des mécanismes de réaction pour la réduction par le CO et par le carbone, incorporant comme étape limite la production d'un composé intermédiaire, qui pourrait être le polysulfide liquide, à partir du Na₂SO₄ et du Na₂S.

ACKNOWLEDGEMENTS

I would like to express my gratitude to Dr A.R.P. van Heiningen for his valuable guidance, encouragement and financial support through out the period it took to complete this thesis. I feel fortunate to have had him as my research supervisor as well as a good friend. I also very much appreciate the friendship developed between his family and me over the years.

I wish to thank Dr. G.J. Kubes, Dr. G.M. Dorris and Prof. Moulijn for their constructive advice and valuable comments.

For his help with analytic work, I would like to thank Mr. J. Ing of the Pulp and Paper Research Institute of Canada.

I would like to sincerely thank Ms. C. Bryce in the Department of Chemical Engineering, McGill University, for her devoted help in the analysis of sulfur and fixed gases for the steam gasification study.

The help of my colleagues, Mr. Y. Ni and Mr. X. Zou with part of the data reduction is gratefully acknowledged.

It has been a very enjoyable time to work with the members of the CRISP research group at McGill University. Special thanks go to Paul, Omar, John, Pritham and Aliye for their friendship, advice and help.

I am also grateful to the Pulp and Paper Research Institute of Canada for the scholarships awarded.

A special word of thanks to Mr. J. Dumont for his very kind help in the selection and ordering of equipment, materials and supplies. I would like to thank Mr. J-F. Bond for translating and typing the French abstract of the thesis. For help on various occasions, I would like to thank Ms. A. McGuinness and Ms. P. McCaffery.

Last, I would like to thank my parents, brother and sisters for their love and moral support during the completion of this work.

TABLE OF CONTENTS

ABSTRACT	
RESUME	
ACKNOWLEDGEMENTS	
TABLE OF CONTENTS	i
LIST OF FIGURES	iv
LIST OF TABLES	ix

CHAPTER 1, INTRODUCTION

BACKGROUND INFORMATION AND LITERATURE REVIEW	1
OBJECTIVES AND STRATEGY	2
OUTLINE OF THE THESIS	3
REFERENCES	5

CHAPTER 2, TRANSPORT PHENOMENA IN A COMMON THERMOGRAVIMETRIC ANALYSIS SYSTEM

ABSTRACT	6
INTRODUCTION	7
BACKGROUND ON TEMPERATURE MEASUREMENT AND NAPHTHALENE SUBLIMATION	8
EXPERIMENTAL APPARATUS AND PROCEDURE	9
PART I GAS TEMPERATURE	14
PART II MASS TRANSFER	22
CONCLUSION	46
NOMENCLATURE	47
REFERENCES	48

CHAPTER 3, KINETICS OF CO₂ GASIFICATION OF FAST PYROLYSIS BLACK LIQUOR CHAR

ABSTRACT	50
INTRODUCTION	51
EXPERIMENTS	53

KINETIC RESULTS	57
DISCUSSIONS	70
CONCLUSION	80
NOMENCLATURE	80
REFERENCES	81

**CHAPTER 4, KINETICS OF GASIFICATION OF
BLACK LIQUOR CHAR BY STEAM**

ABSTRACT	83
INTRODUCTION	84
EXPERIMENTAL	85
RESULTS AND DISCUSSION	86
CONCLUSION	118
NOMENCLATURE	118
REFERENCES	120

**CHAPTER 5, SULFUR EMISSION DURING CO₂
GASIFICATION OF BLACK LIQUOR CHAR**

ABSTRACT	122
INTRODUCTION	123
EXPERIMENTAL	124
DILUTION EFFECT ON GAS ANALYSIS	126
THERMODYNAMIC PREDICTIONS	127
EXPERIMENTAL RESULTS AND DISCUSSION	135
CONCLUSION	145
NOMENCLATURE	146
REFERENCES	147

**CHAPTER 6, SULFUR EMISSION DURING STEAM
GASIFICATION OF BLACK LIQUOR CHAR**

ABSTRACT	149
INTRODUCTION	150
EXPERIMENTAL	150
THERMODYNAMIC ANALYSIS OF THE REACTION SYSTEM	153
EXPERIMENTAL RESULTS	157
DISCUSSION	162
CONCLUDING REMARKS	168

IMPLICATION	172
NOMENCLATURE	172
REFERENCES	173

**CHAPTER 7, KINETICS OF SODIUM SULFATE REDUCTION
BY CARBON MONOXIDE BELOW 800°C**

ABSTRACT	175
INTRODUCTION	176
EXPERIMENTAL	177
RESULTS AND DISCUSSION	183
CONCLUSION	212
NOMENCLATURE	214
REFERENCES	215

**CHAPTER 8, KINETICS OF SOLID STATE REDUCTION OF
SODIUM SULFATE BY CARBON**

ABSTRACT	217
INTRODUCTION	218
BACKGROUND OF REACTOR DESIGN	219
EXPERIMENTAL	220
RESULTS	225
DISCUSSIONS	242
CONCLUSION	256
IMPLICATION	256
NOMENCLATURE	257
REFERENCES	258

CHAPTER 9, GENERAL CONCLUSIONS

GENERAL SUMMARY	259
CONTRIBUTIONS TO KNOWLEDGE	260
RECOMMENDATIONS AND SUGGESTIONS FOR FUTURE WORK	261

LIST OF FIGURES

CHAPTER 2

Figure 1.	Schematic picture of the TGA system.	10
Figure 2.	Close-up of the reactor tube of the TGA system.	12
Figure 3.	System for temperature measurement.	13
Figure 4.	Effect of gas flow rate on gas temperature without baffle.	15
Figure 5.	Effect of gas flow rate on gas temperature with baffle.	16
Figure 6.	Effect of carrier gas type on gas temperature without baffle.	17
Figure 7.	Effect of Sc on mass transfer rate.	26
Figure 8.	Effect of sample form on mass transfer rate.	28
Figure 9.	Effect of sample pan on mass transfer rate.	29
Figure 10.	Effect of baffle on mass transfer rate.	30
Figure 11.	Effect of void height on mass transfer rate without baffle.	32
Figure 12.	Effect of void height on mass transfer rate with baffle.	33
Figure 13.	Correlations for mass transfer without baffle and $H=3.2\text{mm}$.	35
Figure 14.	Sensitivity test of n .	36
Figure 15.	Correlation for mass transfer without baffle and full pan.	38
Figure 16.	Correlation for mass transfer with baffle and $H=3.2\text{mm}$.	39
Figure 17.	Correlation for mass transfer with baffle and full pan.	41
Figure 18.	Comparison of mass transfer data without presence of baffle literature data.	42
Figure 19.	Comparison of mass transfer data with presence of baffle with literature data.	43
Figure 20.	Mass transfer coefficient a function of temperature and gas system.	45

CHAPTER 3

Figure 1.	TGA set-up with gas supply system.	56
Figure 2.	Schematic picture of temperature and weight loss curve from TGA.	58
Figure 3	Measured weight loss and carbon weight loss for a typical run. Note: the inner figure shows the weight increase rate due to COS formation.	60
Figure 4.	Effect of carrier gas on gasification rate.	61
Figure 5.	$1/r_w$ as function of $[CO] / [CO_2]$.	64
Figure 6.	Arrhenius plot of BLC gasification rate.	67
Figure 7.	Gasification rate for black liquor char and alkali metal impregnated activated carbon	68
Figure 8.	Effect of sample preparation on gasification rate.	69
Figure 9.	Effect of pyrolysis rate on gasification.	71
Figure 10.	a) SEM picture of a BLC particle. b) EDS sodium mapping of BLC surface.	74
Figure 11.	a) SEM picture of a IAC particle. b) EDS sodium mapping of IAC surface.	75
Figure 12.	SEM-EDS line scan for sodium and sulfur of BLC	76
Figure 13.	SEM-EDS line scan for sodium of IAC after pyrolysis in He+CO and 775°C	77
Figure 14.	SEM picture of black liquor char obtained by drying in a dish.	78

CHAPTER 4

Figure 1.	Schematic picture of the TGA system.	87
Figure 2.	Thermodynamic equilibrium for steam gasification of carbon.	89
Figure 3.	Thermodynamic equilibrium of H ₂ O-black liquor char as function of steam to carbon ratio.	90
Figure 4.	Thermodynamic equilibrium of H ₂ O-black liquor char as function of hydrogen addition.	91
Figure 5.	Thermodynamic equilibrium of H ₂ O-black liquor	

	char as function of temperature.	92
Figure 6.	Schematic diagram of experimental procedure and results.	94
Figure 7.	A typical output generated by computer.	98
Figure 8.	Gasification rate as function of carbon conversion.	99
Figure 9.	The inverse of gasification rate as function of [H ₂] / [H ₂ O].	101
Figure 10.	Arrhenius plot of steam gasification rate.	102
Figure 11.	Comparison of theoretical and experimental equilibrium constant.	105
Figure 12.	Flow pattern in the reactor tube.	107
Figure 13.	Effect of temperature on [CO ₂]/[CO] ratio.	112
Figure 14.	Effect of steam concentration on [CO ₂]/[CO] ratio.	113
Figure 15.	Effect of hydrogen concentration on [CO ₂]/[CO] ratio.	114
Figure 16.	Reaction scheme proposed by Wigmans [6].	116

CHAPTER 5

Figure 1.	Schematic picture of the TGA system.	125
Figure 2.	Effect of thermodynamic data on sulfurous gas concentration.	130
Figure 3.	Equilibrium composition as function of CO ₂ addition in CO ₂ gasification.	131
Figure 4.	Equilibrium composition as function of CO addition in CO ₂ gasification.	132
Figure 5.	Equilibrium composition as function of temperature in CO ₂ gasification.	133
Figure 6.	COS production rate as function of [CO ₂].	137
Figure 7.	R/k _g as function of CO ₂ concentration.	139
Figure 8.	Effect of carrier gas on COS production rate.	141
Figure 9.	COS production rate as function of CO concentration.	143
Figure 10.	COS production rate as function of Temperature.	144

CHAPTER 6

Figure 1.	Schematic picture of the TGA system.	151
Figure 2.	[H ₂ S] _e as function of temperature.	156
Figure 3.	[H ₂ S] _e as function of H ₂ addition.	158

Figure 4.	[H ₂ S] _e as function of H ₂ O addition.	159
Figure 5.	Effect of gasification temperature on H ₂ S emission.	161
Figure 6.	Effect of [H ₂ O] on H ₂ S emission rate.	163
Figure 7.	Effect of [H ₂] on H ₂ S emission rate.	164
Figure 8.	The normalized H ₂ S production rate as function of temperature.	165
Figure 9.	Calculated and measured H ₂ S production rate.	167
Figure 10.	Comparison of theoretical and experimental equilibrium constants.	169
Figure 11.	The effect of [H ₂ O] on normalized H ₂ S production rate.	170
Figure 12.	The effect of [H ₂] on normalized H ₂ S production rate.	171

CHAPTER 7

Figure 1.	Schematic picture of experimental system.	178
Figure 2.	Porcelain and alumina pan before and after a reduction experiment.	181
Figure 3.	Typical Na ₂ SO ₄ conversion as a function of time.	185
Figure 4.	60.6% Na ₂ SO ₄ sample; a) just before reduction; b) at 30% conversion; c) at 100% conversion.	186
Figure 5.	Reduction kinetics of Na ₂ SO ₄ by CO.	187
Figure 6.	Reduction kinetics of Na ₂ SO ₄ by CO in the presence of CO.	189
Figure 7.	Influence of CO concentration on reaction constants.	191
Figure 8.	Influence of CO ₂ concentration on k of equation (9).	193
Figure 9.	Influence of temperature on reaction constants.	194
Figure 10.	Influence of CO concentration on initiation time.	195
Figure 11.	Influence of CO ₂ concentration on initiation time.	197
Figure 12.	Influence of temperature on initiation time.	198
Figure 13.	Influence of sodium carbonate on reduction rate.	199
Figure 14.	The phase diagram for Na ₂ CO ₃ -Na ₂ S-Na ₂ SO ₄ (from Andersson [16]).	201
Figure 15.	The sulfate conversion for 750, 760 and 800°C at 50% CO and 1.5% CO ₂	202
Figure 16.	The conversion-time results at 800°C for different initial sample weight.	204
Figure 17.	The conversion-time results at 760°C for	

	30% and 50% CO.	207
Figure 18.	The microscopic picture of the sample before a) and after b) the reduction with Fe ₃ O ₄ .	209
Figure 19.	Reduction kinetics of Na ₂ SO ₄ by CO in the presence of TiO ₂ .	210
Figure 20.	Influence of temperature on reduction kinetics in the presence of TiO ₂ .	211
Figure 21.	Arrhenius plot of the reaction constant of sulfate reduction by CO with presence of TiO ₂ .	213

CHAPTER 8

Figure 1.	Schematic picture of the TGA system.	221
Figure 2.	A typical experimental result recorded by computer.	226
Figure 3.	Weight-loss measured by TGA and calculated from CO and CO ₂ .	228
Figure 4.	Sulfate conversion as function of temperature.	230
Figure 5.	Reaction kinetics of sulfate reduction by carbon in black liquor char.	231
Figure 6.	Effect of temperature on reaction rate.	233
Figure 7.	Arrhenius plot of reaction constant for sulfate reduction by carbon.	234
Figure 8.	Effect of sodium sulfate addition on reduction rate.	236
Figure 9.	Effect of sodium carbonate on reduction rate.	237
Figure 10.	Comparison of sulfate reduction by black liquor char and graphite.	238
Figure 11.	Effect of particle size on sulfate reduction rate.	240
Figure 12.	Effect of ambient gas on sulfate reduction rate.	241
Figure 13.	Effect of temperature on CO/CO ₂ ratio.	244
Figure 14.	Effect of carbon to sulfate ratio on CO/CO ₂ ratio.	250
Figure 15.	Effect of carbonate on CO/CO ₂ ratio.	252
Figure 16.	Comparison of CO/CO ₂ ratio in sulfate reduction by black liquor char and graphite.	253
Figure 17.	Effect of ambient gas on CO/CO ₂ ratio.	255

LIST OF TABLES

Table		Page
CHAPTER 2		
Table 1	Gas temperatures	20
Table 2	Sample temperatures	21
Table 3	Physical properties of the gas systems	24
CHAPTER 3		
Table 1	Chemical and elemental analysis of black liquor solids and chars	54
Table 2	Reactivities of carbonaceous materials	64
Table 3	Chemical composition of black liquor solids obtained by different drying methods	70
CHAPTER 4		
Table 1	Gas production balance	96
Table 2	Carbon mass balance	96
Table 3	Comparison of reactivities	103
Table 4	Physical properties and Sc ; mass transfer coefficient in some typical cases	109
CHAPTER 5		
Table 1	Chemical composition of black liquor solids, char and reduced char	126
Table 2	Sulfur mass balance	135
Table 3	Results of mass transfer coefficients	138
CHAPTER 6		
Table 1	Chemical composition of black liquor solids,	

	char and reduced char	152
Table 2	Sulfur mass balance	160

CHAPTER 7

Table 1	Effect of sample pan, carrier gas, temperature and gas composition on reactivity and sulfur mass balance	182
Table 2	Reduction catalyzed by titanium and iron oxide	212

CHAPTER 8

Table 1	Chemical and elemental analysis of black liquor solids	223
Table 2	Sample preparation and composition	223
Table 3	Mass balance	227
Table 4	Kinetic models for solid state reactions	232
Table 5	Carbon gasification rate	243
Table 6	Disproportionation of Na_2SO_3	246
Table 7	Reduction of Na_2SO_3 by CO and graphite	247

CHAPTER 1

INTRODUCTION

BACKGROUND INFORMATION AND LITERATURE REVIEW

One of the most momentous discoveries in the history of mankind is the invention of paper making attributed to a Chinese, Ts'ai Lun (or Cai Lun) in A.D. 105. At about the twelfth century, this art was introduced to Europe where paper making became an industry and modern pulp and paper science was born [1]. Compared to the original Chinese "pulping process" of boiling bamboo in milk of lime for 8 days to release the fibers, the modern chemical pulping processes are much more complicated and sophisticated. However, the basic idea is still the same [2].

Chemical pulping has been the major pulping process for the last two decades [3]. Although the waste streams generated by these processes are considered to be more and more a serious threat to the environment and the capital cost are the highest of all pulping processes, it is likely that chemical pulping will remain the dominant pulping method in the near future. However, improved chemical recovery, minimal pollution and reduced capital cost are challenges which must be met to assure dominance of chemical pulping in the long term.

In kraft pulping, the major chemical pulping process, wood is treated at elevated temperature and pressure with an aqueous solution of NaOH and Na₂S [1, 3]. The spent cooking solution, so called black liquor, contains 50% of dissolved wood substances and pulping chemicals [4, 5]. The recovery of chemicals from the spent liquor goes back to the 1860's, that is, to the inception of the alkali process itself [6]. However, the modern recovery furnace, also known as Tomlinson furnace, was first built in 1934 by a Canadian engineer, G. H. Tomlinson in Windsor, Ontario [6]. Black liquor is

burned in this furnace for its heating value and recovery of pulping chemicals [1-3].

After concentrated black liquor is sprayed into the recovery furnace, the droplets lose the remaining water by evaporation and carbonize in flight and at the bottom of the furnace. Carbon in the char bed at the bottom of the furnace is gasified, providing the reducing atmosphere needed for reduction of sodium sulfate to sodium sulfide. The inorganic salts leave the furnace as a smelt. After dissolving the smelt, a so-called green liquor is obtained containing mostly Na_2CO_3 and Na_2S . The green liquor is sent to the causticizing process where Na_2CO_3 is converted into NaOH with slaked lime so that the resulting white liquor can be reused for pulping.

Although the objective of chemical recovery is adequately achieved in present commercial operation, several major drawbacks are associated with the recovery furnace, such as very high capital cost, the smelt-explosion hazard and the corrosive nature of the smelt. Since the last two decades, numerous studies have been reported on the physical and chemical processes taking place inside the recovery furnace, most of which have been reviewed recently by Blackwell and King [7], and Adams and Frederick [8]. However, because of the many interrelated reactions which take place simultaneously, the corrosive nature and complex composition of the mixture of char and inorganic smelt, fundamental knowledge of the processes occurring in the furnace is still incomplete. Knowledge of the kinetics and mechanism of reactions, such as carbon gasification, reduction of sodium sulfate and sulfur emission is urgently required to improve operation of the conventional recovery furnace and to develop alternative recovery processes.

The above introduction and brief literature review concern the conventional kraft recovery process. However, in each chapter, a comprehensive literature review is given pertaining to the specific topic which is presented. The references are also included therein.

OBJECTIVES AND STRATEGY

The objective of the present study is to obtain better understanding of the processes taking place during gasification and reduction of black liquor char. More specifically, the objective was to determine the mechanism and rate of gasification, reduction and sulfur emission of black liquor char

below or near the melting point of the inorganics. This knowledge will especially be useful for the development of melt-free, low temperature processes such as those employing fluidized beds.

Kraft black liquor obtained by cooking Black Spruce to about 50% was used. A thermogravimetric analysis (TGA) system which operates under differential conditions was selected for kinetic measurements. The heat and mass transfer characteristics of the TGA system were determined by respectively temperature measurement and naphthalene sublimation technique to ensure correct interpretation of reaction rate data. The kinetics of gasification by CO₂ and reduction of sulfate by CO were determined from the weight loss rate. The rate of steam gasification and sulfate reduction by carbon were determined from the CO and CO₂ concentration in the exhaust gas. Sulfur emission during CO₂ and steam gasification was measured by gas chromatographic analysis of the product gas for sulfurous species. The solid samples and products were analyzed by ion chromatography so that mass balances for the inorganics could be made.

OUTLINE OF THE THESIS

This thesis is concerned with the rate processes and mechanism of carbon gasification, sulfate reduction and sulfur emission during gasification and reduction of black liquor char. All experiments were performed with model compounds and black liquor char in a thermogravimetric analysis system at temperatures less than or equal to 800°C. The weight-loss, CO and CO₂ concentration and temperature were continuously recorded and the gaseous and solid products formed during the thermal treatment were analyzed.

In Chapter 2 the transport characteristics of the TGA system are established. The gas temperature in the reactor tube is measured as function of gas flow rate, type of carrier gas and upstream flow configuration, and its influence on sample temperature is discussed. The mass transfer characteristics of the TGA system determined with the naphthalene sublimation technique are presented in the second part of this chapter. The mass transfer rates between the gas stream and hanging sample pan are successfully correlated with the "Usagi and Churchill Equation".

The amount of gas by-passing the sample pan, or the so-called "dilution effect" is quantified for different gas systems.

In Chapter 3 the kinetics and mechanism of CO₂ gasification of black liquor char are presented. The kinetic data for black liquor char are compared with other carbonaceous materials, and explained by differences in degree of sodium dispersion in the carbon matrix. The unique properties of black liquor char in terms of sodium and sulfur distribution are verified by SEM-EDS using the mapping and line scan techniques.

The steam gasification kinetics of black liquor char are presented in Chapter 4. The influence of gas composition and temperature on kinetics and gas product distribution are discussed. The experimentally determined equilibrium constant for the water shift reaction is corrected for the so-called "dilution effect" and compared with theory. A gasification mechanism is proposed to explain the excess production of CO₂.

The sulfur emission during CO₂ and steam gasification of black liquor char are discussed respectively in Chapter 5 and 6. The reaction systems are investigated both experimentally and by thermodynamic analysis. The influence of gas composition and temperature on sulfur emission rate is explained by thermodynamics combined with mass transfer limitation and carbon gasification or by reaction kinetics depending on gasification conditions.

The kinetics of sodium sulfate reduction by CO with or without catalyst are presented in Chapter 7. The sigmoid conversion curves obtained without catalyst are analyzed in terms of an induction and deceleration period. The influence of temperature, gas composition, sodium carbonate concentration and presence of a molten phase are discussed. A reaction mechanism is proposed based on the kinetics and microscopic analysis of the sample. The catalytic activity of iron compounds and TiO₂ on reduction are investigated.

In Chapter 8 the kinetics of sodium sulfate reduction by carbon in black liquor chars are presented. The kinetics are analyzed by fitting the conversion data to different kinetic expressions for solid-solid reactions. The influence of the type of sample, temperature and sample pan shape are investigated. A reaction mechanism is proposed based on the experimental observations and the unique character of black liquor char.

The general conclusion, suggestions for further work and contributions to knowledge are presented in Chapter 9.

The work described in Chapters 2, 3, 4, 5, 6, 7, and 8 have been

written as self-contained papers suitable for publication with little or no further modifications. Thus each chapter has its own abstract, list of symbols and references. As far as possible, uniform and standard symbols are used throughout the thesis. The major content in several chapters has been presented at technical conferences or published in journals. Specifically:

- Chapter 3: presented at **Fall Meeting of the Materials Research Society**, Boston, USA 1987, and **Carbon'88**, Newcastle, UK. The refereed paper is published in **Mat. Res. Soc. Symp. Proc.**, Vol 111, p.441(1988).
- Chapter 4: presented at **19th Biennial Conference on Carbon**, Penn State Univ., 1989.
- Chapter 5 & 6 presented at **Intern. Chem. Recov. Conf.**, Ottawa, Canada, April, 1989.
- Chapter 7: presented at **10th Intern. Symp. on Chem. React. Eng.**, Basle, Switzerland, 1988. The refereed paper is published in **Chemical Engineering Science**, Vol.43, p.2079(1988).

REFERENCES

1. Casey, J.P., editor, **Pulp and Paper**, vol.1, 3rd edition, John Wiley & Sons, N.Y., p.2(1980).
2. Rydholm, S.A., **Pulping Processes**, John Wiley & Sons, N.Y., (1965).
3. Smook, G.A, **Handbook for Pulp & Paper Technologists**, TAPPI & CPPA, Montreal, p.35(1986).
4. Passinen, K., **Proc. Symp. Rec. Pulp. Chem. IUPAC-EUCEPA**, Helsinki, Finland, Eng. Trans., p.188(1969).
5. Annergren, G., **Svensk Papperstid**, 71(15), p.497(1968).
6. Tomlinson, G.H., **Forum on Kraft Recovery Alternatives**, IPC, Appleton, US, p.15(1976).
7. Blackwell, B., and T. King, **Chemical Reactions in Kraft Recovery Boilers**, Sandwell, Vancouver, (1985).
8. Adams, T.N., and Wm.J. Frederick, **Kraft Recovery Boiler Physical and Chemical Processes**, IPC, Inc., Appleton, (1988).

CHAPTER 2

TRANSPORT PHENOMENA IN A COMMON THERMOGRAVIMETRIC ANALYSIS SYSTEM

ABSTRACT

The heat and mass transfer characteristics of a common hanging basket type TGA system are studied by measuring the gas temperature inside the reactor tube and weight loss rate respectively with thermocouples and the naphthalene sublimation technique. At a flow rate higher than 500 scc/min for N₂ or 1000 scc/min for He, the gas temperature is significantly different from the furnace or sample pan temperature. The mass transfer data obtained by naphthalene sublimation are correlated in the form of non-dimensional expressions which differ depending on the degree of filling of the sample pan, presence of a baffle tube or range of Reynolds number. The void height above the sample surface in the sample pan can represent a major resistance to mass transfer. Both heat and mass transfer are enhanced by presence of a baffle tube inside the cylindrical reactor tube. A simple method of performing experiments with respectively He and N₂ as carrier gas, is suggested for detection of gas phase heat and mass transfer limitations. Based on the correlations of mass transfer to the sample pan, a so-called "dilution factor" is defined with which the product gas concentration in the sample pan can be calculated from the concentration in the exhaust and the feed flow rate. Knowledge of the product gas concentration in the sample pan removes one of the major drawbacks of TGA for kinetics studies, compared to investigations with a fixed bed.

INTRODUCTION

An internationally accepted definition of thermogravimetry (TG) is " a technique whereby the weight of a substance, in an environment heated or cooled at a controlled rate, is recorded as a function of time or temperature"[1]. The first thermobalance was developed by a Japanese scientist K. Honda in 1915 [2]. Yet only starting from the late 1940's this important experimental technique became well known and widely used. Since then a large number of further developments have been made. Comprehensive reviews and have been published by Keattch [1] and Wendlandt [3].

Although there are many thermobalance configurations, the most commonly used is the hanging basket type already employed by Honda [2]. In this type of balance, the sample is held in a small basket located in a thick-walled tube surrounded by a furnace. The basket is suspended by a wire from the balance assembly. The balance assembly is shielded from the heated zone by a combination of distance and cool purge gas. This type of balance has been recognized as a useful and simple tool for measuring gas-solid reaction rates and adsorption phenomena. However, difficulties inherent in the design make measurement of intrinsic reaction kinetics unreliable under certain conditions. First, it is the difficult to measure the sample temperature during reaction, as placement of a thermocouple directly in the solid will disrupt weight measurement. Secondly, the reactant gas passes around the sample pan and exchanges mass with the sample only by diffusion via the top exposed surface. Thus gas phase mass transfer external to and within the solid sample are potentially major transport resistances that can obscure measurement of intrinsic reaction kinetics.

To avoid these disadvantages, some new design concepts have been reported, i.e. the internally heated weighed reactor balance [4, 5] and the centrifuged thermobalance [6]. However, these designs suffer from either much lower accuracy or much more complicated operation. Therefore, because of its highly accurate weighing capability, straightforward operation, wide operational range and many application fields, the hanging basket thermobalance is still widely used and will not be replaced in foreseeable future.

The thermocouple used for measurement of sample temperature is normally

placed underneath the basket. The thermocouple and sample are both heated by radiation from the furnace walls and cooled by the reactant gas, because the latter generally has a lower temperature due to the relative short heating zone inside the furnace. It is normally assumed that the thermocouple and sample have the same temperature, although it has been reported that in some cases the gas temperature is only heated to about 100°C with a furnace temperature of 700°C [7].

In order to characterize the effect of mass transfer limitations, preliminary experiments are normally carried out whereby gas flow rate, sample size and particle size are varied [8, 9]. The existence of a reliable mass transfer correlation would eliminate the need for these preliminary experiments. Furthermore, this type of correlation is essential for calculation of gas concentration inside the pan when the TG set-up is not operated differentially. Li [9] used the well known Ranz & Marshall correlation [10]

$$\text{Sh} = 2 + 0.6 \text{Re}^{1/2} \text{Sc}^{1/3} \quad (1)$$

when estimating the relative influence of external mass transfer in a TGA set-up. The only mass transfer correlation for a hanging basket type thermobalance was reported by Wigmans [11] as

$$\text{Sh} = 1.2 + 1.2 \text{Re}^{1/4} \text{Sc}^{3/5} \quad (2)$$

for the range of $0.6 < \text{Re} < 30$. There are, however, some problems associated with this correlation. First, according to theory [12], the power of Sc cannot be larger than 0.5. Secondly, some important operating conditions such as bed height in the pan and the presence (or absence) of a baffle in the reactor are not specified.

Because this hanging basket type thermobalance is still widely used in kinetic studies, knowledge of the heat and mass transfer characteristics would be useful for interpretation of experimental results. In the present study, the temperature of the carrier gas is measured with an aspirated thermocouple. The mass transfer characteristics are established by the naphthalene sublimation technique.

BACKGROUND ON TEMPERATURE MEASUREMENT AND NAPHTHALENE SUBLIMATION

The concept of a shielded high velocity aspirated thermocouple was

developed in the early 1940's [13]. It is based on the fact that convective heat received (or lost) by a thermocouple is equal to the heat lost (or gained) by radiation, i.e.

$$\sigma \epsilon A_1 (T_t^4 - T_w^4) = h A_2 (T_g - T_t) \quad (3)$$

where T_t , T_w and T_g are respectively the thermocouple, wall and gas temperature, A_1 the thermocouple surface area, A_2 the area of gas film around thermocouple, σ the Stefan-Boltzmann constant (5.67×10^{-8} watt \cdot m $^{-2}\cdot$ K 4), and ϵ the thermocouple emissivity. As can be seen from equation (3), if the thermocouple is shielded from the wall by a surface which temperature is closer to that of the thermocouple, the radiation heat received or lost by the thermocouple will be much reduced, resulting in a lower value for $(T_g - T_t)$. More importantly, gas can be aspirated at very high velocities into the annular region formed by the thermocouple and shield. This greatly enhances the heat transfer between the thermocouple and gas so that T_g will be even closer to T_t . It was shown [14] that for a high efficiency shielded thermocouple operating at a gas velocity equivalent to a Mach number of about 0.1 to 0.2, 90 to 95% temperature recovery can be achieved. At a Mach number of about one, 98% temperature recovery can be obtained.

One of the most popular methods to obtain heat and mass transfer data is the naphthalene sublimation technique, developed in the 1940's. This technique permits ease of construction of surfaces and simplicity in measuring both average and local transfer rates. It has been widely used in forced and natural convection studies [15, 16]. One of the classical papers was published by Sogin and Providence [17] in which they gave complete data reduction procedures and a very detailed analysis concerning the problem of calculating the sublimation temperature, as well as data on the diffusion coefficient of naphthalene and naphthalene equilibrium vapor pressures.

EXPERIMENTAL APPARATUS AND PROCEDURE

Thermogravimetric Analysis System

Shown in Figure 1 is a schematic picture of the thermogravimetric analysis set-up including gas supply system. The TGA system is a Cahn

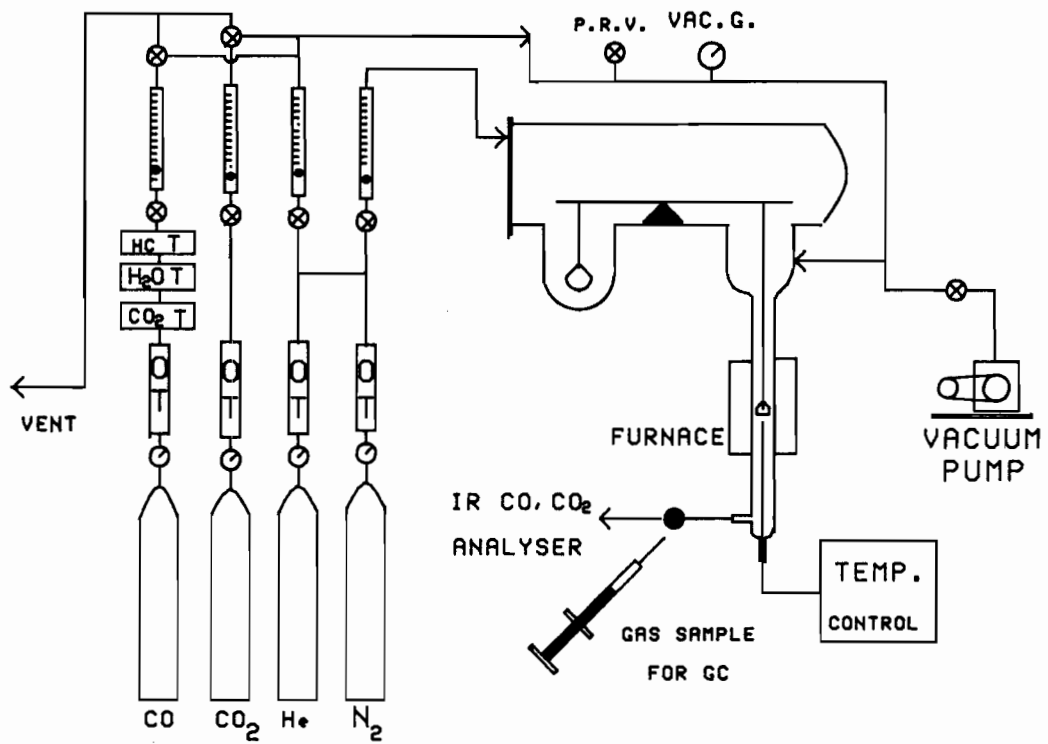


Figure 1. Schematic picture of the TGA system.

113-DC system installed with a Cahn RG-2000 electric-balance. Shown in Figure 2 is a close-up picture of the reactor tube which consists of a quartz baffle tube, a hang-down wire and a suspended sample pan. The quartz baffle serves to minimize noise in the weight signal due to the natural convection currents. It also enhances the heat and mass transfer inside the reactor tube as will be shown later. Also given in Figure 2 are some important dimensions. In a normal TGA experiment the weight change of a sample is recorded as a function of time with an accuracy of 1 to 100 μg depending on the sample weight. The temperature is measured by a K type thermocouple with an accuracy of 5°C (reproducibility 1°C). The gas flow rate was set by a fine metering valve and measured by rotameters calibrated by a bubble meter and wet test meter to an accuracy of 5% of the flow setting.

Temperature Measurement

Shown in Figures 3a and 3b are respectively a schematic picture of the experimental system and aspirated thermocouple. Two thermocouples were installed in the reactor tube. Thermocouple A is a K type used for measurement and control of the furnace temperature. Thermocouple B is the shielded high velocity thermocouple used for measurement of gas temperature. This thermocouple is also a K type thermocouple with a diameter of 1/32 inch inside an alumina tube with an I.D. and O.D. of respectively 1/16 and 1/8 inch. A second shield made of copper tubing is placed on top of the thermocouple. The top opening is about 1/16 inch in diameter. Gas was aspirated into the shielded thermocouple by a vacuum pump at a flow rate equal to that introduced into the balance by controlling valve B so that a soap film in the bubble flow meter was stationary.

Naphthalene Sublimation Technique

80 to 400 mg reagent grade naphthalene was molten in the porcelain sample pan shown in Figure 2. After solidification, the exposed naphthalene surface was leveled and hand polished. After placement of the pan inside the reactor tube, the weight loss rate due to naphthalene sublimation was measured as function of gas flow rate, type of gas, presence of baffle, type of sample pan and fractional filling of sample pan. Four different gases were used: helium, nitrogen, carbon dioxide and freon-12

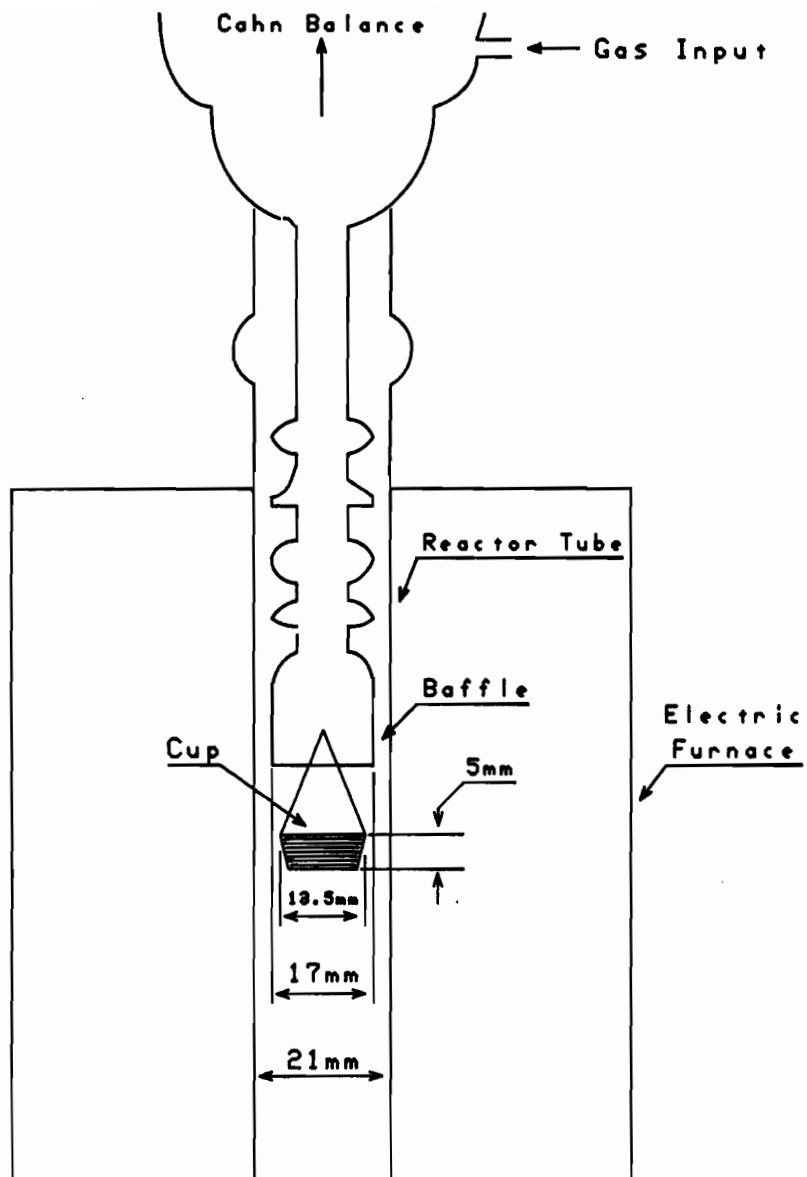
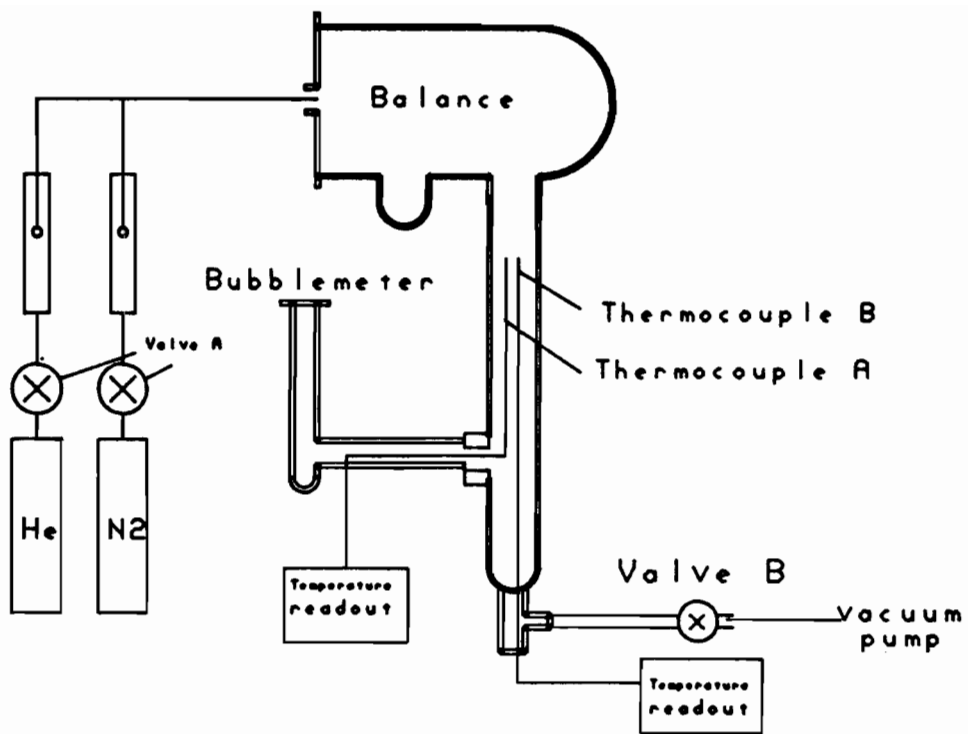
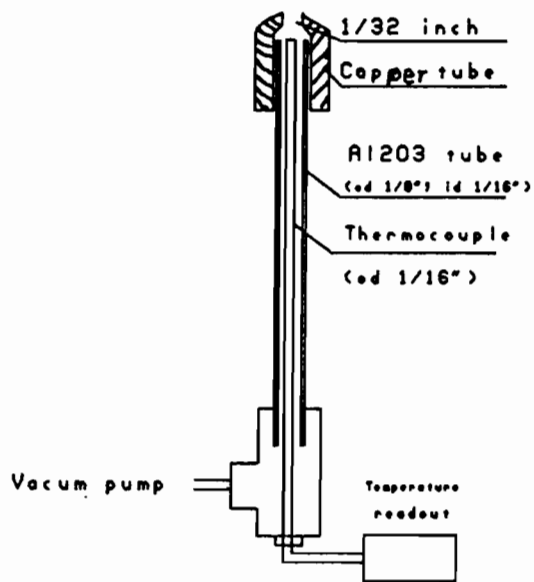


Figure 2. Close-up of the reactor tube of the TGA system.



a)



b)

Figure 3. System for temperature measurement.

(dichlorodifluoromethane). Besides the porcelain pan, two commonly used platinum and quartz pans were also tested. The dimensions of the porcelain pan are given in Figure 2. The platinum pan and quartz pan are in the form of a segment of a sphere with opening of 9 and 8.6 mm O.D. and bed height of 4 and 3.5 mm respectively. A calibrated T-type thermocouple with resolution of 0.1°F was used to measure the carrier gas temperature continuously during every experiment. All experiments were performed at room temperature and atmospheric pressure. The maximum total weight loss with the porcelain sample pan was about 4 mg corresponding to a negligible decrease in surface height of 0.04 mm.

PART I GAS TEMPERATURE

Results

Because the gas side transfer properties are temperature dependent and an inert carrier gas such as helium or nitrogen can only be heated significantly by convection rather than by radiation, the effect of TGA operation on gas temperature in the reactor tube was determined.

Shown in Figure 4 is the temperature of the aspirated thermocouple obtained in the reactor tube without a baffle as a function of gas flow rate at standard conditions (25°C , 1 atm) and 800°C furnace temperature. The furnace temperature is measured by thermocouple A. The results in Figure 4 show that with nitrogen as carrier gas the aspirated thermocouple temperature decreases rapidly with increasing gas flow rate. However with helium as carrier gas the temperature is only slightly influenced at the highest flow rates. This shows that the residence time in the heated section upstream of the thermocouple is not large enough or just sufficient respectively with nitrogen or helium as carrier gas.

Shown in Figure 5 are the results obtained with the presence of the baffle in the reactor tube. The decrease in temperature measured by the aspirated thermocouple with nitrogen as carrier gas is less than that without baffle in Figure 4. Therefore, convective heat transfer to the carrier gas is enhanced by the presence of a baffle.

Shown in Figure 6 is the aspirated thermocouple temperature at constant flow rate as function of He concentration in N_2 . Consistent with the results of Figure 5, the temperature approaches the furnace temperature

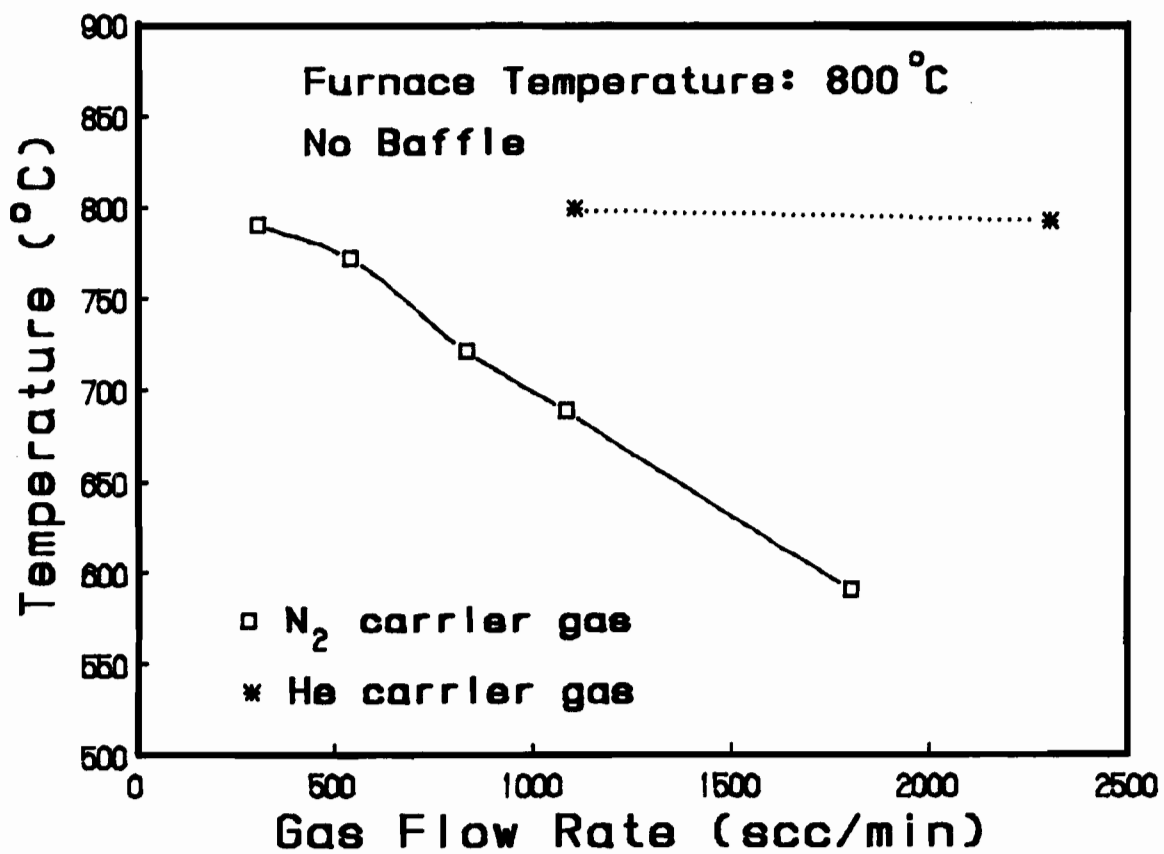


Figure 4. Effect of gas flow rate on gas temperature without baffle.

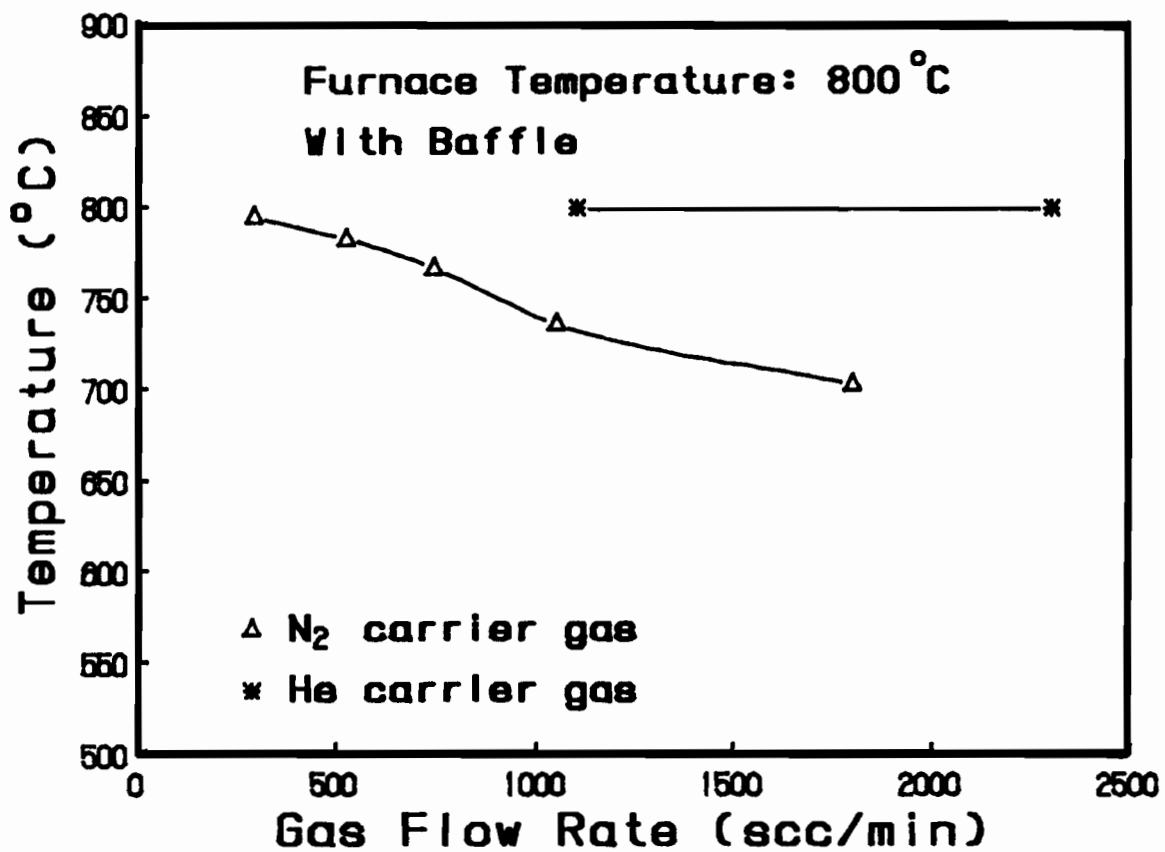


Figure 5. Effect of gas flow rate on gas temperature with baffle.

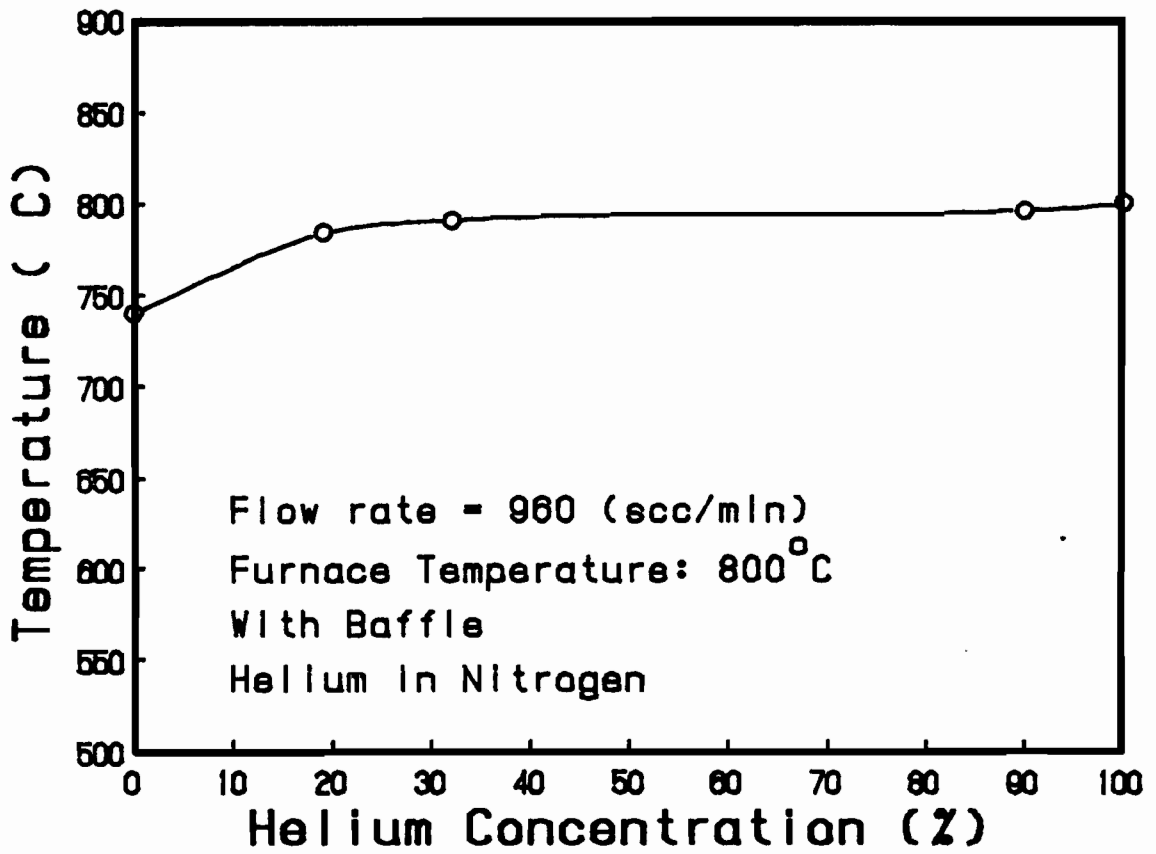


Figure 6. Effect of carrier gas type on gas temperature without baffle.

when the He concentration is increased.

Discussion

a) Gas Temperature

It should be realized that the temperature measured by the aspirated thermocouple is not the true gas temperature. First, the thermocouple shield is also heated by the furnace and the thermocouple is still receiving radiation from the shield. Secondly, because convective heat transfer between the thermocouple and the high velocity gas stream is finite the gas temperature can not be fully recovered by the thermocouple.

The true gas temperature may be estimated by equation (3) when emissivity ϵ , wall temperature T_w and convective heat transfer coefficient h are known, and the surface area of the thermocouple, A_1 , and the film area, A_2 , are assumed to be equal. The emissivity of the thermocouple made of stainless steel with a rough surface can be taken as 0.5 [18]. The shield is heated by the furnace and cooled by the aspirated gas. Because of the high radiative heat transfer, the temperature of the shield would approach the furnace temperature. The convective heat transfer coefficient can be estimated from the stagnation point heat flux correlation for cylindrical blunt bodies [18];

$$Nu = \frac{h d}{k} = 1.14 Re_d^{0.5} Pr^{0.4} \quad (4)$$

where Nu is the Nusselt number, k the thermal conductivity of the gas, Re_d the Reynolds number based on thermocouple diameter d and Pr the Prandtl number of the gas. With these assumptions and equations (3) and (4), the gas temperature, T_g , was calculated and the results are shown in Table I. The results in Table I confirm that convective heat transfer between the high velocity gas and the top of the aspirated thermocouple is large enough so that its indicated temperature is a reasonable approximation of the actual gas temperature.

The gas temperature can also be estimated from an energy balance over the heating zone. The energy received by the gas in the heating zone is

$$q = \bar{h} \pi D l \left[\frac{\Delta T_2 - \Delta T_1}{\ln (\Delta T_2 / \Delta T_1)} \right] = m C_p (T_2 - T_1) \quad (5)$$

with

$$\Delta T_2 = T_w - T_2 ; \quad \Delta T_1 = T_w - T_1$$

where \bar{h} is the mean heat transfer coefficient, D the tube diameter, l the length of the heating zone, T_w the tube wall temperature, m the gas mass flow rate, C_p the gas heat capacity, T_1 the inlet gas temperature, and T_2 the gas temperature at the end of the heating zone. In present study, D and l are 0.021 and 0.06 m respectively. T_w is assumed to be equal to the furnace temperature, 800°C. while T_1 is room temperature at 20°C. Without the presence of a baffle in the reactor tube, the heat transfer coefficient can be estimated with the heat transfer correlation for fully developed flow with developing thermal boundary layer [19]

$$Nu = \frac{\bar{h} D}{k} = 1.86 \left(Re_D Pr \frac{D}{l} \right)^{1/3} \left(\frac{\mu_b}{\mu_w} \right)^{0.14} \quad (6)$$

where Re_D is the Reynolds number based on the tube diameter and μ_b and μ_w the gas viscosity at respectively the bulk and tube wall temperature. With equations (5) and (6), the gas temperature at the end of the heating zone, T_2 , was calculated and the results are also listed in Table I. Since there is no heat transfer correlation available for flow through a tube with a baffle, this case is not considered.

As can be seen from Table I, the calculated gas temperature, T_2 , is also very close to the aspirated thermocouple temperature, T_t , confirming again that the gas temperature is closely approximated by the temperature measured with the aspirated thermocouple.

The results in Table I, show that helium with its high thermal conductivity approaches the furnace temperature at normal operating flow rates, while nitrogen does not at these conditions. However, the gas heating is much less of a problem with the present TGA system than with the Du-Pont system reported by Edelstein (1987). The major reason for this difference must be related to the large difference in length of the upstream heating zone. For example, if the the upstream heating zone is 1 cm instead of 6 cm, the gas temperature without a baffle at maximum N₂ flow rate of 1800 scc/min will be about 170°C instead of 576°C. Furthermore, the convective heat transfer in the upstream heating zone of the present system is enhanced by presence of the baffle.

TABLE I GAS TEMPERATURES

FLOW RATE (scc/min)	GAS TYPE	BAFFLE	T _t (°C)	T _g (°C)	T ₂ (°C)
1800	N ₂	No	590	574	576
1080	N ₂	No	690	678	679
830	N ₂	No	720	710	719
535	N ₂	No	772	767	764
300	N ₂	No	790	788	792
2300	He	No	792	791.7	794
1100	He	No	797.5	797.4	799.7
1800	N ₂	Yes	702	693	
1050	N ₂	Yes	735	727	
745	N ₂	Yes	766	761	
525	N ₂	Yes	782	779	
297	N ₂	Yes	794	793	
2300	He	Yes	799	799	
1100	He	Yes	799	799	

b). Effect of Gas Temperature on Sample Temperature

In most TGA set-up's, including the present, the furnace temperature is controlled by a thermocouple immediately beneath the sample pan. When the carrier gas temperature is lower than the furnace wall temperature, the sample and control thermocouple are heated by radiation from the wall and cooled by the gas. Therefore, the furnace wall temperature will be higher than the control thermocouple and sample pan. Similarly more power will be supplied to the furnace when the cooling effect is larger, resulting in a further increased furnace wall temperature to maintain constant temperature of the control thermocouple.

TABLE II SAMPLE TEMPERATURES

FLOW RATE (scc/min)	GAS TYPE	BAFFLE	Sample Temperature	
			T_s ($^{\circ}C$) $\epsilon_s = 0.25$	T_s ($^{\circ}C$) $\epsilon_s = 1$
1800	N ₂	No	782	843
1080	N ₂	No	789	819
830	N ₂	No	792	812
535	N ₂	No	797.3	803.3
300	N ₂	No	799.1	800.8
2300	He	No	798	803
1100	He	No	799.4	800.6
1800	N ₂	Yes	781	815
1050	N ₂	Yes	791	808
745	N ₂	Yes	797	805
525	N ₂	Yes	798.3	802.1
297	N ₂	Yes	799.4	800.5
2300	He	Yes	799.7	800.4
1100	He	Yes	799.7	800.2

The relation between the furnace wall temperature, T_w , gas temperature, T_g , and control thermocouple, T_{ct} , is given by equation (3) with T_t replaced by T_{ct} as shown in equation (7). The same equation can also be used to related the sample temperature, T_s , to T_g and T_w , as shown in equation (7a).

$$\sigma \epsilon_{ct} (T_{ct}^4 - T_w^4) = h_{ct} (T_g - T_{ct}) \quad (7)$$

$$\sigma \epsilon_s (T_s^4 - T_w^4) = h_s (T_g - T_s) \quad (7a)$$

where ϵ_s and ϵ_{ct} are, respectively, the emissivity of the sample and control thermocouple, and h_s and h_{ct} , respectively, the heat transfer coefficient of the sample and control thermocouple. Since the sample emissivity may vary widely, for example $\epsilon_s = 0.95$ for carbon and $\epsilon_s = 0.5$ for MgO, the effect of emissivity difference between sample and thermocouple on T_s was investigated. The following two cases were examined 1) $\epsilon_{ct} = 0.5$, $\epsilon_s = 0.25$; 2) $\epsilon_{ct} = 0.5$, $\epsilon_s = 1$. With T_g taken as the measured gas temperature in Table

I, $T_{ct} = 800^{\circ}\text{C}$, and h_{ct} calculated with equation (4) (diameter of control thermocouple = 1/8 in), the wall temperature T_w is obtained with equation (7). This value for T_w is used in equation (7a) together with h_g calculated from mass transfer correlations for the present system (which will be presented later) using the analogy between heat and mass transfer to obtain T_s listed in Table II. It should be pointed out that the value of h_g used is the convective heat transfer coefficient for the top surface of the sample pan. Since this value is somewhat higher than the heat transfer coefficient of the entire sample pan, T_s in Table II represents the largest possible influence of gas temperature on sample temperature.

As can be seen from Table II, with these differences in emissivity the maximum deviation of the sample temperature from the control thermocouple temperature set-point of 800°C is negligible with helium as carrier gas and only -19 to $+15^{\circ}\text{C}$ and -18 to $+43^{\circ}\text{C}$ for nitrogen, respectively with or without presence of a baffle. When the N_2 flow rate is lower than 500 or 750 scc/min respectively with or without baffle, the sample temperature is 3 to 5°C different from the control temperature. This is about the same as the absolute error in temperature measurement for most TGA equipment. Because most TGA studies are conducted at flow rates lower than 1000 scc/min, it follows that in general the effect of insufficient heating of the carrier gas on the sample temperature can be neglected. Another factor which improves the gas heating is that hetero-atomic gases such as the gasification gases CO_2 and H_2O are significantly heated by radiation besides convection. Only in some extreme cases such as operation at medium temperature range (300 - 500°C) with a newly polished thermocouple and carbon sample, or with a corroded thermocouple and white crystalline sample, the sample temperature might be significantly different from the set-point. The existence of such a temperature difference can easily be verified by repeating an experiment with N_2 and He as carrier gas, since in the latter case the gas temperature will be very close to the control temperature under all conditions.

PART II

MASS TRANSFER

Data Reduction Techniques

Definition of Mass Transfer Coefficient

The mass transfer coefficient k_g ($\text{m}\cdot\text{s}^{-1}$) is defined by

$$(-r) = k_g S (C_w - C_\infty) \quad (8)$$

where $(-r)$ is the rate of naphthalene sublimation ($\text{mol}\cdot\text{s}^{-1}$) measured by the balance, S the top exposed surface area of the sample pan for sublimation (m^2), and C_w and C_∞ the vapor concentration of naphthalene respectively at the top surface and in the bulk of the gas ($\text{mol}\cdot\text{m}^{-3}$). In the present study, C_∞ is zero, and C_w is calculated from the ideal gas law using the top surface temperature T_w (K) and the saturated vapor pressure of naphthalene p_w (Pa) at this temperature:

$$C_w = \frac{p_w}{R T_w} \quad (9)$$

where R is the gas constant, 8.314 ($\text{kJ}\cdot\text{mol}^{-1}\cdot\text{K}^{-1}$). The mass transfer coefficient k_g was correlated in terms of Sherwood number (Sh), Reynolds number (Re) and Schmidt number (Sc) defined as

$$Sh = \frac{k_g d_c}{D} ; \quad Re = \frac{V \rho d_c}{\mu} ; \quad Sc = \frac{\mu}{\rho D} \quad (10)$$

where d_c is the diameter of the sample pan (m), V the velocity of the carrier gas ($\text{m}\cdot\text{s}^{-1}$), ρ the density of the carrier gas ($\text{kg}\cdot\text{m}^{-3}$), μ the viscosity of the carrier gas ($\text{Pa}\cdot\text{s}$), and D the diffusion coefficient of naphthalene in the carrier gas ($\text{m}^2\cdot\text{s}^{-1}$).

The velocity of the carrier gas was calculated based on the cross sectional area of the reactor tube of 3.462 cm^2 . The density and viscosity of the carrier gas were used because the influence of the vapor pressure of naphthalene on the density is negligible over the temperature range of present study (22° - 25°C).

Saturated Vapor Pressure of Naphthalene

There are many sources of naphthalene saturation vapor pressure data available. Christian and Kezios [20] compared several sets of data and concluded that the differences in vapor pressure were normally within 5% over the temperature range of 12° to 50°C . The latest measurements used by Popiel [21] are also within 5% of the earlier data. The vapor pressure is usually expressed as

$$\log_{10} p_w = B_1 - \frac{B_2}{T_w} \quad (11)$$

where: $B_1 = 13.54$ and $B_2 = 3729$ for p_w in Pa and T_w in degrees Kelvin. These constants were taken from [17] and were previously used by others [15].

Diffusion Coefficient

The diffusion coefficient of naphthalene in the different carrier gases was calculated by Fuller's method [22] as

$$D_{AB} = \frac{10^{-3} T^{1.75} (1/M_A + 1/M_B)^{1/2}}{P [(\sum v_B)^{1/3} + (\sum v_A)^{1/3}]^2} \quad (12)$$

where $\sum v$ is sum of structural volume increments, with $\sum v$ for He, N₂ and CO₂ being respectively 2.88, 17.9 and 26.9 [22]. $\sum v$ for Freon-12 of 102 is the average value calculated from the diffusion coefficient of Freon-12 in different gases [23, 24]. $\sum v$ for naphthalene of 94.9 is determined from the most recent measurement of diffusion coefficient of naphthalene in air by Caldwell [25]. Caldwell's data are 25% higher than those of Mack [26] used by others over the last several decades. The calculated diffusion coefficients at 23°C are listed in Table III.

Schmidt Number

With gas density calculated by the ideal gas law and the viscosity obtained from Perry [27], the Schmidt number at 23°C for different systems was calculated and listed in Table III.

TABLE III PHYSICAL PROPERTIES OF THE GAS SYSTEMS

(1 atm., 296 K)

System (A-Naph.)	Density ($\text{kg} \cdot \text{m}^{-3}$)	Viscosity ($\times 10^{-5} \text{ Pa} \cdot \text{s}$)	Diffusivity ($\times 10^{-6} \text{ m}^2 \cdot \text{s}^{-1}$)	Sc
He - C ₁₀ H ₈	0.165	1.87	29.9	3.79
N ₂ - C ₁₀ H ₈	1.16	1.75	8.55	1.77
CO ₂ - C ₁₀ H ₈	1.82	1.44	6.46	1.23
CCl ₂ F ₂ - C ₁₀ H ₈	4.97	1.3	3.18	0.822

Evaluation of Naphthalene Surface Temperature

The temperature T_w is calculated as the "wet-bulb" temperature of a naphthalene sample subliming into the gas flow. Thus the usual assumption is made that heat transfer by radiation and conduction is very small compared to convection. The equation derived by Sogin [17] is used here to evaluate the difference between the gas temperature T_g and the top surface wall temperature T_w , written as

$$T_g - T_w = \left(\frac{Pr}{Sc}\right)^{2/3} \frac{M_n}{M_g} \frac{\lambda}{C_p} \frac{P_w}{P} \quad (13)$$

where Pr is the Prandtl number of the carrier gas, λ the latent heat of naphthalene sublimation, C_p the specific heat of carrier gas and M_n and M_g the molecular weight of respectively naphthalene and carrier gas. By using equations (11) and (13), ΔT was evaluated to be ≤ 0.1 °C for all carrier gases used. Such a small temperature difference changes the naphthalene vapor pressure by only 1%.

Results of Naphthalene Sublimation

1) Effect of Sc

The effect of Sc on Sh over a wide range of Re was studied by using different carrier gases. It was found that by plotting $Sh/Sc^{1/3}$ against Re rather than Sh versus $Re \cdot Sc^{1/3}$ all the data collapsed onto a single curve. As an example, the results obtained for the case of no baffle present in the reactor tube and a full porcelain pan, are shown in Figure 7. The range of Re is between 10^{-1} to 170. The lower limit of Re is determined by increasing difficulties to control and measure lower flow rates. The lowest Re data were obtained with the lightest gas, He. The higher limit of Re is determined by the onset of strong vibrations of the sample pan. It was found that the onset of strong vibrations occurred at Re of about 170 when no baffle was present and at Re of 130 with baffle, independent of the type of carrier gas used. Unless specified otherwise, all further data presented in this chapter were obtained with He, N₂ and CO₂ as carrier gas.

2) Effect of the Form of Naphthalene Sample

The effect of surface roughness and bed porosity were studied by comparison of the weight loss of molten and subsequently solidified

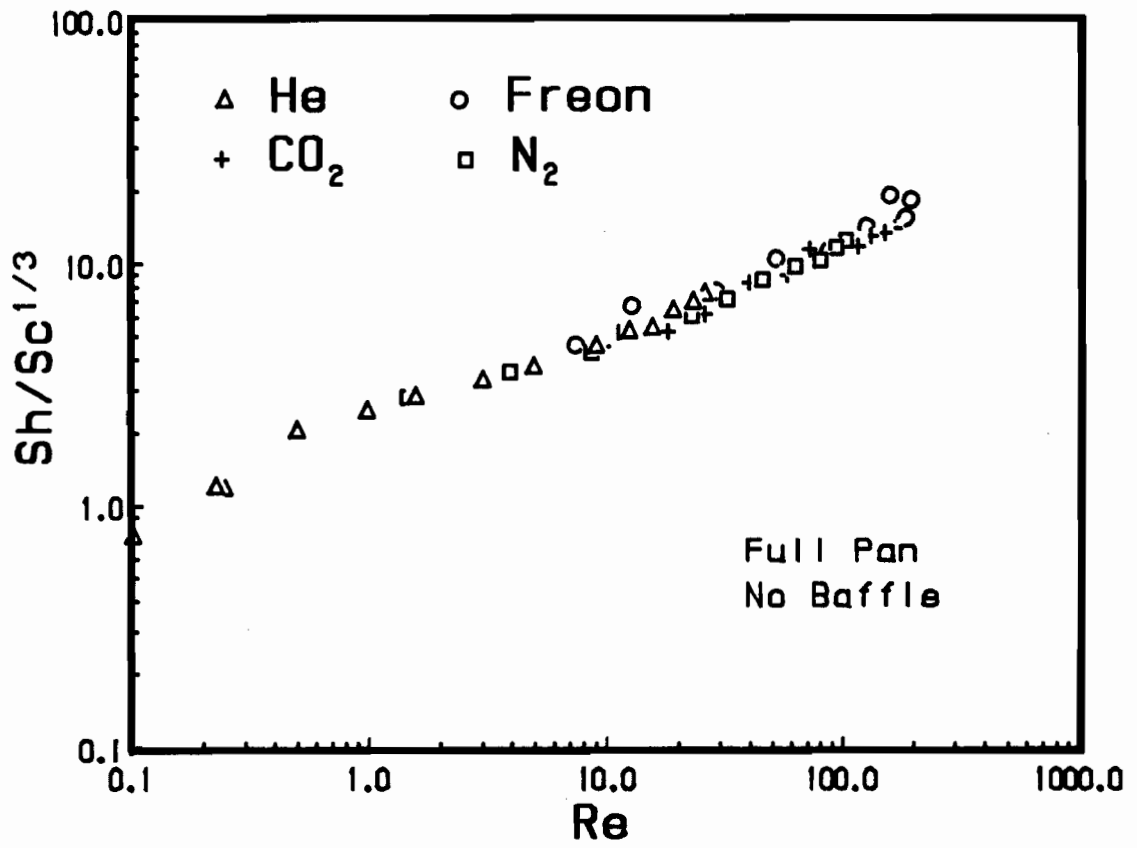


Figure 7. Effect of Sc on mass transfer rate.

naphthalene ("pellet" sample) and of powdered naphthalene pressed to form a flat horizontal exposed top surface ("powder" sample). The porcelain pan was used in both cases. The results in Figure 8 show that there is no difference between the two samples, indicating that surface roughness and bed porosity are unimportant at the conditions of the present study. This information is of interest because TGA studies are mostly carried out with powdered samples. All other data were obtained with the "pellet" sample.

3) Effect of Sample Pan

Three sample pans were compared; the porcelain pan (Coors Co.) and two much used and commercially available (Cahn Inc.) platinum and quartz pans. The naphthalene sublimation tests were done with the baffle present and a fully filled pan. The exposed naphthalene surface areas for the porcelain, platinum and quartz pan are 1.06, 0.636 and 0.478 cm² respectively. The results in Figure 9 show that under the present conditions the type of sample pan only has a small influence on the non-dimensional mass transfer rate ($Sh/Sc^{1/3}$). All further data were obtained with the porcelain pan.

4) Effect of Baffle

The baffle provided with the Cahn TGA system was designed to minimize flow instability as result of natural convection. Earlier it has been shown that convective heat transfer to the sample pan is enhanced by the baffle. Shown in Figure 10 is the effect of presence of the baffle on mass transfer. At low Re the mass transfer rate is not influenced by presence of the baffle. However for $Re \geq 10$, $Sh/Sc^{1/3}$ is higher with baffle and the effect increases with increasing Re . This behavior is caused by the higher gas velocity obtained with the smaller exit diameter of the baffle, while Re contains the average velocity based on the tube diameter. At low Re this effect is not felt because the jet dissipates before reaching the sample pan surface.

Not investigated in the present study is the distance between the exit of the baffle and the sample pan. This distance is about 10 mm in the present set-up. It is anticipated that the Reynolds number limit at which the influence of the baffle on $Sh/Sc^{1/3}$ is felt, will depend on the distance between sample and baffle exit.

5) Effect of Void Height of Sample Pan

Probably the most important, and often ignored geometric factor

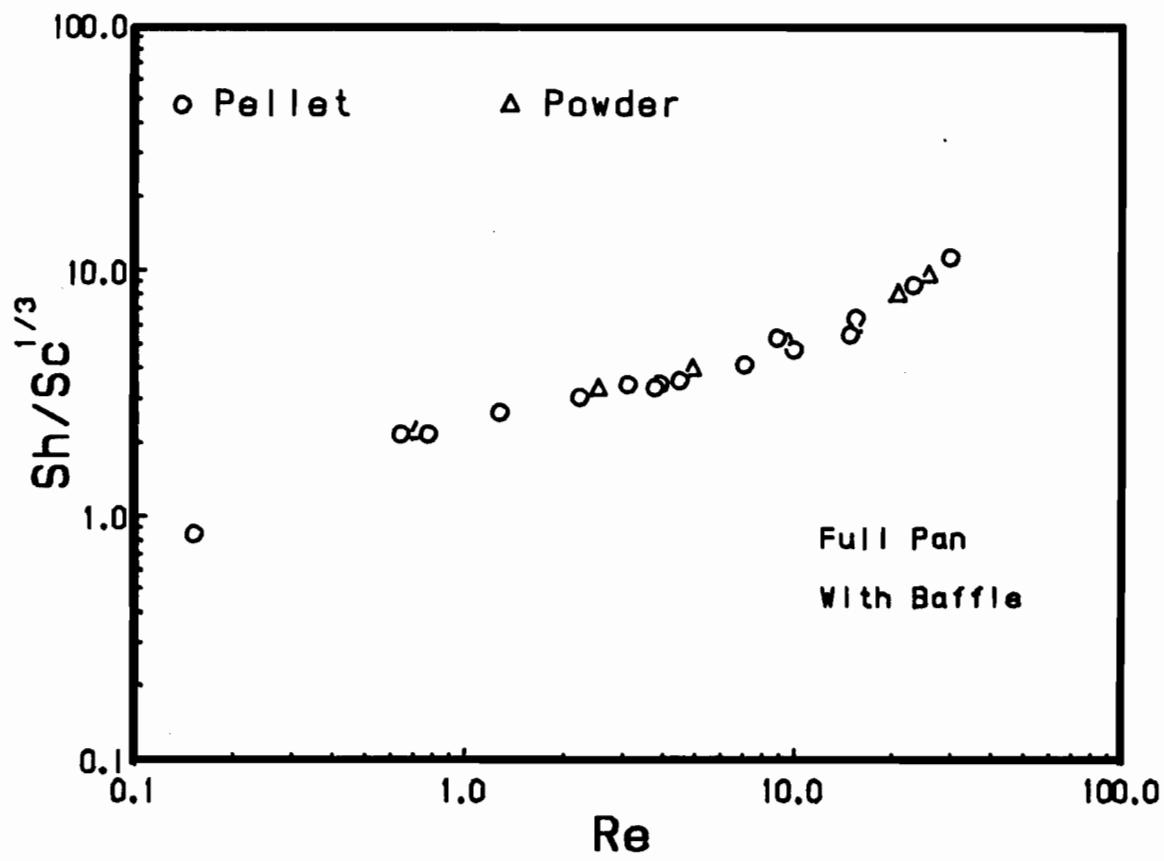


Figure 8. Effect of sample form on mass transfer rate.

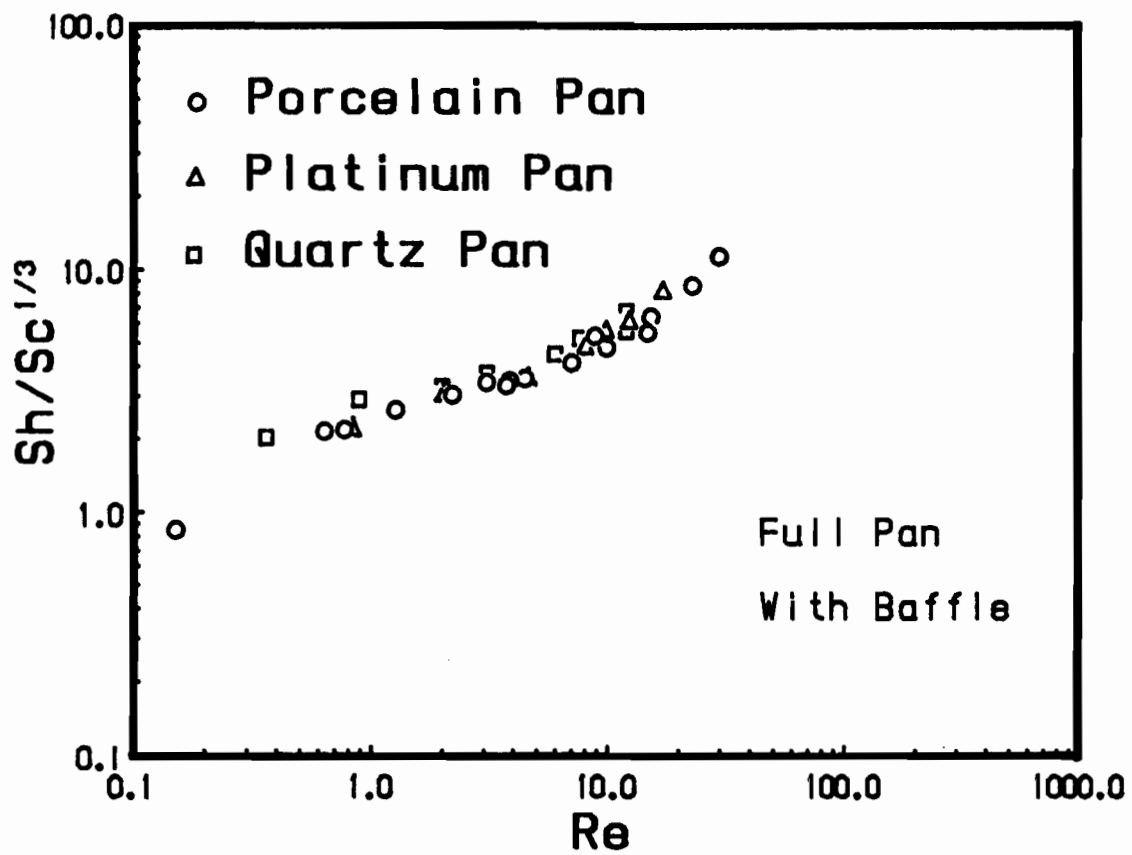


Figure 9. Effect of sample pan on mass transfer rate.

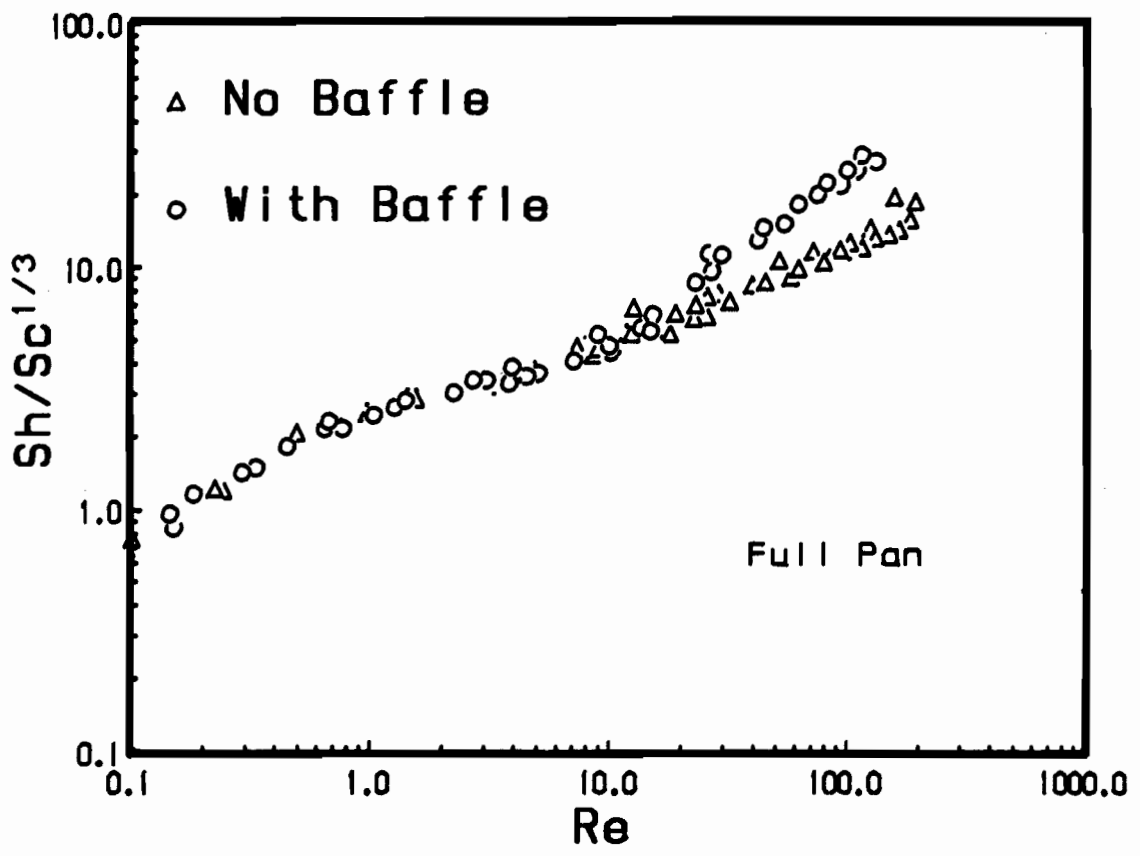


Figure 10. Effect of baffle on mass transfer rate.

influencing the mass transfer rate is the void height, H , between the sample surface and the surface bounded by the rim of the sample pan.

Three cases are considered; $H=0$, 1.1 and 3.2 mm, respectively a full pan, 60% and 5% full. Shown in Figures 11 and 12 are the results obtained with different degrees of sample pan filling, respectively with or without baffle present in the reactor tube. Without baffle, increasing H has a strong negative effect on the mass transfer rate. For $Re \geq 10$, the relative difference in $Sh/Sc^{1/3}$ is independent of Re . At $Re \leq 0.3$, the effect of H on $Sh/Sc^{1/3}$ disappears. With a baffle, the results are different, as can be seen from Figure 12. For $Re > 10$, the effect of H on the relative difference in $Sh/Sc^{1/3}$ diminishes until its influence becomes insignificant at $Re \approx 100$. At $Re < 1.0$, the results are about the same as without the baffle.

The explanation for the decreasing effect of H at $Re < 1.0$ is that the height H becomes less important compared to the thickness of the mass transfer boundary layer external to the surface bounded by the rim of the sample pan. For $Re \geq 1.0$ the additional mass transfer resistance due to the gas layer of thickness H becomes more important and is eventually dominant at $Re \approx 10$. The reason why the influence of H disappears at high Re with a baffle present might be that the gas flow jet formed by the baffle penetrates the gas layer inside the cup. Also the flow disturbances introduced by the expansions and contractions inside the baffle will lead to unsteady and non-axisymmetric impingement of the jet on the sample cup. This in turn leads to unsteady flow inside the sample cup and continuous renewal of the gas layer H above the naphthalene surface.

It should be noted however that under normal conditions H will affect the mass transfer since most TGA studies are performed at $1 < Re < 50$ [9, 11]. Without a baffle the influence of H remains at high Re because the flow is now steady and gas containing high concentrations of naphthalene will be recirculating inside the cup. The importance of minimizing H to increase the mass transfer can be illustrated by the following observation from Figure 11, that the effect of reduction of H from 3.2 mm to 0 mm on mass transfer rate is at least equivalent to increasing Re by one order of magnitude.

Correlation and Discussion

Correlation of the Experimental Results

It is obvious from the presented results that Sh can not be correlated

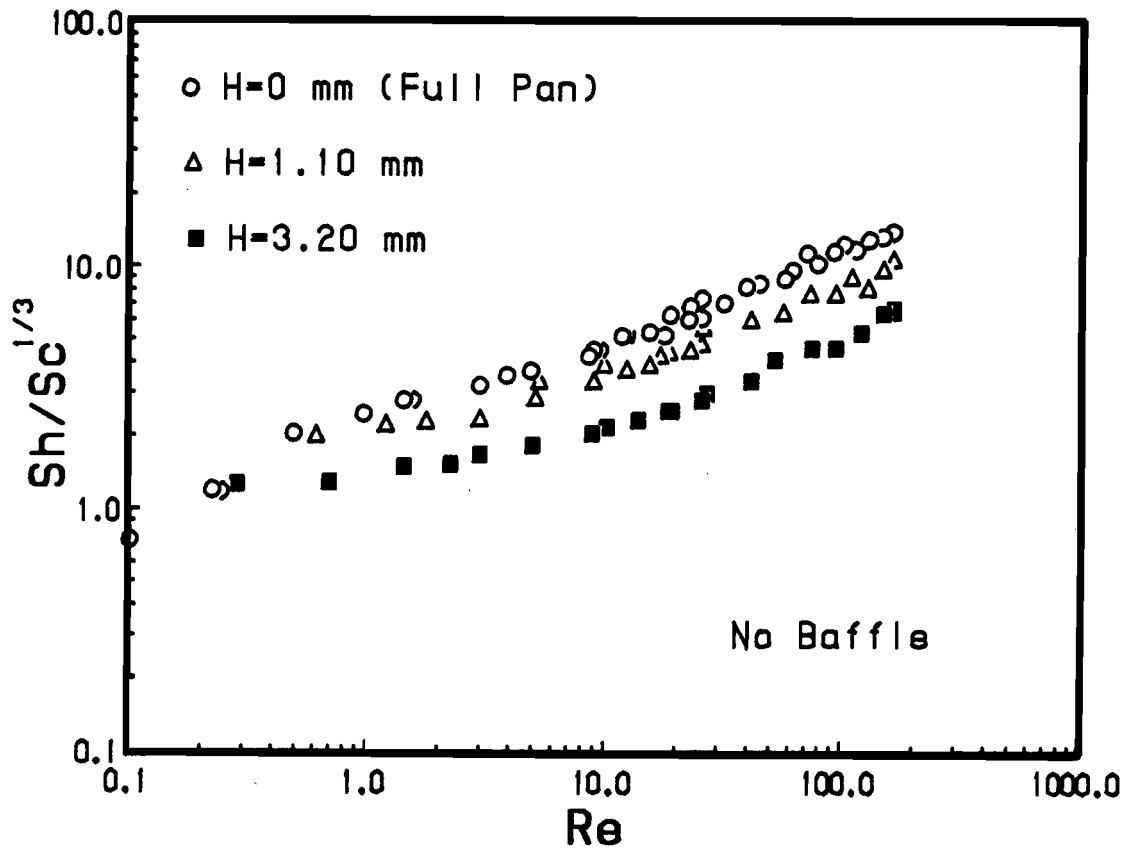


Figure 11. Effect of void height on mass transfer rate without baffle.

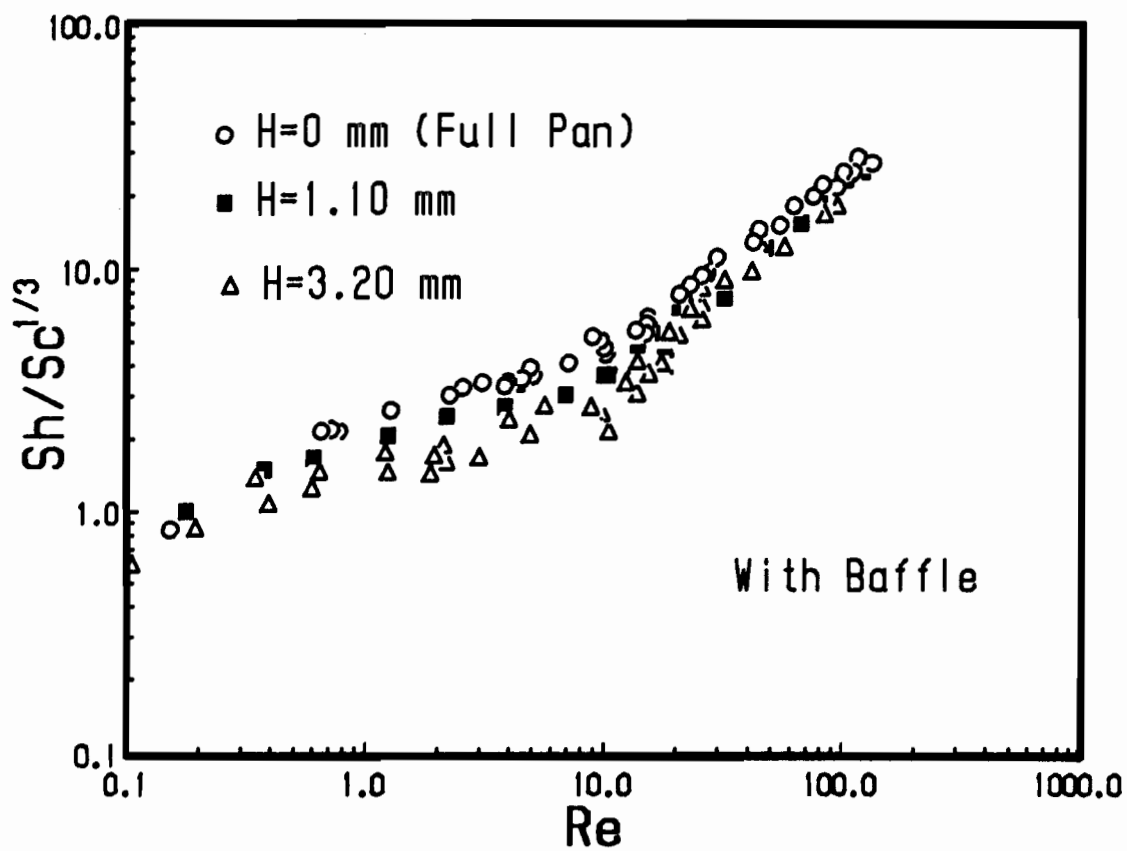


Figure 12. Effect of void height on mass transfer rate with baffle.

by a simple equation as

$$\text{Sh} / \text{Sc}^c = A + B \text{Re}^d \quad (14)$$

over the whole range of Re. Therefore the results were separately correlated for two or three smaller ranges of Re in the form of equation (14). The resulting equations were then combined by the Churchill and Usagi equation or "CUE" [28, 29].

Using a canonical expression to correlate data was developed by Churchill and Usagi [28, 29]. The basic equation can be written as

$$\left(y(x) \right)^n = \left(y_0(x) \right)^n + \left(y_\infty(x) \right)^n \quad (15)$$

where $y_0(x)$ is the asymptote for $x \rightarrow 0$, $y_\infty(x)$ the asymptote for $x \rightarrow \infty$, and n an arbitrary exponent. Equation (15), often referred as the CUE, has the advantages of incorporating the limiting behavior or solutions for both small and large x and of introducing only one arbitrary coefficient. The representation is ordinarily quite insensitive to the choice of n .

Mass Transfer Correlations of TGA System

The mass transfer correlations were obtained for four major cases:

a) For the case of no baffle present and $H=3.2$ mm, the results are correlated over two different ranges of Re as

$$\text{Sh} / \text{Sc}^{1/3} = 0.73 + 0.68 \text{Re}^{1/4} \quad (16)$$

When $0.3 < \text{Re} < 6$.

and

$$\text{Sh} / \text{Sc}^{1/3} = 0.56 + 0.46 \text{Re}^{1/2} \quad (17)$$

When $10 < \text{Re} < 170$.

Using the CUE method, equations (16) and (17) can be combined as

$$\frac{\text{Sh} / \text{Sc}^{1/3}}{0.73 + 0.68 \text{Re}^{1/4}} = \left\{ 1 + \left(\frac{0.56 + 0.46 \text{Re}^{1/2}}{0.73 + 0.68 \text{Re}^{1/4}} \right)^n \right\}^{1/n} \quad (18)$$

when $0.3 < \text{Re} < 170$.

with $n = 4.5$.

The experimental results and equations (16), (17) and (18) are shown in Figure 13. The figure clearly shows the powerful capability of the CUE method. Shown in Figure 14 are plots of Eq. (18) obtained with different n .

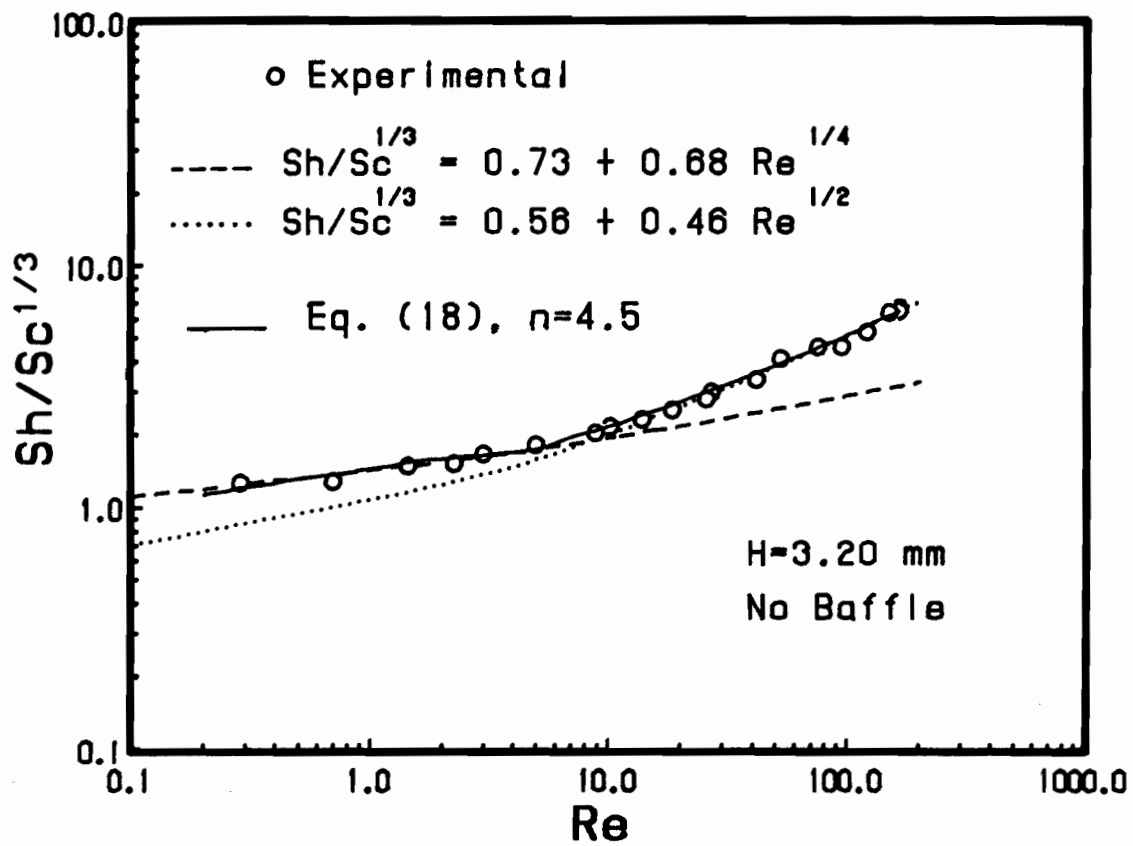


Figure 13. Correlations for mass transfer without baffle and $H=3.2$ mm

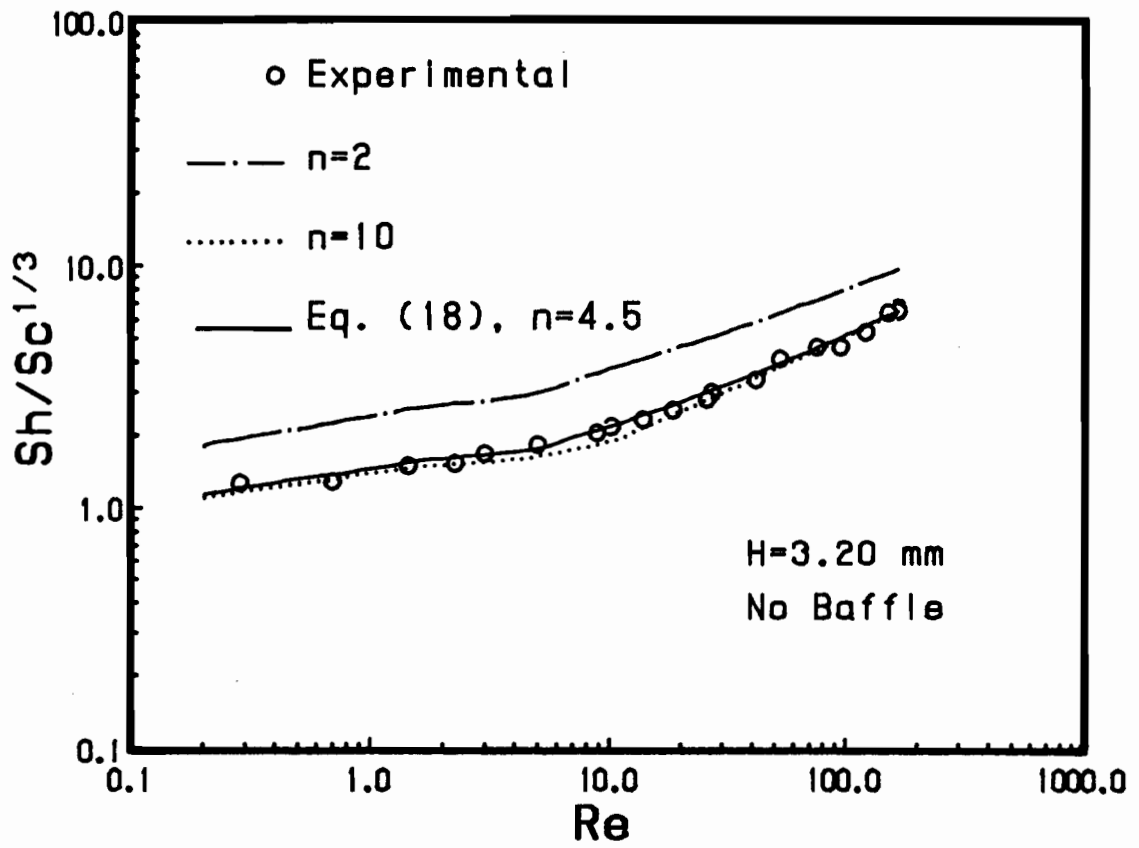


Figure 14. Sensitivity test of n.

It shows that for n larger than a certain value, the left hand side of Eq. (18) becomes insensitive to n .

b) For the case without baffle and a full pan ($H=0$), the results are simply correlated as

$$\text{Sh} / \text{Sc}^{1/3} = 2.02 \text{Re}^{0.37} \quad (19)$$

When $0.1 < \text{Re} < 170$.

The correlation and the experimental results are shown in Figure 15.

c) With a baffle present and $H=3.2$ mm height, the results can be correlated

$$\text{Sh} / \text{Sc}^{1/3} = 0.5 + 0.9 \text{Re}^{0.37} \quad (20)$$

when $0.3 < \text{Re} < 3$,

and

$$\text{Sh} / \text{Sc}^{1/3} = 0.52 \text{Re}^{0.8} - 0.5 \quad (21)$$

when $10 < \text{Re} < 150$.

Using the CUE method, equations (20) and (21) can be combined as

$$\frac{\text{Sh} / \text{Sc}^{1/3} + 0.5}{0.52 \text{Re}^{0.8}} = \left\{ 1 + \left(\frac{1.92}{\text{Re}^{0.8}} + \frac{1.73}{\text{Re}^{0.43}} \right)^n \right\}^{1/n} \quad (22)$$

with $n = 8$,

when $0.3 < \text{Re} < 150$.

The experimental results and equations (20), (21) and (22) are shown in Figure 16.

d) With a baffle and full pan the experimental results can be correlated as

$$\text{Sh} / \text{Sc}^{1/3} = 0.4 + 1.8 \text{Re}^{0.37} \quad (23)$$

when $0.3 < \text{Re} < 10$,

and

$$\text{Sh} / \text{Sc}^{1/3} = 1.63 \text{Re}^{0.6} - 1.68 \quad (24)$$

when $10 < \text{Re} < 170$.

Using the CUE method, equations (23) and (24) can be combined as

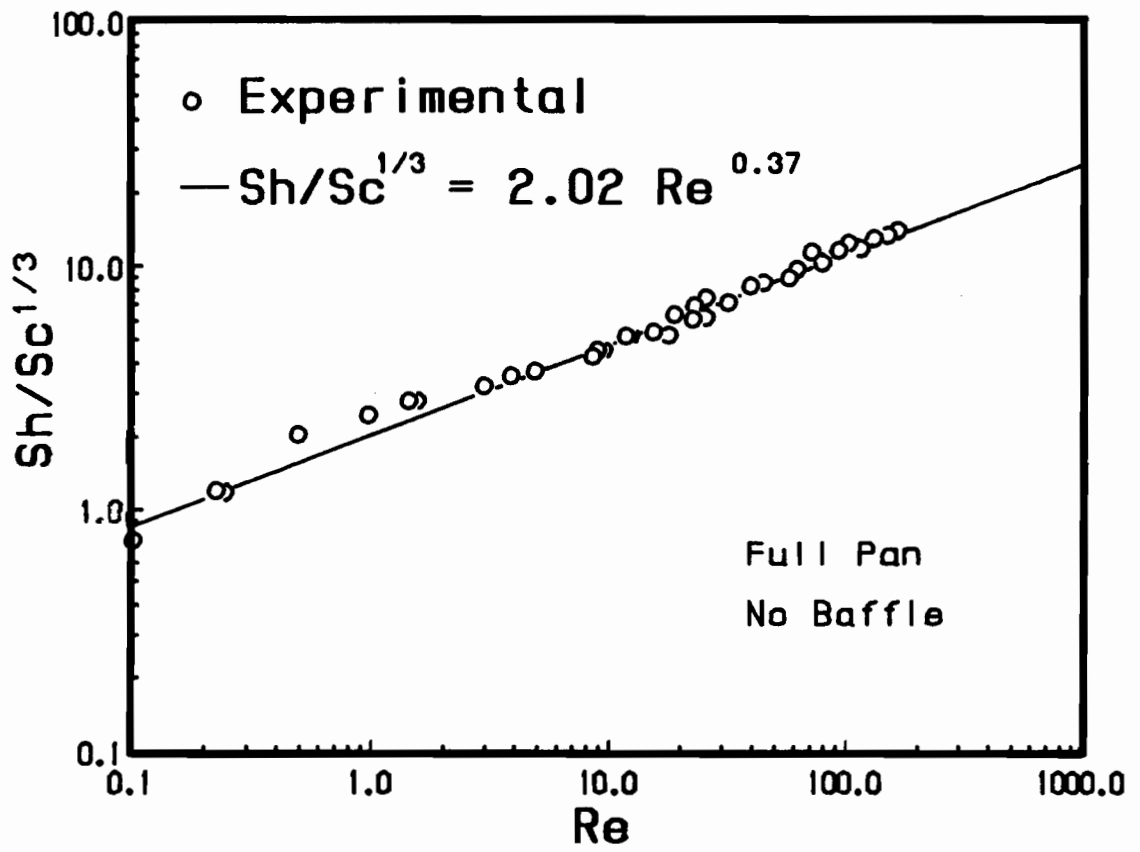


Figure 15. Correlation for mass transfer without baffle and full pan.

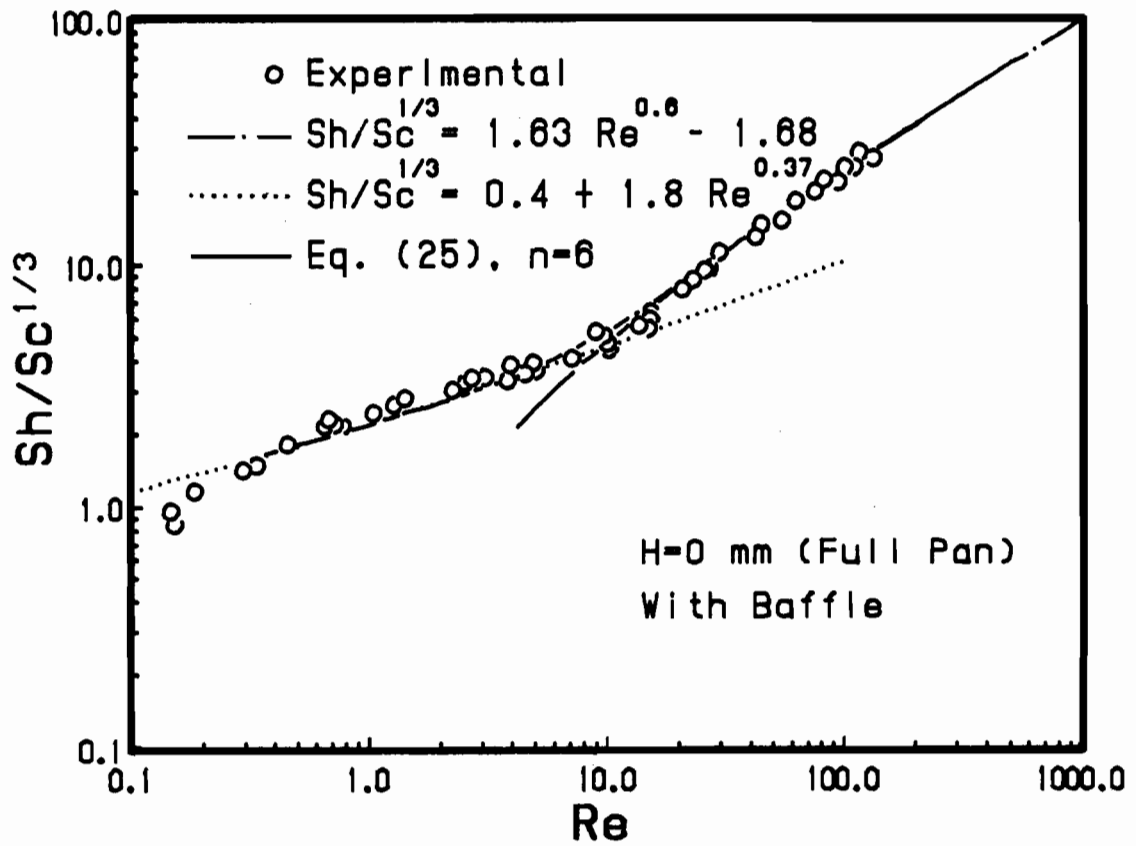


Figure 16. Correlation for mass transfer with baffle and $H=3.2$ mm.

$$\frac{Sh / Sc^{1/3} + 1.68}{1.63 Re^{0.6}} = \left\{ 1 + \left(\frac{1.28}{Re^{0.6}} + \frac{1.1}{Re^{0.23}} \right)^n \right\}^{1/n} \quad (25)$$

with $n = 6$

when $0.3 < Re < 170$.

The experimental results and plots of equations (23), (24) and (25) are shown in Figure 17.

Comparison with Literature Data

In Figures 18 and 19 the present results are compared with some published data. The data of Wigmans were obtained with the naphthalene sublimation technique and a similar TGA system. The Re used Wigmans based on the annular area between tube and sample pan was converted to the present Re based on the reactor tube diameter. Also shown is the Ranz & Marshall [10] correlation, Eq.(1).

The present results without baffle for $H=1.1$ mm closely agree with Wigmans data. Assuming a wall thickness of 0.5 mm for pan 2^b used by Wigmans, a height of 1.5 mm can be calculated from the geometry of the pan. Wigmans data also show that higher transfer rates were obtained with a shallower pan, but he did not comment on it. The Ranz & Marshall equation also gives almost the same results as for the present case with or without baffle and $H=1.1$ mm, and with the presence of a baffle and $H=1.1$ mm for $1 < Re < 20$. This confirms that equation (1) can be used as a first approximation for estimation of the mass transfer in the present TGA system as was done by Li [9].

Application of the Present Results

Evaluation of External Mass Transfer Limitation

Traditionally the influence of external mass transfer on the reaction rate is investigated by changing k_g through variation of gas flow rate. This method has as weakness that in certain situations the mass transfer coefficient k_g is only slightly dependent on flow rate. For example for $Re < 10$, $H=3.2$ mm (or almost empty pan) and the presence of a baffle, a decrease in Re of a factor 20 leads only to a decrease in Sh of a factor 2 (Figure 16). However with known mass transfer characteristics for the

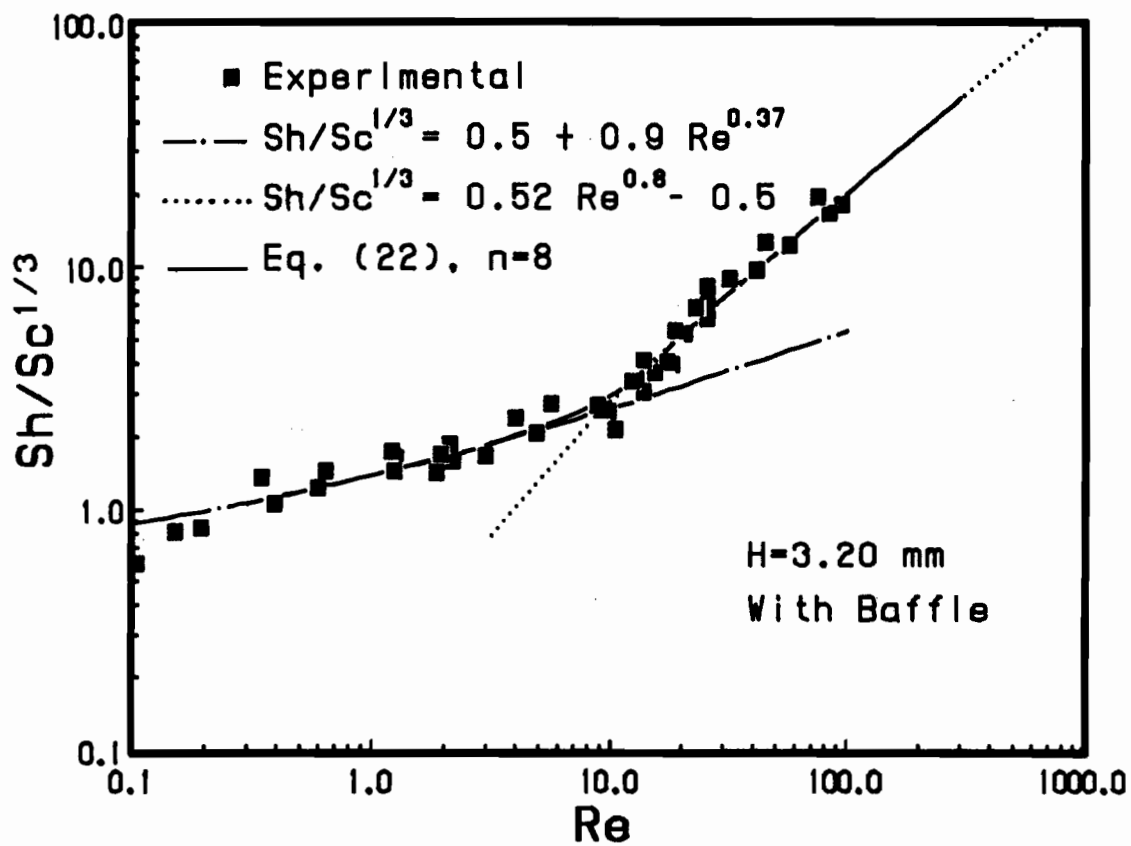


Figure 17. Correlation for mass transfer with baffle and full pan.

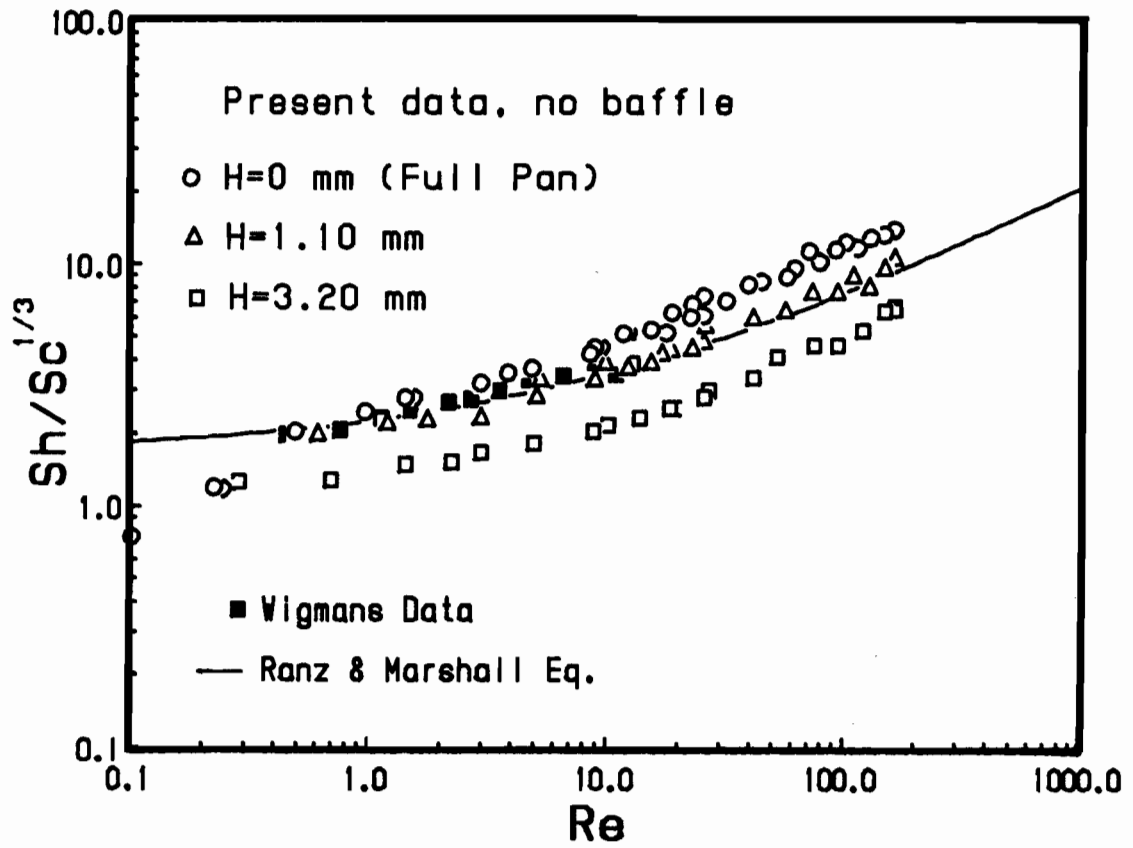


Figure 18. Comparison of mass transfer data without presence of baffle with literature data.

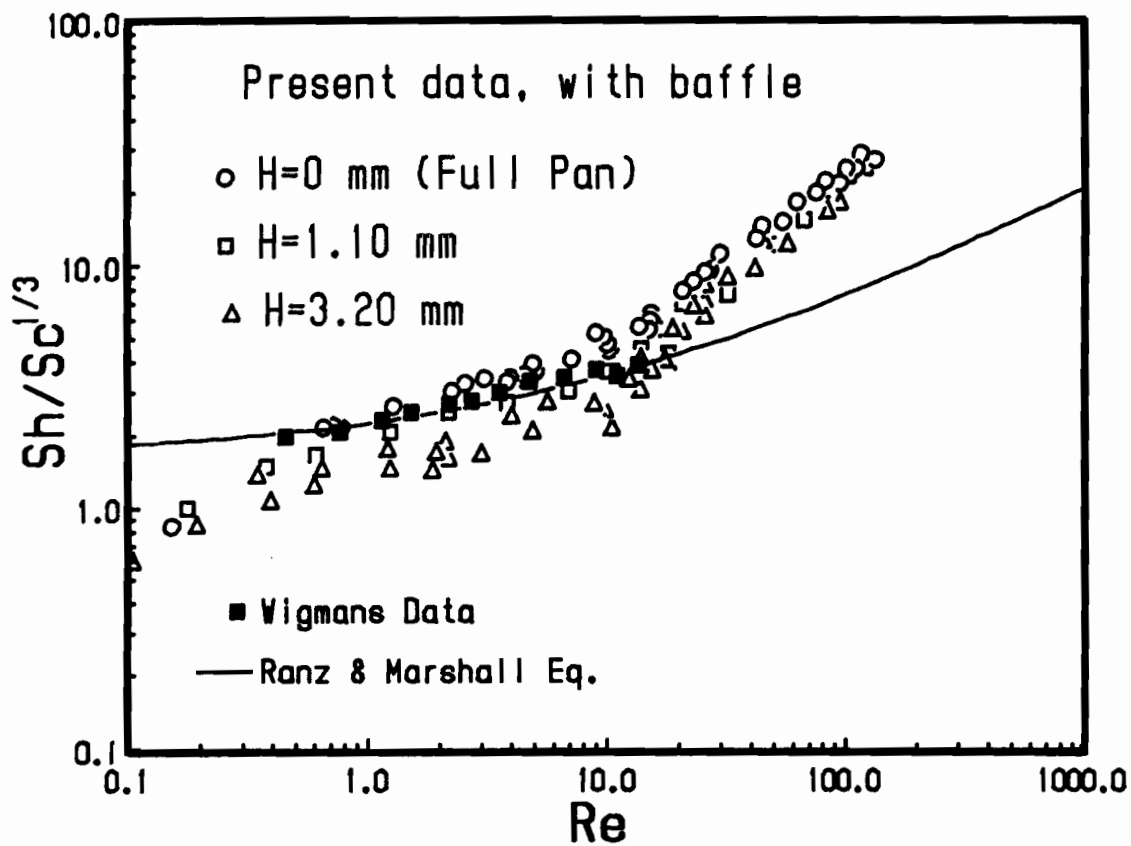


Figure 19. Comparison of mass transfer data with presence of baffle with literature data.

present system, the influence of mass transfer on the measured reaction rate can now be evaluated quantitatively. Thus external mass transfer represents less than 5% of the total resistance of the gas consumption rate of a gas-solid reaction measured with the present TGA system [9], when

$$M_H = \frac{(-r_v) L}{k_g C_b} < 0.05 \quad (26)$$

where $(-r_v)$ is the molar consumption rate per unit bed volume of solid sample, L the characteristic bed dimension, defined as bed volume divided by exposed bed surface height and C_b the molar concentration of reactant gas in the bulk of the gas.

A simple and more conclusive experimental test of absence of both external and internal gas mass transfer limitations on gas reaction consumption rate is when the reaction rates with respectively N_2 or He as carrier gas are the same. This test is only not valid for evaluation of gas phase mass transfer limitation inside the bed, when transport inside the solids is governed by Knudsen diffusion.

Shown in Figure 20 is the mass transfer coefficient as function of temperature calculated from equation (25) for carbon gasification by CO_2 and H_2O with an alumina sample pan in the present TGA set-up with baffle. The results were obtained at the maximum practical flow rate of 1000 scc/min, a pan with an external diameter of 10 mm and a surface area S for mass transfer of 0.5 cm^2 . Figure 20 shows that at higher temperatures the mass transfer coefficient in He is almost twice as large as in N_2 .

Dilution Factor

A disadvantage of the hanging basket TGA technique for study of chemical reactions is that a large amount of gas bypasses the sample pan. This leads to a much lower concentration of product gas in the exhaust gas than existing inside the bed of solids in the sample pan. The dilution factor, Ψ , defined as the ratio of product concentration in the sample pan, $[a]_b$, and in perfectly mixed off-gas at the sample temperature, $[a]_{exh}$, for zero product concentration in the feed is

$$\Psi = \frac{[a]_b}{[a]_{exh}} = \frac{Q_v}{k_g \cdot S} \quad (27)$$

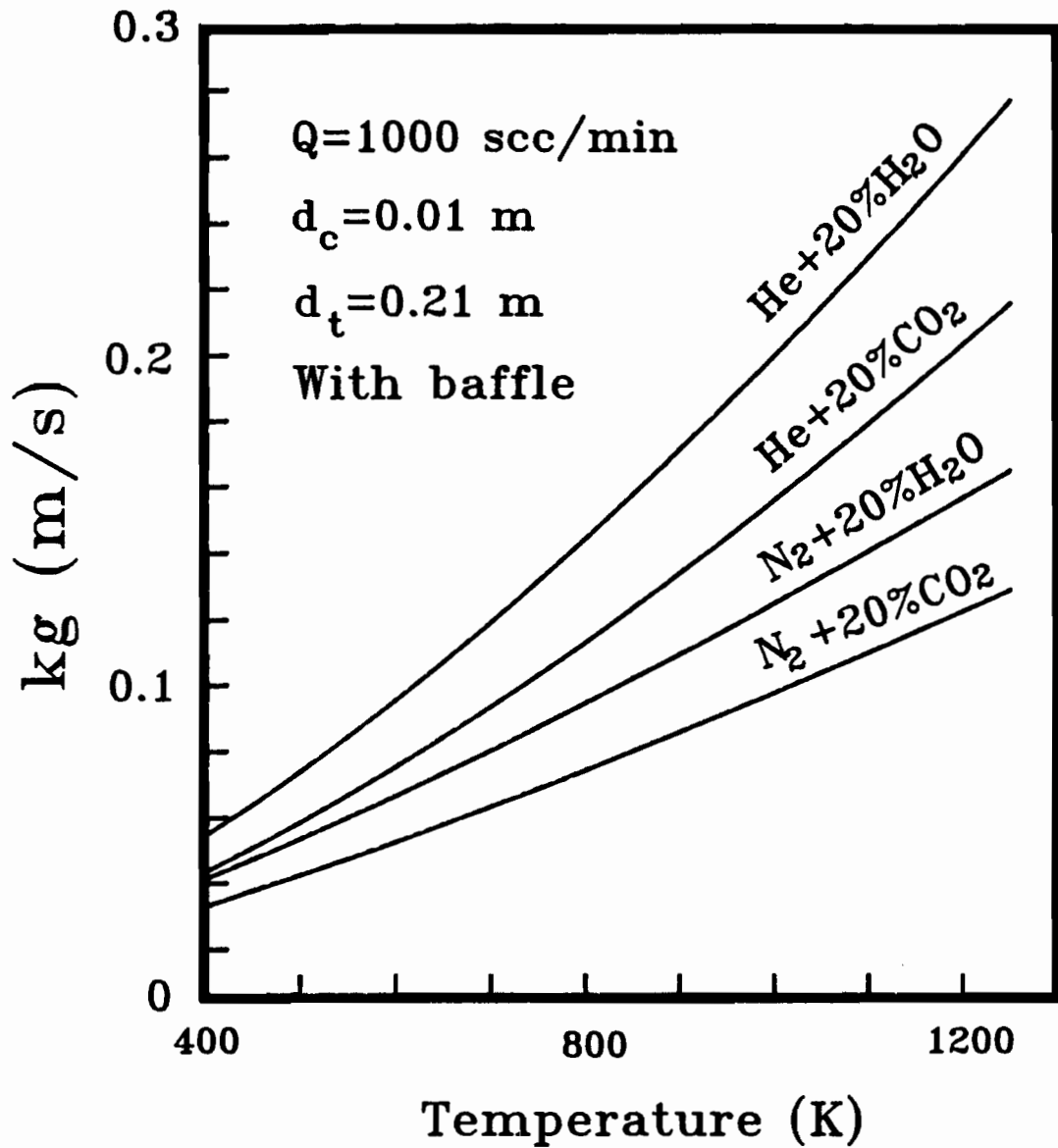


Figure 20. Mass transfer coefficient as function of temperature and gas system.

where Q_v is the total volumetric flow rate of the off-gas at the sample temperature. Since the TGA is operated differentially, the rate of gas produced by reaction can be neglected compared to the feed gas flow rate. With k_g determined from the previous presented correlations and known values for S and Q_v , the dilution factor can be determined. For example, the dilution factors for products H_2 , CO and CO_2 of carbon gasification by 15% H_2O in N_2 at 923 K and 750 scc/min total flow rate are respectively 7, 17 and 20. The product gas concentration in the sample bed expressed in ppm or vol% is subsequently calculated from the dilution factor and the measured gas concentration in the exhaust also expressed in ppm or vol%. Knowledge of [a]_b makes it possible to study the influence of product gas concentration on reaction kinetics, or to determine whether thermodynamic equilibrium exists inside the bed of solids. When the product concentration in the feed is at the percentage level, the dilution factor is very nearly equal to 1.0 because of differential operation of the TGA.

With evaluation of the external mass transfer limitation and knowledge of product gas concentrations in the sample pan, the present TGA technique has an advantage over a packed bed reactor that the weight loss during reaction is also known. Remaining potential disadvantages of the TGA technique compared to a packed bed reactor are low product concentrations in the off-gas and a relative large volume between gas analysis sampling point and sample pan. The latter results in gas mixing and a delay time for analysis which might be unacceptable for study of fast processes such as adsorption or desorption and rapid exchange reactions [30]. However for most reaction systems and with modern gas analysis techniques, these two disadvantages are generally insignificant.

CONCLUSION

The present investigation of heat and mass transfer characteristics of a common hanging basket TGA set-up shows that

- although mono and diatomic gases might not reach the furnace control temperature inside the reactor tube at high flow rate, the sample temperature under most conditions is sufficiently close to the control temperature.
- the mass transfer rate to the sample pan is enhanced by presence of an

upstream baffle tube and by increasing the fractional filling of the sample pan.

- the external mass transfer limitation and product gas concentration in the sample pan can be calculated using correlations for external mass transfer to the sample pan.
- external gas phase heat and mass transfer limitation to the sample pan are negligible when the weight-loss rate is the same with respectively N₂ or He as carrier gas.

NOMENCLATURE

A ₁	= thermocouple surface area, m ² .
A ₂	= area of gas film around thermocouple, m ² .
[a] _b	= gas concentration in sample bed, mol·m ⁻³ .
[a] _{exh}	= gas concentration in exhaust, mol·m ⁻³ .
C _b	= bulk gas concentration, mol·m ⁻³ .
C _w	= vapor concentration of naphthalene at top surface, mol·m ⁻³ .
C _∞	= vapor concentration of naphthalene in bulk gas, mol·m ⁻³ .
C _p	= gas heat capacity, J·mol ⁻¹ ·K ⁻¹ .
d _c	= sample pan diameter, m.
D	= tube diameter, m.
D	= diffusion coefficient, m ² ·s ⁻¹ .
h	= heat transfer coefficient, J/(s·K·m ²).
h _{ct}	= heat transfer coefficient of control thermocouple, J/(s·K·m ²).
h _s	= heat transfer coefficient of sample, J/(s·K·m ²).
H	= void height, mm.
k	= thermal conductivity, J/(s·m·K).
k _g	= mass transfer coefficient, m·s ⁻¹ .
l	= length of heating zone, m.
L	= characteristic length, m.
m	= gas mass flow rate, kg·s ⁻¹ .
M	= molecular weight, g/mol.
Nu	= Nusselt number.
p _w	= partial pressure of naphthalene at surface, atm.
P	= total pressure, atm.
Pr	= Prandtl number.
Q _v	= volumetric gas flow rate, m ³ ·s ⁻¹ .
(-r)	= rate of naphthalene sublimation, mol·s ⁻¹ .

$-r_v$	= rate of reaction, $\text{mol}\cdot\text{m}^{-3}\text{ s}^{-1}$.
R	= universal gas constant, $\text{atm}\cdot\text{l}\cdot\text{mol}^{-1}\cdot\text{K}^{-1}$.
Re	= Reynolds number.
S	= exposed surface area, m^2 .
Sc	= Schmidt number.
Sh	= Sherwood number.
t	= time, min.
T	= temperature, K.
T_g	= gas temperature, K.
T_t	= thermocouple temperature, K.
T_w	= wall temperature, K.
V	= average gas velocity based on reactor tube cross section, $\text{m}\cdot\text{s}^{-1}$.

Greek Symbols

ϵ	= thermocouple emissivity.
Ψ	= dilution factor defined by equation (27).
σ	= Stefan-Boltzmann constant ($5.67\times 10^{-8}\text{ watt}\cdot\text{m}^{-2}\cdot\text{K}^4$).
ρ	= density of the gas mixture, $\text{kg}\cdot\text{m}^{-3}$.
λ	= latent heat, $\text{J}\cdot\text{mol}^{-1}$.
μ	= viscosity, $\text{kg}\cdot\text{m}^{-1}\cdot\text{s}^{-1}$.
$\sum_a v_i$	= sum of diffusion volumes.

REFERENCES

1. Keattch, C.J. and D. Dollimore, "An Introduction to Thermogravimetry", 2nd edit., Heyden & Son Ltd., N.Y., (1975).
2. Honda, K., *Sci. Rep.*, Tohoku Univ., 4, p.97(1915).
3. Wendlandt, W.Wm., "Thermal Methods of Analysis", 2nd edit., John Wiley & Sons, N.Y., (1974).
4. Kapteijn, F., and J.A. Moulijn, *Fuel*, 62, p.221(1983).
5. Treptau, M.H., and D.J. Miller, *IEC Res.*, 26, p.2007(1987).
6. Lee, W-G., and J.Y. Park, *IEC Fundam.*, 25, p.799(1986).
7. Edelstein, S., *Ph.D. thesis*, California Institute of Technology, (1987).
8. Hippo, E. and P.L. Walker, Jr, *Fuel*, 54 (Oct.), p.245 (1975).

9. Li, J. and A.R.P. van Heiningen, **JPPS**, 12 (5), p.1146(1986).
10. Ranz, W.E., and W.R. Marshall, **Chem. Eng. Prog.**, 48, p.173(1952).
11. Wigmans, T. **Ph.D. thesis**, Univ. Amsterdam, (1982).
12. Schlichting, H., "**Boundary-Layer Theory**", 6th edit., McGraw-Hill, p.285(1968).
13. Mullikin, H.F., "**Temperature, Its Measurement and Control in Science and Industry**", Reinhold, p.775(1941).
14. Eber, G.R., "**Physical Measurements in Gas Dynamics and Combustion**", edited by R.W. Ladenburg et al, Princeton Univ. Press, p.186(1954).
15. Sparrow, E.M. and J.E. Niethammer, **J. Heat Transfer, Transaction ASME**, 99, p.507(1977).
16. Sparrow, E.M. and J.E. Niethammer, **J. Heat Transfer, Transaction ASME**, 101, p.404(1979).
17. Sogin, H.H. and P.L. Providence, **Trans. of the ASME**, 80, p.61(1958).
18. Chapman, A.J., **Heat Transfer**, 2nd, edit., Macmillan Co., N.Y., (1970).
19. Bennett, C.O., and J.E. Myers, "**Momentum, Heat, and Mass Transfer**", 3rd edit., McGraw-Hill, p.353(182).
20. Christian, W.J., and S.P. Kezios, **1957 Heat Transfer Fluid Mech. Inst.**, Stanford Univ. Press, p.359(1957).
21. Popiel, Cz.O. and L. Boguslawski, **1986 Heat Transfer Conf.** p.1187(1986).
22. Fuller, E.N., P.D. Schettler, J.C. Giddings, **Ind. Eng. Chem.**, 58, p.19(1966).
23. Lee, C.Y., and C.R. Wilke, **Ind. Eng. Chem.**, 46(11), p.2381(1954).
24. Barr, R.F. and H. Watts, **J. Chem. Eng. Data**, 17(1), p.45(1972).
25. Caldwell, L., **J. Chem. Eng. Data**, 29(1), p.60(1984).
26. Mack, E., **J. Am. Chem. Soc.** 47, p.2468(1925).
27. Perry, R.H. and C.H. Chilton, "**Chemical Engineer's Handbook**", 5th edit., (1973).
28. Churchill, S.W. and R. Usagi, **AIChE J.**, 18, p.1121(1972).
29. Churchill, S.W. and R. Usagi, **Ind. Eng. Chem., Funda.**, 13, P.39(1974).
30. Cerfontain, R., **Ph.D. Thesis**, Amsterdam University, (1986).

CHAPTER 3

KINETICS OF CO₂ GASIFICATION OF FAST PYROLYSIS BLACK LIQUOR CHAR

ABSTRACT

The CO₂ gasification rate of black liquor char (BLC) was studied in a thermogravimetric analysis set-up at temperatures between 600 to 800°C. BLC was prepared via fast pyrolysis of dry solids of spent liquor of the kraft wood pulping process. BLC gasification by CO₂ is well described by Langmuir-Hinshelwood type kinetics. The gasification rate of BLC is one order of magnitude larger than a high surface area activated carbon impregnated with 12% Na₂CO₃. Also, the gasification rate of BLC remains high at sodium/carbon ratios where the rate of Na₂CO₃ impregnated chars would normally be strongly reduced. The rate of BLC gasification was also influenced by the drying method and pyrolysis heating rate. With SEM-EDS and mapping and line scan techniques it is shown that the unique gasification properties of BLC are caused by a very fine distribution of sodium in the carbon matrix. The present data suggests that internal surface area measurements rather than swelling tests might be more appropriate to characterize combustion properties of black liquors.

INTRODUCTION

Black liquor char (BLC) is the pyrolysis product of kraft black liquor solids (BLS). Kraft black liquors are dark viscous liquids resulting from digestion of wood with an aqueous solution of sodium hydroxide and sodium sulfide. In general, during kraft pulping about 50% of the wood enters in solution. This dissolved wood substance originates primarily from hemicellulose and lignin, and is present in the liquor as respectively hydroxy acids and alkali lignin. At the bottom of a chemical recovery furnace, a black liquor char bed is formed after drying, pyrolysis and partial gasification of a spray of concentrated black liquor droplets. The porous char has a very high sodium content and also contains inorganic sulfur compounds like Na_2SO_3 , $\text{Na}_2\text{S}_2\text{O}_3$ and Na_2SO_4 . Gasification of the char provides the reducing atmosphere required to convert the inorganic sulfur compounds to Na_2S , one of the active pulping chemicals. Fundamental knowledge of the processes occurring in a kraft recovery furnace is still incomplete because many interrelated reactions proceed simultaneously. Also the corrosive nature and complex composition of the mixture of char and inorganic smelt complicates kinetic study of the different heterogeneous reactions. Char gasification by CO_2 and H_2O is an area recently identified by Grace et al. [1] where data is urgently needed. This data is also required for development of a proposed alternative low temperature recovery process [2].

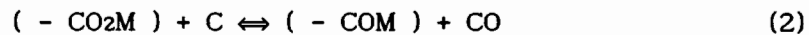
Because black liquor char consists mainly of a mixture of carbon, sodium carbonate and sodium sulfide, alkali catalyzed carbon gasification studies serve as a useful reference for gasification of black liquor char. Comprehensive reviews of gasification of carbonaceous materials catalyzed by alkali metals have been published by McKee [3], Wen [4] and Wood and Sancier [5]. It is generally agreed that presence of alkali metal carbonates leads to a reactivity increase over uncatalyzed CO_2 gasification in the order of 10 to 100, and that the rate generally increases with increasing atom number, i.e. $\text{Li} < \text{Na} < \text{K} < \text{Rb} < \text{Cs}$ [6]. A number of recent studies of the alkali-metal catalyzed Boudouard reaction ($\text{C} + \text{CO}_2 = 2\text{CO}$) deal with influence of changing catalyst/carbon ratio, changing micro-porous structure and internal

surface area development during burn-off [6, 7] on gasification rate.

Since McKee and Chatterji [8] proposed an oxygen transfer mechanism for alkali metal carbonate catalyzed carbon gasification, a number of very detailed mechanistic studies have been reported [9-14]. These investigations have provided more evidence that alkali oxide groups on the carbon surface are involved in the gasification [10, 11]. In one of the latest mechanisms it is proposed by Sams and Shadman [12] that alkali metal carbonate is first reduced



followed by the redox sequence



and



where $(-CO_2M)$ and $(-COM)$ are believed to be carboxylic and phenolic groups observed in IR studies [15, 16]. It is also suggested that the reduction of carboxylic groups, reaction (2), is the rate determining step. From this mechanism it follows that the number of alkali metal oxide surface groups, and thus the dispersion of alkali on the carbon surface, is an important factor determining the rate of carbon gasification. The mechanism proposed by Moulijn et al. [13, 17] involves more reaction steps and intermediates. However the active catalytic species are still alkali C(O) complexes, and their reduction step by carbon is also considered to be rate determining for gasification.

Despite the similarities in chemical composition, there is however, a significant difference between black liquor char and carbonaceous chars doped with alkali metal salts. In the latter case the chars are prepared by either impregnation or by pyrolysis of the char precursor with catalyst powder. Black liquor char on the other hand, is produced from a liquid phase in which sodium is mixed and chemically bound with the char precursor on a molecular scale. This leads to a three dimensional and presumably fine dispersion of the alkali metal catalyst. Another difference is the several times larger initial sodium/carbon atomic ratio for black liquor char. The only study on CO₂ gasification kinetics of "slow pyrolysis" BLC was reported

by the present author [18]. It was found that the gasification rate of BLC is more than one order on magnitude higher than coal char with an optimum alkali metal catalyst loading [19]. Also the BLC gasification rate remains high at sodium metal-carbon ratio far exceeding the optimum ratio for doped coal chars.

In the present investigation, the gasification rate of BLC obtained after fast pyrolysis is studied as a function of CO and CO₂ concentration, temperature, sample preparation method and burn-off. The results are compared with gasification data of other alkali-metal impregnated chars. The unique gasification properties of BLC are explained by the fine dispersion of sodium, quantified by SEM-EDS.

EXPERIMENTS

A. Sample Preparation

An ultimate and chemical analysis of the black liquor solids and black liquor chars are given in Table I. The black liquor used in this study was obtained by cooking black spruce wood chips with an aqueous solution of Na₂S and NaOH at 170°C to about 49% of pulp yield (Kappa No. = 30). The liquor was subsequently oxidized under 200 psig oxygen and 130°C whereby all inorganic sulfur was converted into Na₂SO₄ as can be verified in Table I. It can be calculated from Table I that about 50% of sodium is bound to SO₄²⁻ and CO₃²⁻, indicating that the remaining sodium is chemically linked to lignin and hydroxy acids. This property makes black liquor an unique precursor for sodium impregnated chars.

Black liquor was dried as a thin film on the convex surface of watch glasses below 120°C. This drying method was used to prevent enrichment of the inorganic salts in the mother liquor during the drying process. After scraping from the glass surface, the solids were pyrolyzed for 20 minutes under nitrogen with 10% CO in a tube furnace preheated to 580°C. Swelling occurred during pyrolysis and the final swollen volume was one to two orders of magnitude larger than the original volume of the solids. The pyrolysis yield was about 70%. The resulting char was then ground and the fraction passing a 500 mesh (<25 μm) sieve was used in this study. The chemical composition of the pyrolyzed char is shown in Table 1. Comparing the oxygen

in the inorganic ions with total oxygen, it can be calculated that there is 7% organic oxygen in the char. It also can be seen that the pyrolyzed char still contains 0.5% hydrogen. The organic O and H may be in the form of C-O-H (or its sodium salt) and C-H, which were identified by IR analysis in pyrolyzed lignin [20]. The hydrogen content in the reduced char should be less than that of the non-reduced char. However it was very difficult to obtain reproducible results for H analysis, due to extreme sensitivity of the sample to exposure of air and moisture. In general, the elemental analysis for C, H, N and O is very difficult because the black liquor samples are very corrosive and damaging to the sample holder at the analysis temperatures.

TABLE I. CHEMICAL AND ELEMENTAL ANALYSIS OF BLACK LIQUOR SOLIDS AND CHARs

CHEMICAL ANALYSIS (wt%)							
	[SO ₄ ⁼]	[S ⁼]	[SO ₃ ⁼]	[CO ₃ ⁼]	[S ₂ O ₃ ⁼]	[Na ⁺]	Fixed C
SOLIDS	8.13	< 0.1	< 0.1	7.2	< 0.05	18.6	33
CHAR	13.5	< 0.1	< 0.1	28	< 0.05	25.4	28.7
REDUCED CHAR	<0.1	5.7	< 0.1	33	< 0.05	33.2	28

ULTIMATE ANALYSIS (wt%)								
	C	H	O	S	N	Na	K	Cl
SOLIDS	34.2	4.1	38	4.0	0.2	18.6	0.07	0.2
CHAR	34.8	0.5	33	4.5	0.2	25.4	0.11	0.2
REDUCED CHAR	34.6	-	27	5.7	0.1	33.2	0.13	-

As reference material was used, a coconut shell activated carbon from A.C. Carbon Canada, treated with boiling 4% HCl solution, washed with deionized water and subsequently ground. The fraction passing 500 mesh was impregnated with Na₂CO₃ solution and dried at room temperature. The Na₂CO₃ loading was 12.8%.

To investigate the influence of drying technique on gasification rate,

another BLS was obtained by drying the liquor in drying dishes under IR lamps. Further processing to obtain BLC was the same as described above. The influence of pyrolysis heating rate on reactivity of BLC was studied by comparing the present data with those obtained for "slow pyrolysis" of BLC, prepared with a heating schedule of 20 to 775°C at a rate of 25°C/min. For more information see reference [18]. An interesting difference with the "fast pyrolysis" char is that the "slow pyrolysis" char did not swell at all.

B. Experimental System for Kinetic Study

A Cahn TGA 113 DC thermogravimetric analysis system was used. The schematic picture of the TGA system with auxiliary gas preparation system is shown in Figure 1. Nitrogen (99.998%) and helium (99.995%) are zero grade quality, carbon dioxide anaerobe grade (99.99%) and carbon monoxide ultra-high purity (99.9%). An oxygen trap was used for each gas. CO₂, water and hydrocarbon traps were used for CO because of its relatively low purity. A flat dish shaped sample pan of high purity alumina (99.8%) was used to eliminate chemical interaction with the sample and to minimize the external and internal mass transfer resistances [21].

A gas chromatograph with a flame photometric detector was used for analysis of sulfurous gas components in the exhaust, while a Fisher gas partitioner was used for measurements of fixed gases. CO and CO₂ were also determined continuously with IR analyzers. The inorganic ions in the solid product, such as sulfate, sulfide, sulfite, thiosulfate, carbonate and sodium were measured with a Dionex ion chromatograph with conductivity and electro-chemical detectors. The BET surface area of BLC and activated carbon was measured by CO₂ adsorption with a Flowsorb device of Micromeritics. The catalyst distribution in BLC and impregnated activated carbon was studied by SEM-EDS using a JSM-T300 from JEOL.

C. Experimental Procedures

After adding about 5 mg of "fast pyrolysis" BLC to the pan inside the reactor tube, the system was three times evacuated and refilled with N₂ or He. Then under a He or N₂ flow rate of 400 scc/min, the furnace temperature was raised from 20°C to 775°C at a rate of 25°C/min. At about 500°C 25 scc/min of CO was also added to the carrier gas. After 2 minutes at 775°C

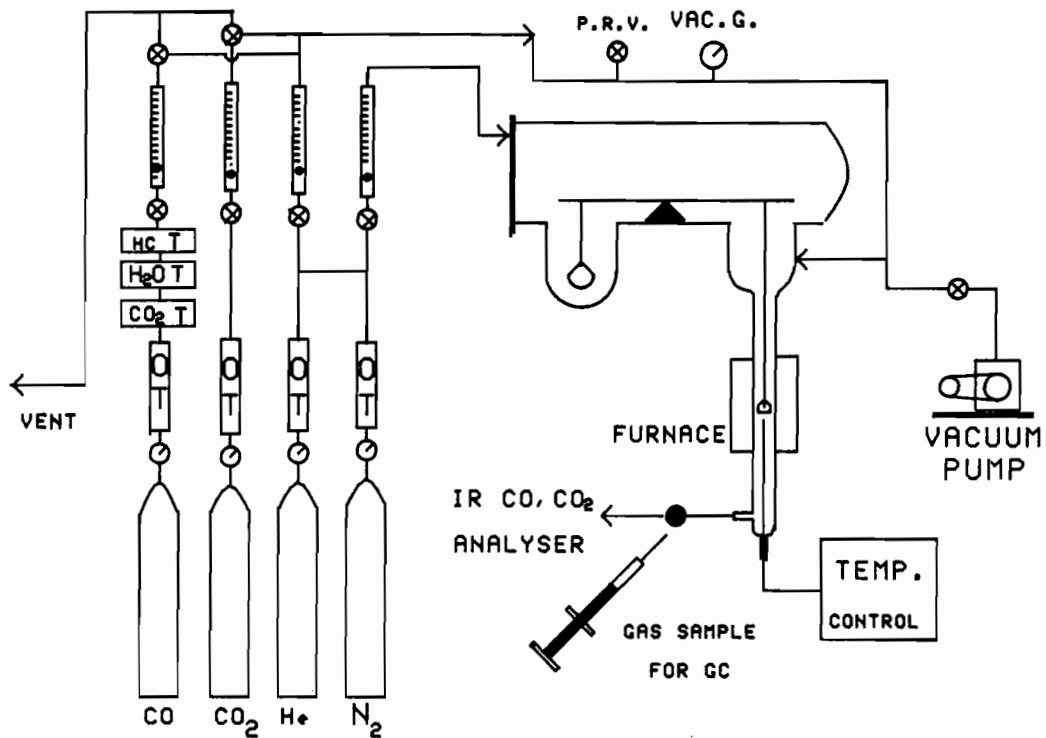


Figure 1. TGA set-up with gas supply system.

the temperature was reduced to the required reaction temperature. When the temperature and sample weight were stabilized, the CO concentration was adjusted and CO₂ was added to obtain the desired gasification atmosphere.

KINETIC RESULTS

A. Data Analysis and Reduction

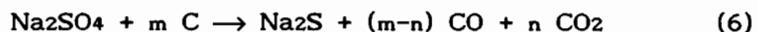
The temperature and weight loss curves for a typical run are shown schematically in Figure 2. The small weight loss below 500°C is due to release of H₂O, CO₂ and CO. An apparent weight increase occurred at 500°C because of the increased drag due to addition of CO to the gas stream. CO was added to prevent



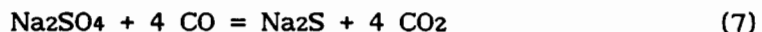
and



which lead to vaporization of sodium and a weight loss [12, 21]. The sample weight decrease recorded between 600°C and final gasification temperature was caused by reduction of Na₂SO₄ by carbon and CO [22, 23] as



and



It is clearly shown in Figure 2 that the sample weight remains constant after the weight loss associated with Na₂SO₄ reduction is complete, indicating that no other reaction is taking place. When CO₂ was added to the system at the reaction temperature, a weight increase was observed as a result of the increased gas velocity and fast chemical reaction between reduced Na₂CO₃-carbon complexes and CO₂ [12, 24]. The ultimate analysis and chemical composition of the reduced black liquor char just before

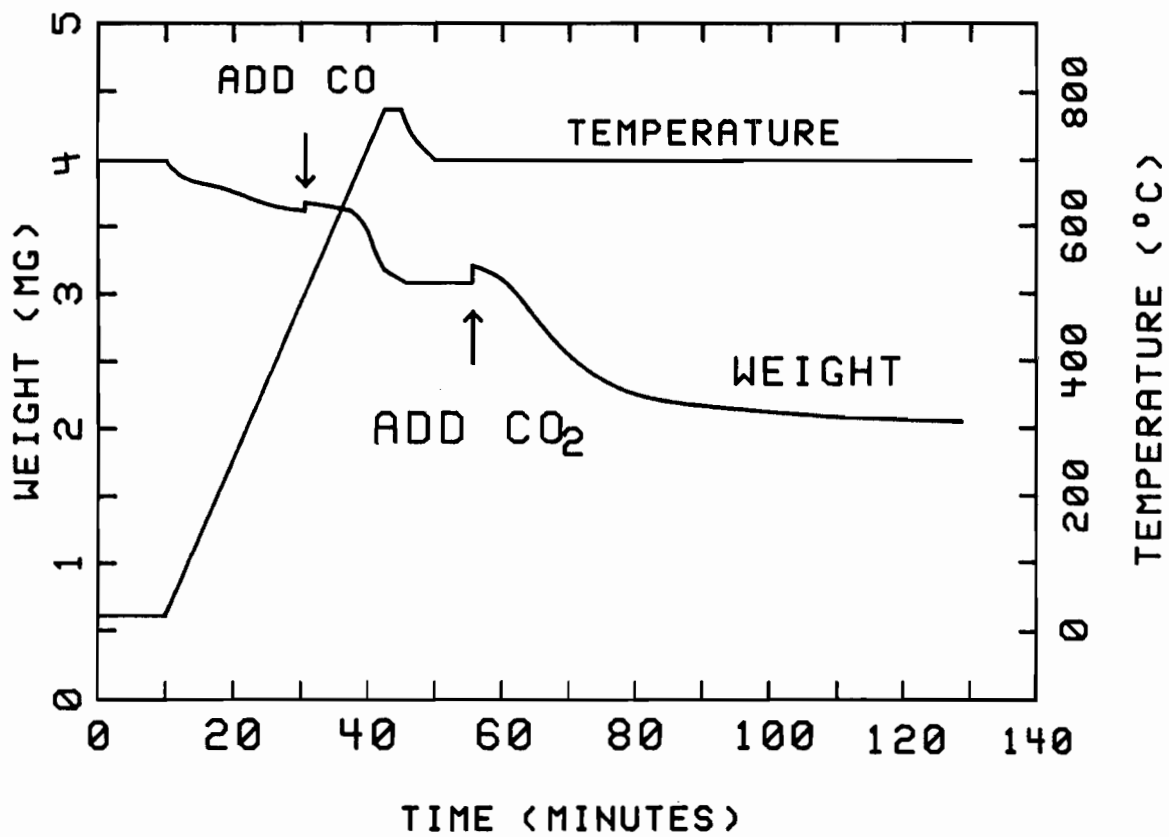


Figure 2. Schematic picture of temperature and weight loss curve from TGA.

gasification are shown in Table I. As can be seen from the Table, the major chemical compounds of the reduced char are 28% fixed carbon, 13% Na₂S and 58% Na₂CO₃.

The weight change during gasification was caused by two reactions:



and



Therefore the carbon gasification rate was obtained after correction of the recorded weight loss by the weight increase caused by reaction (9). Although the COS production was one order of magnitude smaller than CO formed by gasification, the increase in weight due to reaction (9) was not negligible. The correction procedure for a typical run is shown in Figure 3. The COS emission rate shown in the inner figure of Figure 3 was multiplied by 28/60 and then integrated over time to obtain the weight increase resulting from reaction (9). Then it was added to the weight recorded by TGA to obtain the weight loss due to carbon gasification. The effect of reaction (9) is clearly illustrated in Figure 3 where at the end of the experiment the recorded weight increases even though carbon gasification was complete.

The instantaneous rate of gasification (of) is defined as:

$$-r_w = -\frac{1}{W} \frac{dW}{dt} \quad (10)$$

where W is the carbon weight at time t. The gasification rate is obtained by differentiation of the polynomial fitted to the gasification weight loss curve.

It has previously been shown [25] that the presence of heat and mass transfer limitations in a TGA system can easily be detected by varying the type of carrier gas. Helium and nitrogen are most suitable because of their large difference in thermal conductivity and diffusivity. It should be noted that mass transfer resistances due to less common Knudsen or configurational diffusion can only be identified by varying particle size. As can be seen in Figure 4, the CO₂ gasification rates of BLC with He or N₂

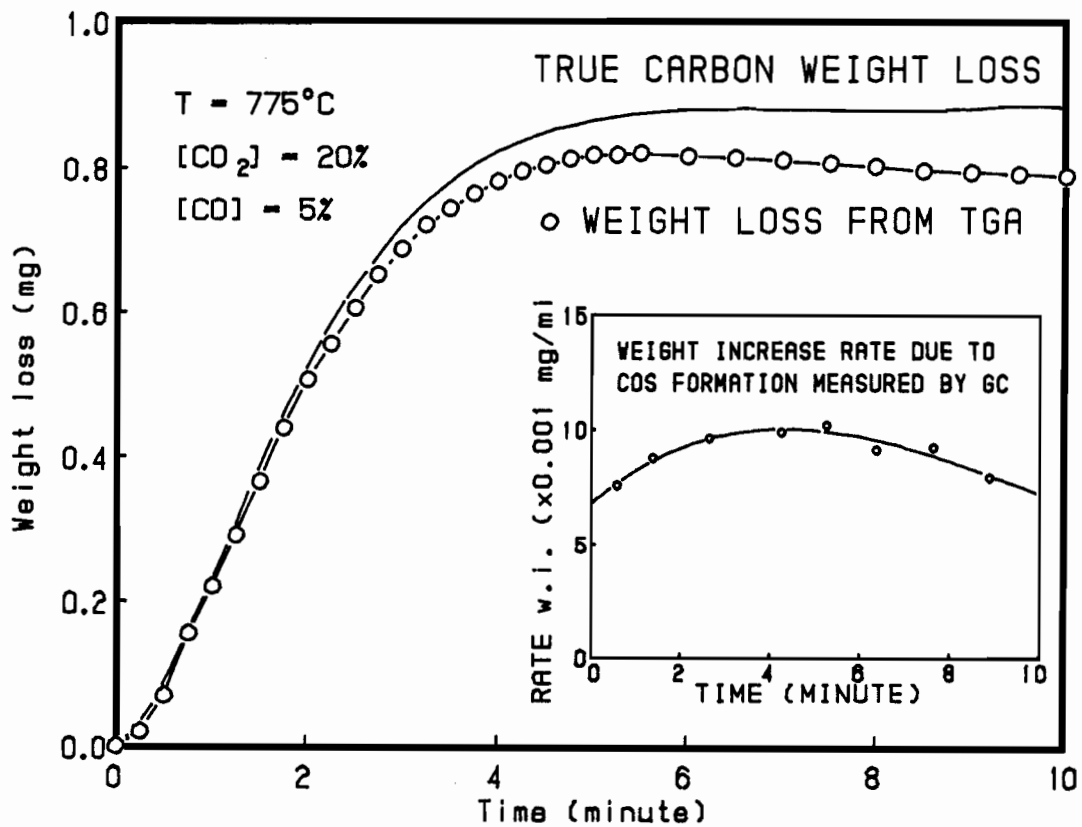


Figure 3 Measured weight loss and carbon weight loss for a typical run. Note: the inner figure shows the weight increase rate due to COS formation.

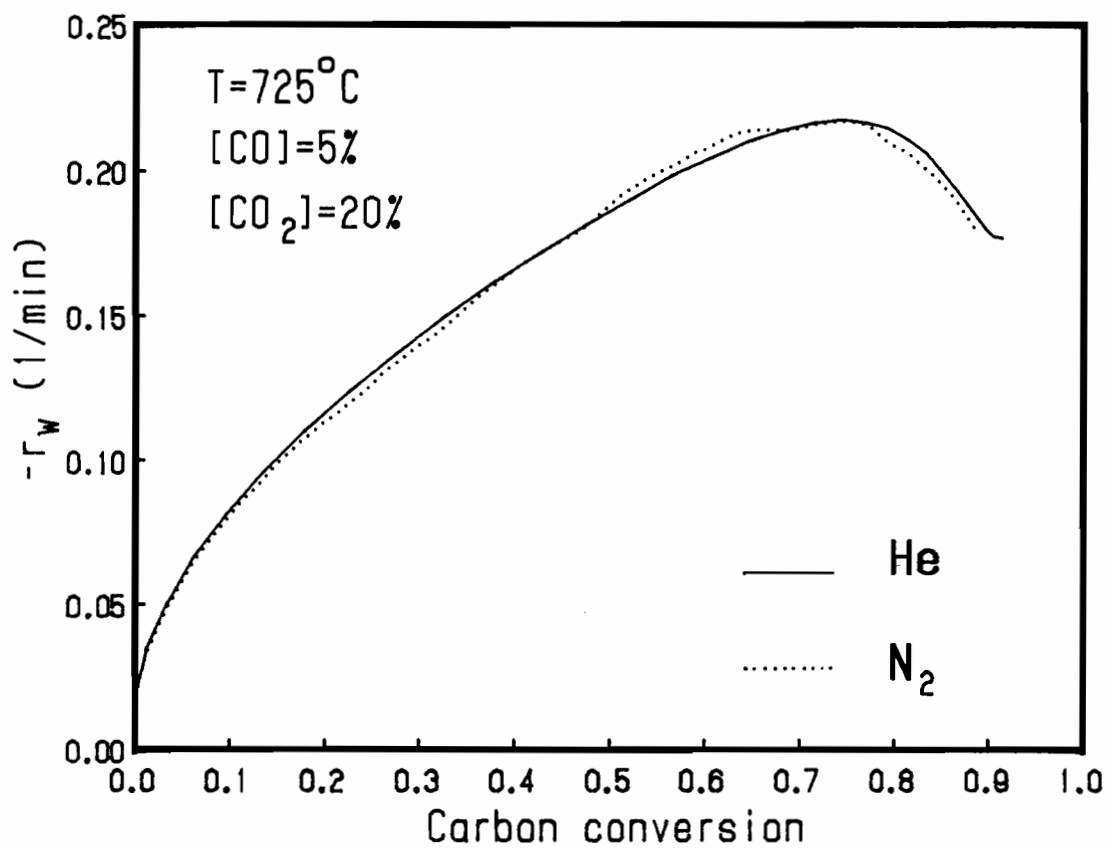


Figure 4. Effect of carrier gas on gasification rate.

as carrier gas are essentially the same, proving that heat and mass transfer resistances were not important in the present experimental system. Unless specified otherwise, all kinetic data were obtained with He as carrier gas.

B. Gasification Kinetics

It has been shown in a number of studies [3, 4, 26] that both the uncatalyzed and catalyzed CO₂ gasification of carbon can be described by the following Langmuir-Hinshelwood kinetic expression:

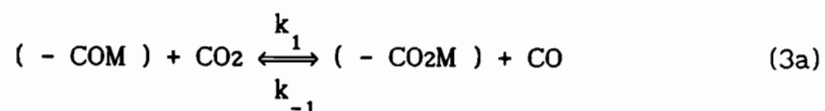
$$-r_w = \frac{K [\text{CO}_2]}{1 + K_{\text{CO}_2} [\text{CO}_2] + K_{\text{CO}} [\text{CO}]} \quad (11)$$

where K ($\text{m}^3 \cdot \text{mol}^{-1} \cdot \text{min}^{-1}$) is the reaction constant and K_{CO_2} ($\text{m}^3 \cdot \text{mol}^{-1}$) and K_{CO} ($\text{m}^3 \cdot \text{mol}^{-1}$) can be considered to be the equilibrium adsorption constants of respectively CO₂ and CO. However, more recent studies [10, 13] indicate that the rate of alkali metal catalyzed gasification of carbon by CO₂ can be described by another Langmuir-Hinshelwood type of expression

$$-r_w = \frac{K' [\text{CO}_2]}{[\text{CO}_2] + K'_{\text{CO}} [\text{CO}]} \quad (12)$$

where K' (min^{-1}) is the reaction constant and K'_{CO} (dimensionless) can be considered to be the equilibrium adsorption constant of CO. It should be noticed that the dimensions of K' and K'_{CO} are different from those of K and K_{CO} . The absolute values of K' and K'_{CO} do not change when different units are used for the gas concentrations.

Both equations (11) and (12) can be derived from the same reaction mechanism proposed by Sams and Shadman [12]. As discussed before, the gasification proceeds via a redox sequence represented by equations (2) and (3), and the reduction of the carboxylic group, reaction (2), is the rate determining step. Therefore, the reaction steps can be rewritten as



and



By assuming that i) reaction (2a) is the rate determining step and ii) formation and destruction of $(-\text{CO}_2\text{M})$ is at quasi steady state, equation (11) is obtained as

$$-r_w = \frac{k_1 [\text{CO}_2]}{1 + \frac{k_1}{k_2} [\text{CO}_2] + \frac{k_{-1}}{k_2} [\text{CO}]} \quad (11a)$$

so that $K = k_1$, $K_{\text{CO}_2} = k_1 / k_2$ and $K = k_{-1} / k_2$. However, one assumes that i) reaction 2a) is the rate determining step and ii) reaction 3a) is at quasi equilibrium, meaning $k_2 \ll k_{-1} [\text{CO}]$, then equation (12) is obtained as

$$-r_w = \frac{k_2 [\text{CO}_2]}{[\text{CO}_2] + \frac{k_{-1}}{k_1} [\text{CO}]} \quad (12a)$$

and thus $K' = k_2$ and $K'_{\text{CO}} = k_{-1} / k_1$. The only additional assumption for derivation of (12a) is that the oxidation reaction (3a) is assumed to be much faster than reduction reaction (2a). In the most recent study, Cerfontain al et [13] showed with labelled reaction gases that this assumption is valid. They found that the oxidation reaction, also defined as oxygen exchange reaction, is three orders of magnitude faster than the reduction reaction or carbon gasification reaction.

Equation (12) can be rewritten as

$$\frac{1}{-r_w} = \frac{1}{K'} + \frac{K'_{\text{CO}}}{K'} \frac{[\text{CO}]}{[\text{CO}_2]} \quad (13)$$

Accordingly the inverse of the carbon gasification rates at 25%, 50% and 75% conversion are plotted as a function of $[\text{CO}]/[\text{CO}_2]$ in Figure 5. Linear relationships are obtained for all three different conversions, confirming the validity of equation (12) for "fast pyrolysis" black liquor char. Similarly it was tested whether equation (11) could represent the data.

Correlation of the data with that equation (11), however, gave negative values for the reaction and both adsorption constants. The reaction and adsorption constants determined from Figure 5 are listed in Table II.

TABLE II. REACTIVITIES OF CARBONACEOUS MATERIALS

TYPE OF CARBON	CONV. X (%)	RATE (min ⁻¹)	K or K'	K _{CO₂}	K _{CO} or K' _{CO}	T (°K)	[CO ₂] (atm)
REDUCED BLC	25	0.132	0.24		4.1	998	0.2
	50	0.185	0.31		3.4		
	75	0.215	0.35		2.9		
ACTIVATED CARBON [27]		0.018	0.024		10	1050	0.15
							**
ELECTRODE CARBON [28]		1.6e-5*	1.1e-5	0.34	4e3	1000	0.2
GRAPHITE 5%K ₂ CO ₃ [29]		3e-5		0.2	1.6	1400	0.2
COAL { 5%Na ₂ CO ₃		4.4e-4				973	1
CHAR { 10%Na ₂ CO ₃		2.0e-3				973	1
[30] 20%Na ₂ CO ₃		2.0e-3				973	1
ACTIVATED CARBON [9]		0.012	4.7e-3	0.47	3.1e2	1175	0.27

* "e" means " times 10 to the power "

** K' and K'_{CO} above this line, K, and K_{CO₂} and K_{CO} below this line.

Also included in Table II are kinetic data from literature for some selected carbonaceous materials. It can be seen that the reactivity of BLC is at least one and three orders of magnitude larger than activated carbon

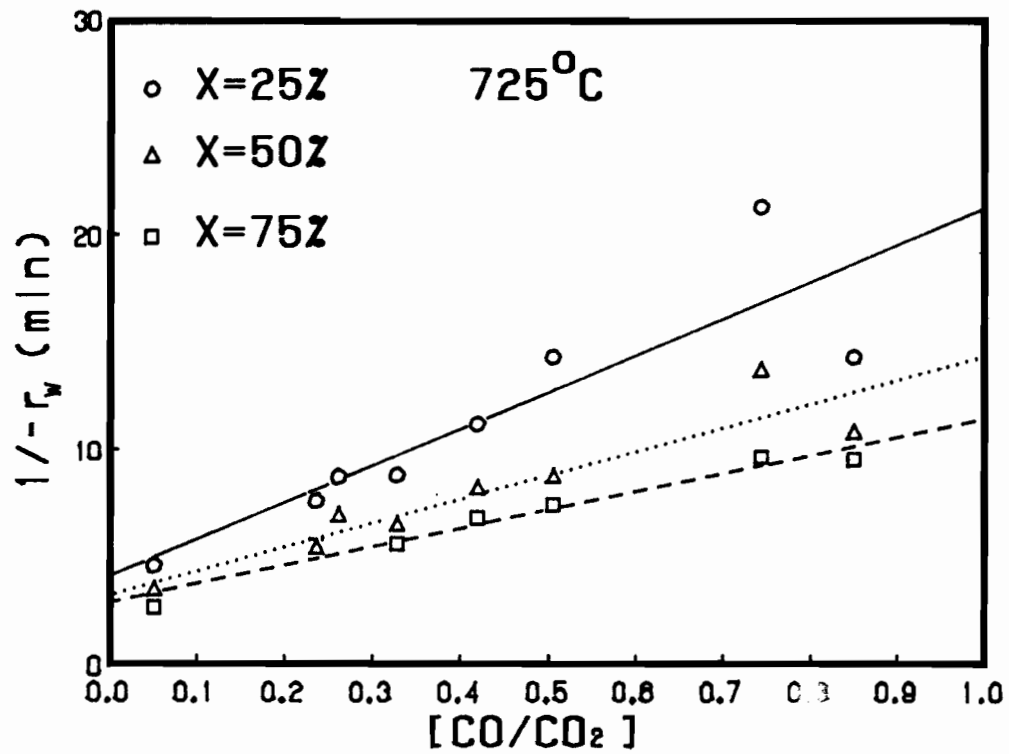


Figure 5. $1/-r_w$ as function of $[CO] / [CO_2]$.

impregnated with 5% K_2CO_3 and electrode carbon respectively. It also can be seen from Table II that the CO adsorption constant for BLC is much smaller than for any other material, indicating that the inhibition of gasification by CO is relatively unimportant for BLC.

The temperature dependence of black liquor gasification was studied at $[CO]=5\%$ and $[CO_2]=20\%$. Shown in Figure 6 is the Arrhenius plot for the gasification rate at different carbon conversions over the temperature range of 675 to 775°C. An activation energy of 60 kcal/mol or 250 kJ/mol is calculated for all three conversions, which is within the range of the activation energies reported for CO_2 gasification catalyzed by alkali metal carbonate [3, 9].

C. Comparison With Na_2CO_3 Impregnated Activated Carbon

The gasification rates of Na_2CO_3 impregnated activated carbon and BLC at 20% CO_2 and 5% CO are plotted versus carbon conversion in Figure 7. It clearly shows that the gasification rate of Na_2CO_3 impregnated activated carbon is one order of magnitude lower than black liquor char over almost the entire range of carbon conversion. It also can be seen that the gasification rate of the impregnated activated carbon reduces dramatically at about 85% conversion while this occurred only at $\geq 95\%$ for BLC. When examining the gasification residue, there were still some black particles in the activated carbon sample, while the BLC residue was a white or grey powder. This suggests that the contact between sodium catalyst and carbon is better in BLC than in the activated carbon sample.

D. Effect of Sample Preparation

A BLC char sample was also prepared by drying black liquor in a dish. The gasification rate at 725°C, 20% CO_2 and 5% CO as function of carbon conversion is given in Figure 8 and compared with the rate of the char obtained by the film drying method. It shows that the reactivity of the char prepared by the dish drying method is about 20 to 30% lower than the film dried sample over almost the entire range of conversion.

During the dish drying method a crust is formed on top of the liquor. It is likely that the crust contains more organics and less inorganic salts than the underlying mother liquor. This was verified by analysis of sulfate and sodium ion content of solids taken from top and bottom of the drying

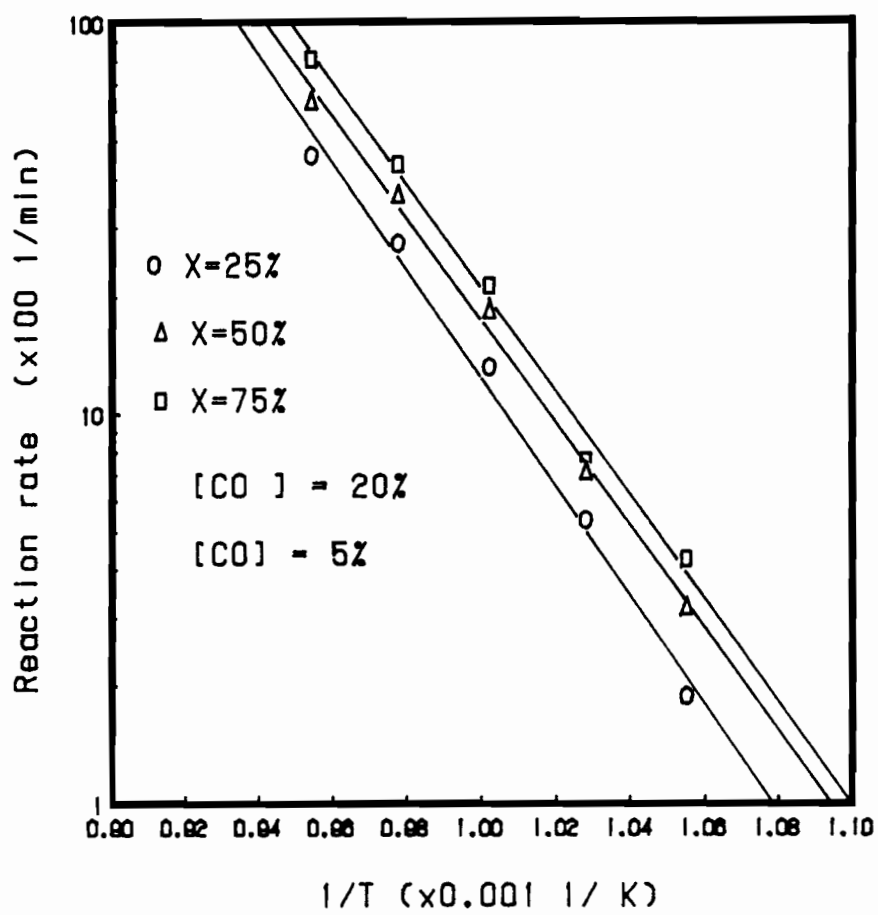


Figure 6. Arrhenius plot of BLC gasification rate.

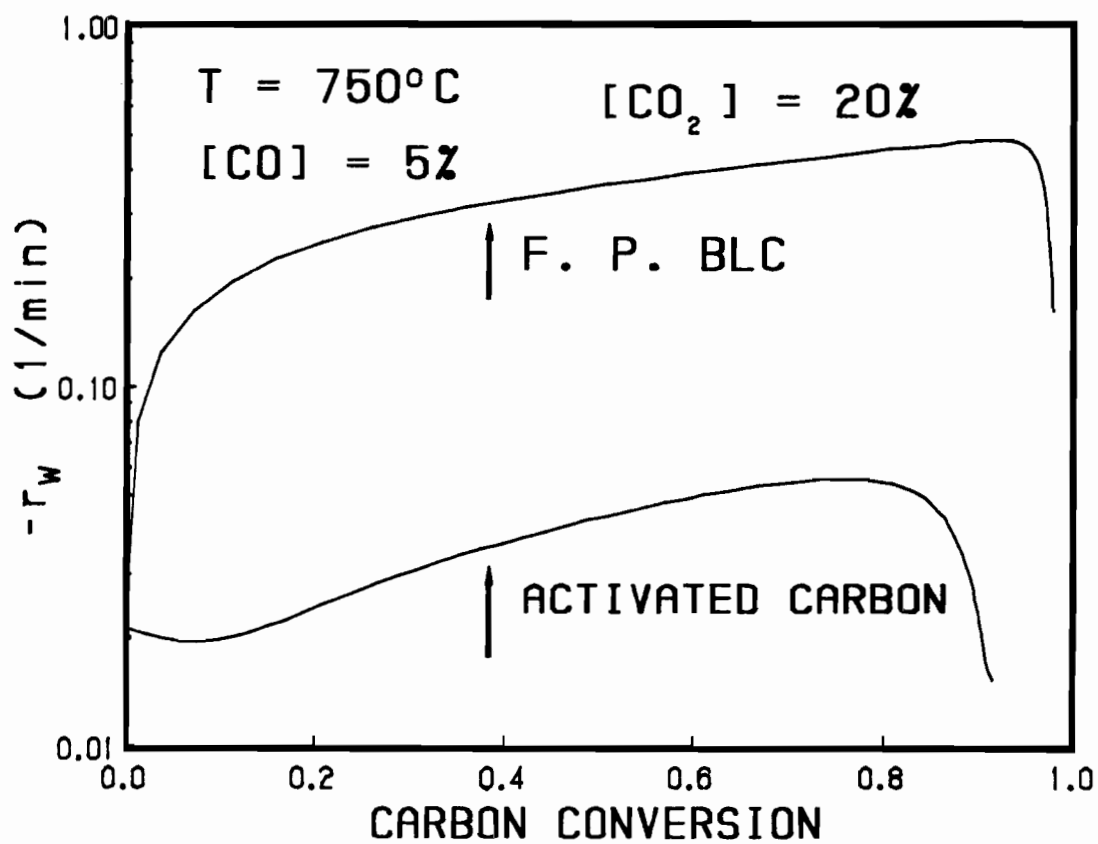


Figure 7. Gasification rate for black liquor char and alkali metal impregnated activated carbon.

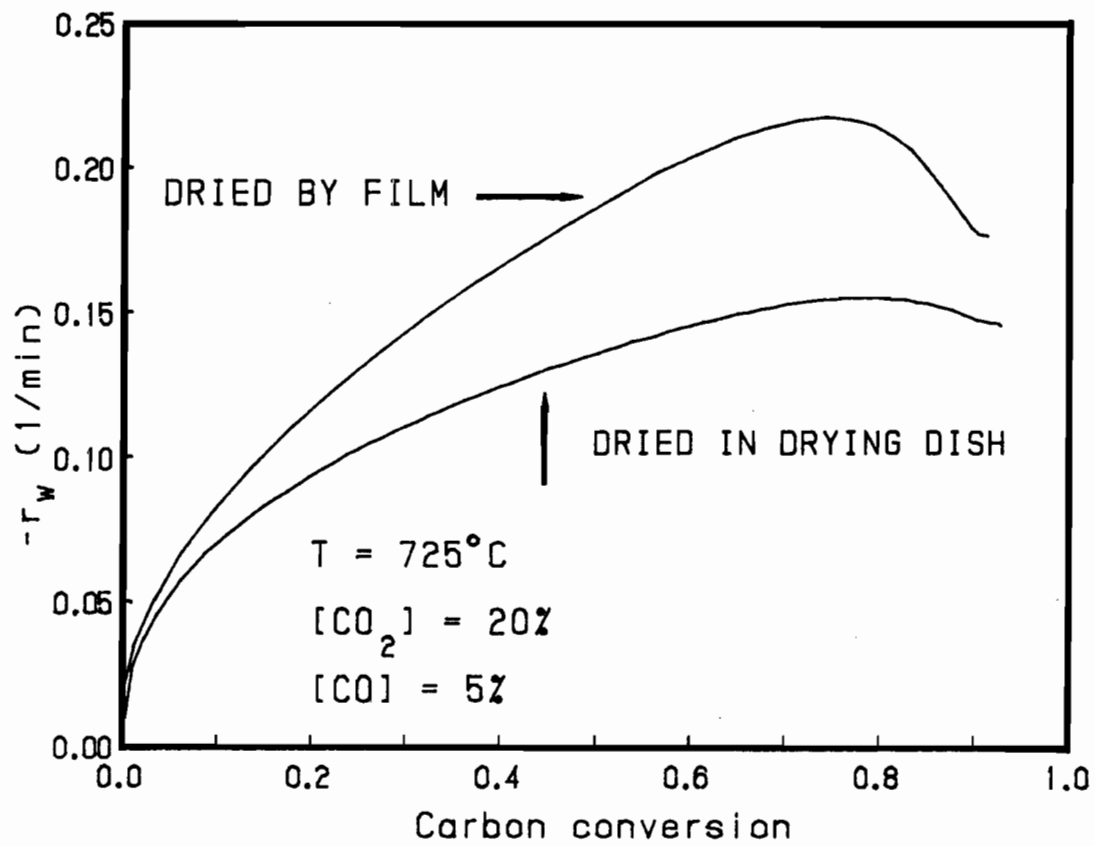


Figure 8. Effect of sample preparation on gasification rate.

dish. The results in Table III show a large difference in sulfate content between the top and bottom sample. The difference in sodium content is smaller, because about half of the sodium is bound to organic compounds, (see previous section on Sample Preparation). Included for comparison in Table 3 is the analysis for the film dried black liquor solids. The intermediate concentrations for the film dried solids proves that enrichment of inorganics in the mother liquor occurs during dish drying. It seems likely that the non-uniform distribution of sodium is responsible for the lower gasification rate of the dish dried black liquor.

TABLE III. CHEMICAL COMPOSITION OF BLACK LIQUOR SOLIDS
OBTAINED BY DIFFERENT DRYING METHODS

SAMPLE	[SO ₄ ⁼] (%)	[Na ⁺] (%)
FILM DRIED	8.13	18.6
DISH { TOP	7.76	18.17
DRIED { BOTTOM	22.9	22.04

E. Effect of rate of pyrolysis

The effect of pyrolysis rate on gasification characteristics was studied by comparing the reactivity of the present "fast pyrolysis" char with that of a "slow pyrolysis" char in Figure 9. Generally the rate of "fast pyrolysis" char is 2 to 5 times larger than that of "slow pyrolysis" char.

DISCUSSION

Catalytic carbon gasification by CO₂ is a heterogeneous gas-solid reaction determined by the degree of catalyst dispersion on the carbon surface [6]. The dispersion of a catalyst, introduced by impregnation to a fixed weight percentage in a char, is expected to improve with increasing internal surface area of the char. Therefore a larger surface area of a

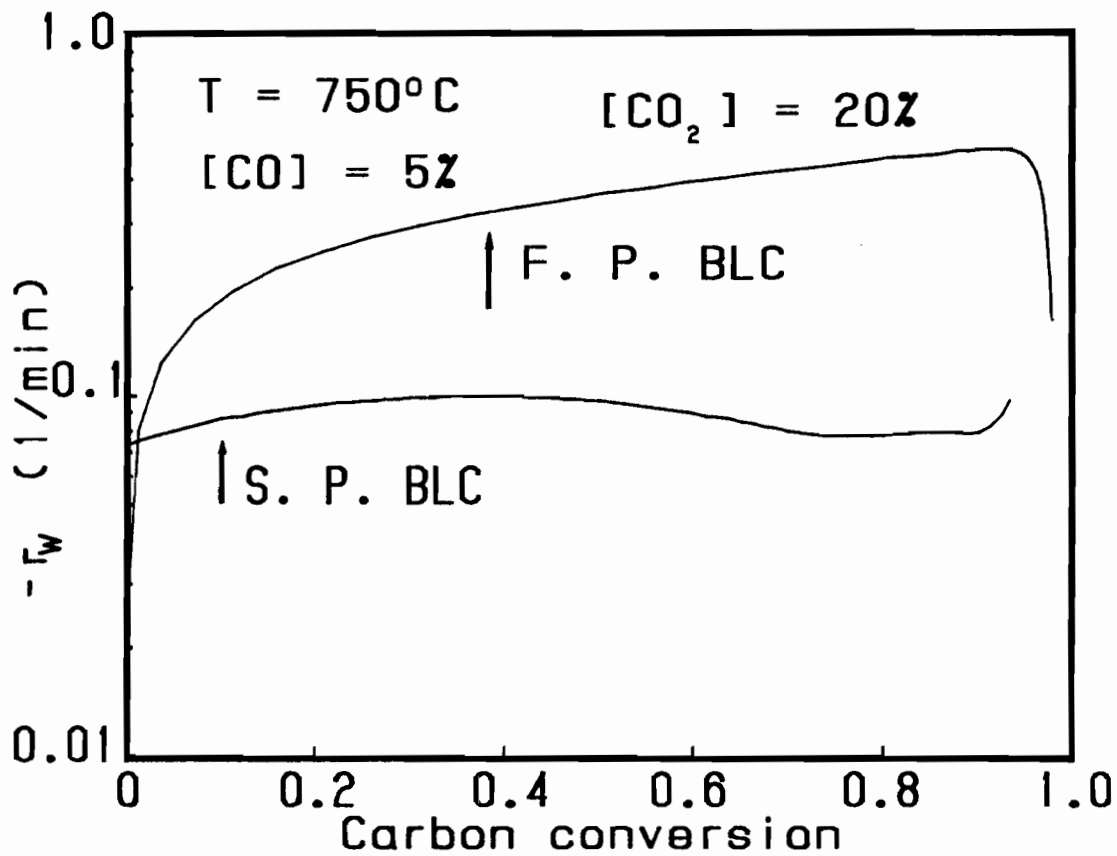


Figure 9. Effect of pyrolysis rate on gasification.

char normally leads to a higher carbon gasification rate. For the same char, the reactivity increases with increasing alkali metal (M) catalyst loading or M/C atomic ratio up to a certain maximum M/C. At higher initial M/C ratios and high carbon conversion, the reactivity decreases again because of pore plugging and surface saturation by alkali metal catalyst [6]. The maximum M/C ratio was reported to be at about 0.04 for a coal char, which is equivalent to about 16% by weight of Na₂CO₃ or 20% K₂CO₃ loading. It is noteworthy that the K₂CO₃ loading in the EXXON coal gasification process [19] is also 20%.

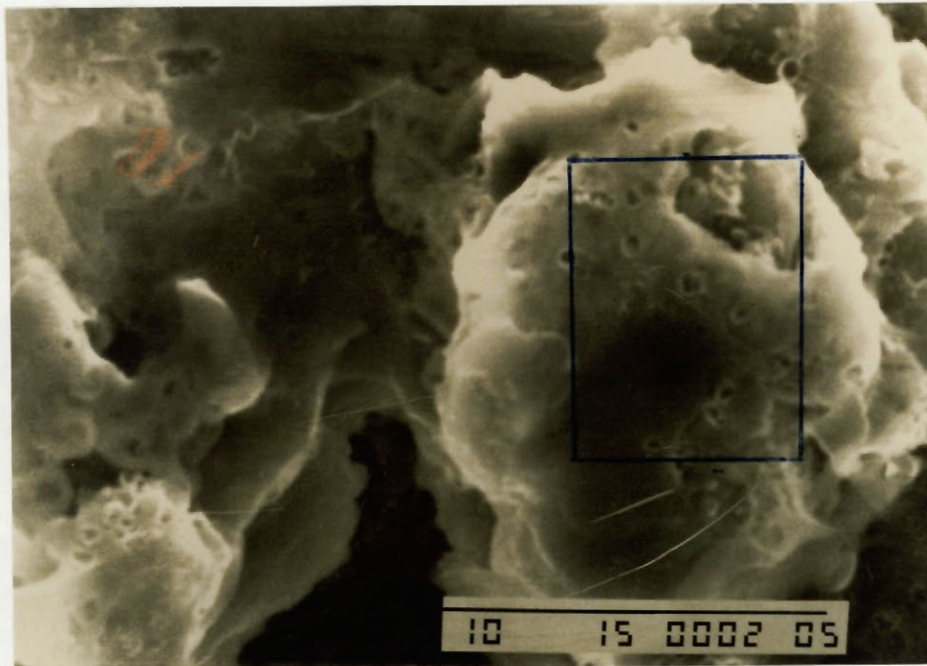
BLC gasification differs from the above described gasification behavior in a number of aspects. First, the Na/C ratio of BLC is 0.48, which is 12 times higher than the optimum ratio for coal char, and 14 times that of the present impregnated activated carbon (IAC). At such a high Na/C ratio the reactivity of any impregnated char would be strongly reduced. However the gasification rate of BLC is one to two order of magnitude larger than that of coal char with optimum Na₂CO₃ impregnation (see Table II). Also the BLC gasification rate remains high up to 95% carbon conversion while coal char gasification decreases above 70% conversion [11]. Secondly, comparison of the gasification rates of "fast pyrolysis" BLC and IAC in Figure 7 shows that the latter is about one order of magnitude lower. However, the BET surface areas of the chars just before gasification are respectively 160 m²/g and 1000 m²/g, i.e. one order of magnitude smaller for BLC. This indicates that the catalyst dispersion in BLC is extremely fine despite its relatively low internal surface area and high Na loading. On the other hand, the type of kinetics and activation energy of gasification are the same for BLC and alkali metal impregnated chars, suggesting a similar reaction mechanism. The extraordinary gasification properties of BLC can be explained by the unique character of the precursor of BLC. BLC is produced from a solution in which sodium is mixed and chemically bound with degraded lignin and carbohydrates on a molecular scale. Therefore the distribution of the catalyst in the solids and subsequently in the carbon matrix of the char is expected to be extremely fine throughout the bulk of the char. It is also interesting to note that a significant amount of sodium already exists as sodium phenolate in black liquor, while sodium phenolate complexes are thought to be the active sites for carbon gasification. In alkali metal impregnated chars, however, the active material is only present on the internal carbon surface, and its distribution is dependent on the volume and size of the different pores.

To prove that the catalyst dispersion is responsible for the difference in reactivity between BLC and IAC, both samples were examined by SEM-EDS. Shown in Figure 10 a) and Figure 11 a) are SEM pictures of particles of respectively film dried, "fast pyrolysis" BLC and IAC. It should be pointed out that the morphological character of this BLC is very similar to that of the activated carbon. The sodium distribution was determined by EDS within the frame shown in the upper figure and displayed in Figure 10 b) and Figure 11 b) for respectively BLC and IAC. The presence of sodium is indicated by the bright spots. When comparing Figure 10 b) with Figure 11 b), one can see that the spot density and intensity is higher for respectively BLC than IAC. This indicates that BLC has a much finer sodium distribution in the carbon matrix than IAC.

In order to quantify the degree of sodium distribution, line scans of sodium content were made on the carbon surface. A line of constant height on the carbon surface was identified with the SEM video picture. This eliminates the influence of surface irregularities on the X-ray intensity. Two elements, sodium and sulfur were scanned along a line for black liquor char while only sodium was scanned for IAC. The results are shown in Figures 12 and 13 for respectively BLC and IAC. The top line scan in Figure 12 is for sodium while the lower scan is for sulfur. The scan length for BLC and IAC are respectively 68 and 53 nm. A comparison of the line scans shows that the sodium distribution in BLC is much more uniform, and that contrary to IAC, there are no regions where sodium is absent.

From these results it can be concluded that the high gasification rates obtained for BLC are caused by fine dispersion of sodium in the carbon matrix. When gasification proceeds, small new catalytic sites will be exposed because of the three dimensional nature of the catalyst dispersion in BLC. This could also explain the sustained high rates at almost complete carbon conversion when catalytic gasification of coal chars is substantially reduced due to pore plugging and catalyst sintering [7].

The importance of the uniformity of dispersion of sodium is also confirmed by the effect of drying method on char reactivity. Further evidence of separation of inorganics and organics during dish drying was obtained by analyzing the "fast pyrolysis" char prepared from a well mixed sample of the dish dried solids. Shown in Figure 14 is a SEM picture of dish dried char particles. The sodium content of the dendritic structures in Figure 14 measured by EDS was much higher than that of surrounding particles, indicating that these are sodium salt crystals. These dendritic

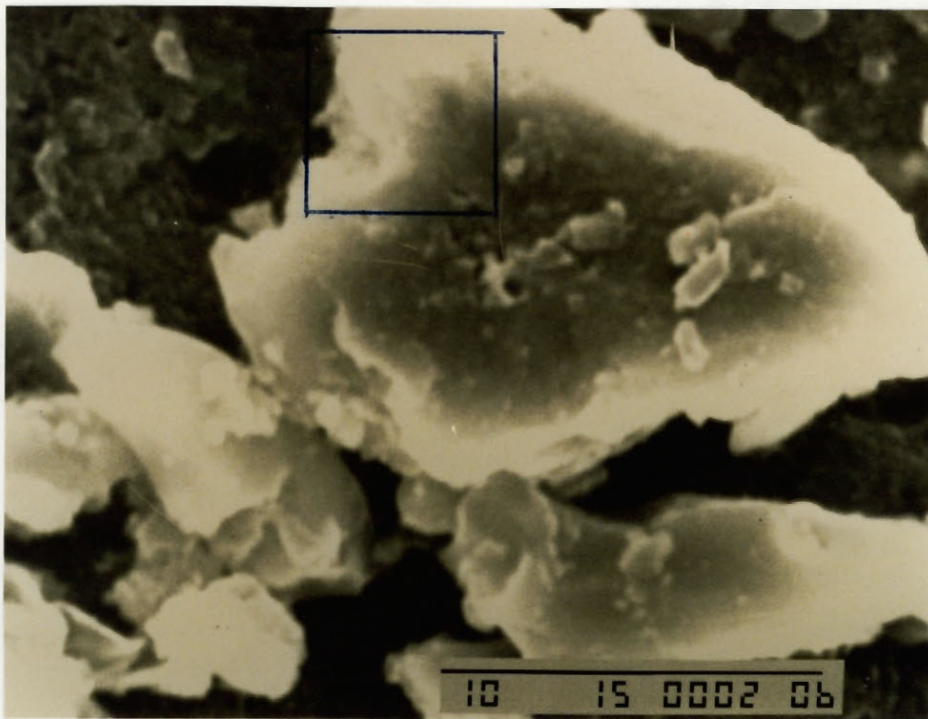


a)

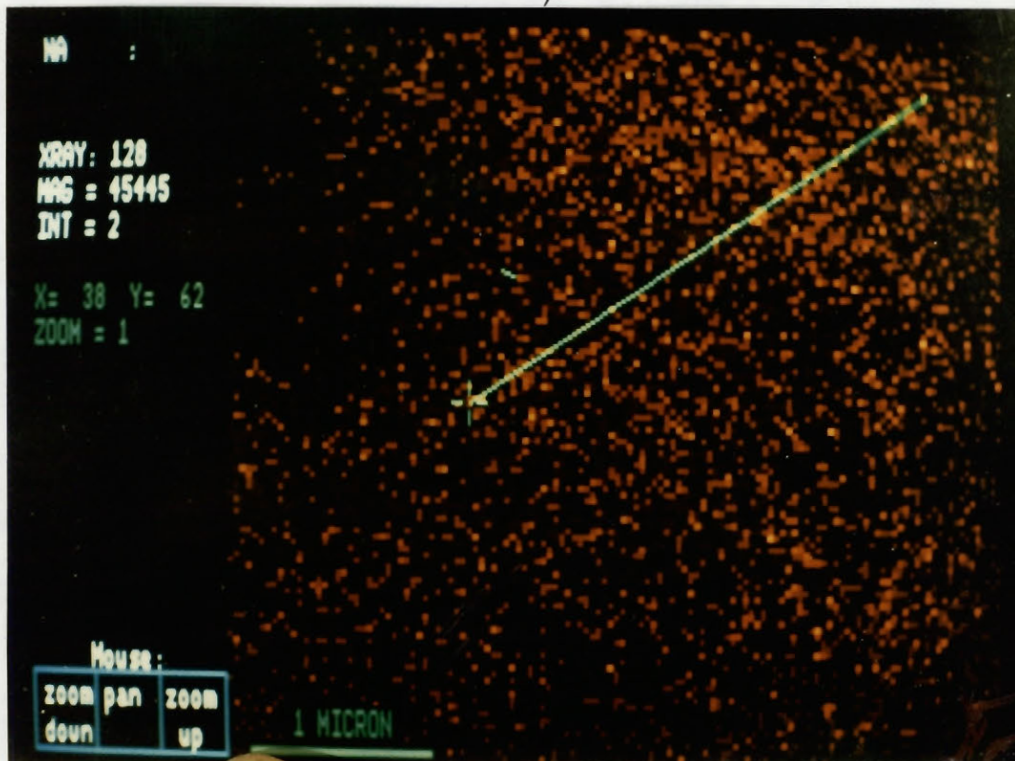


b)

Figure 10, a) SEM picture of a BLC particle. b) EDS sodium mapping of BLC surface.



a)



b)

Figure 11. a) SEM picture of a IAC particle. b) EDS sodium mapping of IAC surface.

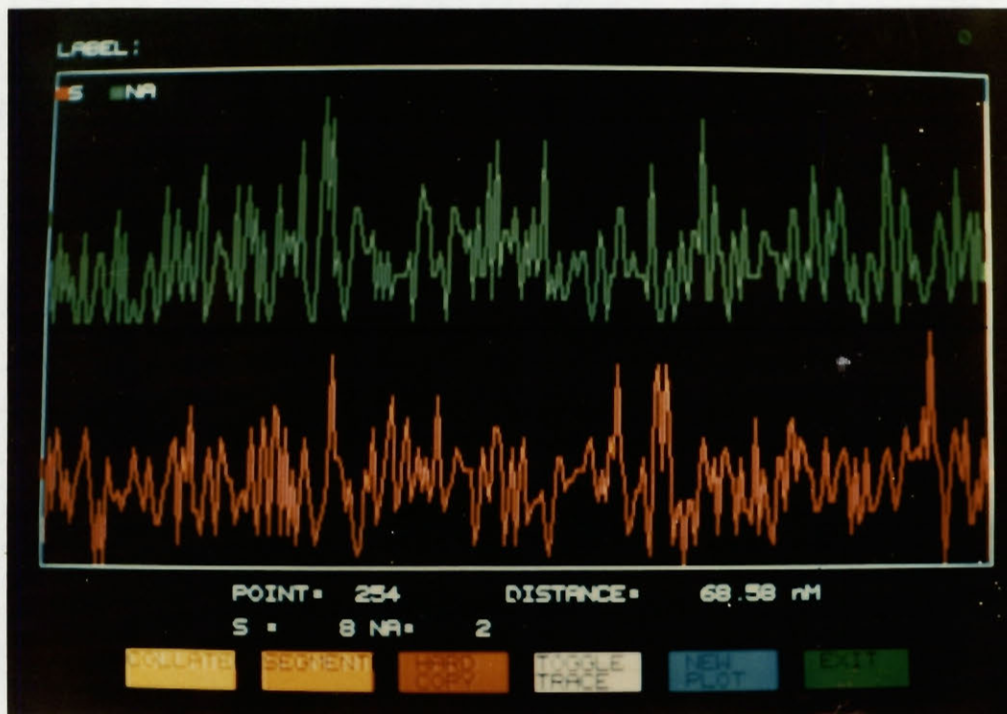


Figure 12. SEM-EDS line scan for sodium and sulfur of BLC.

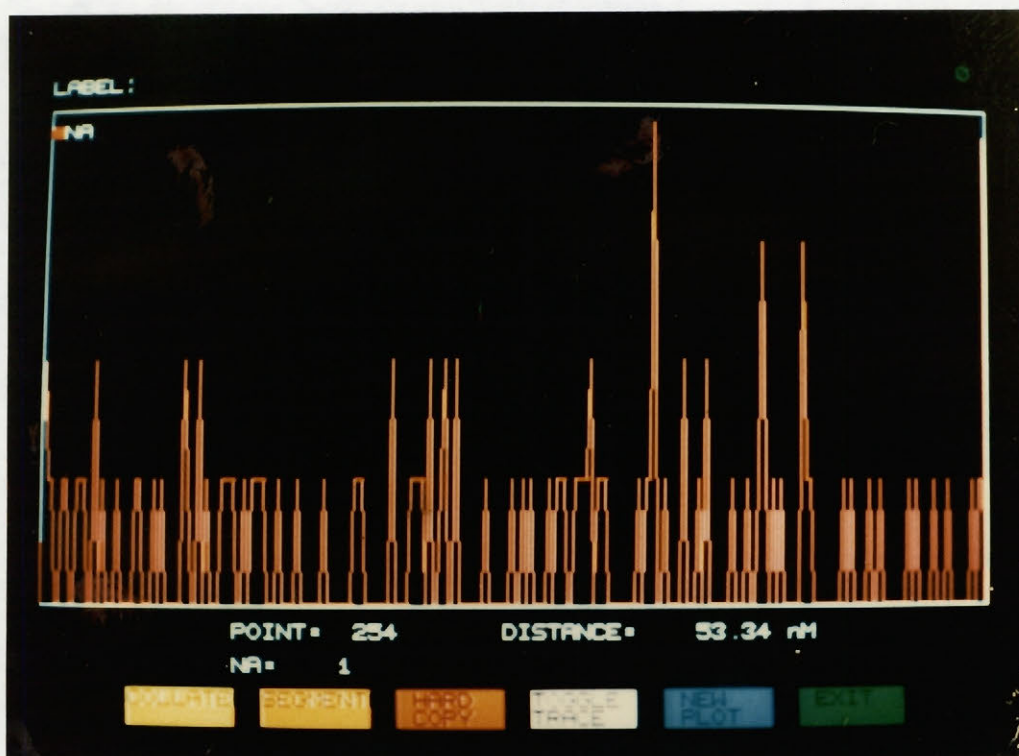


Figure 13. SEM-EDS line scan for sodium of IAC after pyrolysis in He+CO and 775°C.

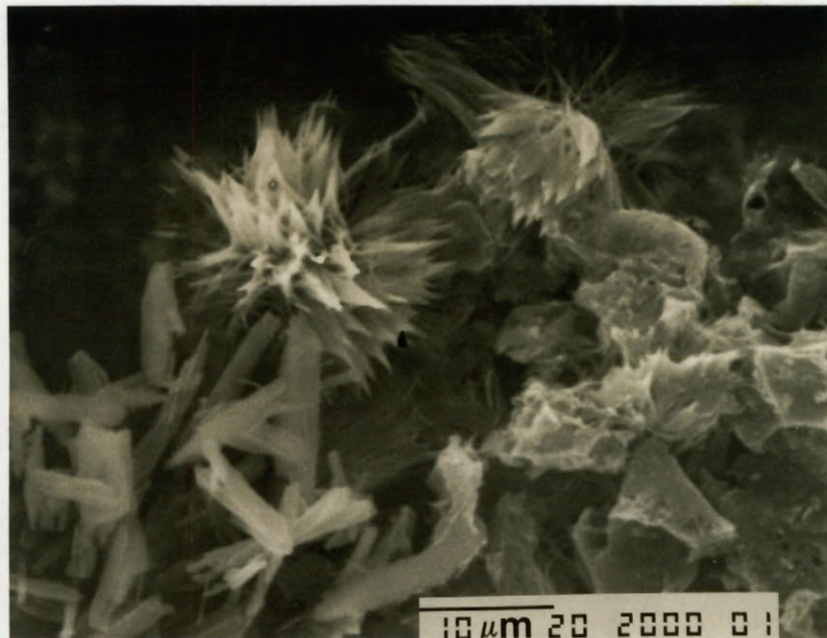


Figure 14. SEM picture of black liquor char obtained by drying in a dish.

crystals were never seen in film dried chars. When comparing Figure 10 a) and Figure 14 one can see that the morphological character of the two types of BLC chars are quite different. Based on the above results and discussion it can be concluded that loss of uniformity of sodium dispersion during dish drying is responsible for the lower gasification rate.

Although the fine dispersion of sodium in BLC is mostly responsible for the extremely high reactivity, other factors still might have an influence on the gasification rate. For example, the results shown in Figure 9 cannot only be explained by degree of catalyst dispersion, because the "slow pyrolysis" char was produced from the same film dried black liquor solids as the "fast pyrolysis" char. Since the sodium dispersion is established during the drying process, it is unlikely that the dispersion will be strongly influenced by the pyrolysis technique. However, it is known that pyrolysis time at the highest temperature is an important parameter influencing dispersion of sodium catalyst in coal char gasification [11]. In order to eliminate this effect, the pyrolysis time at the highest temperature, 780°C, was kept the same for both "slow" and "fast" pyrolysis char. Therefore the only obvious differences between the "fast pyrolysis" and "slow pyrolysis" chars are that the former has a significantly larger porosity (degree of swelling) and internal surface area. Specifically, the surface areas of the "fast" and "slow" pyrolysis chars are respectively 160 m²/g and 30 m²/g for respectively .

It has been shown that the carbon combustion rate of black liquor is related to degree of swelling during pyrolysis [31]. Since the present set-up is free of significant heat and mass transfer resistances [25], only the larger internal surface area of the "fast pyrolysis" char might explain its higher reactivity. Implicit is the assumption that the concentration of active sites of alkali metal surface oxides is the same for both chars. When comparing the two chars in Figure 9, it can be seen that the ratio of the gasification rates at 50% conversion is about the same as the ratio of their internal surface area.

A recent study [32] has shown that swelling of black liquor in air with or without ignition (respectively 700°C and 420°C) does not always give a good indication of the combustion rate for laboratory liquors. Unreported work by Hupa and co-workers [33] even showed that there was no correlation between swelling and combustion properties when industrial liquors were analyzed. The present data suggests that it might be more relevant to correlate the combustion properties of black liquors with internal surface

of their respective chars obtained by pyrolysis under inert conditions at 700 - 800°C.

CONCLUSIONS

Black liquor char is a unique carbonaceous material because of its fine dispersion of sodium throughout the bulk of the carbon matrix. The fine dispersion of sodium in the carbon structure, is confirmed by SEM-EDS techniques. The high loading and fine distribution of sodium is responsible for a gasification rate, at least one order of magnitude higher than that obtained for activated carbon or coal chars impregnated with an optimal loading of Na₂CO₃. The fine dispersion of sodium in the bulk of the carbon structure of BLC rather than just on the internal surface is probably responsible for the sustained high gasification rates at Na/C ratios where the rate for Na₂CO₃ impregnated chars is normally strongly reduced due to pore plugging and sintering of the catalyst. The method of drying of BLC has an influence on the gasification rate because it influences the sodium dispersion. The influence of gas composition on BLC gasification rate can be described by Langmuir-Hinshelwood type kinetics. This behavior as well as the activation energy are the same as for alkali metal catalyzed carbon gasification. This indicates that despite the much higher reactivity, the mechanism of carbon gasification by CO₂ for BLC is the same as for other alkali metal impregnated chars. The internal surface area rather than porosity of BLC also appears to have an influence on the gasification rate. This suggests that internal surface area measurements rather than swelling tests might be more appropriate to characterize combustion properties of black liquors.

NOMENCLATURE

- k_x = elementary reaction constant.
K = reaction constant, m³·mol⁻¹·min⁻¹.
K' = reaction constant, min⁻¹.

K_{CO}	= equilibrium adsorption constant of CO, $m^3 \cdot mol^{-1}$.
K'_{CO}	= equilibrium adsorption constant of CO.
K_{CO_2}	= equilibrium adsorption constant of CO ₂ , $m^3 \cdot mol^{-1}$.
-rw	= reaction rate based on carbon weight W, min^{-1} .
t	= reaction time, min.
W	= carbon weight at time t, mg.

REFERENCES

1. Grace, T.M., and et al, 1989 Intern. Chem. Recov. Conf., Ottawa, April, p.1(1989).
2. van Heiningen, A.R.P., J. Li, and J. Fallafollita, Canadian Patent Application, #583,409, Nov.17, (1988).
3. McKee, D.W., Chemistry and Physics of Carbon, 16, pp.1-118(1981).
4. Wen, W.-Y., Catal. Rev.-Sci. Eng., 22(1), 1(1980).
5. Wood, B.J., and K.M. Sancier, Final Report for DOE, SRI International, DOE Contract No. DE-AC21-80MC1 4953(1984).
6. Kapteijn, F., et al, Fuel, 63(8), 1056(1984).
7. Hamilton, R.T., et al, Fuel, 63(7), 1008(1984).
8. McKee, D.W. and D. Chatterji, Carbon, 12, p.453(1975).
9. Wigmans, T., Ph.D. Thesis, University of Amsterdam (1982).
10. Mims, C.A., and J.K. Pabst, Fuel, 62(2), 176(1983).
11. Sams, D.A., Ph.D. thesis, University of Arizona, 1985.
12. Sams, D.A., and F. Shadman, AIChE J., 32(7), 1132(1986).
13. Cerfontain, M.B., et al, J. of Catalysis, 107, 173(1987).
14. Cerfontain, M.B. Ph.D. thesis, University of Amsterdam, (1987).
15. Freriks, I.L.C., and et al, Fuel, 60, 463(1981).
16. Yuh, S.L., and E.E. Wolf, Fuel, 63, 1604(1984).
17. Moulijn, J.A. and F. Kapteijn, Sci. & Tech., Jan., p.15(1987).
18. Li, J., and A.R.P. van Heiningen, Can. J. Chem. Eng., 67,p.693(1989).
19. Nahas, N.C., Int. Symp. on Fund. of Cat. Coal of Carbon Gasification, Amsterdam, Sept. (1982).
20. Oren, M.J., et al, Can. J. Spectrosc., 29(1), p.10(1984).
21. Li, J., and A.R.P. van Heiningen, J. of Pulp and Paper Sci., 12(5), J146(1986).
22. Li, J., Ph.D Thesis (this thesis), Chapter 5.

23. Li J., **Ph.D Thesis** (this thesis), Chapter 6.
24. Cerfontain, M.B., et al, **Carbon**, 25 (3), 351(1987).
25. Li J., **Ph.D Thesis** (this thesis), Chapter 2.
26. Walker, P.L. Jr. and et al, **Advan. Catal.**, 11, 133(1959).
27. Kapteijn, F., and J.A. Moulijn, **Fuel**, 62(2), 221(1983).
28. Austin, L.G., and P.L. Walker, Jr., **AIChE J.**, 9(3), 303(1963).
29. McKee, D.W., **Carbon**, 20(1), 59(1982).
30. Spiro, C.L., et al, **Fuel**, 62(3), 323(1983).
31. Milanova, E, and G.L. Kubes, **71st Ann. Conf. of CPPA**, Montreal, Jan., B67(1985).
32. Noopila, T., and et al, **1989 Intern. Chem. Recov. Conf.**, Ottawa, April, 75(1989).
33. Hupa, M., **Private Communication**.

CHAPTER 4

KINETICS OF GASIFICATION OF BLACK LIQUOR CHAR BY STEAM

ABSTRACT

The steam gasification kinetics of kraft black liquor char were studied in a thermogravimetric analysis reactor. Gas products, CO, CO₂, H₂, CH₄, H₂S and COS were analyzed by infrared gas analyzers and gas chromatographic techniques. The effect of steam and hydrogen concentration on gasification rate can be described by Langmuir-Hinshelwood type kinetics. An activation energy of 210 kJ/mol was obtained. The methane formation was negligible over the temperature range studied, 873 to 973 K. The CO₂ concentration was higher than calculated for the water-shift reaction at equilibrium. A gasification mechanism is proposed whereby CO₂ is one of the primary gasification products.

INTRODUCTION

Black liquor is the spent liquor resulting from digestion of wood in a solution of NaOH and Na₂S. The dried product, black liquor solids (BLS), consist of 50% dissolved wood and 50% inorganics. Black liquor char (BLC), the pyrolysis product, consists mainly of a mixture of carbon, Na₂CO₃, Na₂S and Na₂SO₄. In a conventional chemical recovery furnace, concentrated black liquor is introduced as a spray. After drying, pyrolysis and partial combustion, the droplets fall onto a char bed at the bottom of the furnace where the remaining carbon is gasified and inorganic oxy-sulfur compounds are reduced to sodium sulfide. Because of the complexity, corrosive nature and heterogeneous character of the reactor system, present knowledge of all these reactions is far from complete. Steam gasification of black liquor char, for example, has never been studied. Information about steam gasification kinetics will not only lead to better understanding of the conventional furnace, it is also needed for several proposed alternative kraft recovery processes [1-3] which incorporate gasification as one of the key steps.

Because the chemical composition of BLC and alkali carbonate impregnated chars are similar, extensive studies on catalytic gasification of the latter chars serve as a useful reference. Alkali-metal salts are among the oldest known additives which markedly increase the rate of steam gasification of carbonaceous materials [4]. Since then numerous studies have been performed, and the general effectiveness of alkali metals as catalysts for gasification is well established. Steam and CO₂ gasification catalyzed by alkali metal salts are similar in a number of aspects, such as increased reactivity with better catalyst dispersion [5], higher alkali metal/carbon ratio [6] and order of catalytic activity of alkali metals (Cs>Rb>K>Na>Li) [7]. The present state of knowledge of alkali-metal catalyzed carbon gasification by CO₂ has been summarized recently by Moulijn [7]. Detailed reaction mechanisms are given in [8-10].

A mechanism of alkali-metal catalyzed carbon gasification by steam was proposed a decade ago by McKee and Chatterji [11]. It has been postulated [6, 12-13] and recently shown [5, 14-15] that alkali metal oxide complexes on the carbon surface are the active sites which correlate quantitatively with steam gasification rate [15]. In the reaction scheme of potassium

catalyzed steam gasification proposed by Huttinger [16] every potassium salt has to be activated to form an oxygen surface group, $K(O)$, before it becomes reactive. However, the complete reaction mechanism is still not firmly established. The major uncertainties are related to which products are formed on the surface, how the products dissociate from the surface and what the product distribution such as the CO_2/CO ratio is. These questions are difficult to answer because the water shift reaction takes place simultaneously with gasification. Therefore, research of the water shift reaction has been the objective of several gasification studies [17-18]. It was found that the water shift reaction rate is a function of CO and H_2O concentration [17], retarded by CO_2 and not affected by H_2 [18]. A complicating factor to formulate a reaction mechanism is that for alkali metal carbonate catalyzed gasification it has been found [6, 19-20] that more CO_2 is formed than thermodynamically possible based on simple overall reaction steps. Except for alkali metal carbonate catalyzed steam gasification, no other steam gasification studies have reported such a behavior.

Like alkali-metal catalyzed gasification, it is expected that steam gasification of BLC would have many similarities with CO_2 gasification of BLC. The CO_2 gasification study of BLC performed by the present author has shown that the rate is one or three orders of magnitude higher than that of coal char respectively with or without impregnation of alkali metal carbonate [21-23, chapter 3]. The extremely high reactivity of BLC is explained by very fine dispersion of Na_2CO_3 in the carbon matrix as a result of formation of the char from a liquid precursor. This is confirmed by a comparative SEM-EDS study of the sodium distribution on the surface of BLC and activated carbon impregnated with Na_2CO_3 .

In the present investigation, the reaction system is first analyzed thermodynamically. Then the gasification rate of BLC is studied experimentally as function of H_2O and H_2 concentration, temperature and carbon conversion. The equilibrium constant of the water-shift reaction is determined experimentally and compared to that at thermodynamic equilibrium. Factors influencing the product distribution are discussed.

EXPERIMENTAL

Experimental System

A schematic picture of the experimental system, a standard TGA from Cahn with auxiliaries, is shown in Figure 1. The differences with the CO₂ gasification set-up are: a) addition of a steam generation system and heating tape to lines containing water vapor; b) on-line computerized data acquisition of temperature, sample weight and CO and CO₂ concentration. Steam was generated by injecting deionized water with a calibrated syringe pump in a heated tube. The exhaust gas was dried by bubbling through 96% H₂SO₄ and then fed to IR analyzers for CO and CO₂ content. The dry gas was also analyzed for other fixed gases and sulfurous gases by two GC's with TCD and FPD respectively. The solid gasification residues were analyzed by an IC with CD and ECD for respectively sulfate, sulfite, thiosulfate, carbonate, sodium, and sulfide content.

Material

The same BLC sample is used as in the CO₂ gasification study (Chapter 3). The composition of BLC at the start of gasification is 60% Na₂CO₃, 13.9% Na₂S and 25% fixed carbon. Detailed information concerning the BLC sample can be found in chapter 3 of this thesis.

Experimental Procedure

After about 5 mg BLC was added to the sample pan, the whole system was purged with N₂ at 600 scc/min for 40 minutes. The furnace temperature was then raised from 20 to 775°C at a rate of 25°C/min under 400 scc/min N₂. At 500°C, CO was added at 25 scc/min to prevent Na₂CO₃ decomposition [23]. After 2 minutes at 775°C, reduction of Na₂SO₄ to Na₂S was complete, and the temperature was reduced to the required gasification temperature. When the temperature was stabilized at gasification temperature, the addition of CO was stopped. After 10 to 15 minutes to allow complete removal of CO from the system, gasification was started by injecting water into an inert carrier gas mixed with various levels of H₂ concentrations.

RESULTS AND DISCUSSION

Thermodynamic Prediction of the Reaction System

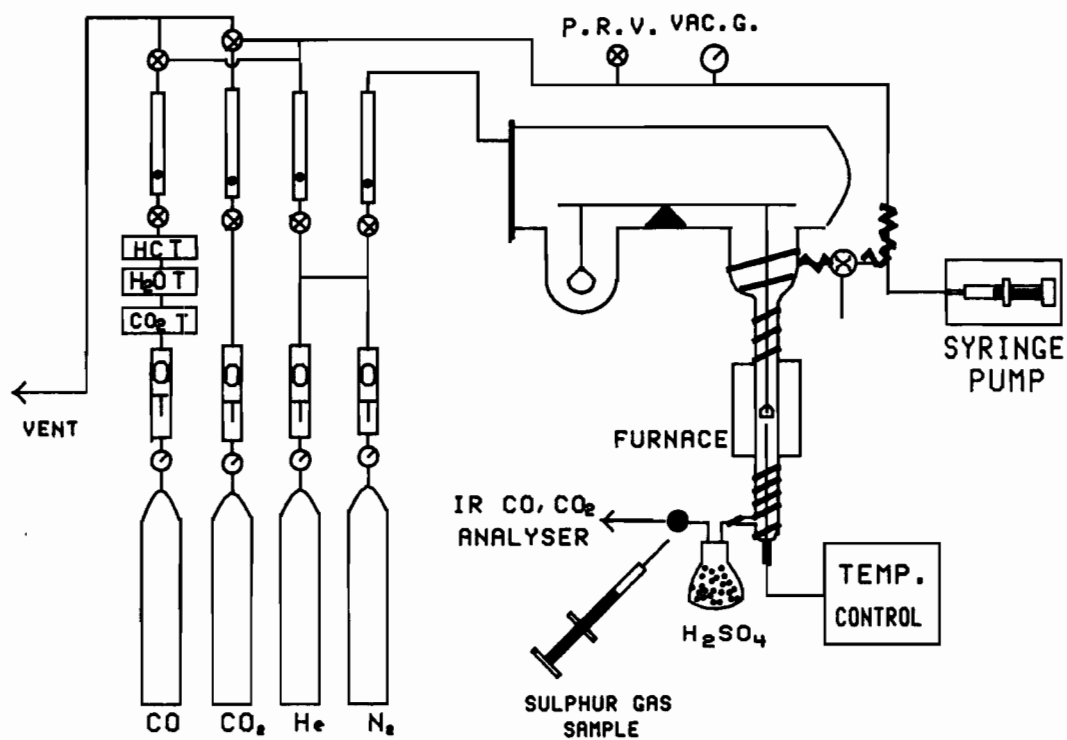
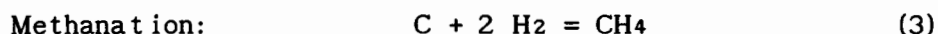
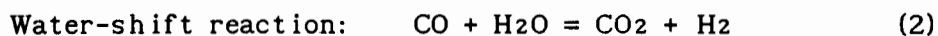


Figure 1. Schematic picture of the TGA system.

Thermodynamic calculations were performed with the EQUILIBRIUM program of the FACT system of the McGill University Computer Center. The EQUILIBRIUM program is the latest version of SOLGASMIX [24]. A detailed description of the calculation procedure and strategy of the program has been given by Pejryd and Huppa [25].

Under steam gasification conditions, the following reactions occur:



The equilibrium gas composition of a mixture of steam and excess carbon as function of temperature is shown in Figure 2. The total pressure is 1 atm. It can be seen that at low temperatures, CH₄ and CO₂ are the main products besides unconverted steam, while CO and H₂ are the only products at high temperature.

The equilibrium compositions for the present reaction system of 1 mole Na₂S, 3.1 moles of Na₂CO₃ and 10.76 moles of carbon as function of steam to carbon ratio, hydrogen addition and temperature are shown respectively in Figures 3, 4 and 5. The gas composition and total moles of gas are displayed in the top figures, while the liquid and solid phase composition is shown at the bottom. Again the system pressure was kept at one atmosphere.

The effect of steam to carbon ratio at 923 K in Figure 3 shows that at a ratio of about 1.7, all carbon is gasified. At higher steam to carbon ratios the CO and CH₄ concentration decrease rapidly, while the CO₂ concentration increases. At very high steam to carbon ratios, the CH₄ concentration is two to three orders of magnitude smaller than CO or CO₂. All sulfur is volatilized at a very low steam to carbon ratio of 2.8. The H₂S concentration is always about two orders of magnitude higher than the COS concentration.

Shown in Figure 4 is the effect of hydrogen addition at 923 K and steam to carbon ratio of 1.04. With increasing hydrogen addition, all product concentrations decrease except the methane concentration. More carbon is gasified at higher hydrogen addition because more methane is formed. Sulfur emission decreases slightly with increasing hydrogen addition.

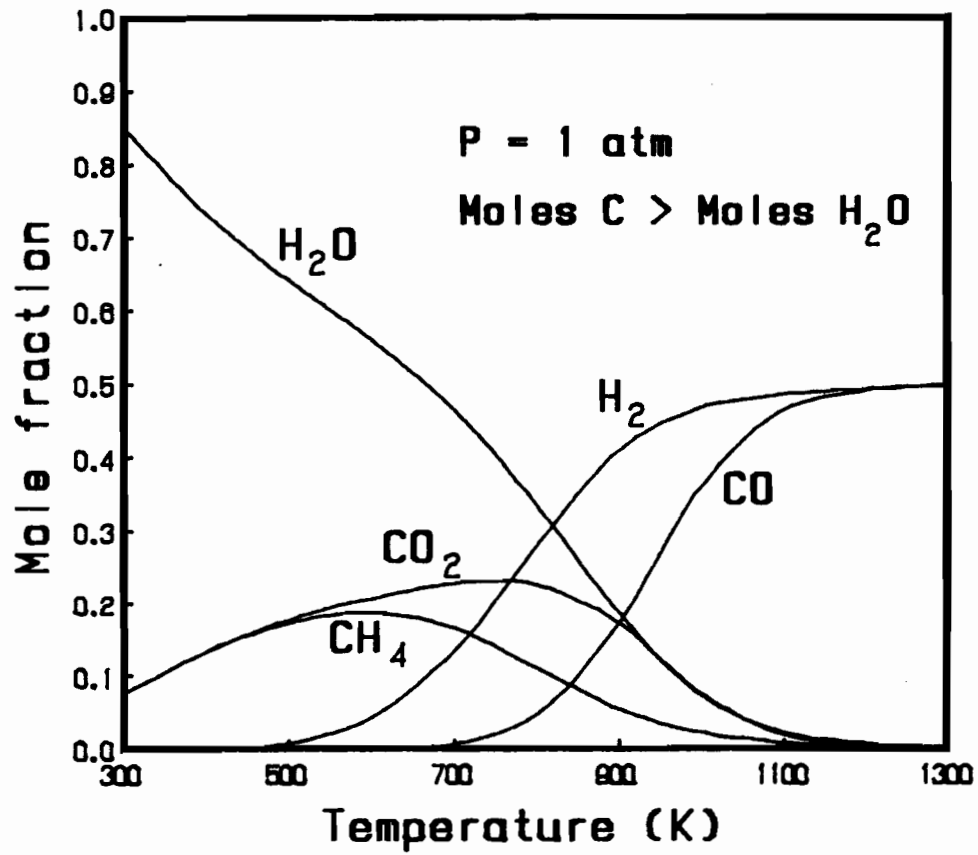


Figure 2. Thermodynamic equilibrium for steam gasification of carbon.

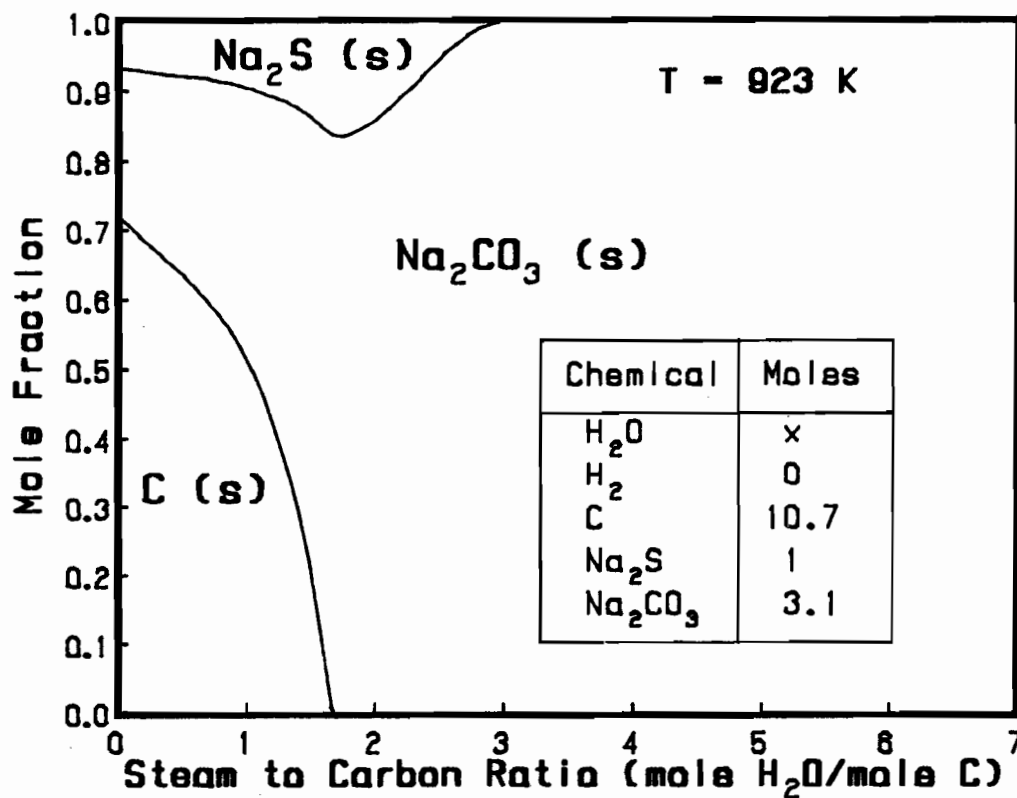
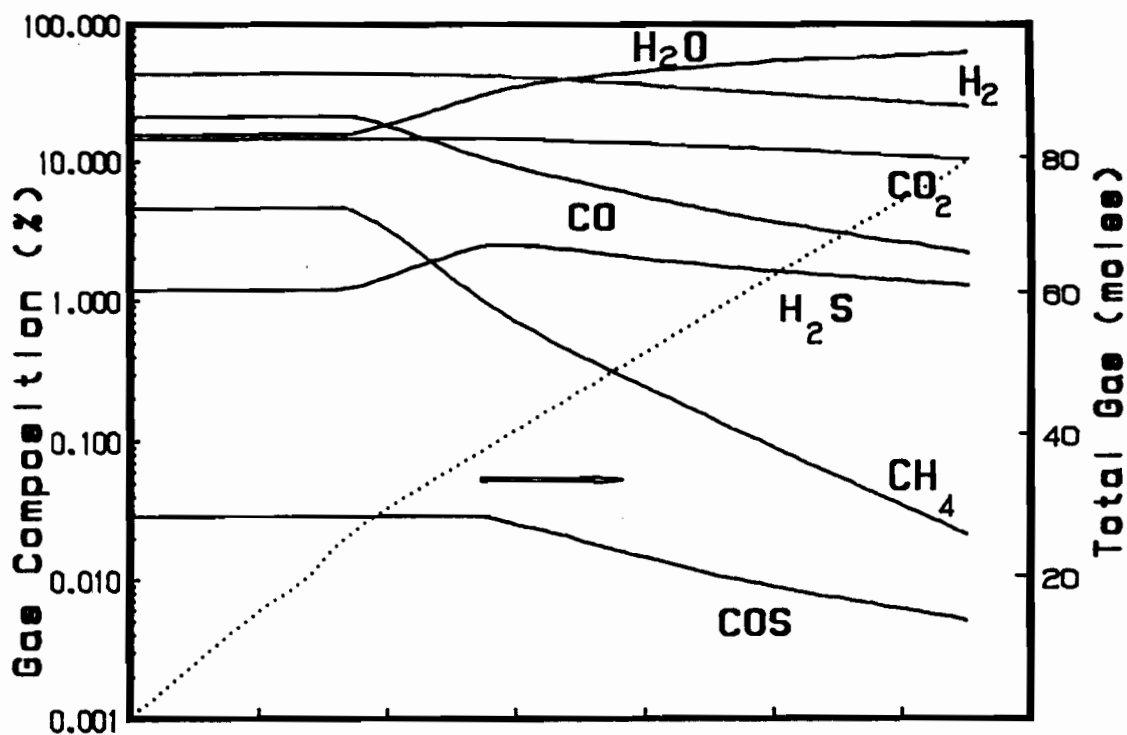


Figure 3. Thermodynamic equilibrium of H₂O-black liquor char as function of steam to carbon ratio.

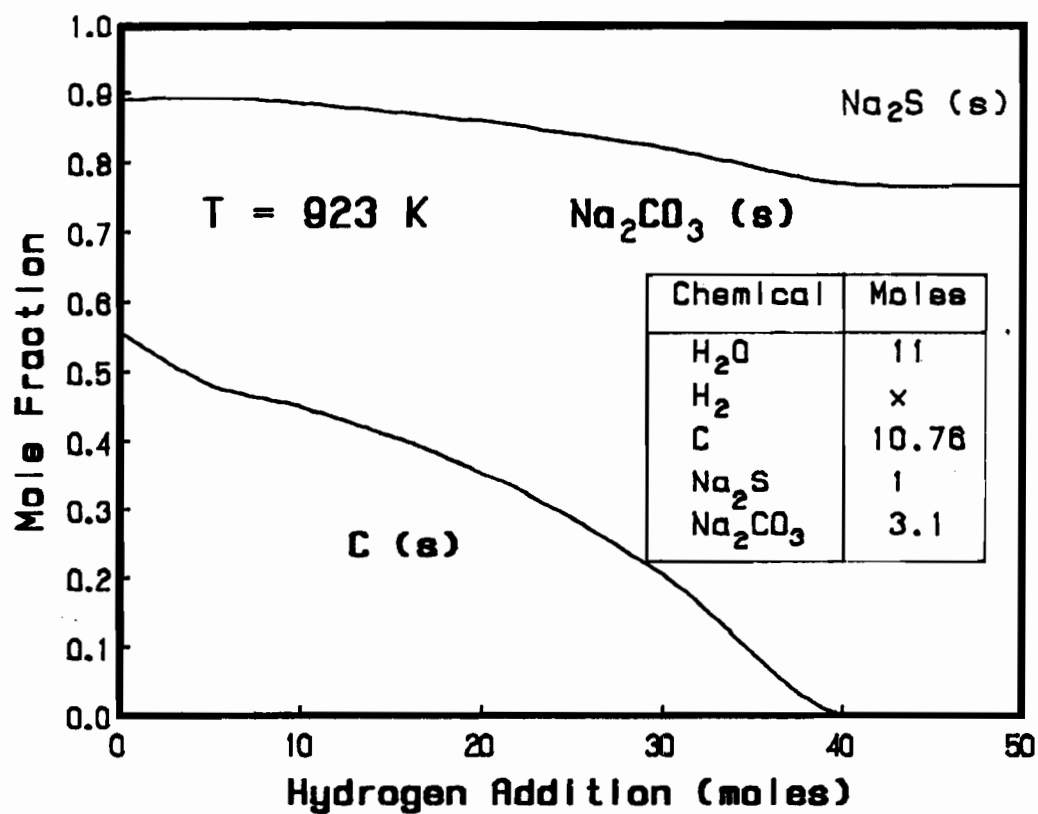
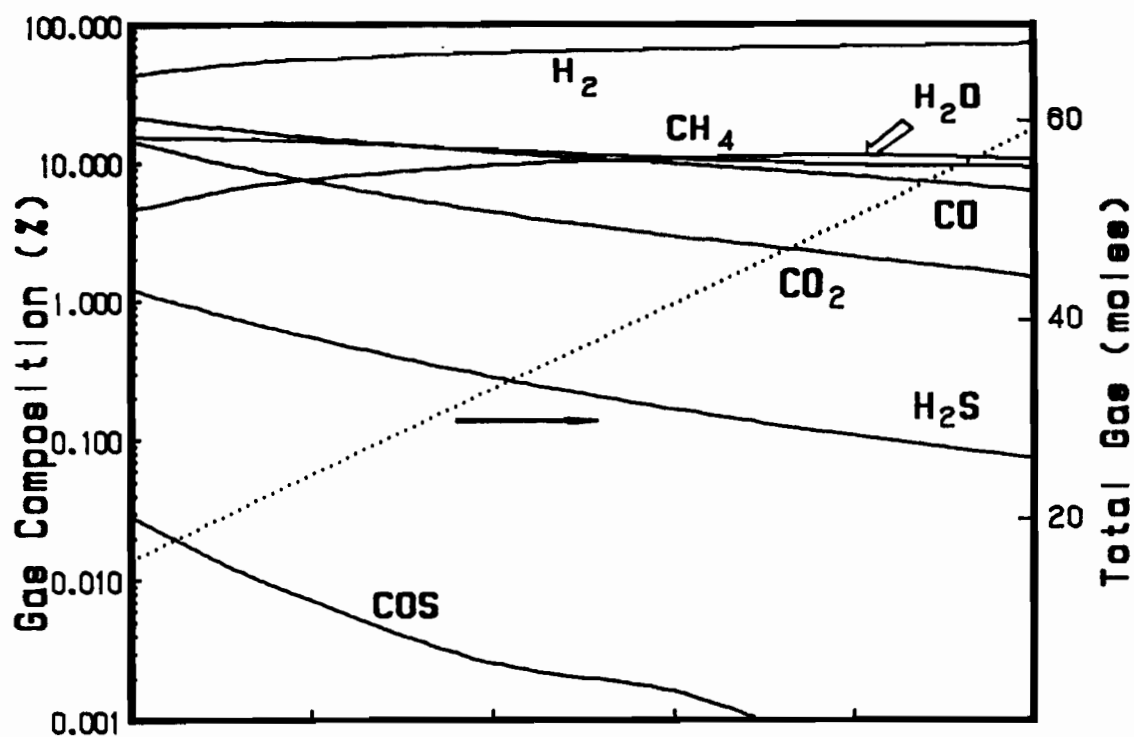


Figure 4. Thermodynamic equilibrium of H_2O -black liquor char as function of hydrogen addition.

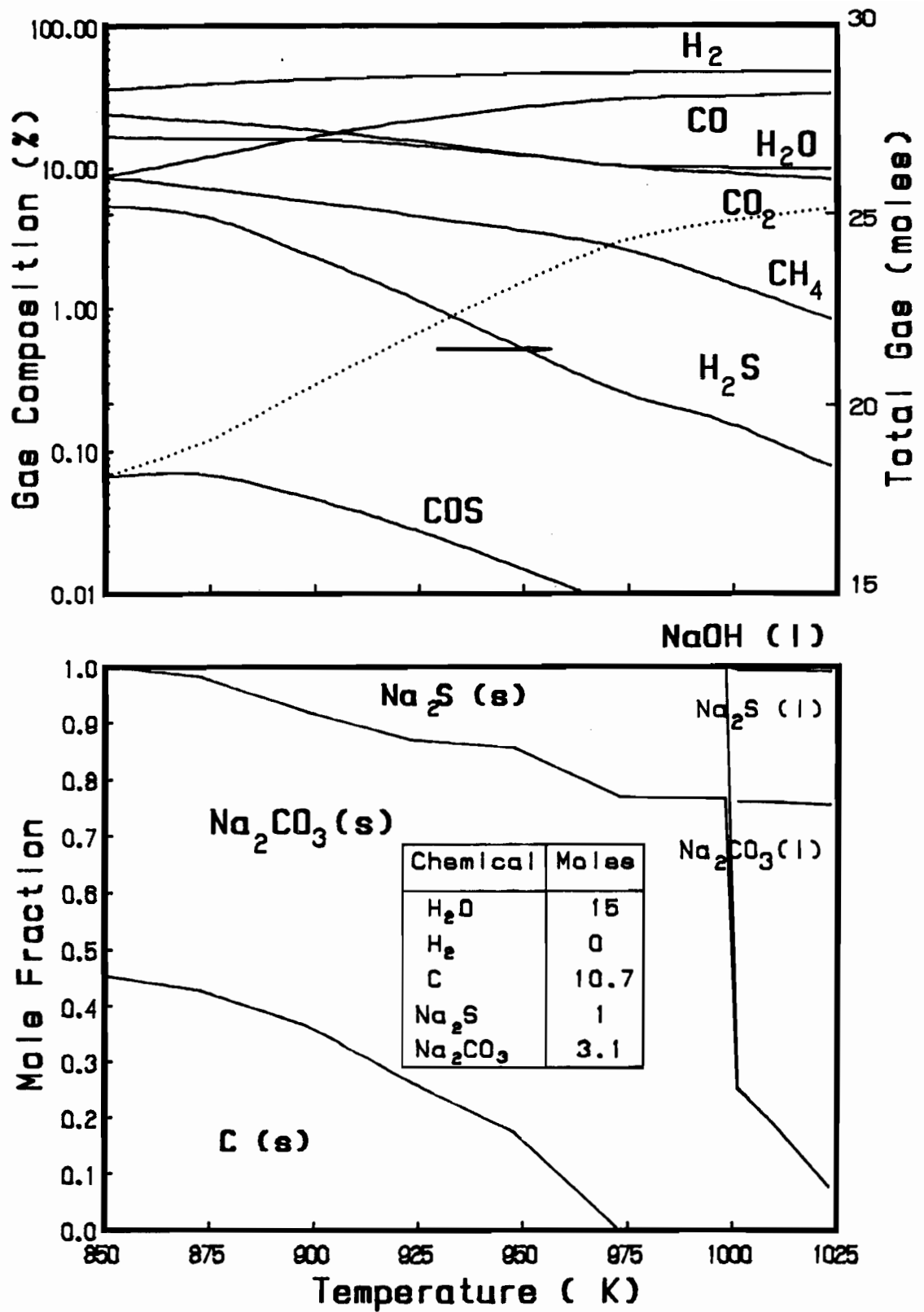


Figure 5. Thermodynamic equilibrium of H₂O-black liquor char as function of temperature.

Shown in Figure 5 is the equilibrium composition of the system at steam to carbon ratio of 1.415 over the temperature range of 850 to 1025°C. At high temperatures, CO becomes the other major gasification product besides H₂. The methane concentration is about one order of magnitude lower than the CO or CO₂ concentration. A liquid phase of Na₂S and Na₂CO₃ appears at about 1000 K. The H₂S and COS concentrations decrease with increasing temperature.

Since the present reactor was operated differentially, which is equivalent to a high steam to carbon ratio, it follows from Figure 3 that under equilibrium conditions the methane formation would not be important. Figure 3 also suggests that complete carbon gasification will be obtained in the TGA set-up with gasification reaction (1) controlled by reaction kinetics. Reaction (4) will also go to completion at high steam to carbon ratios (Figure 3). The extent of sulfur emission at complete carbon gasification under the present gasification condition will therefore depend on the relative rates of gasification and H₂S formation, respectively reactions (1) and (4). The sulfur emission results are presented in chapter 6. The water shift reaction (2) is expected to have a strong influence on the present off-gas composition. The chemical equilibrium constant, K_t , of reaction (2) defined as

$$K_t = \frac{[H_2] [CO_2]}{[H_2O] [CO]} \quad (5)$$

was correlated as function of temperature from the concentrations in Figure 5 as

$$\log K_t = -1.761 + \frac{1.886 \times 10^3}{T} \quad (6)$$

where T is in degrees Kelvin. This correlation agrees closely with literature [26].

Kinetics of Gasification

Data Reduction

Shown in Figure 6 is a schematic graph of the TGA output for a typical run with BLC. The weight loss below 500°C was due to generation of H₂O and

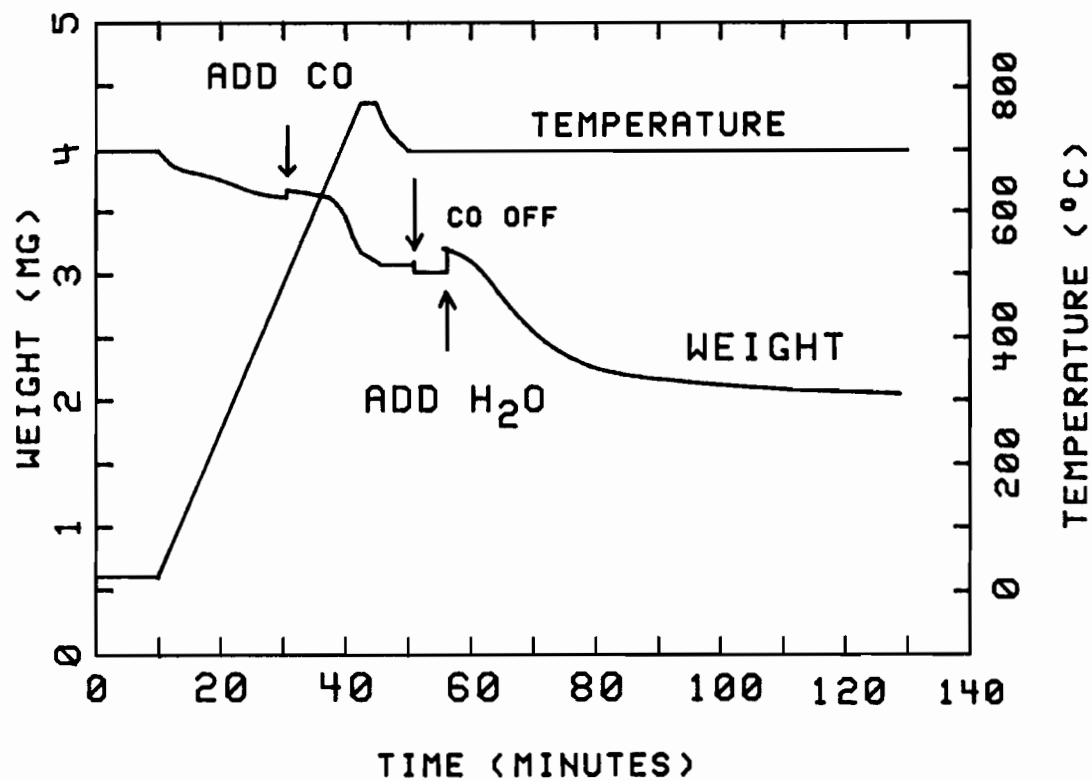


Figure 6. Schematic diagram of experimental procedure and results.

CO₂. A sudden weight gain at about 500°C occurs when CO was added to the carrier gas. Above 600°C, the reduction of Na₂SO₄ by CO and carbon started, resulting in a rapid weight loss as discussed in chapter 8. After two minutes at 780°C the reduction is complete as indicated by stabilization of the weight loss and confirmed by chemical analysis of the sample for sulfide and sulfate. Again a sudden weight increase was recorded at the start of gasification when steam was introduced because of increased drag on the sample pan resulting from the increased gas flow.

The gasification rate, $-r$, is defined as absolute rate, $dW_{c,t}/dt$, divided by the remaining carbon weight at the same time, $W_{c,t}$, i.e.

$$-r = - \frac{1}{W_{c,t}} \frac{dW_{c,t}}{dt} \quad (7)$$

The gasification rate is calculated from the measured CO and CO₂ concentrations as:

$$-r = \frac{[p_{CO}(t) + p_{CO_2}(t)] M_c Q / TR}{W_{c,o} - \frac{M_c Q}{TR} \int_0^t [p_{CO}(t) + p_{CO_2}(t)] dt} \quad (8)$$

where p_{CO} and p_{CO_2} are the partial pressures of CO and CO₂, M_c the molecular weight of carbon, Q the gas flow rate, T the temperature, R the gas constant, and $W_{c,o}$ the weight of carbon at time zero.

Under the present conditions the methane concentration was at least two orders of magnitude lower than the CO or CO₂ concentrations, in agreement with thermodynamic prediction. Therefore the rate of methane formation was not included in the calculation of overall gasification rate. Since CO₂ formed by gasification is consumed by the H₂S emission reaction (4), the total gasified carbon includes carbon in form of CO and CO₂, as well as an equimolar amount of H₂S as carbon. However, as the H₂S formation accounts for about 5 to 10% of the carbon loss, the total gasification rate was calculated based on the CO and CO₂ concentration only.

Shown in Table I is a mass balance which shows that the gas analysis data are internally consistent. From reactions (1) and (2) it follows that per mole of CO or CO₂ formed, respectively one or two moles of H₂ will be produced. Also for every mole of H₂S produced in reaction (4) one mole of CO₂ is consumed which previously was co-produced with two moles of H₂. So

the H₂ concentration can be calculated from the measured CO, CO₂ and H₂S concentrations, respectively [CO]_m, [CO₂]_m and [H₂S]_m, as

$$[\text{H}_2]_{\text{cal}} = [\text{CO}]_m + 2 [\text{CO}_2]_m + 2 [\text{H}_2\text{S}]_m \quad (9)$$

The difference between [H₂]_m and [H₂]_{cal} is shown in the last column of Table I. The difference of less than 8% shows that the gas analysis data are internally consistent.

TABLE I. MOLAR GAS BALANCE

[CO ₂] _m ppm	[CO] _m ppm	[H ₂ S] _m ppm	[H ₂] _m ppm	[H ₂] _{cal} ppm	Δ [H ₂] %
315	6	6	600	648	-7.4
250	5	2	510	509	+0.2
200	3	2	400	407	-1.7
780	35	60	1750	1695	+3.2

Some carbon mass balance results are summarized in Table II. W_{c,m} is the amount of total gasified carbon calculated from the measured CO and CO₂ concentrations during the duration of an experiment. W_{c,c} is the amount of initial carbon calculated from the initial sample weight and fixed carbon content and ΔW_c is the difference between W_{c,m} and W_{c,c}. As can be seen from the table, the difference between W_{c,m} and W_{c,c} is less than 5%. This confirms that the gasification rate can be accurately calculated from the CO and CO₂ production rates.

Table II CARBON MASS BALANCE

W _{c,m} (mg)	W _{c,c} (mg)	ΔW _c (%)
1.19	1.13	+ 4.8
0.95	0.948	+ 0.2
1.075	1.1	- 2.2
1.39	1.36	+ 2.4

Shown in Figure 7 are the sample weight and CO and CO₂ concentrations for a typical run at 700°C, 15% H₂ and 15% H₂O. The noise on the weight curve was due to flow disturbances generated by gas sampling with a syringe for H₂S analysis. These peaks were used as time markers for the gas samples. It can also be seen in Figure 7 that a certain amount of CO was already present in the inert off-gas before introduction of steam. The CO cannot be explained as a rest concentration of previously added CO (see experimental procedure) because about 20 reactor gas volumes were flushed out between turning off the CO flow and starting gasification. However the presence of CO can be explained by decomposition of the alkali oxygen surface complexes [7, 10]. When gasification starts, this decomposition is prevented as indicated by the same amount of sodium in the sample before and after gasification.

Effect of Conversion

Shown in Figure 8 is the gasification rate as function of carbon conversion obtained at 15% H₂, 15% H₂O and 650°C. The independence of -r on conversion X shows that the gasification rate is first order in carbon. The explanation for the noisy signal at high conversions is that the concentration of CO and CO₂ approaches the lower detection limit of the IR analyzers, and W_{c,t} is determined by subtraction of two almost equal quantities.

Effect of Gas Composition

The influence of gas composition on gasification rate was examined by two Langmuir-Hinshelwood type kinetic expressions:

$$-r = \frac{K [\text{H}_2\text{O}]}{1 + K_{\text{H}_2\text{O}} [\text{H}_2\text{O}] + K_{\text{H}_2} [\text{H}_2]} \quad (10)$$

and

$$-r = \frac{K' [\text{H}_2\text{O}]}{[\text{H}_2\text{O}] + K'_{\text{H}_2} [\text{H}_2]} \quad (11)$$

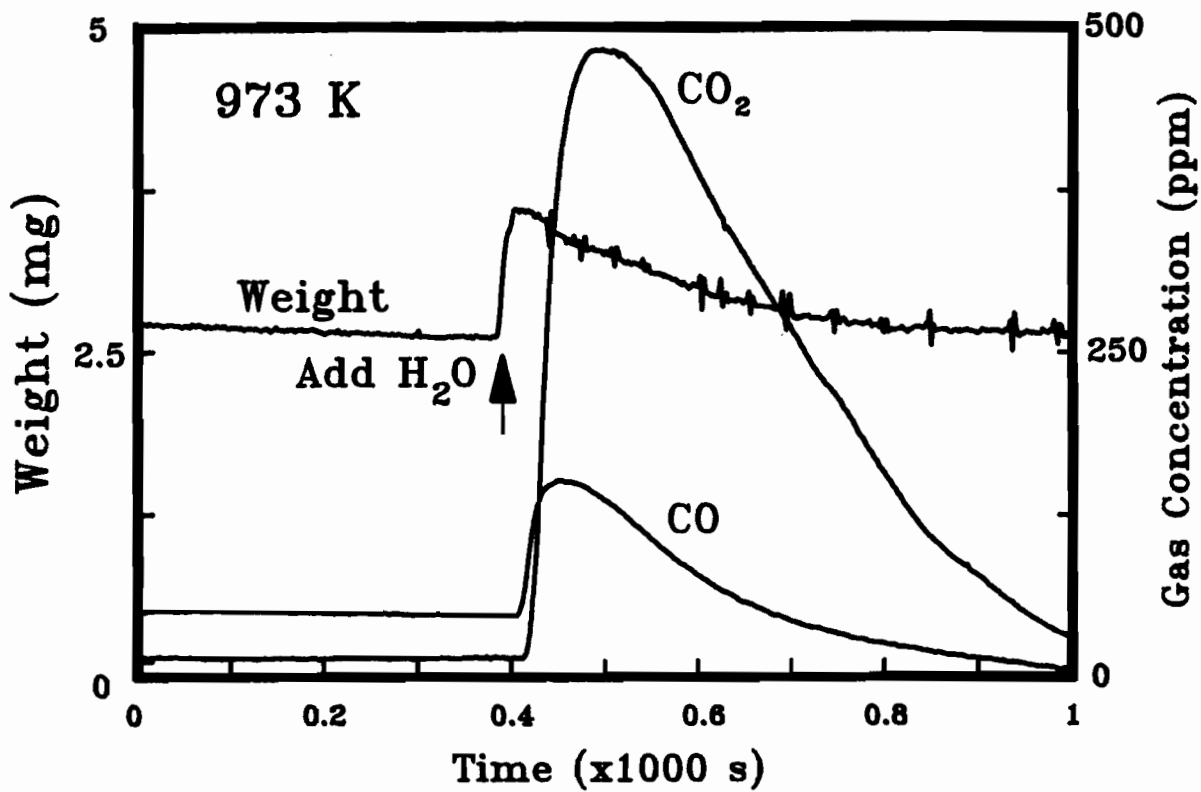


Figure 7. A typical output generated by computer.

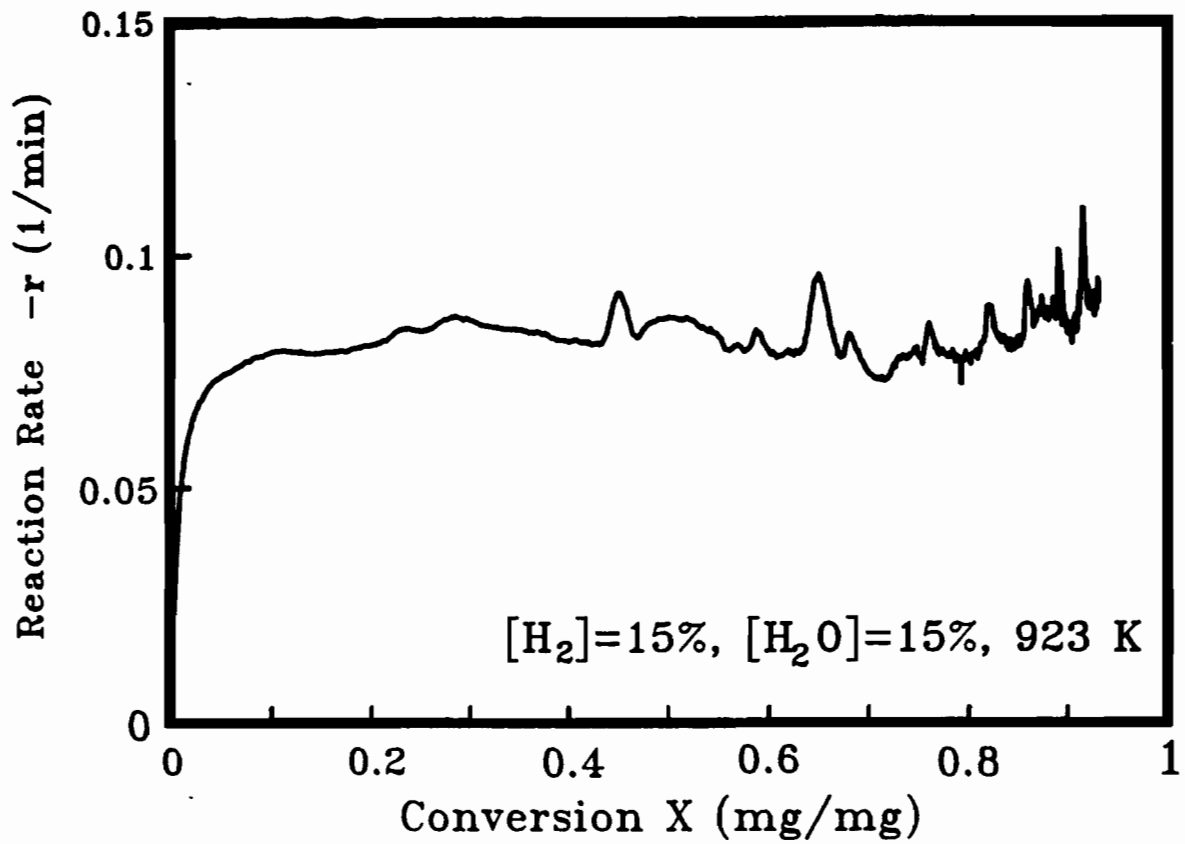


Figure 8. Gasification rate as function of carbon conversion.

where K ($\text{m}^3 \cdot \text{mol}^{-1} \cdot \text{min}^{-1}$) and K' (min^{-1}) are the reaction constants, and $K_{\text{H}_2\text{O}}$ ($\text{m}^3 \cdot \text{mol}^{-1}$), K_{H_2} ($\text{m}^3 \cdot \text{mol}^{-1}$) and K'_{H_2} can be considered as the adsorption constants of H_2O and H_2 , respectively. It is generally accepted that the effect of gas composition on the rate of uncatalysed steam gasification of carbon can be described by equation (10) [27]. However, more recent studies (7, 8, 9, 14, 15) suggest that the rate of alkali metal catalyzed gasification of carbon by steam is better described by equation (11).

In order to test the validity of equations (10) and (11) for steam gasification of BLC, two sets of experiments were performed whereby respectively the steam and hydrogen concentration were varied. In the former case the hydrogen concentration was fixed while in the latter the steam concentration was kept constant. The temperature was kept at 923 K. To test for equation (10) the inverse of the BLC gasification rates were plotted against $[\text{H}_2\text{O}]^{-1}$ and $[\text{H}_2]$, and linear relationships were obtained. However, the constants, K , $K_{\text{H}_2\text{O}}$ and K_{H_2} , calculated from the correlations of the straight lines were all negative, indicating that BLC gasification by steam cannot be described by equation (10). Similarly, to test for equation (11) the inverse of the BLC gasification rates are plotted as a function of $[\text{H}_2]/[\text{H}_2\text{O}]$ in Figure 9. The good linear relationship and positive values of K' and K'_{H_2} obtained, confirm that BLC gasification by steam can be described by equation (11). The constants of K' and K'_{H_2} in equation (11) obtained from the linear relationship are respectively 0.20 min^{-1} and 1.42.

Effect of temperature

The effect of temperature on gasification rate was studied at temperatures of 873 to 973 K, 15% of hydrogen and 15% of steam. From the Arrhenius plot of the gasification rates in Figure 10, an apparent activation energy of $210 \pm 10 \text{ kJ/mol}$ is obtained.

Discussion

In Table III, the reactivity of BLC is listed together with those of some other carbonaceous materials. In the last column the reactivities are compared at conditions of $[\text{H}_2\text{O}]=2.67\%$ and 1000 K. It can be seen that the rate of BLC gasification is 1 or 3 orders of magnitude higher than the rate for activated carbon respectively with or without alkali metal carbonate

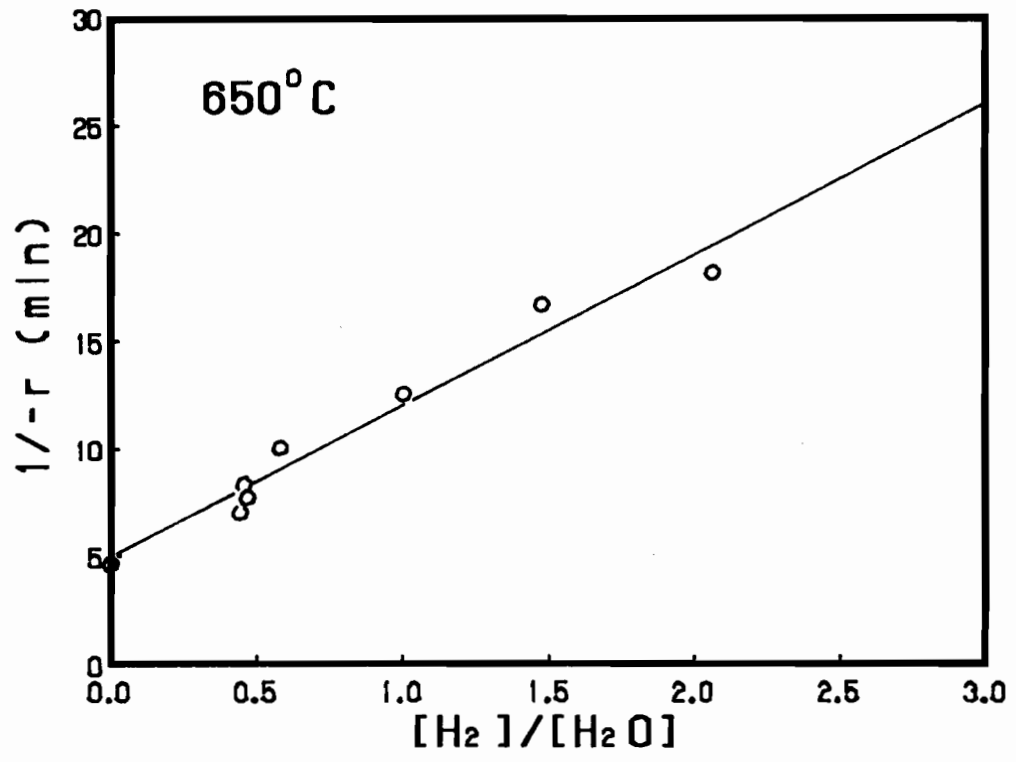


Figure 9. The inverse of gasification rate as function of [H₂] / [H₂O].

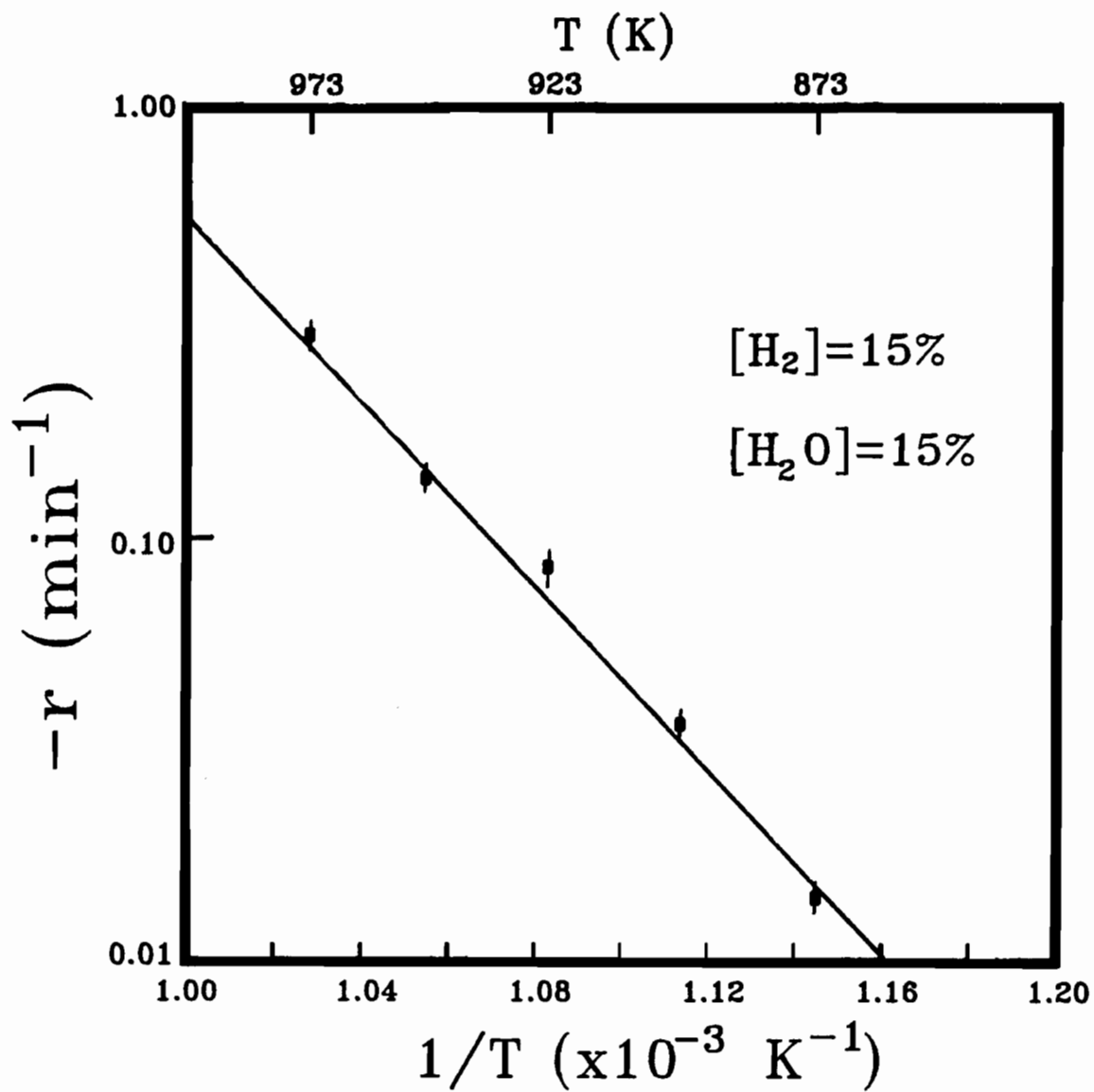


Figure 10. Arrhenius plot of steam gasification rate.

TABLE III. COMPARISON OF REACTIVITIES

CARBON	CAT.	T K	[H ₂ O] %	E _a kJ/mol	-r* 1/min	-r** 1/min
coal char[6]	none	1000	2.67	270	6.0×10^{-5}	6.0×10^{-5}
activated carbon[6]	none	1000	2.67	245	6.6×10^{-4}	6.6×10^{-4}
activated carbon[6]	10% K ₂ CO ₃	1000	2.67	180	2.4×10^{-2}	2.4×10^{-2}
coal char[29]	10% K ₂ CO ₃	1000	49	164	1.8×10^{-2}	3.9×10^{-3}
BLC		923	15	210	2.0×10^{-1}	1.6

-r*: The rate at [H₂].

-r**: The rate at [H₂O]=2.67%, [H₂]=0% and 1000 K.

impregnation. Similarly it is 2 or 4 orders of magnitude higher than the rate for coal char respectively with or without alkali metal carbonate impregnation. The reason for such a high reactivity is the extremely fine dispersion of sodium in the carbon matrix, resulting from formation of BLC from a liquid precursor which contains chemically bound sodium and sodium salts mixed on a molecular scale. It has been found by number of studies [9-10, 14] that the alkali oxygen surface groups of phenolic and carboxylic type, are the active catalytic intermediates. Significant amounts of these groups already exist in the char precursor in the form of alkali lignin and sugar acids. It is likely that a number of these groups would survive the pyrolysis stage. This would eliminate the need of formation of these groups which has been proposed as one of the major rate limiting step in alkali metal catalyzed gasification [16, 28]. For a more detailed analysis and discussion of the effect of the unique BLC properties on gasification reactivity one is referred to the CO₂ gasification study in chapter 3.

Gas Product Distribution

Mass Transfer in Steam Gasification and Data Reduction

In order to examine the extent of the water shift reaction, the experimental equilibrium constant, K_e , defined as

$$K_e = [H_2] [CO_2] / ([H_2O] [CO]) \quad (12)$$

is compared with the theoretical equilibrium constant, K_t , given by equation (6). One way to determine K_e is to use the measured concentrations of CO, CO₂ at the exhaust gas and calculate the H₂ concentration as

$$[H_2] = [CO] + 2 [CO_2] \quad (13)$$

The difference in H₂ concentration calculated with equations (7) or (13) is less than 6% because the amount of H₂S produced is more than one magnitude smaller than CO₂. The steam concentration used in the calculation is the input steam concentration because the system is operated differentially in steam.

Shown in Figure 11 is K_e/K_t plotted as a function of carbon conversion for two typical experiments. The data shows that K_e/K_t is almost two orders

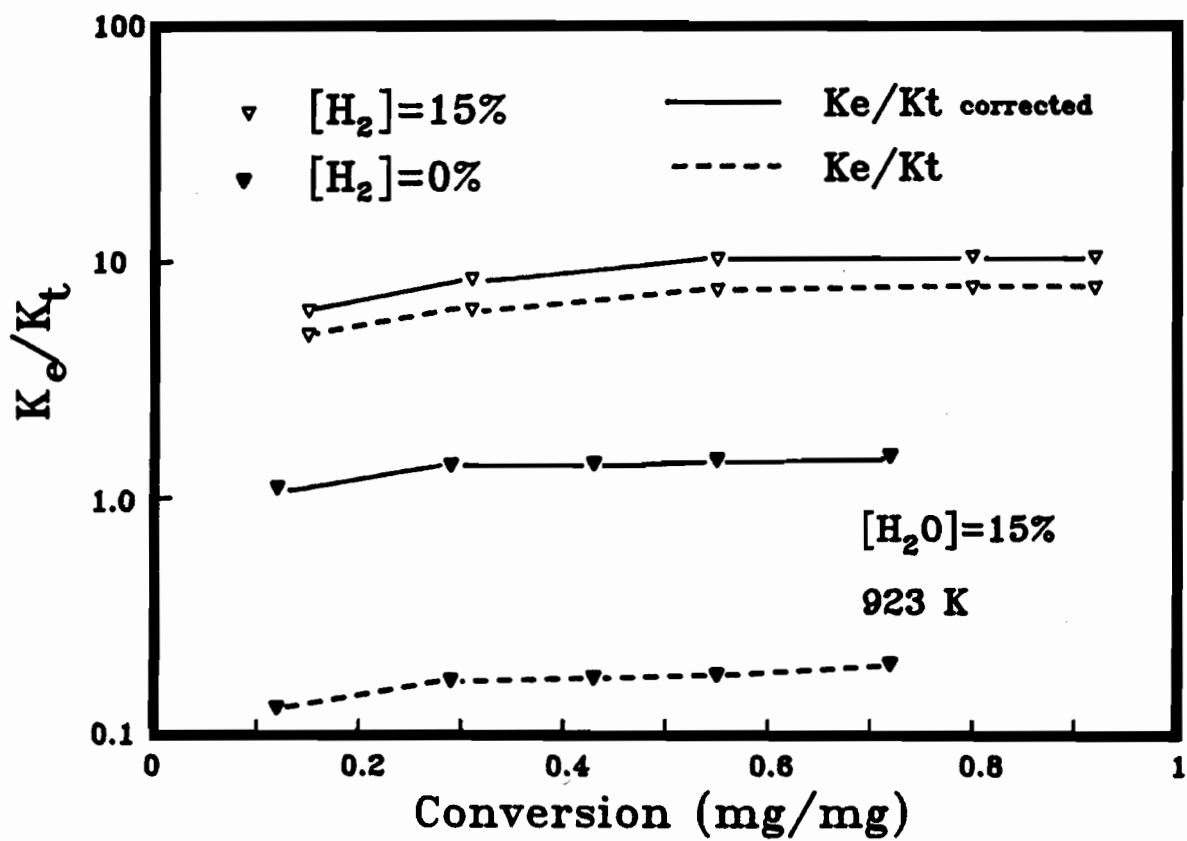


Figure 11. Comparison of theoretical and experimental equilibrium constant.

of magnitude lower at 0% H₂ than at 15% H₂. This difference can be explained by non-differential operation of the TGA system for hydrogen when no hydrogen is supplied to the feed gas as will be shown below.

Shown in Figure 12 is the flow pattern around the sample pan inside the reactor tube. Since the exposed char bed surface area in a sample pan is only 10 to 30% of the tube cross section (12% in present system), a large amount of steam will by-pass the sample pan without coming in contact with the char. This is regarded as one of major disadvantage of the conventional thermogravimetric analysis system [Chapter 2]. The result of this so called dilution effect, is that the product gas concentration in the exhaust is much lower than in the sample bed. So any calculation of K_e should correct for this dilution effect.

It has been shown [30] that the concentration gradient inside the char bed and char particles can be neglected for the present bed height of less than 0.5mm and particle size < 25µm. Therefore the concentration of species a in the bulk of the bed, [a]_b (mol·m⁻³), is related to the rate of production of species a, r_a (mol·s⁻¹), and the concentration of species a in the feed, [a]_i, as

$$[a]_b = [a]_i + \frac{r_a}{k_g S} \quad (14)$$

where k_g (m·s⁻¹) is the mass transfer coefficient, and S (m²) the exposed surface area of the bed. The exposed char bed surface area in the present study was 0.38 cm². For CO, CO₂ and H₂, r_a was calculated from the concentrations measured in the exhaust gas, [a]_{exh} and gas flow rate, Q (m³·s⁻¹), as

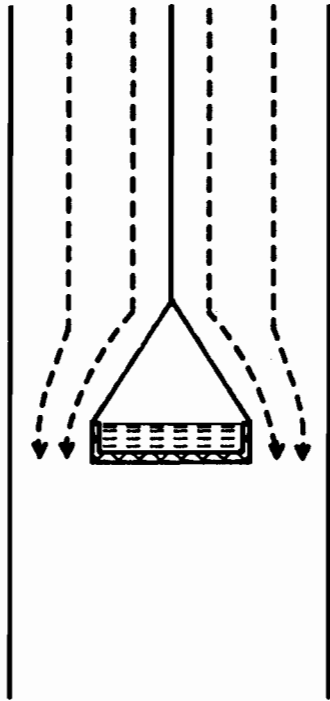
$$r_a = Q [a]_{exh} \quad (15)$$

The rate of steam consumption, -r_{H₂O}, was equated to r_{H₂}.

k_g was calculated from the mass transfer correlation obtained by the naphthalene sublimation technique (see chapter 2) for the present reactor geometry (full sample pan and presence of baffle as shown in Figure 12)

$$\frac{Sh/Sc^{1/3} + 1.68}{2.88 + 1.2 Re^{0.5}} = \left\{ 1 + \left[\frac{1.63 Re^{0.6}}{2.88 + 1.2 Re^{0.5}} \right]^6 \right\}^{1/6} \quad (16)$$

Balance



$$-r = S \, k_g ([a]_b - [a]_i)$$

$$k_g = \frac{Sh \, D}{d_c}$$

$$Sh = f(Re, Sc)$$

Dilution factor: $[a]_b/[a]_o = \frac{Q}{S \, k_g}$
 $([a]_i=0)$

Figure 12. Flow pattern in the reactor tube.

where $Sh (=k_g d_c/D)$, $Sc (=μ /ρ D)$ and $Re (=V d_c ρ/ μ)$ are the Sherwood, the Schmidt and the Reynolds numbers respectively. Equation (15) is valid for $0.6 < Re < 200$. The parameters in the nondimensional groups of Sh , Sc and Re are defined as:

D_{a-m} = the diffusion coefficient of "a" in the gas mixture, $m^2 \cdot s^{-1}$;

d_c = the sample pan diameter, m (=0.0135m in present study);

$μ$ = the viscosity of the gas mixture, $kg \cdot m^{-1} \cdot s^{-1}$;

$ρ$ = the density of the gas mixture, $kg \cdot m^{-3}$;

V = the average gas velocity based on the reactor tube cross section, $m \cdot s^{-1}$.

The diffusion coefficient D_{a-mix} was calculated as [31]

$$D_{a-m} = \frac{1 - y_a}{\sum_{i=1}^n \frac{y_i}{D_{ai}}} \quad (17)$$

where y is the mole fraction of each component in the mixture. D_{ai} is the binary diffusion coefficient of "a" in "i", which was calculated by Fuller's method [32]:

$$D_{ai} = \frac{10^{-3} T^{1.75} (1/M_a + 1/M_i)^{1/2}}{P \left[(\sum_a v_i)^{1/3} + (\sum_i v_i)^{1/3} \right]^2} \quad (18)$$

where M is molecular weight, $\sum_a v_i$ the sum of the diffusion volumes. The viscosity of the feed gas mixture was calculated by a simple correlation [33]:

$$\mu_m = \frac{\sum y_i \mu_i (M_i)^{1/2}}{\sum y_i (M_i)^{1/2}} \quad (19)$$

where μ_i is the viscosity of each component. The difference between equation (19) and μ_m calculated with Wilke's correlation [34] is less than

TABLE IV. PHYSICAL PROPERTIES AND Sc ;
MASS TRANSFER COEFFICIENT FOR SOME TYPICAL CASES

System		[H ₂ O]=15%	[H ₂ O]=15%	[H ₂ O]=15%
		[H ₂]=0%	[H ₂]=15%	[H ₂]=15%
		923 K	923 K	973 K
μ_m	($\times 10^{-5}$ kg/(s·m))	3.91	3.80	3.95
ρ_m	(kg/m ³)	0.350	0.299	0.283
D_{CO-m}	($\times 10^{-4}$ m ² /s)	1.53	1.72	1.89
D_{CO_2-m}	($\times 10^{-4}$ m ² /s)	1.23	1.39	1.52
D_{H_2-m}	($\times 10^{-4}$ m ² /s)	5.62	5.64	6.18
D_{H_2O-m}	($\times 10^{-4}$ m ² /s)	1.91	2.18	2.39
Sc_{CO-m}		0.731	0.739	0.738
Sc_{CO_2-m}		0.911	0.919	0.917
Sc_{H_2-m}		0.199	0.226	0.226
Sc_{H_2O-m}		0.586	0.586	0.584
Q_v	($\times 10^{-6}$ m ³ /s)	39.0	39.0	41.1
Re		13.61	11.94	11.50
Sh_{CO-m}		5.07	4.83	4.76
Sh_{CO_2-m}		5.45	5.20	5.12
Sh_{H_2-m}		3.29	3.26	3.21
Sh_{H_2O-m}		4.71	4.47	4.41
kg_{CO-m}		0.057	0.062	0.067
kg_{CO_2-m}		0.050	0.053	0.058
kg_{H_2-m}		0.137	0.136	0.147
kg_{H_2O-m}		0.067	0.072	0.078

5% for the present system. Shown in Table IV are some physical properties

and Sc for a few typical cases. It can be seen that the physical properties are changing with feed gas composition and condition, while Sc_{a-m} is almost constant except for Sc_{H_2-m} .

Also shown in Table IV are mass transfer coefficients for the different species. It can be seen that the mass transfer coefficient for hydrogen is about 2-3 times larger than those of the other species.

After evaluation of the mass transfer coefficient, $k_{g_{a-m}}$, the dilution effect for the case of $[a]_i=0$ can be quantified with a dilution factor as

$$\frac{[a]_b}{[a]_{exh}} = \frac{Q_v}{k_{g_{a-m}} \cdot S} \quad (20)$$

which is obtained by combining equation (14) and (15). With product "a" absent in the feed as is the case for CO, CO₂ and occasionally for H₂, equation (20) shows that the dilution effect is the ratio of volumetric flow rate and volumetric mass transfer rate. The dilution effect for H₂, CO and CO₂ when $[a]_i$ is zero is around 7, 17 and 20 at the first condition given in Table IV. It is also important to point out that the difference of bed and exhaust concentration generally is less than 10% when $[a]_i$ is in the percentage level because of the differential operation of the TGA system.

Effect of Mass Transfer on K_e

The equilibrium constant ratio of K_e/K_t is now recalculated based on the concentrations inside the char bed and is also shown in Figure 11. With 15% H₂ in the feed gas K_e/K_t is only slightly changed because the effect of increased CO and CO₂ concentration in K_e approximately cancel each other. However without H₂ in the feed, K_e/K_t increases by about one order of magnitude because the $[H_2]$ is 7 times higher inside the bed than in the exhaust.

Probably the most interesting result in Figure 11 is that the ratio K_e/K_t is higher than 1.0 in both cases. Specially with 15% H₂ added in the feed, when the ratio is about 10. This overshoot of the water shift reaction for alkali carbonate catalyzed gasification has been noticed as early as 1952 by Long and Sykes [19] and later by Kayembe and Pulsifer [20], Wigmans [6] and Carrazza et al [35]. The only adequate explanation suggested earlier by Wigmans [5] is that CO₂ is a primary gasification

product besides CO and H₂ in alkali carbonate catalyzed gasification.

Effect of Experimental Conditions on Product distribution

Shown in Figure 13 is the $[CO_2]/[CO]$ plotted against carbon conversion at 15% H₂, 15% steam and temperatures of 923, 948 and 973 K. The results at lower temperature are more noisy, because the CO concentration was close to the detection limit. The results in Figure 13 show that the $[CO_2]/[CO]$ ratio decreases with increasing temperature. Another result shown in Figure 13 is that the ratio increases with increasing carbon conversion. The latter can be interpreted that the $[CO_2]/[CO]$ ratio increases with increasing sodium carbonate concentration. Both the temperature and sodium concentration effects were also observed by [6] .

Shown in Figure 14 is the effect of steam concentration on the $[CO_2]/[CO]$ ratio at 923 K. The ratio decreases with decreasing steam concentration.

Shown in Figure 15 is the effect of hydrogen concentration on the ratio at 923 K. Note the logarithmic scale for the $[CO_2]/[CO]$ ratio, the ratio decreases with increase in hydrogen concentration. In all experiments the $[CO_2]/[CO]$ ratio increases with increasing in carbon conversion.

Discussion

The effect of variations in reaction conditions such as in temperature, [H₂] and [H₂O], on the product distribution is as predicted according to water shift reaction equilibrium. However, it was also shown that CO₂ cannot only be formed via the water shift reaction during steam gasification of BLC. More specifically, it was suggested that both CO and CO₂ are formed directly on the active sites. The explanation for the effect of reaction conditions is that the back reaction of water shift equilibrium converts CO₂ in H₂O and CO when the temperature and [H₂] are increased or the [H₂O] is decreased.

The only mechanistic explanation given of the over-shoot of CO₂ production was reported by Wigmans [6]. Based on his experimental observations, Wigmans drew a reaction scheme for the potassium catalyzed steam gasification of activated carbon, which is shown in Figure 16. In the scheme potassium acts as an oxygen transferring medium, while water adsorption takes place on a reduced site. This explains the relatively high

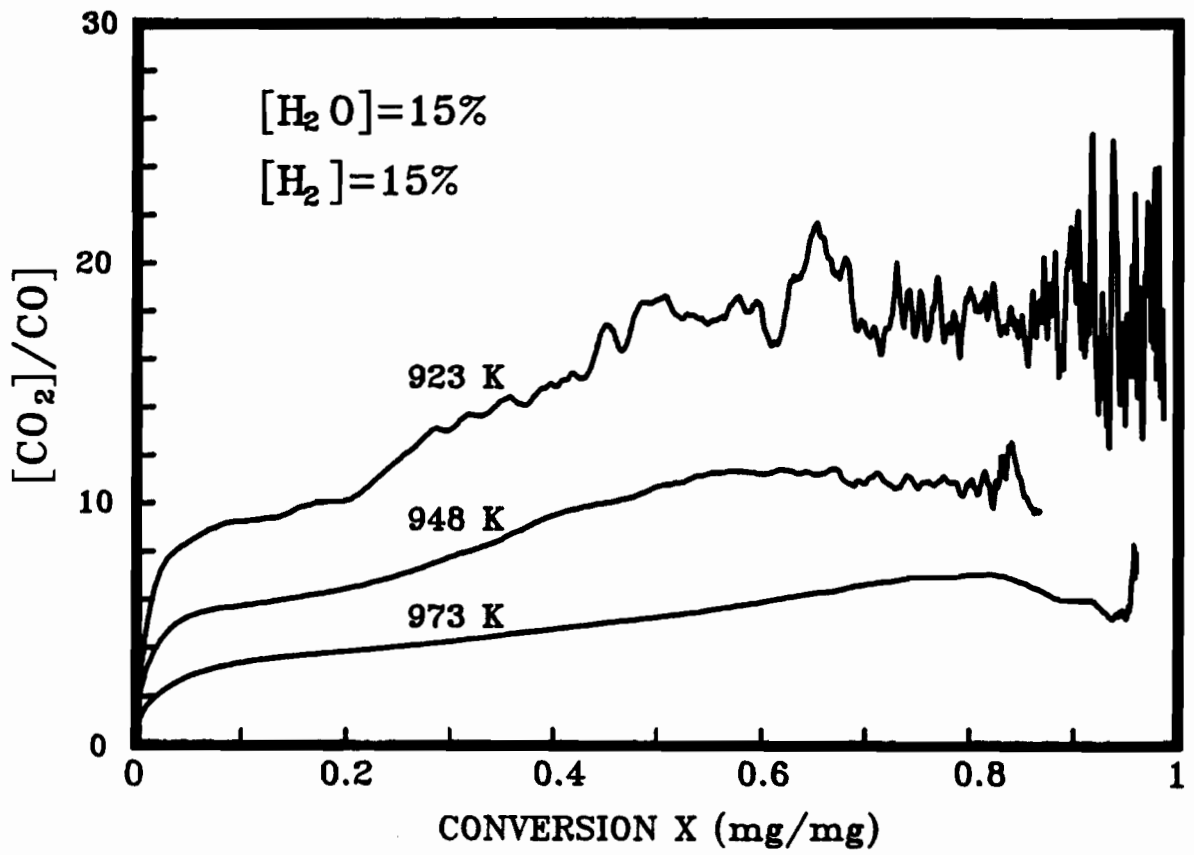


Figure 13. Effect of temperature on $[CO_2]/[CO]$ ratio.

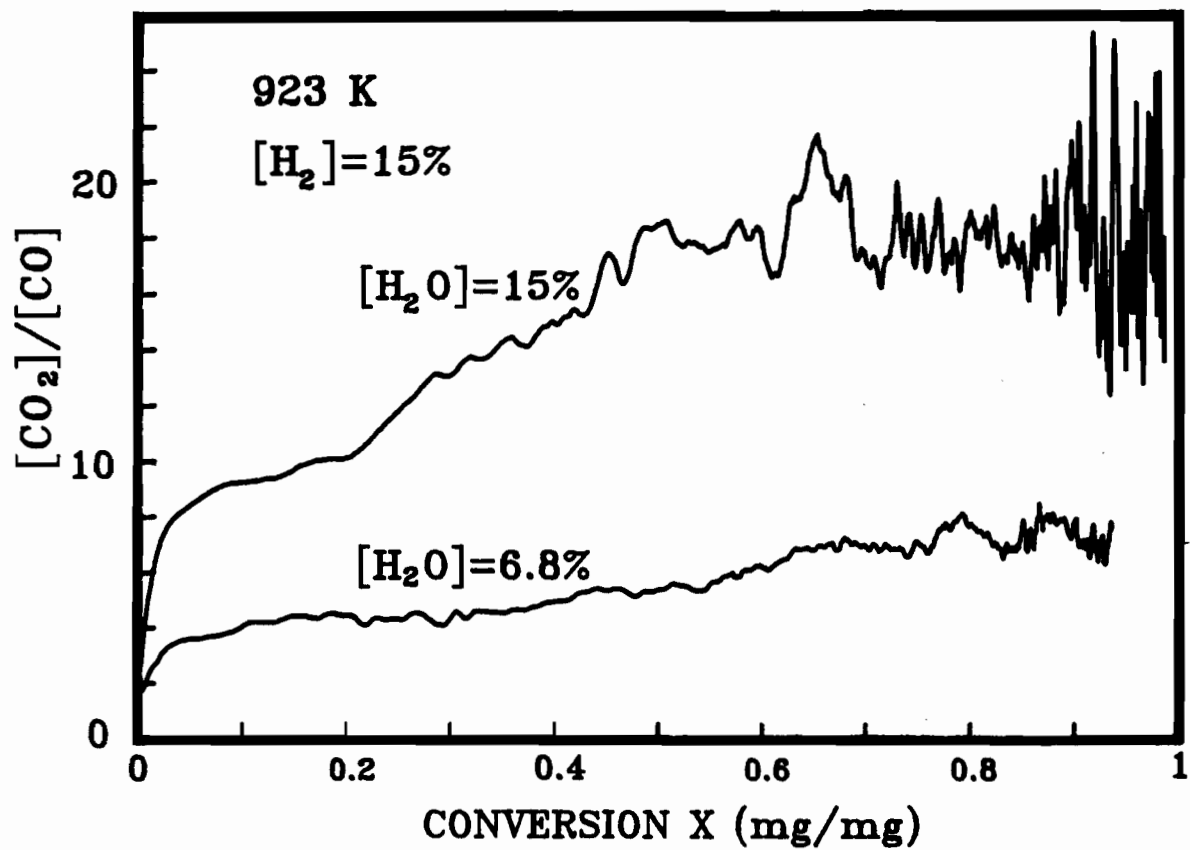


Figure 14. Effect of steam concentration on [CO₂]/[CO] ratio.

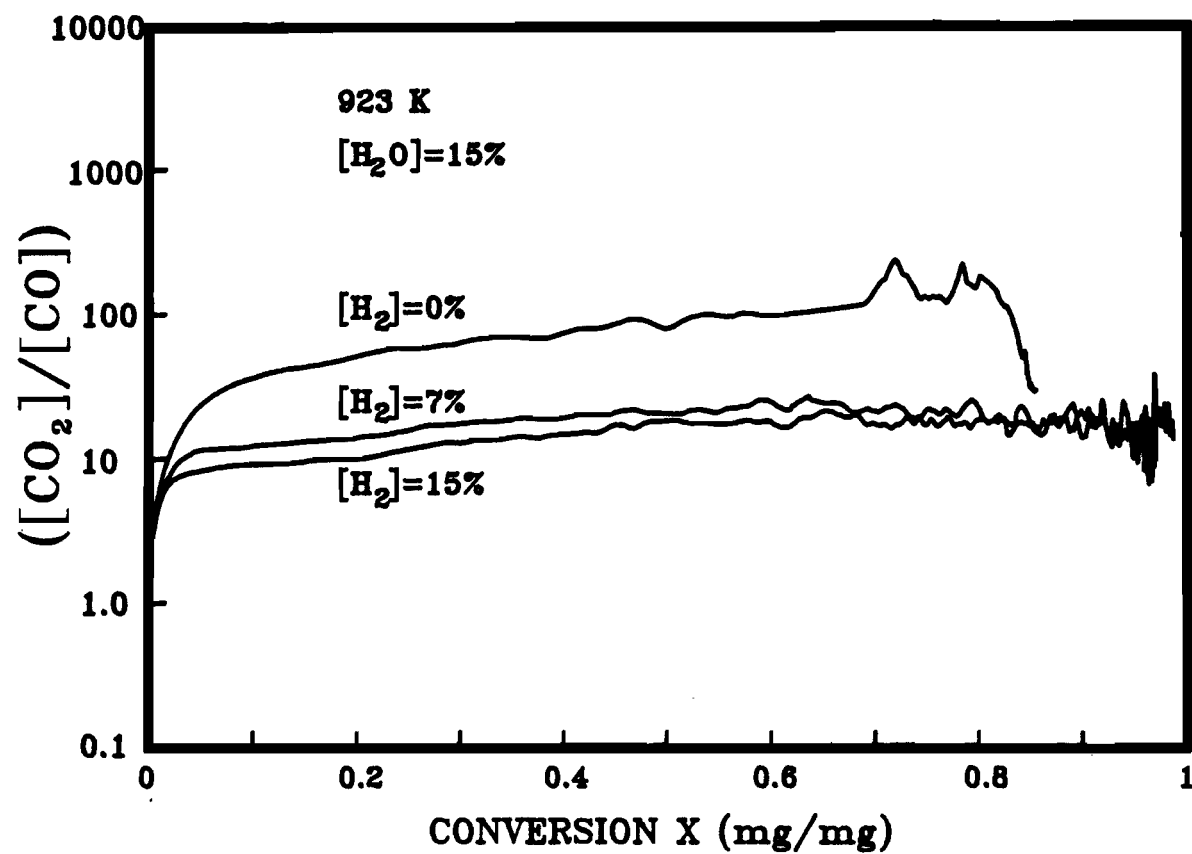


Figure 15. Effect of hydrogen concentration on [CO₂]/[CO] ratio.

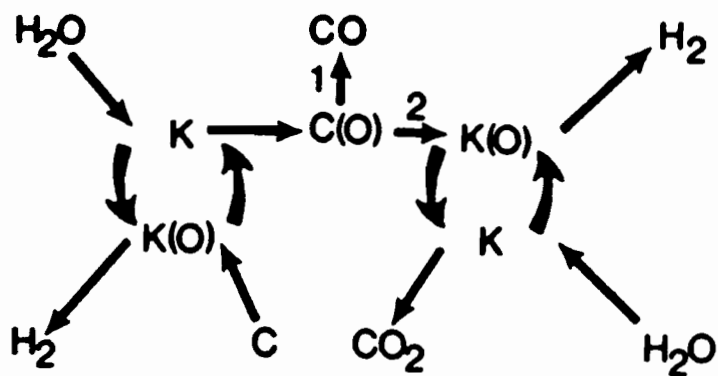


Figure 16. Reaction scheme proposed by Wigmans [6].

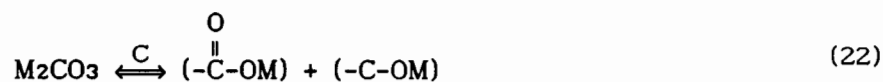
values found for K_{H_2O} , which increase with at increasing K/C ratio in his experiments. The reducing agents in this redox mechanism are C (route 1) and C(O) (route 2). This explains how CO (route 1) and CO₂ (route 2) are both primary products of different pathways. And also according to this scheme, at high K/C ratio the reaction:



is more favorable than CO desorption. This reaction scheme can successfully explain the effect of catalyst concentration on the CO₂/CO ratio. However, the effect of H₂ and steam concentration on the CO₂/CO ratio can only be explained assuming it is due to the back reaction of the water shift equilibrium.

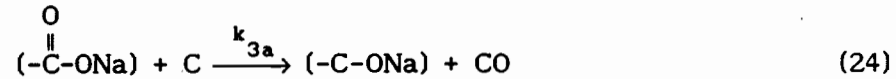
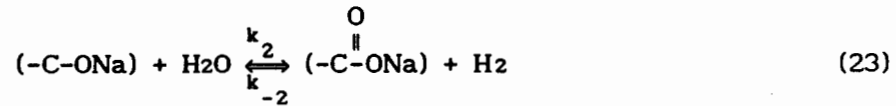
As pointed out in the introduction, CO₂ production higher than predicted by thermodynamics is only observed for alkali carbonate catalyzed steam gasification. Thus this behavior must be related to the nature of the alkali carbonate and the active intermediates formed from alkali carbonate during gasification.

Following the ideas of the mechanism proposed by Sams and Shadman [10], we propose the following redox mechanism involving transformation of the surface oxygen complexes in steam gasification. Following Shadman [28] and Moulijn [9] it is first assumed that the alkali metal surface oxide complexes are formed by reduction of carbonate by carbon as

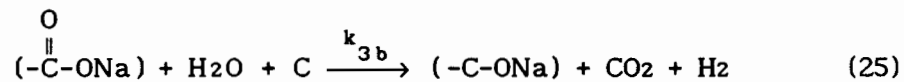
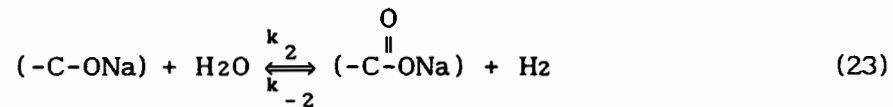


It should be noted that these surface complexes may already exist in the BLC carbon matrix as was discussed before. The catalytic carbon gasification proceeds via a combination of oxidation and the reduction reactions of these surface complexes involving carbon and H₂O molecules. CO₂ and CO are formed via two routes as shown in equations (23) to (25):

Route 1:



Route 2:



In route 1 a phenolic group is oxidized by H₂O into a carboxylic group (reaction (23)), followed by reduction of the carboxylic group on the carbon surface to CO and a phenolic group (reaction (24)). The overall reaction of (23) and (24) is gasification reaction (1). In route 2 the oxidation of the phenolic group is same as in route 1, but then the carboxylic group is reduced into a phenolic group on the carbon surface by H₂O whereby CO₂ is formed (reaction (25)). The overall reaction of route 2 is that one carbon atom reacts with two H₂O molecules to form one CO₂ and two H₂ molecules, i.e. the gasification plus water shift reaction. The above reaction mechanism can be summarized that CO₂ is formed via decomposition of carboxylic groups, while CO is formed via reduction of the carboxylic groups.

The above proposed mechanism can also be related to the Langmuir-Hinshelwood type kinetic expression (equation (11)) used to described the influence of the gas composition. With the assumptions that i) the reduction of (-COONa), i.e. reaction (24) or (25) is rate determining, ii) reaction (23) is at a quasi equilibrium, meaning $k_{3x} \ll k_{-2}[\text{H}_2]$, the following equation can be derived

$$-r = \frac{k_{3x} [\text{H}_2\text{O}]}{[\text{H}_2\text{O}] + \frac{k_{-2}}{k_2} [\text{H}_2]} \quad (26)$$

where 3x is either 3a or 3b.

CONCLUSIONS

From present work, the following conclusions can be drawn:

- The effect of gas atmosphere on the rate of steam gasification of black liquor char can be described by Langmuir-Hinshelwood type kinetics.
- An activation energy of 210 kJ/mol obtained is for BLC similar to that of coal char catalyzed by alkali carbonate.
- The CO₂ concentration was higher than predicted by assuming that the water-shift reaction is at equilibrium.
- It is proposed that CO₂ is one of the primary gasification products.
- A mechanism for steam gasification is proposed which explains the direct formation of CO₂ during gasification and which is also in agreement with the experimentally found Langmuir-Hinshelwood kinetics.

NOMENCLATURE

[a] _b	= gas concentration in sample bed, mol·m ⁻³ .
[a] _{exh}	= gas concentration in exhaust, mol·m ⁻³ .
[a] _i	= gas concentration in feed, mol·m ⁻³ .
d _c	= sample pan diameter, m.
D	= diffusion coefficient, m ² ·s ⁻¹ .
E _a	= apparent activation energy, kJ·mol ⁻¹ .
k _g	= mass transfer coefficient, m·s ⁻¹ .
k _{nx}	= reaction rate constant for elementary reactions.
K	= reaction constant, m ³ mol ⁻¹ min ⁻¹ .
K'	= reaction constant, min ⁻¹ .

K_e	= experimental equilibrium constant for water shift reaction.
K_{H_2}	= adsorption constant of H_2 , $m^3 \text{mol}^{-1}$.
K'_H	= adsorption constant of H_2 .
K_{H_2O}	= adsorption constant of H_2O , $m^3 \text{mol}^{-1}$.
K_t	= equilibrium constant for water shift reaction.
M	= molecular weight.
M_c	= molecular weight of carbon.
P_{CO}	= partial pressures of CO , atm.
P_{CO_2}	= partial pressures of CO_2 , atm.
Q	= gas flow rate at standard conditions, $sl \cdot \text{min}^{-1}$.
Q_v	= volumetric gas flow rate, $m^3 \cdot s^{-1}$.
$-r$	= gasification rate, min^{-1} .
r_a	= production rate of species a, $\text{mol} \cdot s^{-1}$.
R	= universal gas constant, $\text{atm} \cdot l \cdot \text{mol}^{-1} \cdot K^{-1}$.
Re	= Reynolds number.
S	= exposed surface area, m^2 .
Sc	= Schmidt number.
Sh	= Sherwood number.
t	= time, min.
T	= temperature, K.
V	= average gas velocity based on reactor tube cross section, $m \cdot s^{-1}$.
$W_{c,o}$	= weight of carbon at time zero, mg.
$W_{c,t}$	= remaining carbon weight at time t, mg.
$W_{c,c}$	= amount of carbon calculated from initial sample weight, mg.
$W_{c,m}$	= amount of carbon measured from CO and CO_2 production, mg.
ΔW_c	= difference between $W_{c,m}$ and $W_{c,c}$, %.
X	= carbon conversion, mg/mg.
y	= mole fraction.

Greek Symbols

Ψ	= dilution factor defined by equation (1).
ρ	= density, $kg \cdot m^{-3}$.
μ	= viscosity, $kg \cdot m^{-1} \cdot s^{-1}$.
$\sum_a v_i$	= sum of diffusion volumes.

REFERENCES

1. van Heiningen, A.R.P., J. Li, and J. Fallafollita, **Canadian Patent Application**, #583,409, Nov. 17, (1988).
2. Daurai-Swamy, **Intern. Chem. Recov. Conf.**, p.217(1989).
3. Stuart, P. **Ph. D. thesis**, McGill University, (1989).
4. Tessie du Motay, C.M., and C.R. Marechal, **British patent**, 2548, (1867).
5. Mims, C.A., and et al, **J. Am. Chem. Soc.**, 104(24), p.6887(1982).
6. Wigmans, T., **Ph. D. thesis**, University of Amsterdam (1982).
7. Moulijn, J.A., and F. Kapteijn, **Carbon and coal gasification**, Nato Asi Series E, No. 105, p.181 (1986).
8. Cerfontain, M.B., and et al, **J. Catalysis**, 107, p.173(1987).
9. Moulijn, J.A., and F. Kapteijn, **Sci. & Tech.**, 40 (1), p.15(1987).
10. Sams, D.A., and F. Shadman, **AIChE J.**, 32(7), p.1132(1986).
11. McKee, D.W., and D. Chatterji, **Carbon**, 16(1), p.53(1978).
12. Long, F.J., and W.W. Sykes, **J. Chem. Phys.**, 47, p.361(1950).
13. Delannay, F., and et al, **Carbon**, 22(4), p.401(1984).
14. Mims, C.A., and J.K. Pabst, **Fuel**, 62(2), p.176(1983).
15. Mims, C.A., and J.K. Pabst, **J. Catalysis**, 107, p.209(1987).
16. Huttinger, K.J., and R.Minges, **Carbon and coal gasification**, Nato Asi Series E, No. 105, p.197 (1986).
17. Huttinger, K.J., and et al, **Fuel**, 65(7), p.932(1986).
18. Meijer, R., and et al, **Carbon'88**, Newcastle, UK, p.431(1988).
19. Long, F.J., and K.W. Sykes, **Proc. Roy. Soc.**, A215, London, p.100 (1952).
20. Kayembe, N., and A.H. Pulsifer, **Fuel**, 55, p.211(1976).
21. Li, J., and A.R.P. van Heiningen, **Mat. Res. Soc. Symp. Proc.**, vol.111, p.441 (1988).
22. Li, J., and A.R.P. van Heiningen, **Carbon'88**, Newcastle, UK, p.428 (1988).
23. Li, J., and A.R.P. van Heiningen, **Can. J. Chem. Eng.**, 67(4), p.693 (1989).
24. Eriksson, G. **Chemica Scripta**, 8, p.100(1970).
25. Pejryd, L., and Huppa, **1984 Tappi Pulping Conf.**, San Francisco, p1(1984).
26. Smith, J.M., and H.C. van Ness, **Introduction to Chemical Engineering Thermodynamics**, McGraw-Hill book comp. 3ed edit. p.300(1982)

27. Walker Jr., P.L., and et al, **Advan. Catal.**, 11, p.133(1959).
28. Shadman, F, and et al, **Fuel**, 66(12), p.1658(1987).
29. Veraa, M.J., and A.T. Bell, **Fuel**, 57, p.194(1978).
30. Li, J., and A.R.P. van Heiningen, **J. Pulp & Paper Sci.**, 12(5), p.J146(1986).
31. Treybal, R.E., **Mass-Transfer Operation**, McGaw-Hill Book Company, N.Y., 2nd edit., p.24(1968).
32. Fuller, E.N., and et al, **Ind. Eng. Chem.**, 58(5), p.19(1966).
33. Perry, R.H., and C.H. Chilton, **Chemical Engineers' Handbook**, 5th, edit., McGraw-Hill, p.3-211, 3-249 (1969).
34. Wilke, C.R., **J. Chem. Phy.**, 18, p.517 (1950).
35. Carrazza, J., and et al, **J. Catalysis**, 94, p.234 (1985).

CHAPTER 5

SULFUR EMISSION DURING CO₂ GASIFICATION OF BLACK LIQUOR CHAR

ABSTRACT

The COS emission during CO₂ gasification of pyrolyzed and reduced black liquor char was studied from 675 to 750°C in a thermogravimetric analysis set-up. COS is the major sulfur containing gaseous product under all conditions while elemental sulfur, S₂, is suggested as another important sulfur gas product when the CO concentration is low. The COS formation is promoted by both CO and CO₂. The rate limiting step for COS emission from a sample pan with char bed height of less than 0.5 mm at relative low CO₂ concentration or high temperature is external mass transfer. In these cases, the COS concentration inside the char bed is determined by thermodynamics. The calculated equilibrium concentration of COS inside the char bed varies considerably depending on the choice of thermodynamic properties for Na₂S.

INTRODUCTION

Sulfur emission control is one of the major objectives of the kraft recovery process, in addition to chemical recovery and steam generation, because of the toxic and odorous nature of the gases. It is agreed that sulfurous gases are produced during pyrolysis, combustion and gasification of black liquor in the recovery furnace. Yet knowledge concerning the origin of the gases, the reaction rate and mechanism of their formation is still incomplete. This is partly due to the fact that the majority of studies dealing with the recovery furnace are difficult to interpret because several operations are carried out simultaneously within the same reactor. Also the laboratory investigations were almost exclusively focused on sulfur emission during pyrolysis of black liquor.

Since the early 60's many studies have focused on the effect of operating variables on sulfur emission from the chemical recovery furnace [1-5]. Most studies indicate that sulfur emission decreases with increasing bed temperature, solids content, degree of oxidation and liquor droplet size. The only detailed study concerning the origin of sulfur emission inside the recovery furnace was made by Borg et al [5]. They found that about one third of the total sulfur emission originated from the primary air and char bed level, while the other two thirds came from the secondary air and spray level. The sulfur compounds above the char bed were mainly present as H_2S . Most theoretical studies on sulfur emission are based on thermodynamic analysis of the recovery furnace system [6, 7]. The calculated results agree reasonably with actual measurements.

Several bench scale studies have been reported on sulfur emission during pyrolysis of real kraft black liquor or of inorganics in simulated liquors [8-13]. The only study of sulfur emission during combustion of black liquor was performed with a single droplet reactor [14]. It was found that sulfur emission decreased with increasing droplet size and solids content, in agreement with mill studies. Sulfur emission during CO_2 gasification of black liquor char was only previously studied by the present author [12]. It was found that COS emission was promoted by the presence of both CO_2 and CO during gasification of a char obtained by slow pyrolysis of black liquor solids.

The processes taking place in the furnace char bed are mainly

gasification and reduction, because insufficient primary air is supplied to achieve oxidative conditions at the bed surface. Therefore in order to understand the sulfur emission from the char bed the reaction mechanism and rate controlling parameters of sulfur emission during gasification of black liquor char must be known. This knowledge is also needed for development of alternative recovery processes which employ gasification as a separate process step [15].

In this work, sulfur emission from kraft black liquor char under CO₂ gasification conditions was investigated in a thermogravimetric analysis (TGA) system. The emission rate was studied as function of temperature, CO₂ and CO concentration, and type of carrier gas. The results are used to explain some phenomena observed in a recovery furnace and suggestions are made on how to minimize sulfur emission in a proposed [15] low temperature recovery process.

EXPERIMENTAL

Shown in Figure 1 is a schematic picture of the Cahn TGA 113-DC thermogravimetric balance with auxiliary gas preparation system used for CO₂ gasification of kraft black liquor char. A Fisher gas partitioner was used for fixed gas analysis. A Hewlett Packard GC with FPD and an 18 inch column with acetone washed Poropack QS packing, operated at 45°C, was used for sulfur gas analysis [16]. The initial sample and gasification residues were analyzed for sulfate, sulfite, sulfide, thiosulfate, carbonate, sodium and potassium content by immersing the samples in deoxygenated, deionised water and analyzing the solution with a Dionex IC with CD and ECD. The total sulfur was obtained by measuring the amount of sulfate in the sample solution after oxidation of all sulfur species into sulfate by H₂O₂. This oxidation procedure was compared with the Schöninger combustion method and shown to give to the same results. The oxidation by H₂O₂ was adopted for most char samples because the technique is simple and fast, and leads to minimum sample loss and contamination.

Kraft black liquor, obtained by cooking Black Spruce to about 49% yield at a charge of 15% Na₂O on wood and a sulfidity of 30%, was oxidized under 200 psi oxygen at 130°C to convert all inorganic sulfur into sulfate. The liquor was subsequently dried below 120°C as a thin film on the convex surface of watch glasses to minimize separation of inorganic salts from

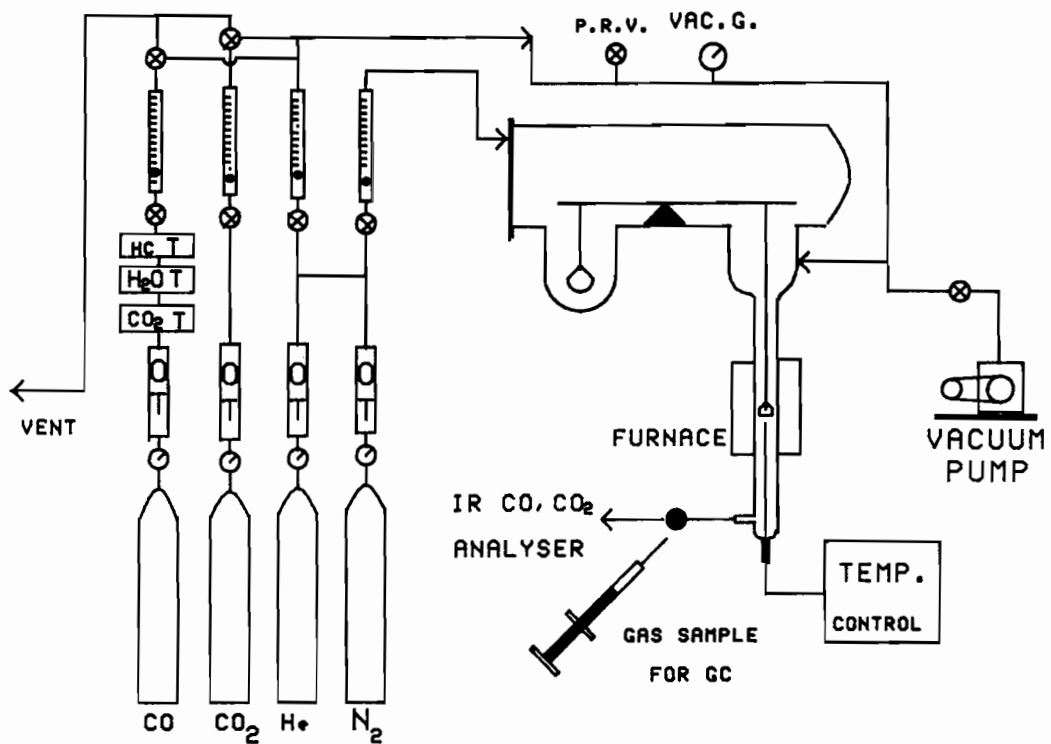


Figure 1, Schematic picture of the TGA system.

organic compounds. The solids were removed from the drying surface and pyrolyzed for 20 min under N₂ with 10% CO in a tube furnace preheated to 580°C. The resulting char was ground and the fraction passing 500 mesh (<25µm) was used in gasification experiments. The chemical composition of the black liquor solids and chars is shown in Table 1.

TABLE 1 CHEMICAL COMPOSITION OF BLACK LIQUOR SOLIDS, CHAR AND REDUCED CHAR

	[Na ⁺] (%)	[SO ₄ ⁼] (%)	[S ⁼] (%)	[CO ₃ ⁼] (%)	[S ₂ O ₃ ⁼] (%)
solids	18.6	8.13	< 0.1	7.2	< 0.05
char	25.4	13.5	< 0.1	28	< 0.05
reduced char	34.2	< 0.1	5.7	34	< 0.05

About 5 mg of the char (BLC) was added to the pan of the TGA system which had previously three times been evacuated and refilled with N₂ or He. The furnace temperature was then raised from 20°C to 775°C at a rate of 25°C/min under a He or N₂ flow rate of 400 scc/min. At about 500°C, 25 scc/min of CO was added to the carrier gas to prevent Na₂CO₃ decomposition [17]. After 2 minutes at 775°C the reduction of Na₂SO₄ to Na₂S is complete, and the temperature was reduced to the required gasification temperature. When the temperature and sample weight were stabilized, a gasification experiment was started by changing to the desired gasification gas composition. At the start of gasification the char consists of 13.9% Na₂S, 58% Na₂CO₃ and 28% organic carbon, Table 1. This corresponds to a molar ratio of 1 Na₂S : 3.1 Na₂CO₃ : 13 C. Further information on experimental procedures and gasification reactions can be found elsewhere [18, 19 and Chapter 3].

DILUTION EFFECT ON GAS ANALYSIS

It was pointed out in Chapter 2 that one of the major disadvantages of the conventional thermogravimetric analysis system is the large amount of gas by-passing the sample pan without contacting the solid reactant. The result is that the product gas concentration in the exhaust is much lower than that existing in the sample bed when this product gas is not present at

a significant concentration in the feed gas. Since the present feed gas was free of sulfur containing gases, the sulfur species gas concentration in the sample bed, $[a]_b$, can be calculated from the sulfur species concentration in the exhaust, $[a]_{exh}$ and the so called dilution factor Ψ defined in Chapter 2 as

$$\Psi = \frac{[a]_b}{[a]_{exh}} = \frac{Q_v}{k_g \cdot S} \quad (1)$$

where $[a]_b$, $[a]_{exh}$ and Q_v are all at the furnace pressure and temperature. k_g ($m \cdot s^{-1}$) is the mass transfer coefficient between the exposed external surface of the char bed and feed gas while S (m^2) is the exposed surface area of the bed and Q_v is the gas flow rate ($m^3 \cdot s^{-1}$). k_g can be calculated from the mass transfer correlation obtained by the naphthalene sublimation technique for the present reactor geometry (Chapter 2). as

$$\frac{Sh/Sc^{1/3} + 1.68}{2.88 + 1.2 Re^{0.5}} = \left\{ 1 + \left(\frac{1.63 Re^{0.6}}{2.88 + 1.2 Re^{0.5}} \right)^6 \right\}^{1/6} \quad (2)$$

where Sh ($=k_g d_c/D$), Sc ($=\mu / \rho D$) and Re ($=V d_c \rho / \mu$) are the Sherwood, Schmidt and Reynolds numbers respectively. Equation (2) is valid for $0.6 < Re < 200$. Details of the calculation procedure for k_g can be found in Chapters 2 and 4.

The concentration in the char bed, $[a]_{exh}$, is uniform in the bed because it has been shown [20] that concentration gradients inside the char bed and char particles are negligible. The maximum difference in concentration of a gaseous species at the exhaust and in the bed is less than 10% when this species is present at the percentage level in the feed, because of differential operation of the TGA.

THERMODYNAMIC PREDICTIONS

Reaction System

The initial composition of the reaction system is 1.0 mole of Na_2S , 3.1

moles of Na₂CO₃ and 100 moles of a mixture of CO, CO₂ and N₂. The presence of carbon in the reduced char is indirectly taken into account by changing the CO and CO₂ concentration of the initial gas mixture. The system pressure was kept at one atmosphere. Except for soot formation at high CO/CO₂ ratios, the major reactions taking place in this system are the following sulfur emission reactions:

1) COS formation



2) Oxidation of Na₂S to S₂



3) Oxidation of Na₂S to SO₂



In the gas phase, the following reactions are also possible:



Since there is only one mole of Na₂S, the amount of gas at equilibrium will be between 99 and 100 moles. This leads to relative small changes in CO and CO₂ concentration, comparable to those obtained under differential operation of the TGA system.

System Analysis

Thermodynamic calculations were performed with the latest version of SOLGASMIX [21]. Pejryd [7] has given a detailed description of the calculation procedure and strategy of the program. However, the thermodynamic property data for Na₂S used in this program is taken from "Thermochemical Properties of Inorganic Substances" (1977) [22]. The listed Na₂S melting point T_m, standard enthalpy ΔG_{298K} and melting enthalpy ΔH_m are 1251 K, -374.468 kJ/mol and 26.359 kJ/mol respectively. It has been reported by Warnqvist [23] that those values were incorrect because they were obtained with impure Na₂S. With better experimental techniques, Warnqvist reported that T_m, ΔG₂₉₈ and ΔH_m for Na₂S are respectively 1443±10

K, -386.6 kJ/mol and 30.1 kJ/mol. By replacing the old data with Warnqvist's data in the same program, Backman [24] calculated the phase diagrams for system $\text{Na}_2\text{CO}_3\text{-Na}_2\text{S-Na}_2\text{SO}_4$, and obtained very close agreement with experimental results. Therefore, Warnqvist's data were used in the present thermodynamic calculations. The effect of thermodynamic data of Na_2S on sulfur emission as function of temperature is shown in Figure 2. The COS concentration obtained with the old thermodynamic data for Na_2S is about one order of magnitude higher than with the new data.

Calculation Results

The predictions are shown in Figures 3, 4 and 5. The top graph shows the equilibrium gas phase composition, while the liquid and solid phase compositions are shown in the bottom graph.

Shown in Figure 3 is the equilibrium composition of the system at 998 K and 5 moles of CO addition as function of CO_2 addition. For present the CO_2 addition range, sulfur containing gases with concentration higher than 1 ppm are COS, S_2 , SO_2 and CS_2 . COS is the major sulfurous gas, while $[\text{S}_2]$ is about one to two orders of magnitude and $[\text{SO}_2]$ and $[\text{CS}_2]$ are respectively 3 and 4 orders of magnitude lower. The concentrations of all sulfurous gases increase rapidly with increasing CO_2 concentration. Besides S_2 , SO_2 and CS_2 , another oxidation product of Na_2S is liquid poly-sulfide at CO_2 addition above 60 moles. Liquid poly-sulfide is in the form of Na_2S_2 , NaS_2 and Na_2S_3 and only exists when there is a liquid phase of Na_2S and Na_2CO_3 . The concentration of the type of poly-sulfide decreases about one to two orders of magnitude in the order of $[\text{Na}_2\text{S}_2] > [\text{NaS}_2] > [\text{Na}_2\text{S}_3]$. The total amount of poly-sulfide is shown in Figure 3 as Na_2S_x .

Shown in Figure 4 is the effect of CO addition on sulfur emission at 998 K and 20 moles of CO_2 addition. The results show that at very low CO concentration large amounts of S_2 and SO_2 are formed. The concentration of S_2 and SO_2 is very sensitive to the $[\text{CO}]$ and decreases to lower than 1 ppm at 2 to 3% of CO. Some Na_2S_x is also formed at low CO concentrations. For almost the entire CO addition range, the equilibrium COS concentration, $[\text{COS}]_e$, remains constant, in agreement with reaction (3) which requires that $[\text{COS}]_e$ is not affected by CO. Only at very low and very high CO addition, $[\text{COS}]_e$ changes slightly because at zero CO addition $[\text{CO}_2]_e$ is 20% lower due to formation of CO and SO_2 , and at above 55 mole CO addition $[\text{CO}_2]$ is 20% higher due to soot formation from CO.

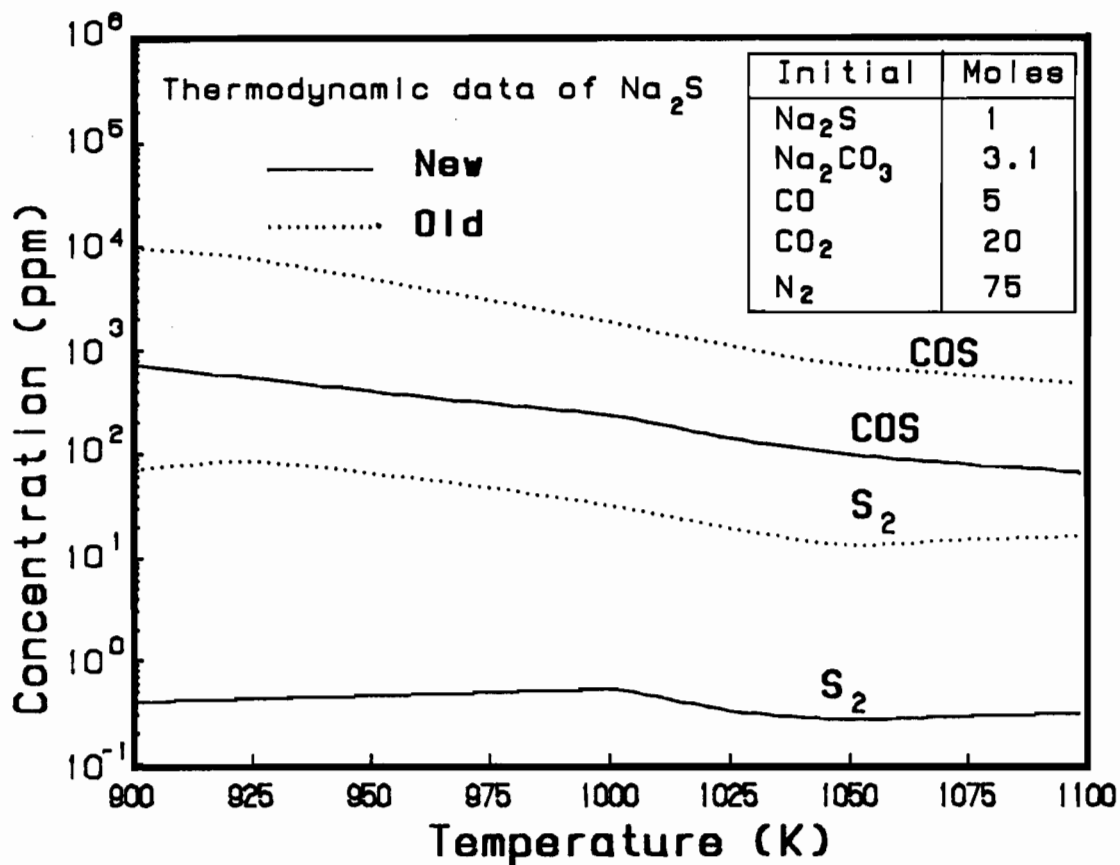


Figure 2, Effect of thermodynamic data on sulfurous gas concentration.

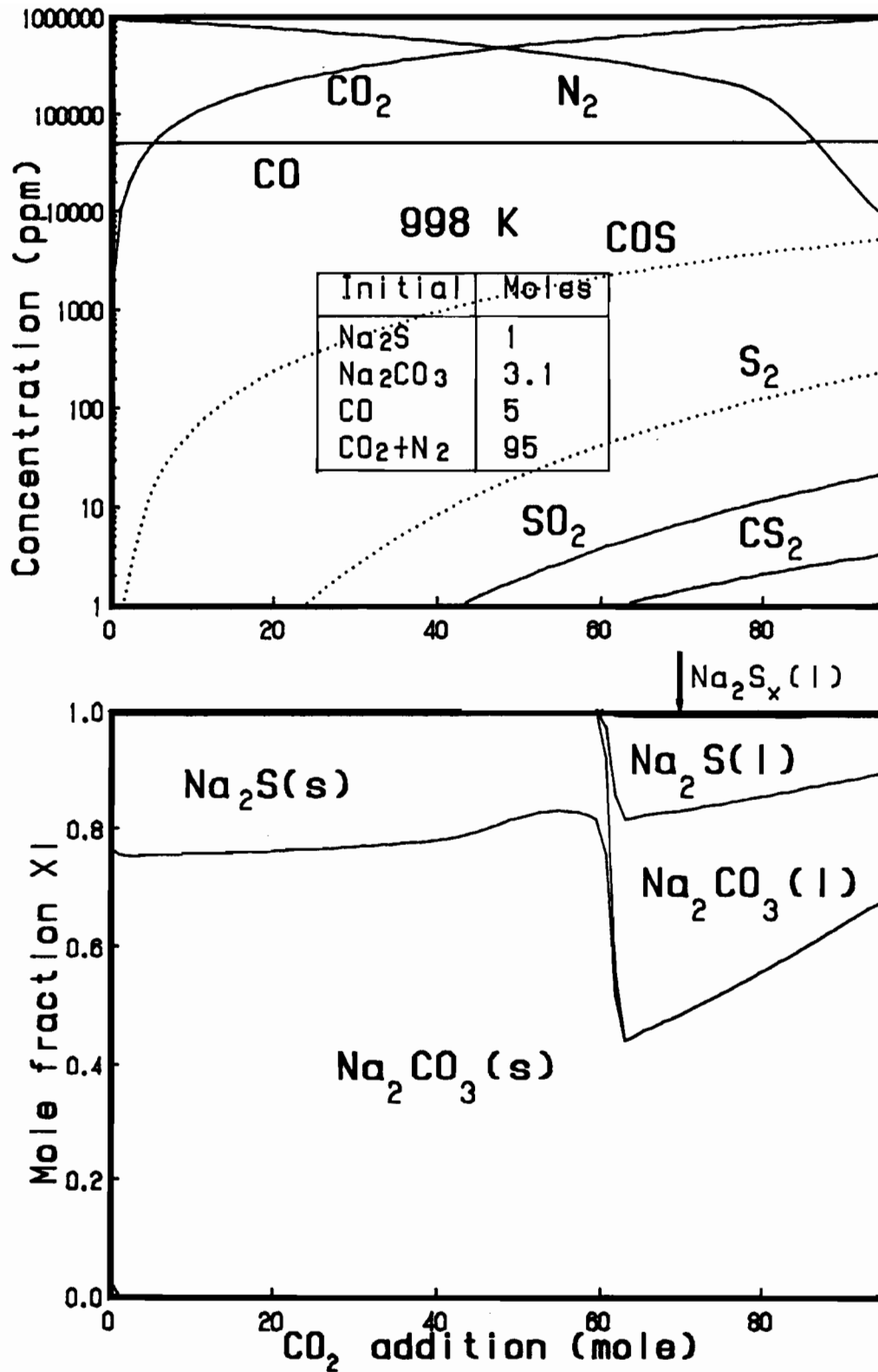


Figure 3, Equilibrium composition as function of CO₂ addition in CO₂ gasification.

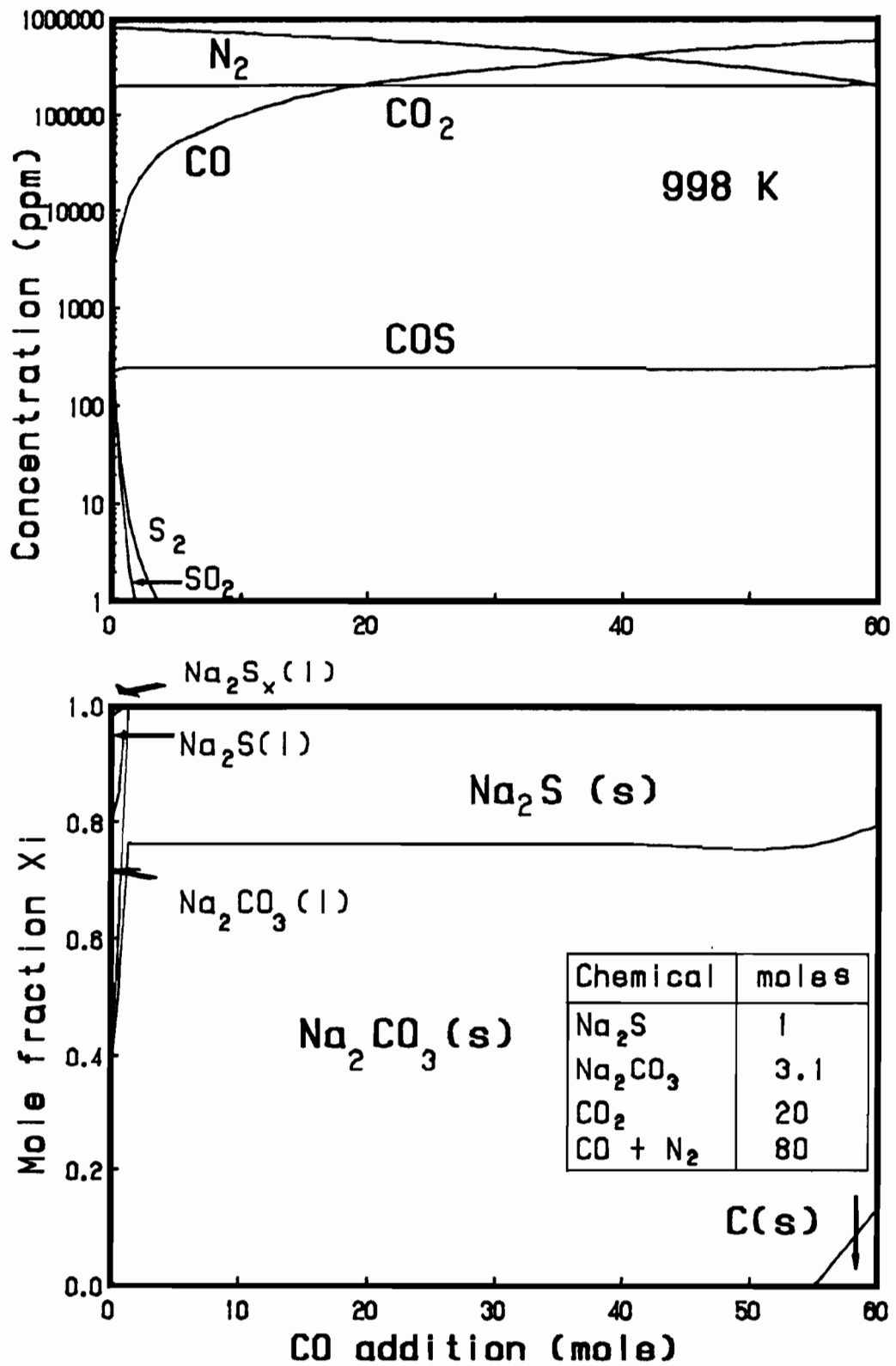


Figure 4, Equilibrium composition as function of CO addition in CO_2 gasification.

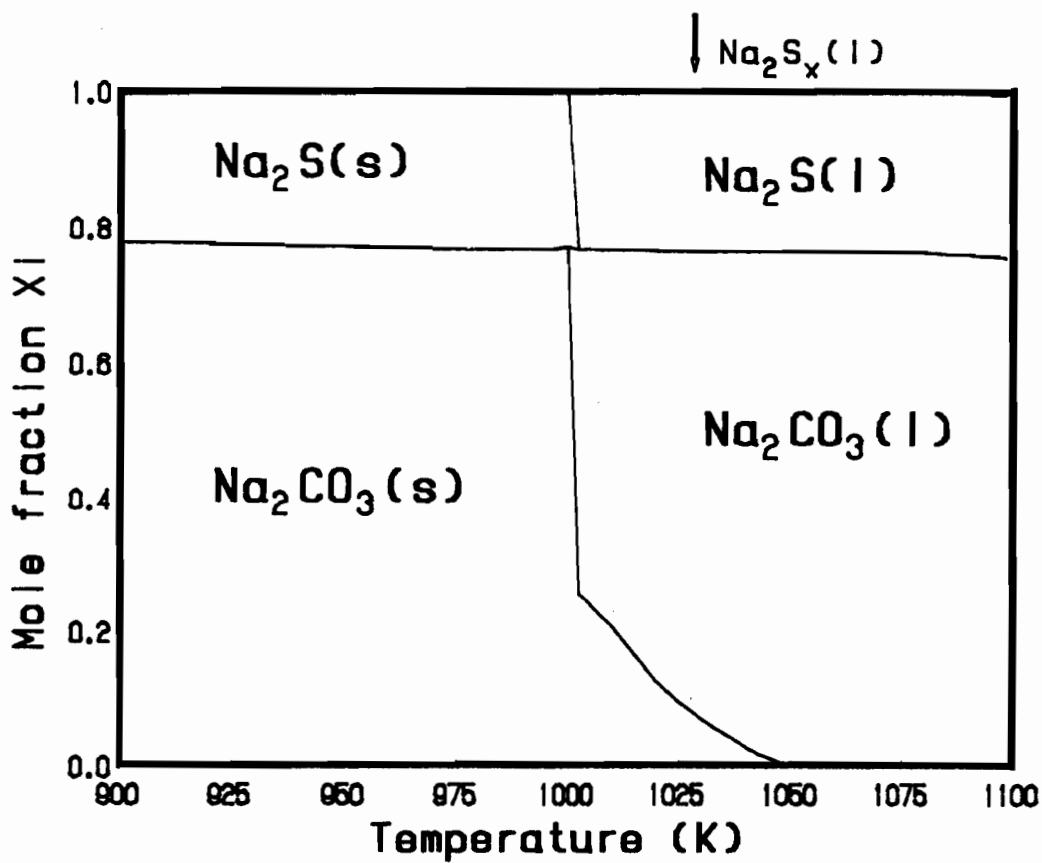
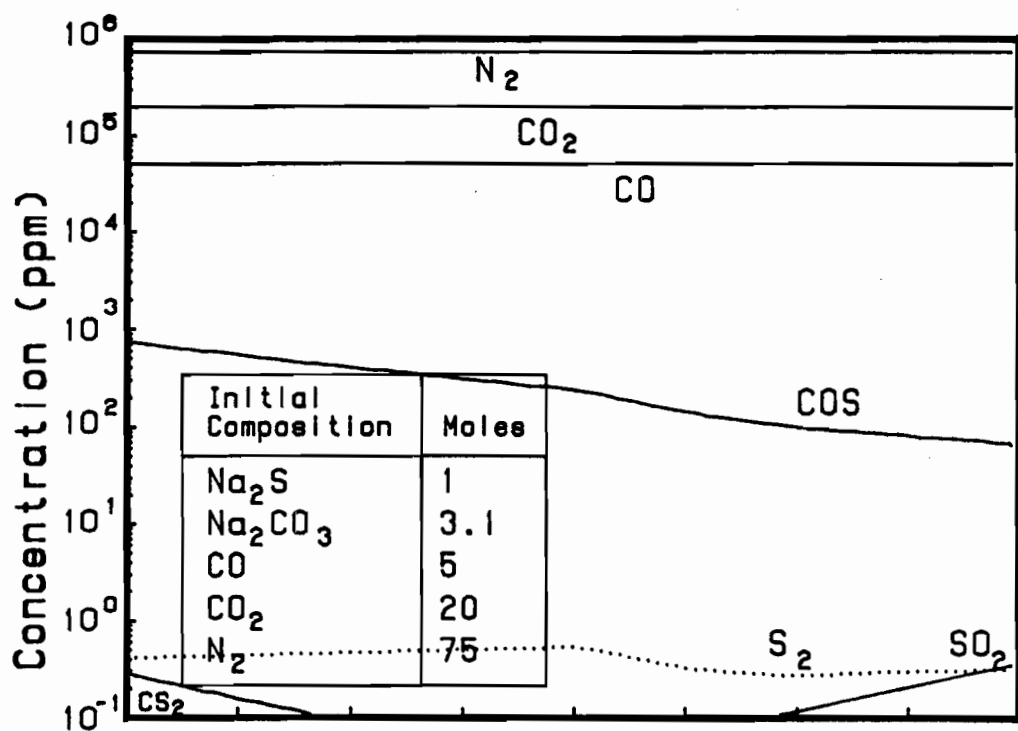


Figure 5, Equilibrium composition as function of temperature in CO₂ gasification.

Shown in Figure 5 is the effect of temperature on sulfur emission at approximately constant CO and CO₂ concentrations, [CO]≈5% and [CO₂]≈20%. Over the present temperature range of 900-1100 K, the sulfur containing gases with concentration higher than 1 ppm are COS, S₂, SO₂ and CS₂. [S₂] is about two to three orders of magnitude lower than [COS]. Only a small amount of SO₂ and CS₂ is formed at respectively below 940 K and above 1050 K. The COS concentration decreases over the entire temperature range, while S₂ is not affected by the system temperature. A liquid phase is formed above 1000 K.

Based on these calculation, the equilibrium composition of sulfur species for a system simulating CO₂ gasification of black liquor char in a TGA set-up can be summarized as follows: a) COS, S₂ and SO₂ are the major sulfur containing gases while only a very small amount of CS₂ is formed at low temperatures and high [CO₂]; b) COS formation decreases with increasing temperature and decreasing CO₂ concentration. c) Sulfur emission in the form of S₂ and SO₂ can be important without the presence of CO.

From the data shown in Figure 5, the equilibrium constants for reactions (3), (4) and (5) can be calculated as function of temperature as:

$$\log K_{\text{COS}} = 7.727 - 5428 / T \quad (6)$$

and

$$\log K_{\text{SO}_2} = - 0.9916 + 9437 / T \quad (7)$$

for 900 < T < 1100 K.

And

$$\log K_{\text{S}_2} = 5.100 + 976.5 / T \quad (8)$$

for 900 < T < 1000K.

where K_{COS} , K_{S_2} and K_{SO_2} are defined as

$$K_{\text{COS}} = \frac{[\text{COS}]}{[\text{CO}_2]^2}; \quad K_{\text{S}_2} = \frac{[\text{S}_2] [\text{CO}]^2}{[\text{CO}_2]^4}; \quad K_{\text{SO}_2} = \frac{[\text{SO}_2] [\text{CO}]^3}{[\text{CO}_2]^4} \quad (9)$$

EXPERIMENTAL RESULTS AND DISCUSSION

Sulfur Mass Balance

Because elemental sulfur, S_2 , could not be measured with the present experimental system and analysis techniques, COS was the only sulfur containing component detected in the off-gas during gasification. Shown in Table II are the sulfur mass balances for several experiments. W_S^o is the amount of sulfur in the sample at the start of gasification, W_{SGC} is the cumulative amount of sulfur removed with the off-gas as COS, W_{SIC} is the amount sulfur in the gasification residue, W_{St} is the sum of W_{SGC} and W_{SIC} , and ΔW_S the percent difference between W_S^o and W_{St} .

Table II. SULFUR MASS BALANCE

No	T ($^{\circ}$ C)	[CO ₂] (%)	[CO] (%)	W_S^o (mg)	W_{SGC} (mg)	W_{SIC} (mg)	W_{St} (mg)	ΔW_S (%)
41	998	20	4.8	0.245	0.21	0.01	0.22	- 10
33	998	15	5.0	0.194	0.209	< 0.005	0.209	+ 7.7
34	998	11.0	4.6	0.237	0.217	0.03	0.247	+ 4.2
35	998	5.4	4.6	0.241	0.115	0.148	0.263	+ 9.1
17	998	19.8	1.0	0.226	0.077	0.03	0.107	- 53
43	998	18.8	9.6	0.210	0.204	< 0.005	0.204	- 3
19	998	19.5	14.6	0.234	0.211	< 0.005	0.211	- 9.4
22	948	20	5.0	0.222	0.149	< 0.005	0.150	- 32
20	973	20	5.0	0.201	0.161	0.01	0.171	- 20
23	1023	20	4.9	0.233	0.153	0.056	0.209	- 10

As can be seen from Table II, there are some cases in which the sulfur mass balance closure is off by more than 20%. The explanation for the large value of ΔW_S in run No.17 is that a large amount of elemental sulfur, S_2 , was produced in this experiment performed at a relatively low CO concentration of 1%. This is based on the thermodynamic prediction in Figure 4, which shows that the molar concentration of S_2 is not negligible compared to that of COS at such a low CO concentration. Also since S_2 contains twice the amount of sulfur on a molar basis than COS, formation of S_2 can lead to a

substantial sulfur loss. The other two cases are run No. 22 and 20. The reason for these two large values of ΔW_S is not known, although some of the error might be explained by the high initial peak of COS emission, which could be missed by the present sampling technique. In all other cases the sulfur mass balance in Table II is acceptable, which suggest that the formation of S₂ is negligible when the CO concentration is sufficiently high and the temperature 998 K or higher.

Effect of CO₂ Concentration

The CO₂ gasification of reduced black liquor char was carried out at CO₂ concentrations varying from 5 to 20%, CO concentrations from 0 to 15% and temperatures from 948 to 1023°K. Helium was used as carrier gas in all experiments except one run as will be discussed later.

The COS emission rate, r_{cos} (1/min), is calculated as

$$r_{\text{cos}} = 1.324 \times 10^{-3} \frac{Q}{W_S^0} [\text{COS}] \quad (10)$$

where W_S^0 is the sulfur weight (mg) in the char at the start of gasification, Q the flow rate (standard liter/min), and [COS] the measured COS concentration (ppm). The COS emission rate as function of CO₂ concentration at 998 K and 5% CO is plotted in Figure 6 versus conversion, X, of reaction (3). The COS emission rate at low sulfur conversion increases strongly with increasing CO₂ concentration. Another interesting result in Figure 6 is that the COS formation rate at low CO₂ concentration and relative small values of X is not a function of the amount of sulfur remaining in the char. However when the conversion X or CO₂ concentration is relatively large, the COS emission rate decreases with increasing X. Most experiments were terminated when gasification of carbon is complete, indicated by Fc in Figure 6.

The independence of the COS emission rate on X at low [CO₂] in Figure 6 suggests that either the rate is reaction controlled and zero order in Na₂S, or that the COS concentration is at thermodynamic equilibrium in the char, and the rate is controlled by mass transfer between the sample and carrier gas. Because the sulfur emission rate depends on Na₂S conversion at high [CO₂], it seems unlikely that the sulfur emission is first order in Na₂S. In the other case, the overall measured rate, R(mg/min), must be

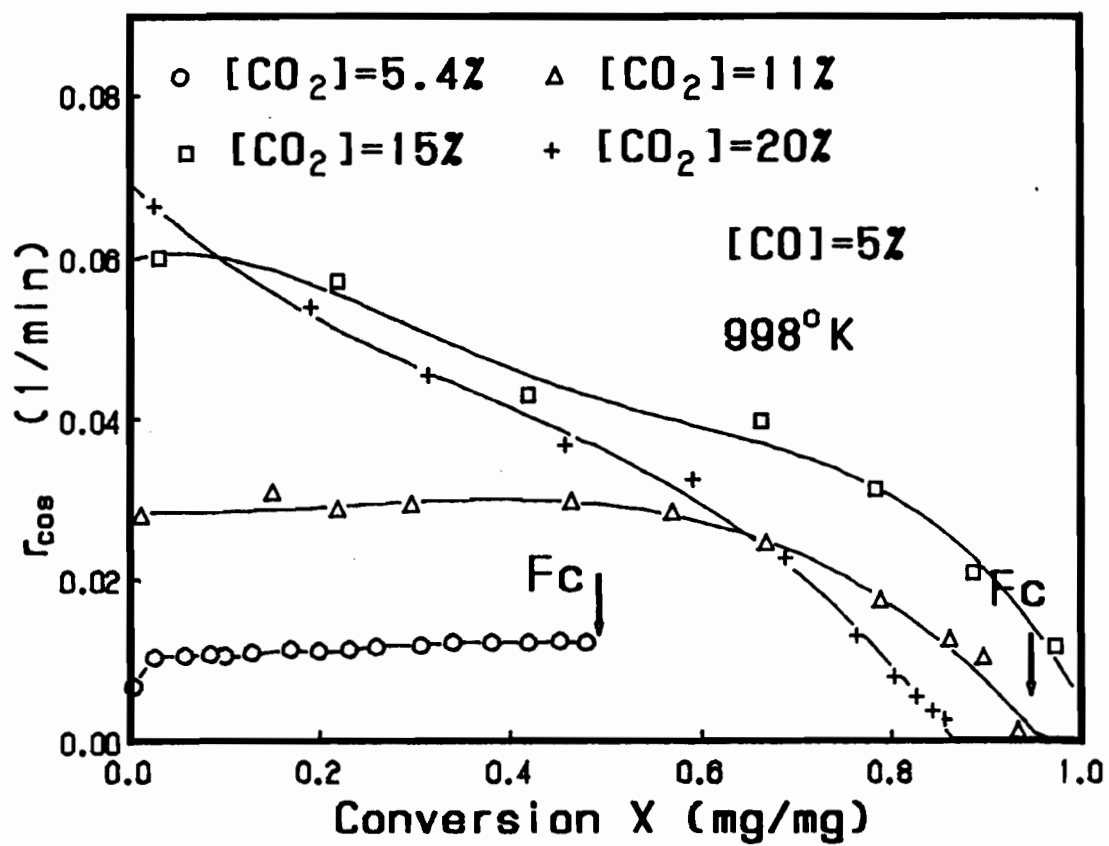


Figure 6, COS production rate as function of [CO₂].

proportional to the thermodynamic equilibrium concentration, $[\text{COS}]_e$, and the external mass transfer coefficient, k_g . According to reaction (3), $[\text{COS}]_e$ should be proportional to $[\text{CO}_2]_e^2$. Thus if the COS concentration in the char bed is at thermodynamic equilibrium, the rate of COS formation, R , can be written as

$$R = S k_g [\text{COS}]_e = S k_g K_{\text{COS}} [\text{CO}_2]_e^2 \quad (11)$$

where S is the exposed char bed surface area. The mass transfer coefficient, k_g , can be obtained from equation (2) and the results are given in Table III. Plotted in Figure 7 is R/k_g against $[\text{CO}_2]$ at small sulfur conversions ($X \approx 0.02$) and $[\text{CO}_2]$ below 15%. Correlation of the data gives

$$R / k_g = S[\text{COS}]_e = 1.74 \times 10^{-5} [\text{CO}_2]^{1.86} \quad (12)$$

The power 1.86 of $[\text{CO}_2]$ is about 7% different from 2 which is required when equilibrium is achieved. This small difference could be due to experimental error and some influence of chemical kinetics at higher $[\text{CO}_2]$. The findings that $R/(k_g \cdot S)$ is almost proportional to $[\text{CO}_2]_e^2$ and that r_{COS} is independent of X at low $[\text{CO}_2]$ (Figure 6) suggest that the COS concentration in the char bed is at thermodynamic equilibrium and that COS emission rate is controlled by external mass transfer rate.

TABLE III. RESULTS OF MASS TRANSFER COEFFICIENTS

$[\text{CO}_2]$ (%)	$[\text{CO}]$ (%)	Q_v (at 295 K) (cc/min)	D (cm^2/s)	Re	Sc	Sh	k_g (m/s)
5.4	4.6	441	2.62	1.50	1.85	3.28	0.086
11	4.6	451	2.32	2.00	1.60	3.39	0.079
15	4.9	453	2.14	2.37	1.47	3.46	0.074

At 20% CO_2 concentration, the COS emission rate depends again on conversion X , indicating that $[\text{COS}]_b$ is not at thermodynamic equilibrium but determined by reaction kinetics.

In order to confirm that COS emission is limited by external mass transfer at relative low $[\text{CO}_2]$, the experiment with 5.4% CO_2 and 4.6% CO in

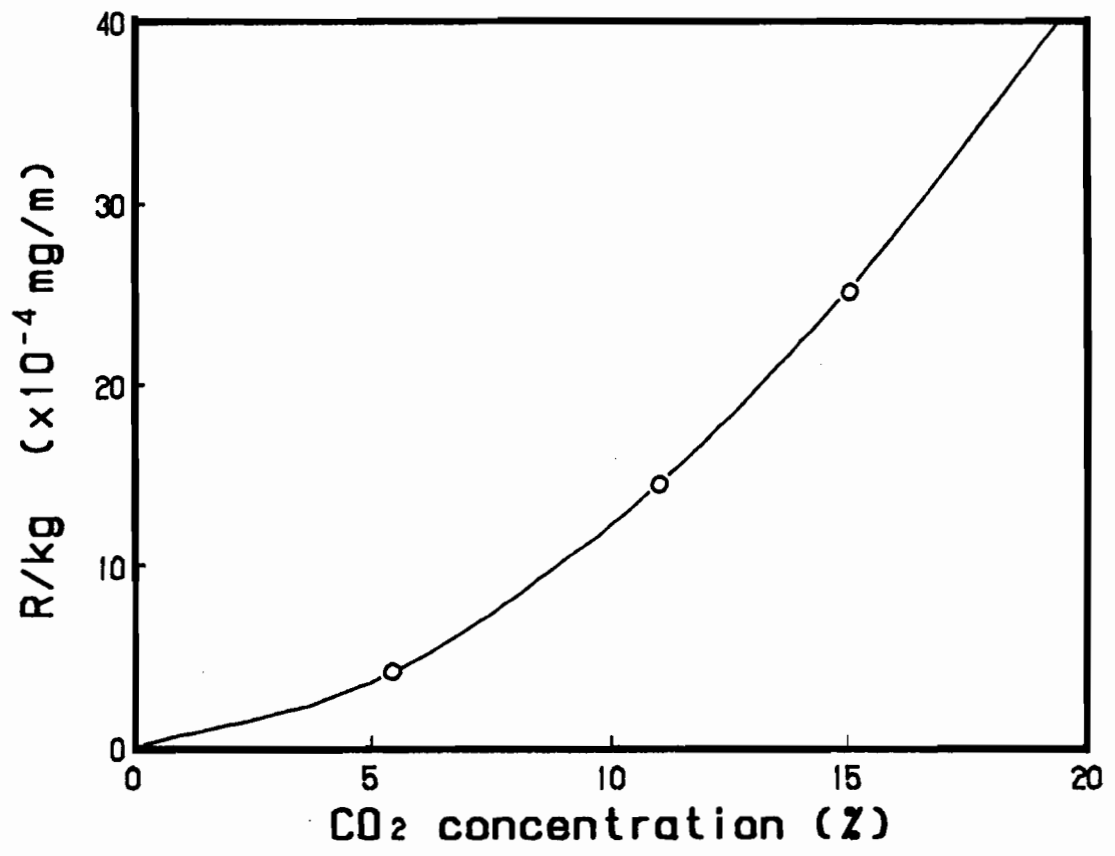


Figure 7, R/kg as function of CO₂ concentration.

helium at 998°K was repeated with nitrogen as carrier gas. The sample weights at the start of CO₂ addition were similar, respectively 4.23 and 4.0 mg. The COS emission for the two experiments are plotted in Figure 8 as emission rate (mg/min), R, against time. It can be seen that the shape of the two curves are almost exactly the same and that the emission in nitrogen is lower than that in helium by a factor of 1.8.

When the COS concentration in the char bed is at thermodynamic equilibrium, the emission rate is controlled by external mass transfer. Since all experimental conditions are the same in the two runs except for the mass transfer coefficient k_g as a result of the different carrier gases, the ratio of the two emission rates is

$$\frac{R_{\text{cos,He}}}{R_{\text{cos,N}_2}} = \frac{k_{g\text{cos-He mix}}}{k_{g\text{cos-N}_2 \text{ mix}}} \quad (13)$$

From equation (2), the mass transfer coefficients for COS in N₂ and He gas mixtures, $k_{g\text{cos-He mix}}$ and $k_{g\text{cos-N}_2 \text{ mix}}$, are calculated as 0.086 and 0.047 m/s respectively. The ratio of 1.83 is exactly the same as the ratio of the measured emission rates. This confirms that the COS emission rate is external mass transfer controlled. The COS emission rate in Figure 8 increases slightly with progress of gasification. This may be explained by a small increase in effective external mass transfer area because of progressive gasification of carbon while a substantial fraction of Na₂S is still unconverted. At complete carbon gasification the Na₂S conversion in He and N₂ are respectively 49 and 27%.

The COS concentration in the char bed can be calculated from the COS concentration in the off-gas and the dilution factor, Ψ , defined by equation (1). With a gas flow rate of 1510 cc/min at 998 K and an exposed surface area of 0.5 cm², the dilution factor for COS in He and N₂ gas mixture are respectively 5.85 and 10.7. Since the COS concentration in the exhaust during the experiments are about 4.6±0.4 and 2.5±0.3 ppm with respectively He and N₂ as carriers gas, the COS concentration in the char bed is calculated as 27 ppm. This compares reasonably well with a value of 17.5 ppm calculated from thermodynamics as shown in Figure 3. The difference between the theoretical and measured [COS] in the char bed is most likely caused by inaccuracies in the thermodynamic data of the FACT program.

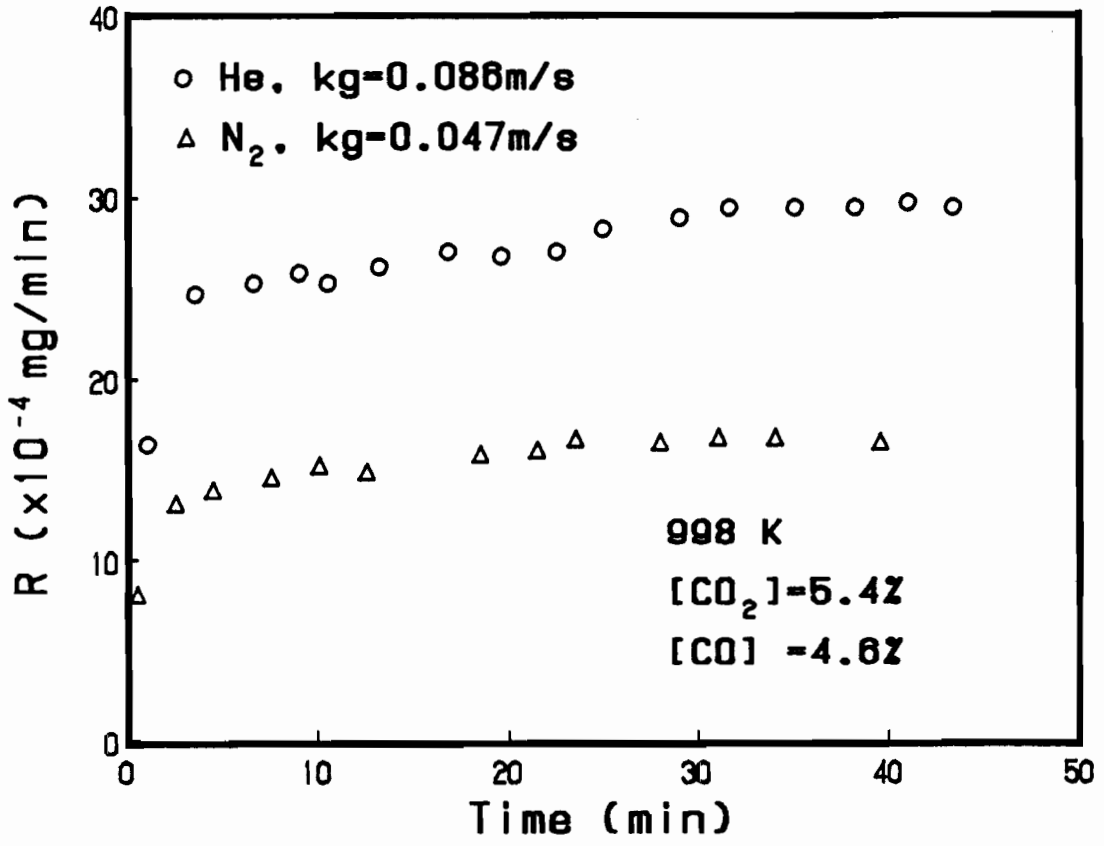


Figure 8, Effect of carrier gas on COS production rate.

Effect of CO Concentration

Shown in Figure 9 is the effect of CO concentration on COS emission rate at 20% CO₂ and 998 K. The results show that at a [CO] of 1% the COS emission rate is much lower than the rate at [CO] above 5%. Another phenomena is that the COS emission rate at [CO] = 1% decreases to a small value even though the Na₂S conversion calculated from integration of the [COS] is far from completion. Both these facts might be explained by formation of S₂ from COS via reaction (4) or (4a). Lowering the [CO] results in a shift of the equilibrium of reaction (4) to the right and a higher [S₂] (Figure 4). At thermodynamic equilibrium, the [COS] in the bed is solely determined by the [CO₂]. Therefore it appears that conversion of COS in S₂ occurs in the hot gas phase downstream of the sample pass via reaction (4a). The lower [COS] at lower [CO] leads to an underestimation of the extend of Na₂S conversion. This is confirmed by analysis of the sample after reaction with 20% CO₂ and 1% CO which showed only 13% sulfur remaining compared to 66% calculated from the original sulfur content and COS emitted. Experiments with higher [CO] show a much better sulfur balance (Table II) indicating that in these cases sulfur emission as S₂ is relatively small compared to sulfur emission as COS. Comparison of the predictions shown in Figure 4 and the data in Figure 9 for [CO]=1% shows that the predicted concentration of S₂ is much lower than suggested from Figure 9. The difference again might be the result of inaccuracies in the thermodynamic data for the gaseous sulfur species, especially S₂.

Effect of Temperature

The COS emission rate as function of sulfur conversion at different temperatures is shown in Figure 10. The CO and CO₂ concentrations are 5% and 20% respectively. At 998 K and lower, the rate decreases with increasing sulfur conversion. However at 1023K the rate is essentially not affected by the sulfur conversion when $X < 0.4$. The reaction rate reduces dramatically at 1023 K when $X > 0.4$, and becomes negligible at $X \approx 0.65$ when all carbon is gasified as indicated by F_c in Figure 10.

It has been shown that [COS]_e decreases with increasing temperature. However chemical reaction rates increase with increasing temperature. Therefore it is expected that at sufficiently high temperature the kinetics of COS formation via reaction (3) are fast enough so that thermodynamic

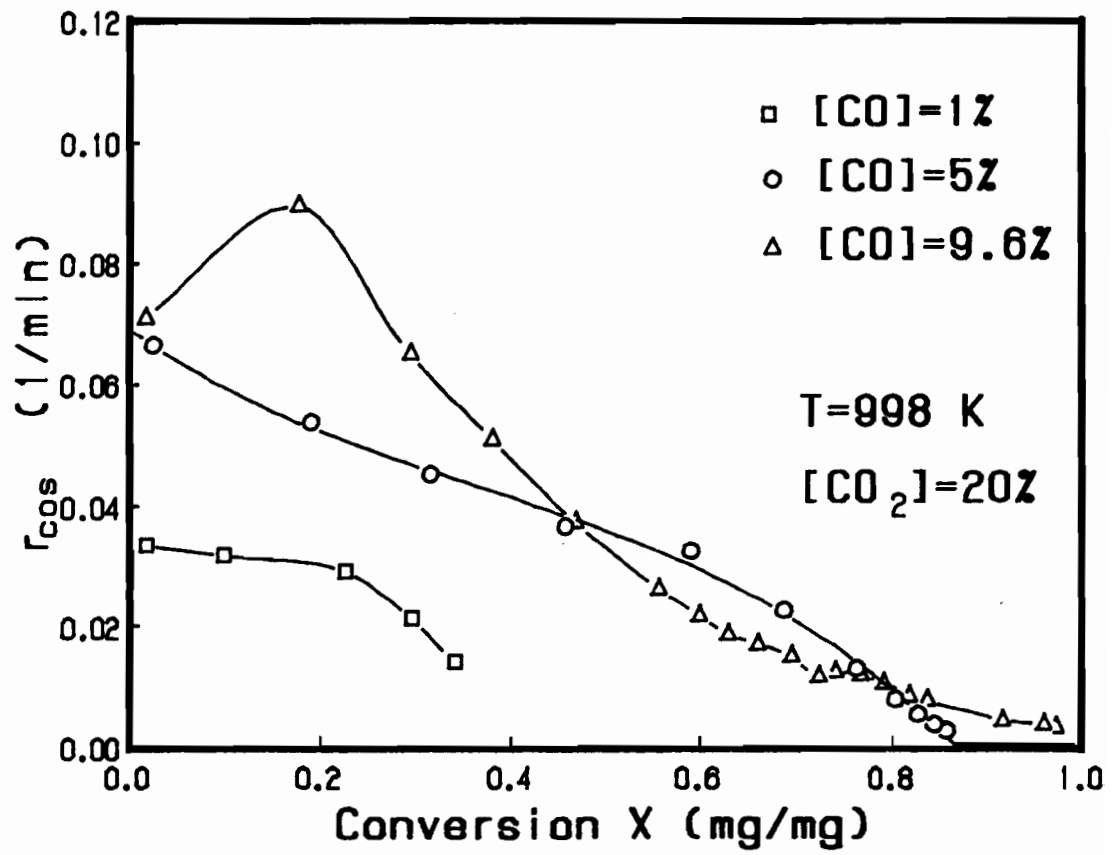


Figure 9, COS production rate as function of CO concentration.

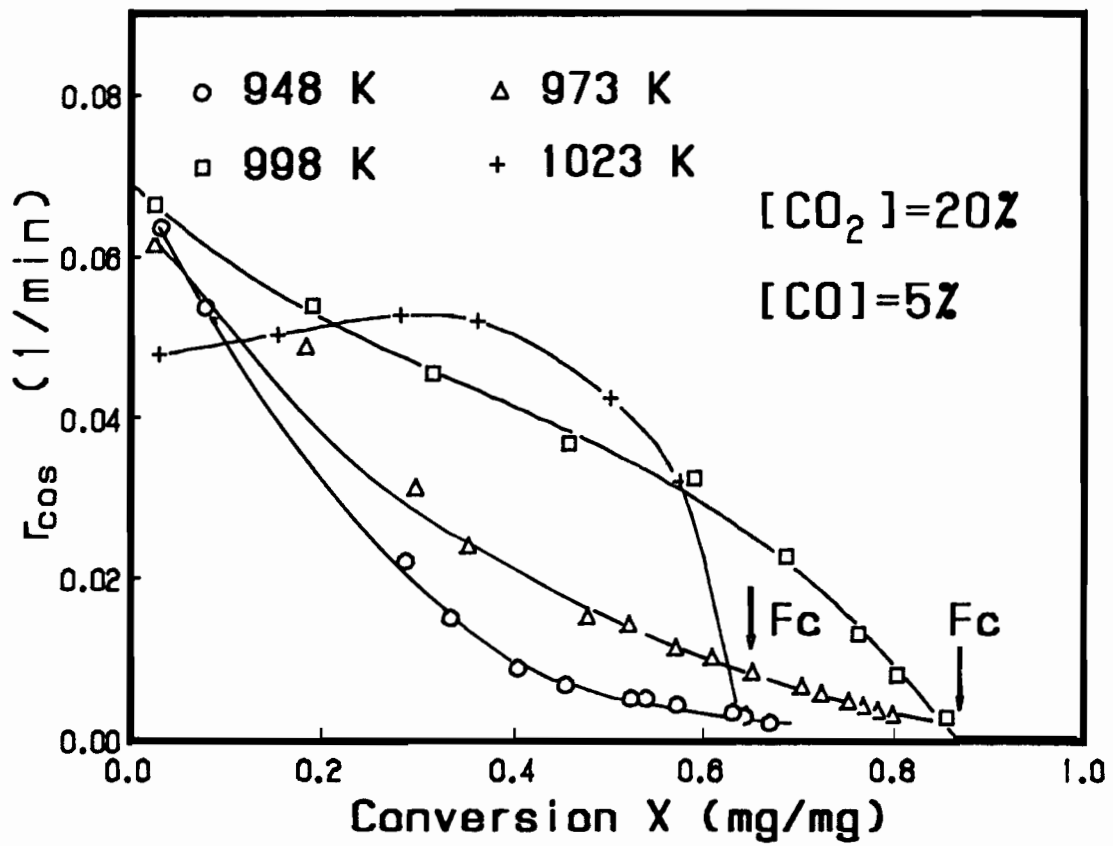


Figure 10, COS production rate as function of Temperature.

equilibrium will be reached and the COS emission rate will be controlled by mass transfer. This might explain why the COS emission at the highest temperature of 1023 K, is not a function of conversion for $X \leq 0.4$. Further confirmation of existence of thermodynamic equilibrium is obtained when the COS concentration in the char bed, $[\text{COS}]_b$, is calculated as $[\text{COS}]_{\text{exh}} \cdot \Psi$ at 20% CO_2 and 1023 K and compared with $[\text{COS}]_b$ calculated from equation (12) with $[\text{CO}_2] = 20\%$ and $S = 0.5 \text{ cm}^2$. These values of $[\text{COS}]_b$ at 1023 and 998°K are respectively 188 ppm and 307 ppm giving a ratio of 0.612. This compares very favorably with the ratio $K_{\text{cos},1023\text{K}} / K_{\text{cos},998\text{K}}$ of 0.606 calculated from equation (6). The good agreement between the two ratios shows that the COS emission rates are consistent with each other assuming thermodynamic equilibrium.

The reason for the rapid decrease in COS formation rate when $X > 0.4$ at 1023°K might be related to the fact that at 1023°K and $X \approx 0.4$ gasification nears completion so that the inorganic salts can form a uniform melt. This was verified by examining the sample remaining after complete carbon conversion which showed a uniform solid mass rather than a powder. The fact that melting took place at 1023 K, 12°C below the eutectic melting point of 1035 K of the $\text{Na}_2\text{CO}_3\text{-Na}_2\text{S}$ system [24] can be explained by presence of potassium (from wood) and other small contaminants. Since mass transfer in the melt is slow, the explanation for the rapid decrease could be that the COS formation is limited by diffusion of CO_2 in the melt.

If the COS emission was governed by thermodynamic equilibrium, the COS emission rate would decrease by a factor 1.7 according to equation (11) when the temperature increases from 948 to 998°K. However, the initial reaction rates at 948, 973 and 998°K are similar, and show a trend opposite to thermodynamics with increasing Na_2S conversion. This behavior might be explained by that at lower temperature and increasing Na_2S conversion the emission rate is limited by reaction kinetics. An Arrhenius plot of the reaction rate at conversions of 20%, 30%, 40% and 50% leads to activation energies increasing respectively from 120 to 230 kJ/mole.

CONCLUSIONS

Based on the present study, the following conclusions can be drawn:

- COS is the major sulfur gas product formed during gasification of

reduced black liquor char by CO₂, while significant amounts of S₂ appear to be formed when the CO concentration is very low.

- According to thermodynamic calculation, some poly-sulfide is formed from Na₂S under CO₂ gasification conditions.
- COS production is promoted by both CO and CO₂; The effect of CO is much smaller and can be explained by the formation of COS from CO and S₂ in the gas phase.
- At relative low [CO₂] and high temperature, the rate of COS formation during gasification of reduced black liquor char is limited by external mass transfer. Under these conditions the COS concentration inside the char is determined by thermodynamics.

NOMENCLATURE

[a] _b	= gas concentration in bed, mol·m ⁻³ .
[a] _{exh}	= gas concentration in exhaust, mol·m ⁻³ .
d _c	= sample pan diameter, m.
D _{a-m}	= diffusion coefficient of "a" in gas mixture, m ² ·s ⁻¹ .
k _g	= mass transfer coefficient, m·s ⁻¹ .
K _{COS}	= equilibrium constant for COS.
K _{S₂}	= equilibrium constant for S ₂ .
K _{SO₂}	= equilibrium constant for SO ₂ .
r _{cos}	= COS emission rate, min ⁻¹ .
R	= over all COS emission rate, mg·min ⁻¹ .
Re	= Reynolds number.
Q	= gas flow rate at standard conditions, sl·min ⁻¹ .
Q _v	= volumetric gas flow rate, m ³ ·s ⁻¹ .
S	= exposed surface area, m ² .
Sc	= Schmidt number.
Sh	= Sherwood number.
T	= temperature, K.
V	= average gas velocity based on reactor tube cross section, m·s ⁻¹ .
W _S ^o	= initial sulfur weight, mg.
W _{Sgc}	= cumulative weight of sulfur removed with off-gas as COS, mg.
W _{Sic}	= amount of sulfur in the gasification residue, mg.
W _{St}	= sum of W _{Sgc} and W _{Sic} , mg.

ΔW_S = percent difference of W_S^o and W_{St} , %.
X = sulfide conversion, mg/mg.

Greek Symbols

Ψ = dilution factor defined by equation (1).
 ρ = density of the gas mixture, $\text{kg}\cdot\text{m}^{-3}$.
 μ = viscosity of the gas mixture, $\text{kg}\cdot\text{m}^{-1}\cdot\text{s}^{-1}$.

REFERENCES

1. Thoen, G.N., and et al, *Tappi*, 51(8), p.329(1968).
2. Walther, J.E. and H.R. Amberg, *Tappi*, 55(8), p.1185(1972).
3. Lang, C.J., and et al, *Tappi*, 56(6), p.115(1973).
4. Lange, H.B., and et al, *Tappi*, 57(7), p.105(1974).
5. Borg, A., and et al, *Tappi*, 57(1), p.(1974)
6. Rosen, E., *Trans. of the Royal Inst. of Technology*, No.223, Stockholm, Sweden, (1964).
7. Pejryd, L., and M. Huppa, 1984 *Tappi Pulping Conf.*, San Francisco, p.1(1984).
8. Feuerstein, D., and et al, *Tappi*, 50(6), p.258(1967).
9. Brink, D.L., and et al, *Tappi*, 50(6), p.276(1967).
10. Brink, D.L., and et al, *Tappi*, 53(5), p.837(1970).
11. Douglass, I.B., and Lawrence Price, *Tappi*, 51(2), p.465(1968).
12. Li, J., *Master Thesis*, McGill University, Canada, (1986).
13. Strohbeen, D.T., *Ph. D. Thesis*, IPC, Appleton, US, (1981).
14. Cantrell, J.G., and et al, *AICHE 1986 Fall National Meeting*, Boston, E5(1986).
15. Fallavolita, J.A., and et al, *Can. J. Chem. Eng.*, 65(Oct.), p.815(1987).
16. De Souza, T.L.C., and et al, *Anal. Chem.* 47(3), p.543(1975).
17. Li, J., and A.R.P. van Heiningen, *Can. J. Chem. Eng.*, 67(Aug), p.693(1989).
18. Li, J., and A.R.P. van Heiningen, *Mat. Res. Soc. Symp. Proc.*, Vol. 111, p.441(1988).
19. Li, J. A.R.P. van Heiningen, *Carbon'88*, Newcastle, UK, p.428(1988).

20. Li, J., and A.R.P. van Heiningen, *JPPS*, 12(5), p.J146(1986).
21. Eriksson, G., *Chemica Scripta*, 8, p.100(1975).
22. Barin, I., and et al, *Thermochemical Properties of Inorganic Substances*, Springer-Verlag, Berlin, (1977)
23. Warnqvist, B., *Thermochemica Acta*, 37, p.343(1980).
24. Backman, R., *Ph. D. Thesis*, ABO AKADEMI, Finland, (1989).

CHAPTER 6

SULFUR EMISSION DURING STEAM GASIFICATION OF BLACK LIQUOR CHAR

ABSTRACT

The sulfur emission during steam gasification of pyrolyzed and reduced black liquor was studied in a thermogravimetric analysis set-up from 600 to 700°C. H₂S is the only detectable sulfur containing gas product. Below 650°C all Na₂S is converted into H₂S. The H₂S concentration is at thermodynamic equilibrium with the gasification gas mixture. H₂S production rate is controlled by the carbon gasification rate. The influence of temperature, H₂O and H₂ concentration on H₂S emission rate follow thermodynamic prediction. Good agreement between experimental and theoretical equilibrium constants suggests that Warnqvist's Na₂S property data are more accurate than those previously used. An equation is derived which can closely predict the H₂S emission rate. The implications of the present results for an alternative low temperature fluidized bed recovery process involving carbon gasification are discussed.

INTRODUCTION

In several proposed alternative kraft chemical recovery processes [1-3], gasification has been suggested as one of the process steps. It has been shown that gasification of black liquor char can be performed at relative low temperatures because its reactivity is probably the highest among all carbonaceous materials [4-7, and chapters 3 and 4]. However there are still a number of questions which have to be answered in order to prove the feasibility of the process. Probably the most important question is what the effect of gasification conditions is on the fate of sulfur in the char.

Although many studies concerning sulfur emission from the conventional kraft recovery process have been reported [chapter 5], very little information is available about sulfur emission during black liquor char gasification, especially with steam. The only data for steam gasification of black liquor was reported by Durai-Swamy et al [2] who employed a so-called pulse-enhanced indirect gasification process. They found that most of the sulfur was emitted as H_2S at gasification temperatures between 550 to 630°C. Other relevant data on sulfur emission during CO_2 gasification of black liquor char were presented in the previous chapter and the M. Eng. thesis of the present author [4]. It was shown that COS was the major sulfur gas formed at relatively high CO concentration and that S_2 is likely also an important part of sulfur emission at low CO concentration. It was also shown that the COS concentration reached thermodynamic equilibrium in a char bed of 0.5 mm height at low CO_2 concentrations and higher temperatures [chapter 5]. As result, the COS emission was controlled at these conditions by external mass transfer to the char bed.

In the present study, sulfur emission during steam gasification of black liquor char was studied as function of steam and hydrogen concentrations, temperature and carbon gasification rate.

EXPERIMENTAL

Shown in Figure 1 is a schematic picture of the Cahn TGA 113-DC thermogravimetric balance with auxiliary gas preparation system used for

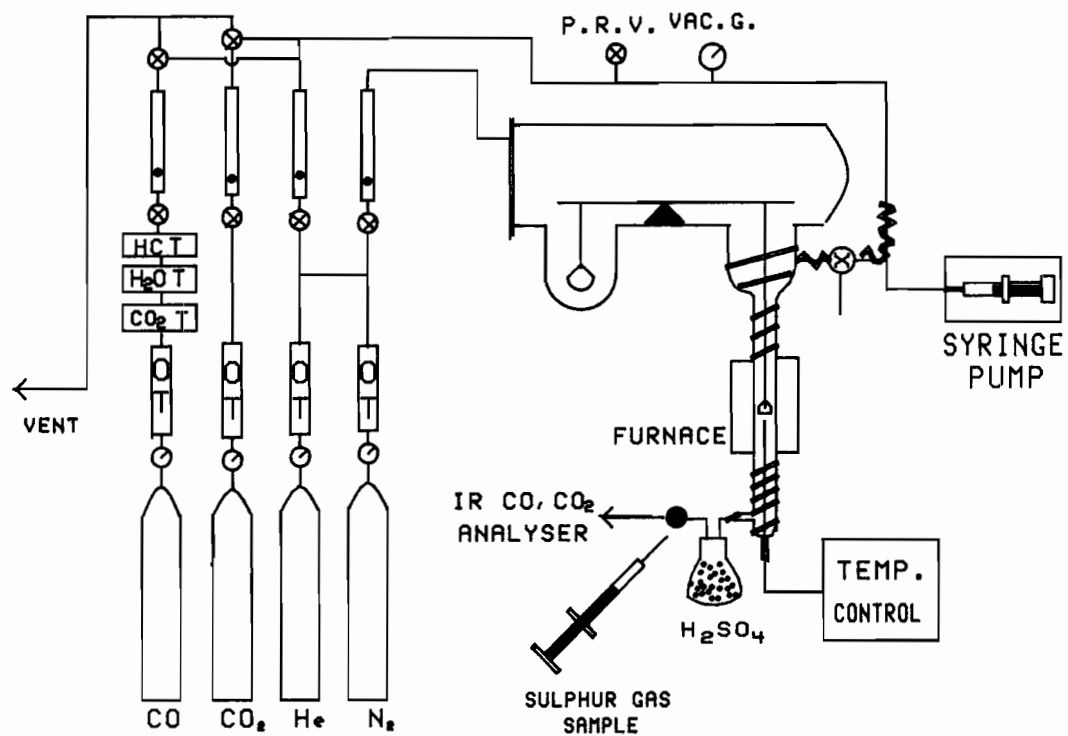


Figure 1, Schematic picture of the TGA system.

steam gasification of kraft black liquor char. A Fisher gas partitioner was used for fixed gas analysis. A Hewlett Packard GC with FPD and an 18 inch column with acetone washed poropack QS packing operated at 45°C was used for sulfur gas analysis [8]. The initial sample and gasification residues were analyzed with a Dionex IC with CD and ECD for sulfate, sulfite, sulfide, thiosulfate, carbonate, sodium and potassium content.

An oxidized black liquor char with particle size <25µm was used. Detailed information concerning the sample preparation can be found in chapter 3. Shown in Table I is the chemical composition of the black liquor solids, char and reduced char.

TABLE 1 CHEMICAL COMPOSITION OF BLACK LIQUOR SOLIDS, CHAR AND REDUCED CHAR

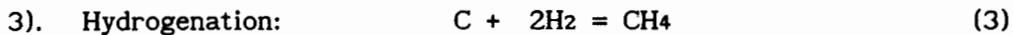
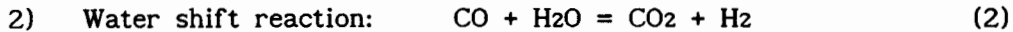
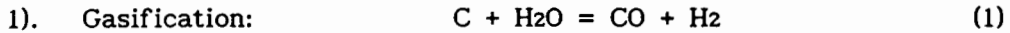
	[Na ⁺] (%)	[SO ₄ ⁼] (%)	[S ⁼] (%)	[CO ₃ ⁼] (%)	[S ₂ O ₃ ⁼] (%)
solids	18.6	8.13	< 0.1	7.2	< 0.05
char	25.4	13.5	< 0.1	28	< 0.05
reduced char	34.2	< 0.1	5.7	34	< 0.0

After addition of about 5 mg char (BLC) to the pan of the TGA equipment, the system was flushed with N₂ for about 1 hr at a flow rate of 400 scc/min to remove any air. The furnace temperature was then raised from 20°C to 775°C at a rate of 25°C/min under a N₂ flow rate of 400 scc/min. At about 500°C, 25 scc/min of CO was added to the carrier gas to prevent Na₂CO₃ decomposition [5]. After 2 minutes at 775°C the reduction of Na₂SO₄ to Na₂S was complete, and the temperature was reduced to the required gasification temperature. When the temperature and sample weight were stabilized, the CO flow was turned off. After CO was flushed out of the system in 10 to 15 minutes, a mixture of steam, hydrogen and nitrogen was added to the system to start a gasification experiment. At the start of gasification the char consists of 13.9% Na₂S, 60% Na₂CO₃ and 25% organic carbon. This corresponds to a molar composition of 1 Na₂S : 3.1 Na₂CO₃ : 11 C. Further information concerning the experimental procedures and gasification reactions can be found in chapter 4 of this thesis.

THERMODYNAMIC ANALYSIS OF THE REACTION SYSTEM

System Analysis

Under steam gasification conditions, the following reactions occur simultaneously:



At temperatures of 850 to 1000 K, the carbon gasification is controlled by reaction kinetics [chapter 4] and the water shift reaction is close to equilibrium for alkali carbonate catalyzed gasification [chapter 4]. Methane formation is negligible according to the equilibrium calculations.

The equilibrium constants of reaction (4) and (2) are respectively:

$$K_1 = \frac{[H_2S]_e}{[H_2O]_e \cdot [CO_2]_e} \quad (5)$$

$$K_2 = \frac{[CO_2]_e \cdot [H_2]_e}{[CO]_e \cdot [H_2O]_e} \quad (6)$$

where all concentrations are in mole fraction. Neglecting the formation of methane and assuming that all carbon added to a confined system is gasified, the following equation is valid when the system is at equilibrium:

$$N_c / N_g = [CO]_e + [CO_2]_e + [H_2S]_e \quad (7)$$

where N_c and N_g are respectively the moles of carbon added to the system and the total moles in the gas phase at equilibrium. Combining equations (5), (6) and (7) and eliminating $[CO]_e$ and $[CO_2]_e$, the equilibrium H_2S concentration can be expressed as:

$$[\text{H}_2\text{S}]_e = \frac{K_1 [\text{H}_2\text{O}]_e^2 (N_c / N_g)}{[\text{H}_2\text{O}]_e + K_1 [\text{H}_2\text{O}]_e^2 + [\text{H}_2]_e / K_2} \quad (8)$$

The major advantage of equation (8) is that when a reactor is operated differentially with respect to $[\text{H}_2]$ and $[\text{H}_2\text{O}]$ the H_2S equilibrium concentration can be easily calculated from the operation conditions. Equation (8) shows that the equilibrium H_2S concentration is linearly proportional to the amount of carbon added to the system. It is also important to note that $[\text{H}_2\text{S}]_e$ is not linearly proportional to $[\text{H}_2\text{O}]$ as expected from equation (5), but it is changing from 2nd order at low $[\text{H}_2\text{O}]_e$ to zero order at high $[\text{H}_2\text{O}]_e$. Increasing H_2 concentration has a decreasing effect on the equilibrium H_2S concentration.

FACT Program and Thermodynamic Data of Na_2S

Thermodynamic calculations were performed with the latest version of SOLGASMIX [9] which is the equilibrium part of the FACT program on the McGill University MUSIC system. Pejryd [10] has given a detailed description of the calculation procedure and strategy of the program and will not be repeated in the present paper.

It was noticed that the thermodynamic property data for Na_2S used in this program was taken from "Thermochemical Properties of Inorganic Substances" [11]. The melting point T_m , standard enthalpy $\Delta G_{298\text{K}}$ and melting enthalpy ΔH_m of Na_2S are listed as 1251 K, -374.468 kJ/mol and 26.359 kJ/mol respectively. It has been reported by Warnqvist [12] that these values are incorrect because they were obtained with impure Na_2S . With better experimental technique, Warnqvist reported that for Na_2S the T_m , ΔG_{298} and ΔH_m are 1443 ± 10 K, -386.6 kJ/mol and 30.1 kJ/mol respectively. With this new data for Na_2S included in the same program, Backman [13] found that the phase diagram for system Na_2CO_3 - Na_2S - Na_2SO_4 agreed closely with experimental results. It was also shown by the present author that predictions of sulfur emission for CO_2 gasification of black liquor char obtained with the FACT program using Warnqvist's data were more in agreement with experimental results than when using the old data for Na_2S [chapter 5]. Therefore, Warnqvist's data for Na_2S was used in the following thermodynamic calculations.

The initial composition of the reaction system is 1.0 mole of Na₂S, 3.1 moles of Na₂CO₃, 100 moles of a mixture of H₂, H₂O and N₂ and a variable amount of carbon. The system pressure was kept at one atmosphere. The calculated equilibrium H₂S concentration will be presented versus amount of carbon added with temperature and H₂ and H₂O addition as parameters.

It was found in all cases that the COS and SO₂ concentrations were at least two orders of magnitude smaller than the H₂S concentration. The methane concentration was more than two orders of magnitude smaller than the CO or CO₂ concentration. All carbon added was gasified. N_g was always between 99 to 100 moles because only 1 mole of Na₂S and less than 0.5 mole of carbon were added to the system. As a result, N_w and N_h, respectively the number of moles of H₂O and H₂ added to the system, were numerically almost equal to [H₂O]_e and [H₂]_e expressed in vol.%. Only small values of N_c/N_g (≤0.005) were investigated to allow comparison with the results obtained in the differentially operated TGA system. From a mass balance it follows that an equilibrium concentration of about 10,000 ppm H₂S corresponds to complete conversion of reaction (4).

Thermodynamic Results

Shown in Figure 2 is [H₂S]_e as function of temperature. It shows that [H₂S]_e decreases with increasing temperature and increases approximately linearly with amount of carbon added. The small deviation from the linear behavior required according to equation (8) is due to small changes in H₂ and H₂O concentration at equilibrium as a result of reactions (1) and (2). At 998 K, a liquid phase is formed, and a certain amount of Na₂CO₃ is converted into liquid NaOH according to:



Thus more CO₂ is available to convert Na₂S according to reaction (4), and [H₂S]_e will be higher. This can be noticed in Figure 2 where at low carbon addition the [H₂S]_e at 998 K is higher than the [H₂S]_e at 973 K. This effect becomes smaller at higher carbon addition because the presence of more CO₂ will shift reaction (9) to the left. The formation of a liquid phase reduces K₁ slightly. The equilibrium constant, K₁, of reaction (4) can be correlated over the temperature range of 850 K to 1000 K by:

$$\log K_1 = -7.210 + 6.426 \times 10^3 / T \quad (10)$$

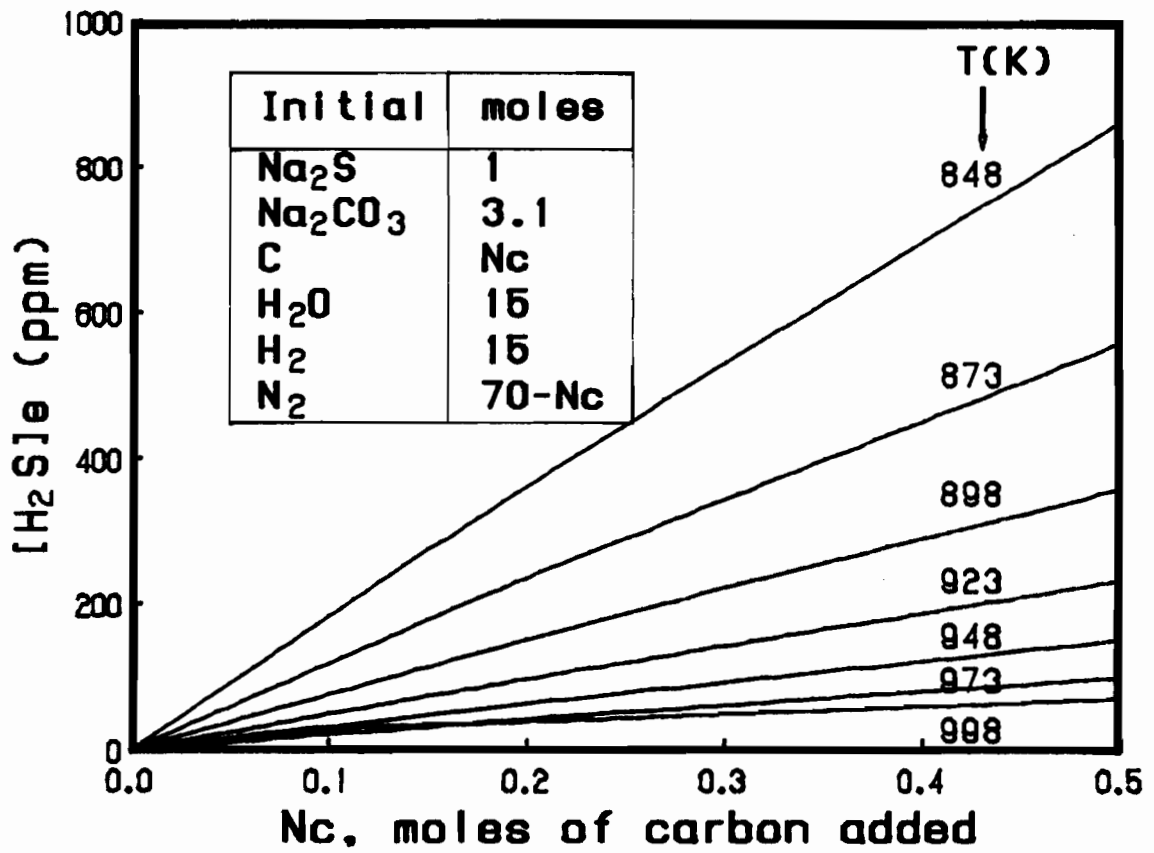


Figure 2, $[\text{H}_2\text{S}]_e$ as function of temperature.

Shown in Figure 3 is $[H_2S]_e$ as function of H_2 addition at 923K. $[H_2S]_e$ decreases with increasing H_2 addition. However the effect is rather small and decreases with increasing H_2 addition, which is expected according to equation (8).

Shown in Figure 4 is $[H_2S]_e$ as function of the amount of H_2O added at 923 K. As expected according to equation (8), $[H_2S]_e$ increases strongly with H_2O addition at low H_2O concentrations, i.e. $[H_2S]_e$ doubled when $[H_2O]$ only increased from 5 to 7.5%. At high H_2O concentrations, the $[H_2O]$ effect on $[H_2S]_e$ becomes smaller, i.e. when $[H_2O]$ increased from 15 to 30%, $[H_2S]_e$ doubled in value.

Correlation of K_2 obtained from the equilibrium concentration gave

$$\log K_2 = -1.761 + 1.886 \times 10^3 / T \quad (11)$$

with T in $^{\circ}K$. This correlation for the equilibrium constant of the water-shift reaction agrees closely with those in literature [14].

EXPERIMENTAL RESULTS

Sulfur Mass Balance

The gasification was studied at steam concentrations of 7 to 30%, H_2 concentrations of 0 to 20% and temperatures from 873 to 973 $^{\circ}K$. H_2S concentrations varying between 0.3 and 60 ppm were detected in the exhaust gas during gasification. The COS and SO_2 concentrations were less than the detection limit of 0.1ppm. The sulfur mass balance was checked for every experiment by comparing the measured total sulfur content before and after gasification and the total amount of sulfur emitted as H_2S during gasification. Shown in Table II are sulfur mass balance results for six experiments. In the table, W_S° is the amount of sulfur in the initial sample, W_{SGC} the amount of sulfur in the off-gas in the form of H_2O , W_{IC} the amount sulfur in the gasification residue, W_{St} the sum of W_{SIC} and W_{SGC} , and ΔW_S the difference between W_{St} and W_S° divided by W_S° in percent.

As can be seen from Table II, the over all sulfur mass balance agrees within 10%. Except run No. 15, the total amount of sulfur as H_2S is larger than the sulfur loss calculated for the solid analyses by 7 to 10%. This suggests that there might be a systematic error in the sulfur analysis.

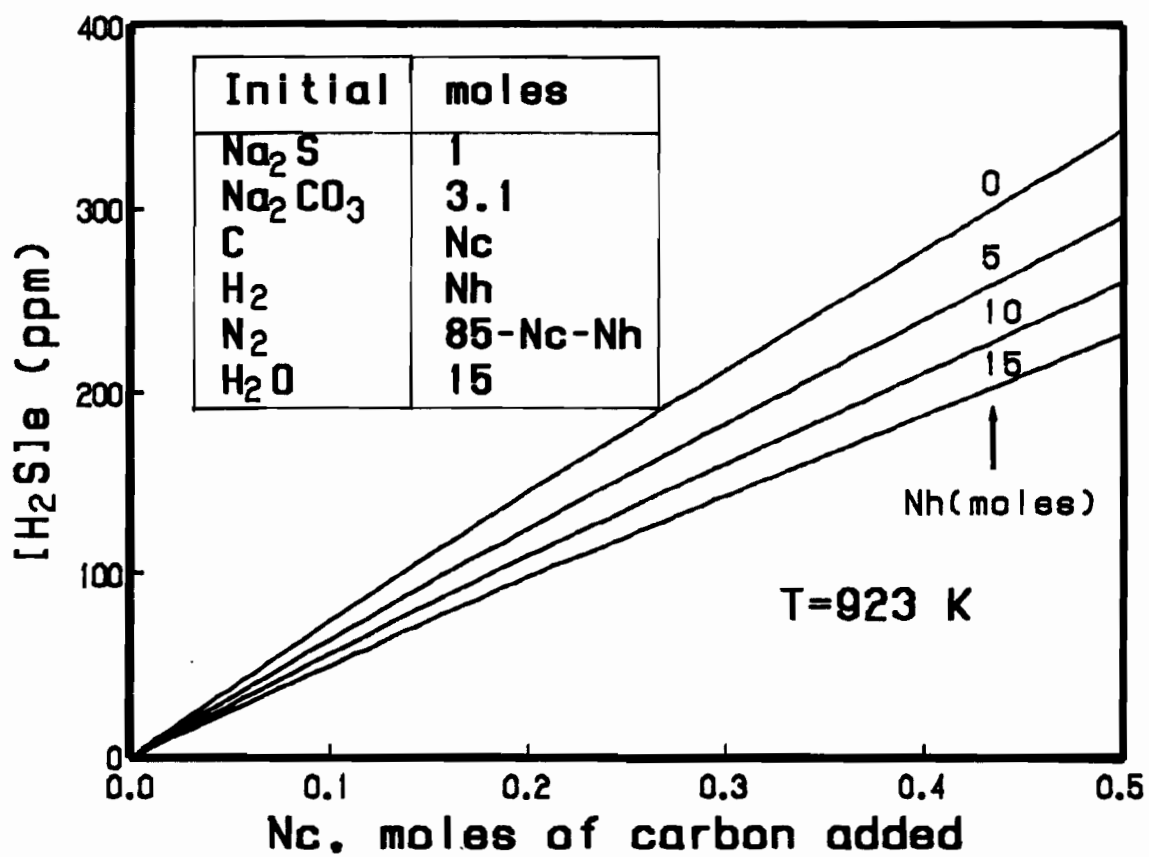


Figure 3, [H₂S]_e as function of H₂ addition.

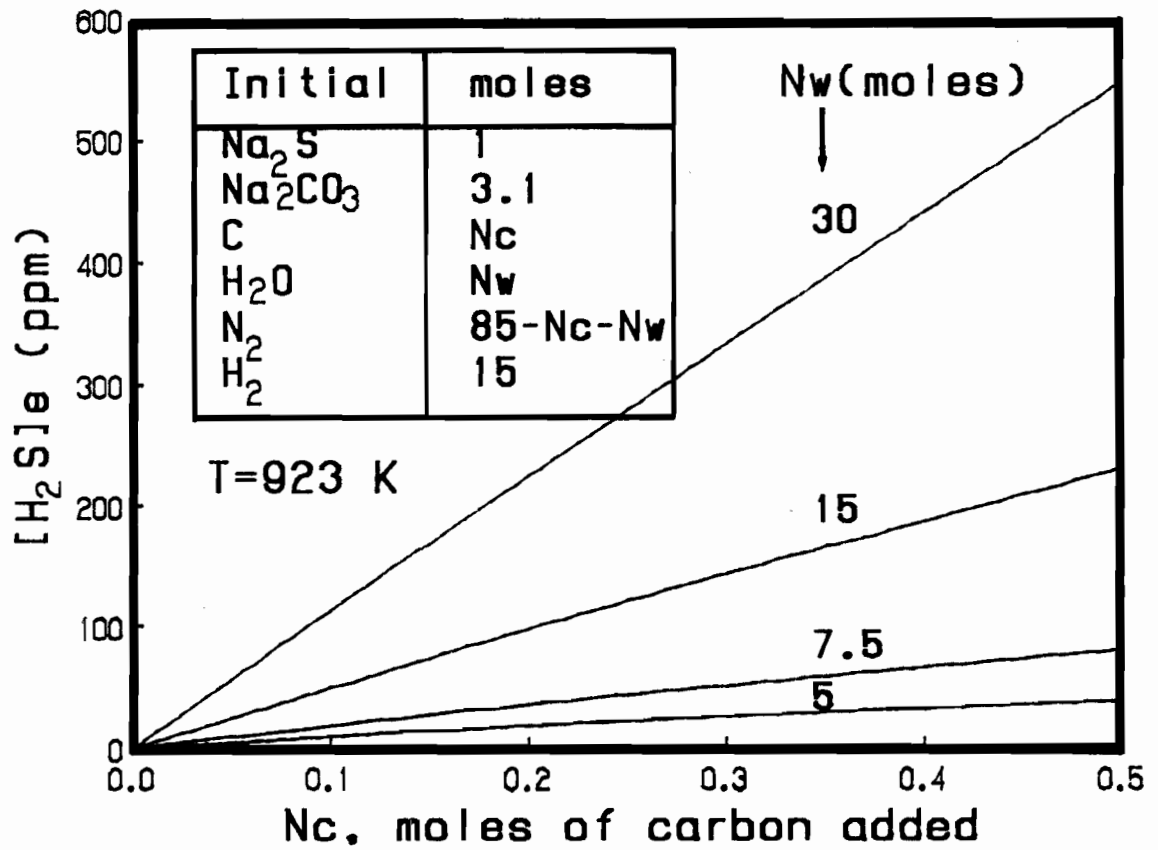


Figure 4, [H₂S]_e as function of H₂O addition.

Table II. SULFUR MASS BALANCE

No	T (K)	[H ₂ O] (%)	[H ₂] (%)	W _S ^o (mg)	W _{SGC} (mg)	W _{SIC} (mg)	W _{St} (mg)	ΔW _S (%)
17	923	6.8	14	0.334	0.360	0.01	0.37	+ 10
15	923	14.7	12.6	0.37	0.303	0.03	0.333	- 10
14	873	15.0	15.0	0.457	0.496	0.008	0.504	+ 10
13	973	15.0	15.1	0.235	0.108	0.144	0.252	+ 7.2
12	898	15.0	15.1	0.314	0.338	0.000	0.338	+ 7.6
11	948	15.0	15.1	0.267	0.206	0.08	0.286	+ 7.1

Effect of Temperature

The H₂S production rate, $r_{\text{H}_2\text{S}}$ (1/min), is calculated as

$$r_{\text{H}_2\text{S}} = 1.324 \times 10^{-3} \frac{Q}{W_S^o} [\text{H}_2\text{S}] \quad (12)$$

where W_S^o is the sulfur weight (mg) in the char at the start of gasification, Q the flow rate (standard liter/min), and $[\text{H}_2\text{S}]$ the measured H₂S concentration (ppm).

The rate of H₂S production versus Na₂S conversion, X , as function of gasification temperature is plotted in Figure 5. The input gas composition was 15% H₂ and 15% steam in N₂. All these gasification experiments were terminated when carbon was completely gasified as indicated by F_c in Figure 5. It can be seen that the H₂S emission rate is still significant at $X=1.0$ and 873 and 898°K. This behavior can be explained by a systematic positive error in the gaseous sulfur analysis of about 10%. The rate of H₂S production increases with increasing temperature up to 923°K, while at higher temperatures a decrease in reaction rate was observed. It is important to note that the H₂S production stops where all carbon is gasified indicated by F_c at about 76 and 46% Na₂S conversion at respectively 948 and 973°K.

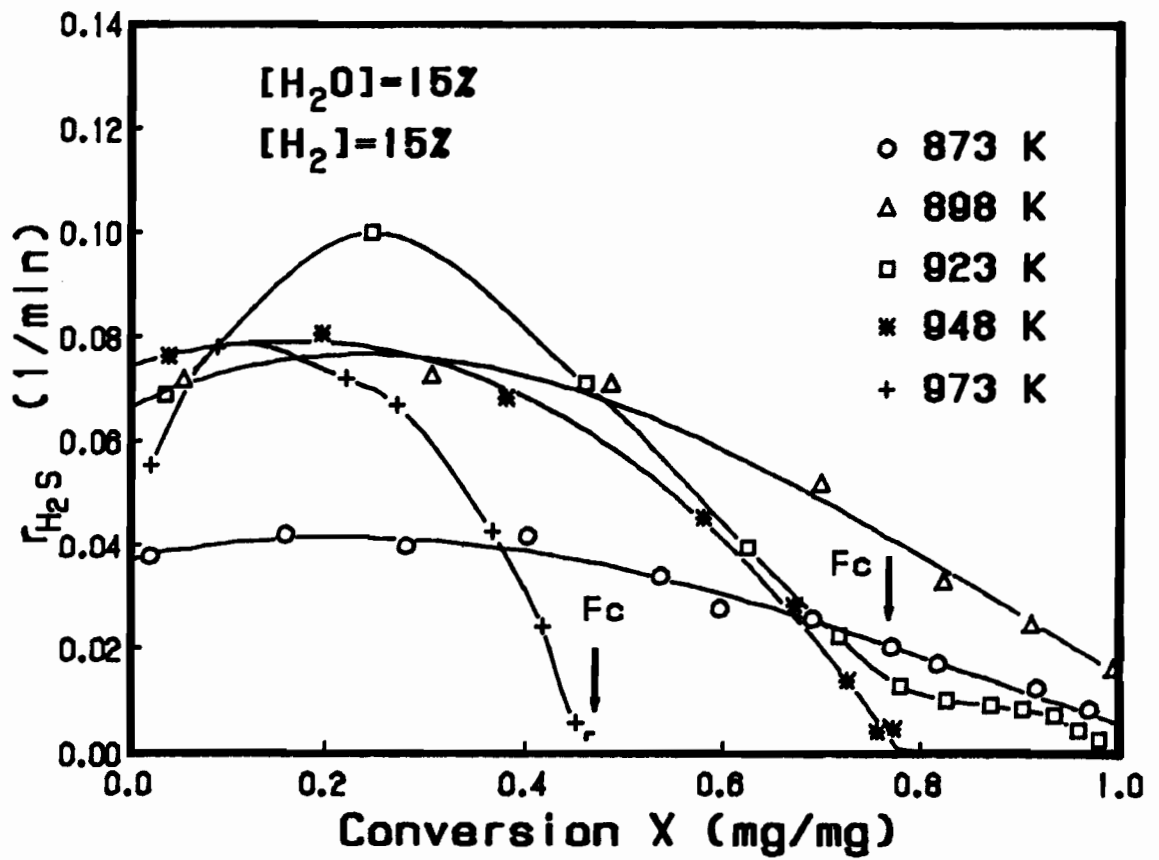


Figure 5, Effect of gasification temperature on H₂S emission.

Effect of Steam Concentration

Shown in Figure 6 is the H₂S formation rate as a function of steam concentration at T=923°K and [H₂]=15%. At relatively low Na₂S conversion the rate increases with increasing steam concentration. However at high conversion of Na₂S the dependence of the H₂S emission rate on the steam concentration is reversed.

Effect of Hydrogen Concentration

The effect of H₂ concentration on H₂S formation at 923°K and 15% H₂O concentration is shown in Figure 7. The finding that the experimental H₂S formation rate is strongly influenced by the H₂ concentration is not in agreement with thermodynamic predictions.

DISCUSSION

The H₂S emission rate shown in Figure 5 reaches a maximum at 923 K, indicating that the H₂S emission rate cannot be controlled by chemical kinetics and that another step must be rate limiting. As shown by equation (8) and the thermodynamic predictions, the H₂S emission is directly proportional to the amount of carbon available in the system. So when all carbon is gasified, H₂S emission should stop. This is confirmed by the results obtained at 948 and 973 K shown in Figure 5.

Since CO₂ is needed for H₂S production (equation (4)) and all CO₂ is formed by the water-shift reaction, $r_{\text{H}_2\text{S}}$ should be indirectly influenced by both the carbon gasification rate and K₂. This effect can be eliminated by dividing $r_{\text{H}_2\text{S}}$ in Figure 5 by the total CO₂ formation rate, $r_{\text{CO}_2}^{\circ}$, defined as the rate of CO₂ formation before any CO₂ has been consumed by reaction (4). The normalized H₂S rate, $r_{\text{H}_2\text{S}}/r_{\text{CO}_2}^{\circ}$, is shown in Figure 8 as function of temperature versus Na₂S conversion. Contrary to the results in Figure 5, the normalized H₂S rate in Figure 8 decreases continuously with increasing temperature, in agreement with the thermodynamics of reaction (4).

Similar to equation (7), the following equation is valid

$$r_c^* / Q = [\text{CO}] + [\text{CO}_2] + [\text{H}_2\text{S}] \quad (7a)$$

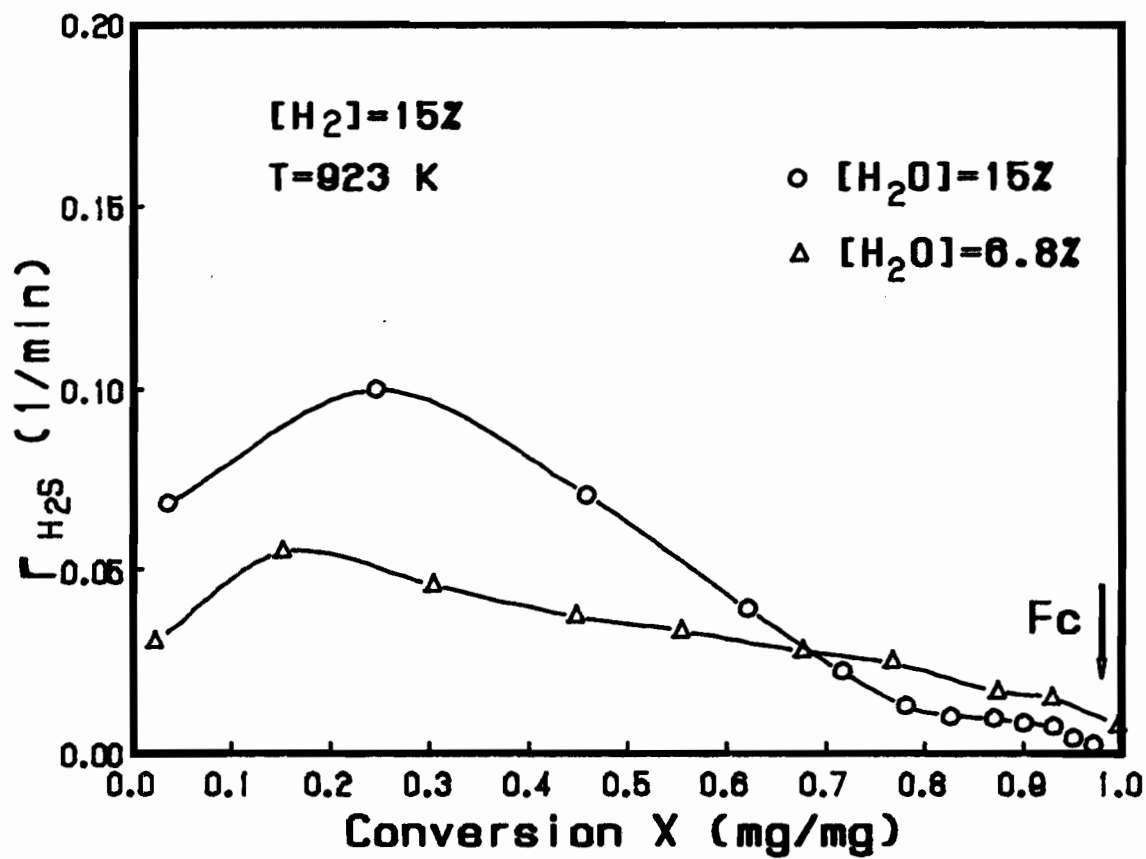


Figure 6, Effect of $[H_2O]$ on H_2S emission rate.

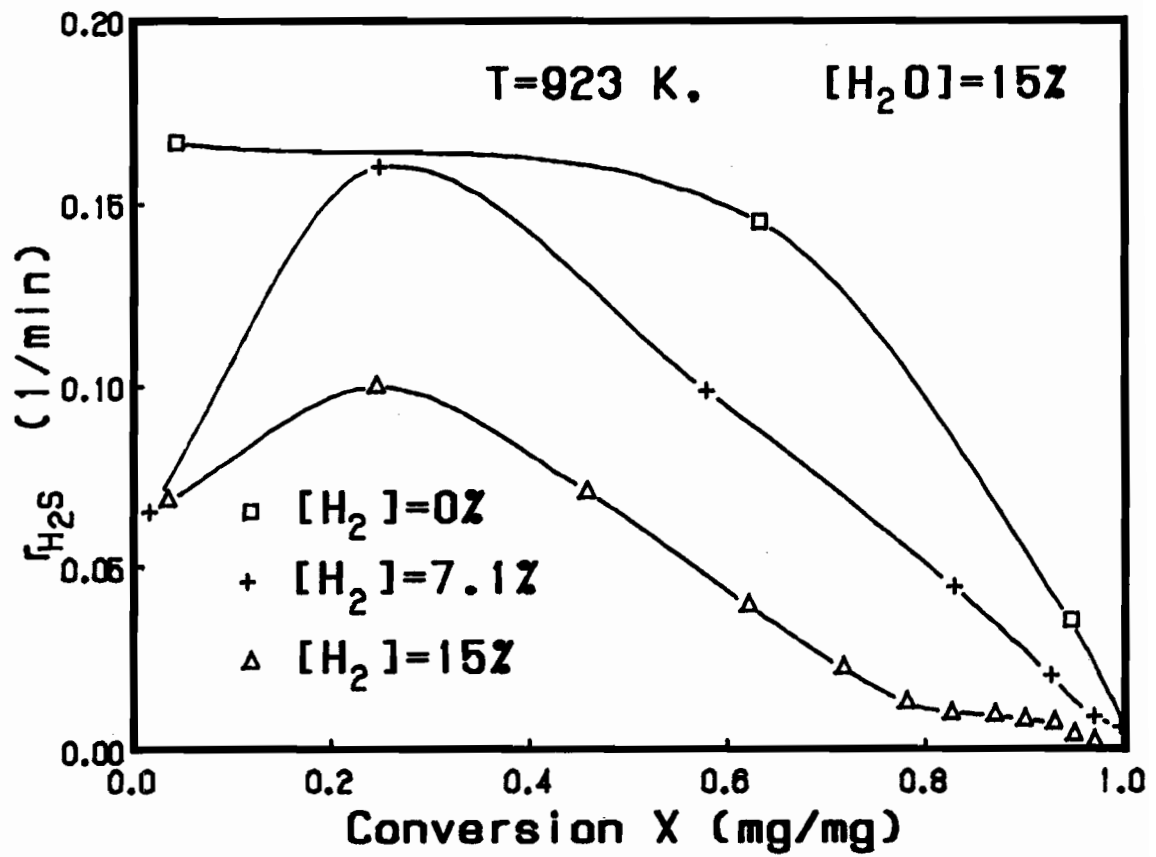


Figure 7, Effect of [H₂] on H₂S emission rate.

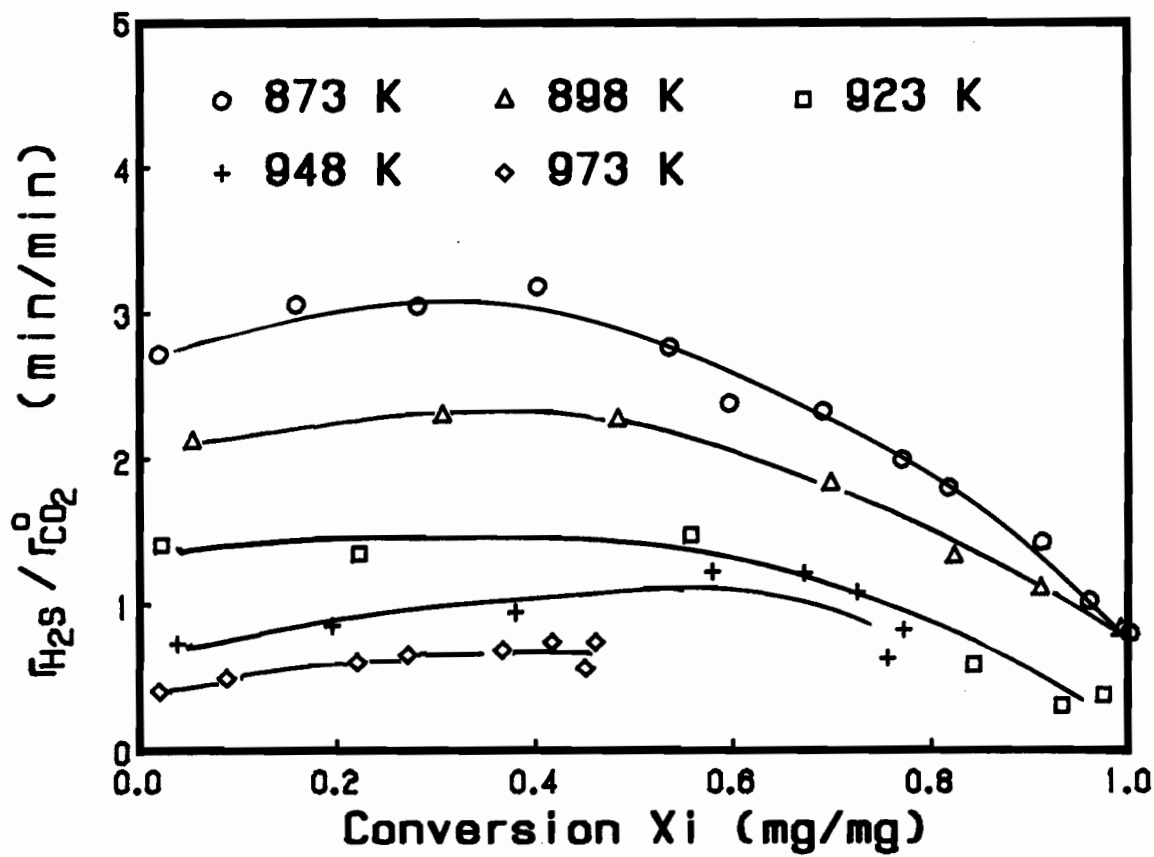


Figure 8. The normalized H₂S production rate as function of temperature.

where r_c^* is carbon gasification rate in mol/min, and Q total gas flow rate in mol/min. If the concentrations of H₂S, CO and CO₂ in the char bed are at equilibrium, then the H₂S production rate, r_{H_2S} , can be calculated based on a modified form of equation (8) as

$$r_{H_2S}^{(1/min)} = \frac{K_1 [H_2O]^2 (-r_c) \alpha \frac{M_s}{M_c}}{[H_2O] + K_1 [H_2O]^2 + [H_2]/K_2} \quad (8a)$$

where $(-r_c)$ is the carbon gasification rate in (1/min), α the weight percentage ratio of carbon and sulfur in the remaining black liquor char at time t, M_s and M_c the molecular weight of sulfur and carbon. K_1 and K_2 can be calculated with equations (10) and (11). From the kinetic study of carbon gasification [chapter 4], it was found that at 15% H₂O and 15% H₂, the carbon gasification rate can be expressed as

$$(-r_c) = 0.017 \text{ Exp} \left[\frac{E_a}{R} \left(-\frac{1}{873} - \frac{1}{T} \right) \right] \quad (13)$$

where E_a the apparent activation energy of gasification (210 kJ/mol), R the gas constant and T the temperature in K.

The H₂S production rate calculated with equations (8a) (10), (11) and (13) is compared with the measured rate at X=0.1 in Figure 9. The trend of the predicted H₂S production rate is similar to the measured rate but its value is smaller by factor of 1.3 to 2. This may be result of a number of factors. The first is that there might be still a small error in the theoretical equilibrium constant for reaction (4). Secondly, the ten times higher experimental value [chapter 4] for the water shift equilibrium constant, K_2 , will result in a higher H₂S production rate. This is shown in Figure 9 where the recalculated H₂S production rate with 10K₂ is much closer in agreement with the measured rate. The third factor is that the [H₂S]/[CO₂] ratio in the bed is lower than in the bulk gas because the external mass transfer coefficient, k_{g,H_2S} , for H₂S is slightly higher than the k_{g,CO_2} for CO₂ resulting from the difference in diffusion coefficients (D_{H_2S} =1.59 cm²/s at 923 K and D_{CO_2} =1.39 cm²/s at 923 K in this gas mixture). The lower ratio leads to a higher H₂S production rate. However, this error is smaller than 15%.

Further confirmation of existence of thermodynamic equilibrium for H₂S

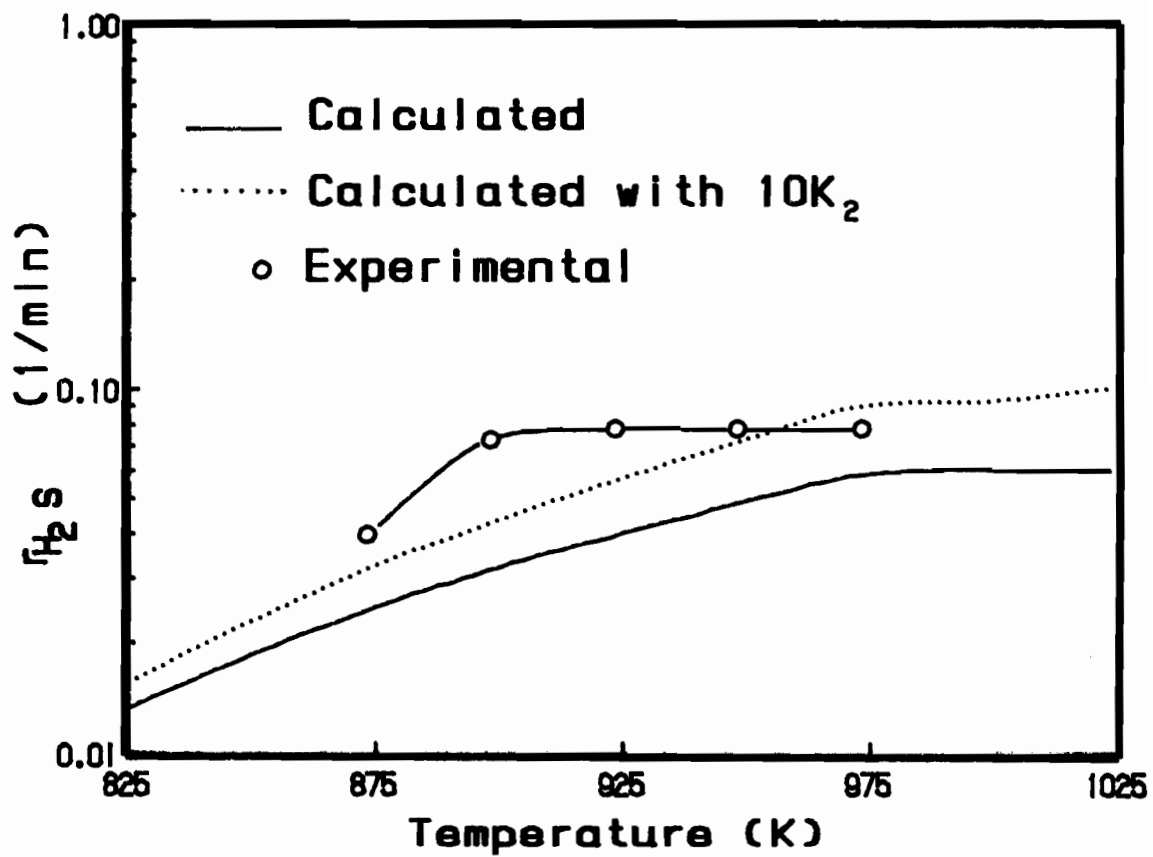


Figure 9. Calculated and measured H₂S production rate.

is obtained by calculating the ratio of the equilibrium constant K_1 and the experimental constant $K_{1e}=[\text{H}_2\text{S}]/[\text{H}_2\text{O}][\text{CO}_2]$ determined from concentrations in the exhaust. Shown in Figure 10 is K_1/K_{1e} as function of Na_2S conversion at different temperatures. Mostly the values of K_1/K_{1e} are between 0.5 to 1 for all temperatures and Na_2S conversions up to about 50%, indicating that the H_2S concentration is at thermodynamic equilibrium. The reasons why K_1/K_{1e} is slightly lower than 1 might again be due to a small error in K_{1e} and the difference in diffusion coefficients. The effect of the CO_2 concentration being higher than thermodynamic equilibrium has been eliminated in Figure 9 because the measured CO_2 was used in the calculations.

Shown in Figure 11 is the normalized H_2S production rate $r_{\text{H}_2\text{S}}/r_{\text{CO}_2}^0$ versus X at two steam concentrations. Contrary to $r_{\text{H}_2\text{S}}$ in Figure 6, the normalized H_2S production rate does not depend on Na_2S conversion over a wide range of Na_2S conversions, which again indicates that the H_2S concentration is at thermodynamic equilibrium. The increase in normalized H_2S production rate with steam concentration is less than predicted by thermodynamics (Figure 3). Part of this difference might be due to experimental error.

Shown in Figure 12 is the normalized H_2S production rate at different $[\text{H}_2]$. This figure confirms that the normalized H_2S production rate is not influenced by the $[\text{H}_2]$ as expected from both thermodynamics and the overall reaction equation. Thus, the strong effect of H_2 on the H_2S production in Figure 7 can be attributed to the combined effect of decreasing CO_2 concentration and carbon gasification rate with increasing $[\text{H}_2]$ [chapter 4].

CONCLUDING REMARKS

During steam gasification of reduced black liquor char, Na_2S is converted into H_2S via reaction (4)



Over the range of conditions studied, the H_2S concentration in the char bed appears to be in thermodynamic equilibrium with steam and CO_2 , the later being produced by carbon gasification. Therefore, the H_2S emission rate is governed by the thermodynamic equilibrium of reaction (4), carbon gasification kinetics and gasification product distribution.

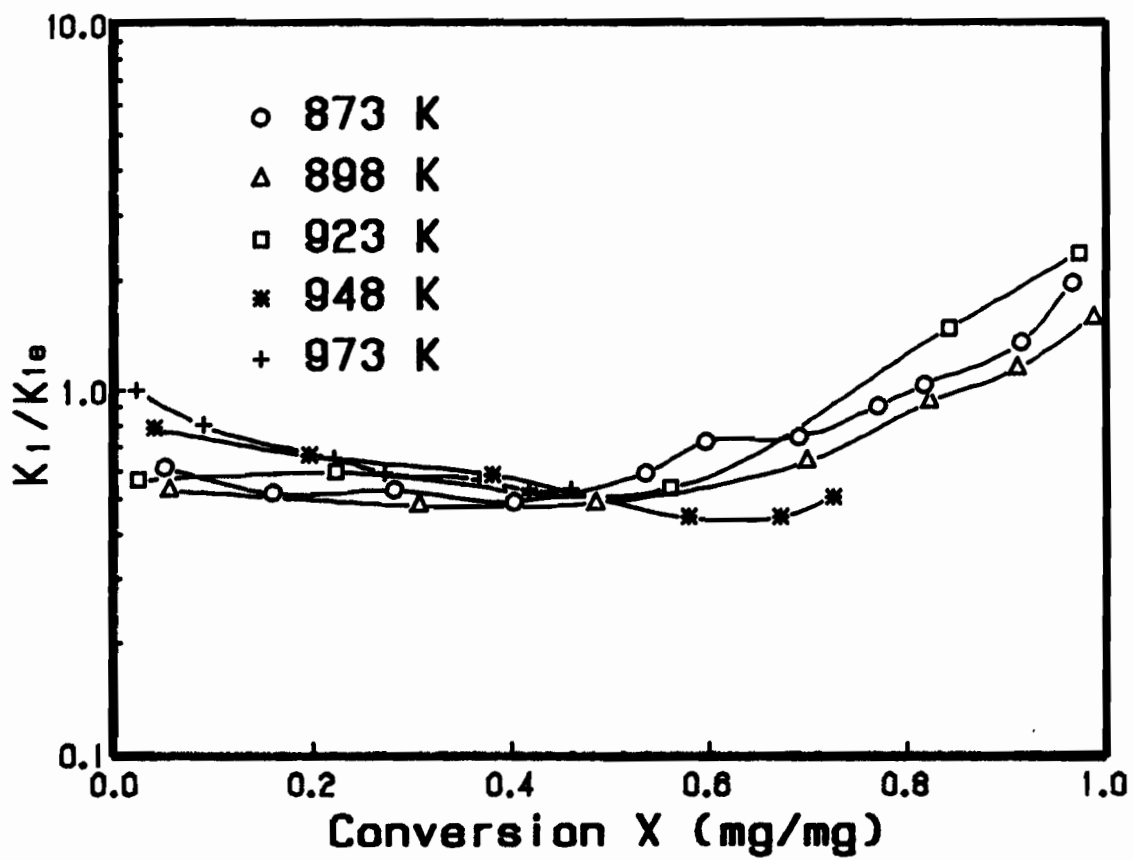


Figure 10. Comparison of theoretical and experimental equilibrium constant

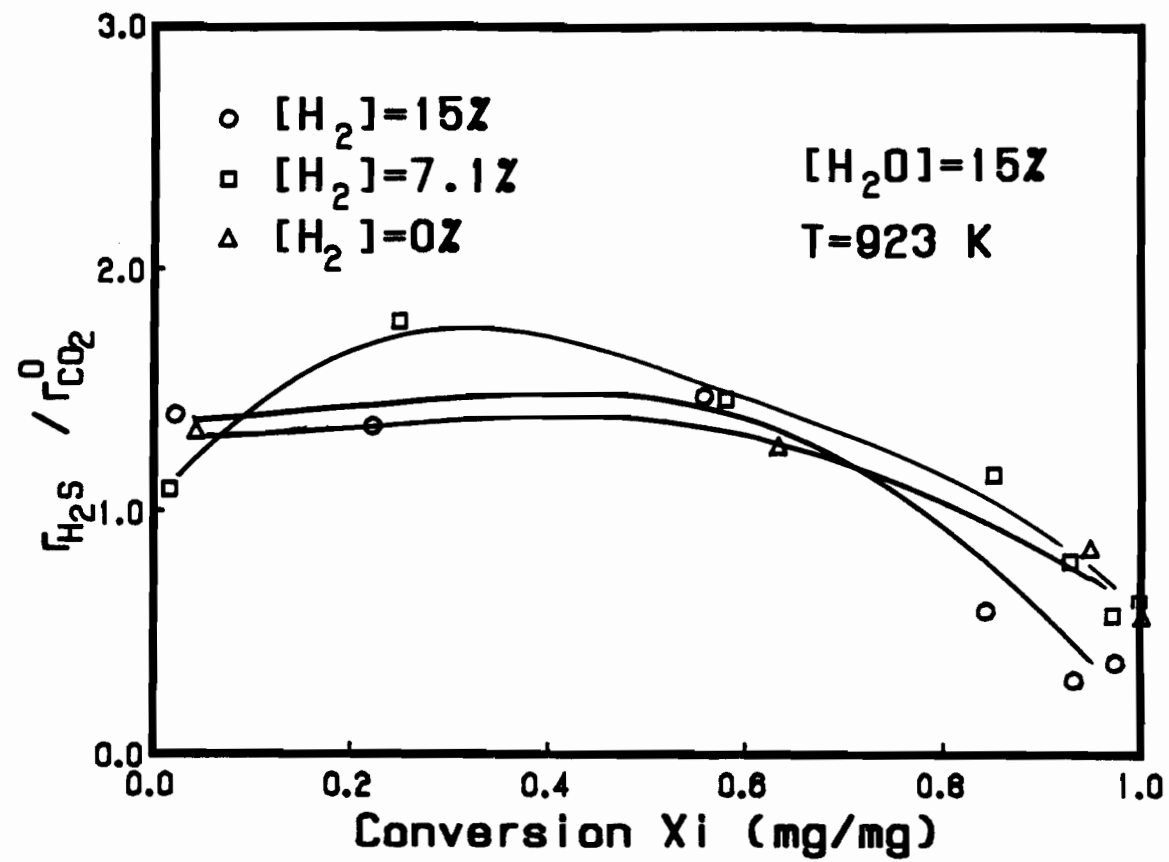


Figure 12. The effect of $[H_2]$ on normalized H_2S production rate.

IMPLICATIONS

The high sulfur emission rates measured in the present study demonstrate that gasification of black liquor char below the melting point of the inorganics will mostly lead to complete loss of sulfur to the gas phase. The emission will especially be high when both steam and CO₂ are present at high concentration. This indicates that partial or complete gasification or pyrolysis of black liquor char should be performed below the onset formation of Na₂S from Na₂SO₄. The presence of steam and CO₂ should then be minimized during the subsequent reduction step. An alternative is to volatilize all sulfur during the gasification of black liquor char and preferentially absorb H₂S from the product gas with a solution of Na₂CO₃.

NOMENCLATURE

D	= diffusion coefficient, m ² ·s ⁻¹ .
E _a	= apparent activation energy of gasification, kJ/mol.
k _g	= mass transfer coefficient, m·s ⁻¹ .
K ₁	= equilibrium constant for H ₂ S.
K _{1e}	= experimental equilibrium constant for H ₂ S.
K ₂	= equilibrium constant for water shift reaction.
M _c	= molecular weight of carbon.
M _s	= molecular weight of sulfur.
N _c	= moles of carbon added to the system.
N _g	= total moles in gas phase at equilibrium.
(-r _c)	= carbon gasification rate, min ⁻¹ .
r _c [*]	= carbon gasification rate in mol/min.
r _{CO₂} ^o	= rate of CO ₂ formation before any consumption, min ⁻¹ .
r _{H₂S}	= H ₂ S emission rate, min ⁻¹ .
R	= gas constant.
Q	= gas flow rate at standard conditions, mol·min ⁻¹ .

T	= temperature, K.
W_S^0	= initial sulfur weight, mg.
W_{Sgc}	= cumulative weight of sulfur removed with off-gas as H ₂ S, mg.
W_{Sic}	= amount of sulfur in gasification residue, mg.
W_{St}	= sum of W_{Sgc} and W_{Sic} , mg.
ΔW_S	= percent difference of W_S^0 and W_{St} , %.
X	= sulfide conversion, mg/mg.

Greek Symbols

α	= weight percentage ratio of carbon and sulfur in remaining black liquor char at time t.
----------	--

REFERENCE

1. van, Heiningen, A.R.P., J. Li, and J. Fallafollita, **Canadian Patent Application**, #583,409, Nov. 7, (1988).
2. Fallavolita, J.A., and et al, **Can. J. Chem. Eng.**, 65(Oct.), p.815(1987).
3. Durai-swamy, K, and et al, 1989 **Intern. Chem. Recov. Conf.**, Ottawa, p.217(1989).
4. Li, J., **Master thesis**, McGill University, Canada, (1986).
5. Li, J., and A.R.P. van Heiningen, **Can. J. Chem. Eng.**, 67(4), p.693 (1989).
6. Li, J., and A.R.P. van Heiningen, **Mat. Res. Soc. Symp. Proc.**, Vol.111, p.441(1988).
7. Li, J., and A.R.P. van Heiningen, **19th Biennial Carbon Conference**, Penn State Univ., June 25-30, p.570(1989).
8. De Souza, T.L.C., and et al, **Anal. Chem.**, 47(3), p.543(1975).
9. Eriksson, G., **Chemica Scripta**, 8, p.100(1975).
10. Pejryd, L., and M. Huppa, **1984 Tappi Pulping Conf.**, San Francisco, p.1(1984).
11. Barin, I. and et al, **Thermochemical Properties of Inorganic Substances**, Springer-Verlag, Berlin, (1977).
12. Warnqvist, B., **Thermochimica Acta**, 37, p.343(1980).

13. Backman, R., **Ph.D thesis**, ABO AKADEMI, Finland, (1989).
14. Smith, J.M., and H.C. Van Ness, **Introduction to Chemical Engineering Thermodynamics**, McGraw-Hill book Company, 3rd Edt., p.390 (1982)

CHAPTER 7

KINETICS OF SODIUM SULFATE REDUCTION BY CARBON MONOXIDE BELOW 800°C

ABSTRACT

The kinetics of Na₂SO₄ reduction by CO below 800°C is studied in a thermogravimetric system. The reduction is auto catalytic and the conversion-time behavior can be described by an initiation, acceleration and deceleration period. The major deceleration period is described by phase boundary reaction controlled or product diffusion controlled solid-solid kinetics for respectively reduction with or without the presence of CO₂. The reduction rate during the deceleration period is only slightly affected by CO and strongly retarded by CO₂. The gas-solid reaction between CO and Na₂SO₄ is identified as the initiation reaction. The initiation reaction is first order in CO and has an activation energy of about 250 kJ/mol. Na₂CO₃ does not have a catalytic effect on the reduction, but may influence the reduction rate due to formation of a ternary melt system. When a molten phase is formed, the reduction rate is controlled by mass transfer of CO in the liquid melt. Na₂SO₄ reduction by CO is catalyzed by TiO₂ and Fe₃O₄. The reduction in the presence of TiO₂ is not auto catalytic and well described by ash diffusion controlled kinetics for gas-solid reactions.

INTRODUCTION

In kraft pulping, wood is treated at elevated temperature and pressure with an aqueous solution of NaOH and Na₂S. About 50% of the wood, mostly lignin and some carbohydrates, is dissolved in the cooking liquor. From the spent liquor, called black liquor, both NaOH and Na₂S are regenerated and the organics are burned in a recovery process. Black liquor droplets are sprayed into a recovery furnace where they dry and pyrolyze before reaching the char bed at the bottom. The remaining carbon in the bed is gasified at temperatures above 800°C, and provides the reducing atmosphere for the conversion of Na₂SO₄ to Na₂S. The inorganic salts, mainly Na₂CO₃ and Na₂S, leave the furnace as a smelt and are dissolved in water. The resulting green liquor is sent to the causticizing plant where Na₂CO₃ is converted into NaOH so that the resulting white liquor can be reused for pulping .

Although the objective of chemical recovery is adequately achieved in present commercial operations, there are still many unanswered questions regarding the complicated and interrelated processes in the furnace. One of the key questions is what mechanism and which parameters are governing the reduction of sulfate to sulfide. The answer to this question would lead to better operation of existing furnaces and aid development of alternative recovery processes. The incentives for the search for an alternative recovery process are the very high capital cost, the smelt-explosion hazard and the corrosive nature of the smelt associated with the present recovery furnace. Potentially safer and less capital intensive alternatives are the fluidized bed processes proposed by Nguyen [1] and Fallavollita et al. [2]. In these processes black liquor is combusted or gasified in fluidized beds and the resulting inorganics are reduced by H₂, CO or carbon with or without the presence of a metal oxide catalyst. No smelt is formed in both the oxidation and reduction steps. An additional advantage of auto causticizing metal oxides such as titanium dioxide and iron oxide is that white liquor rather than green liquor is produced. However, further study is required to optimize the reactor design and operating conditions, in particular of the low temperature reduction step.

Very little information is available concerning the kinetics of the reduction of Na₂SO₄. The reduction of Na₂SO₄ by H₂, CO or carbon has recently been studied in molten carbonate [3-6]. The only two studies of

Na_2SO_4 reduction by CO in the solid state were reported many decades ago [7, 8]. Budnikoff [7] stated that Na_2SO_4 could not be reduced by CO below 850°C . White and White [8] reported that reduction of Na_2SO_4 by CO was slower than with H_2 . They also conclude that Na_2SO_4 and Na_2S form an eutectic slightly below 700°C and that the reduction with H_2 proceeds relatively rapid at 704°C as long as a solid phase is present. The reduction is retarded at higher temperatures because of slow diffusion of H_2 in the molten mass. Sjoberg and Cameron [4] reported that reduction of Na_2SO_4 by CO in molten Na_2CO_3 was zero order in sulfate, first order in CO and had an activation energy of 115 kJ/mol. They did not observe a catalytic effect for Fe , Fe_2O_3 and $\text{Fe}_2(\text{SO}_4)_3$, or an auto catalytic behavior as found by Birk et al [3] for the reduction with hydrogen. However, other investigators [9, 10] did find the auto catalytic behavior in the molten sodium sulfate reduction by CO. They also found that the reduction was catalyzed by several metals of which iron was the most active.

The objectives of this study are to develop kinetic rate equations for solid state reduction of Na_2SO_4 by CO as a function of CO, CO_2 and Na_2CO_3 concentration, and to investigate the catalytic effect of metal oxides known for their auto causticizing properties. The results of this study will aid the development of a melt-free reduction reactor as part of an alternative low temperature kraft recovery process.

EXPERIMENTAL

Experimental Apparatus

A standard thermogravimetric analysis system was used to obtain kinetic data. A schematic picture of the Cahn TGA 113-DC system with auxiliary gas preparation system is shown in Figure 1. N_2 (99.998%) and He (99.995%) are zero grade quality, CO_2 is anaerobe grade (99.99%), and CO ultra-high purity (99.9%). An oxygen trap is used for each gas. Additionally, a CO_2 , H_2O and hydrocarbon (HC) trap are used for CO because of its relatively low purity. 1C, and the accuracy is better than $\pm 5\text{C}$ absolute.

A GC with FPD was used for analysis of sulfurous gas components in the exhaust, while a Fisher gas partitioner was used for measurement of the

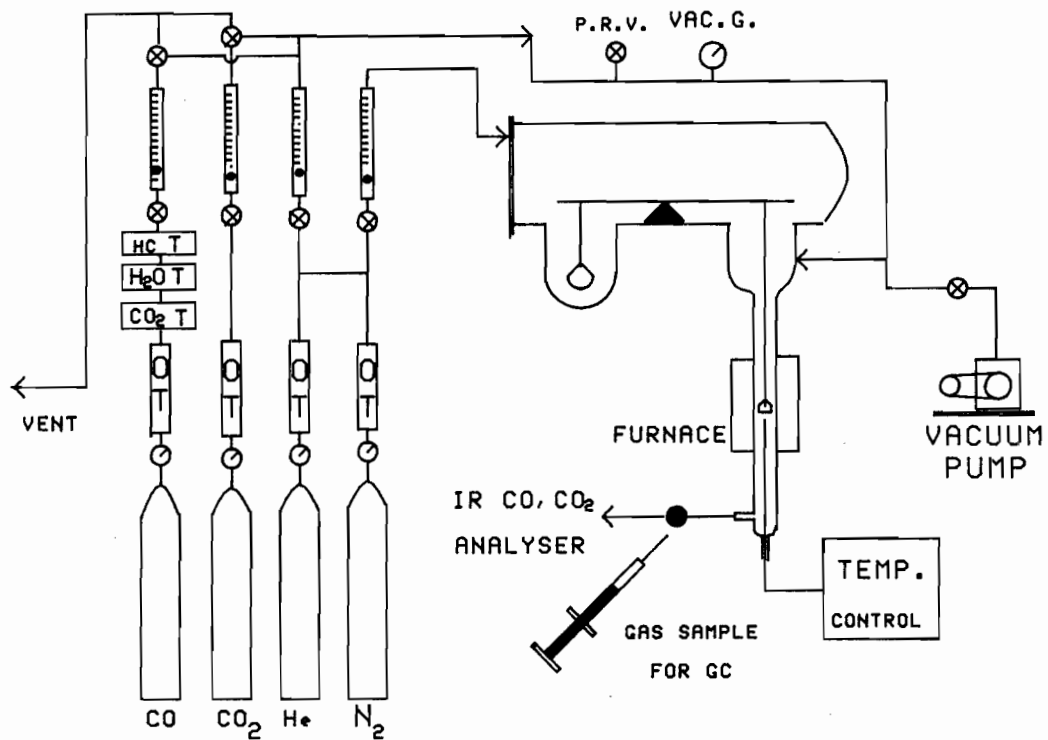


Figure 1, Schematic picture of experimental system.

fixed gases. CO and CO₂ were also determined continuously with IR analyzers. The reproducibility of measurement for fixed and sulfurous gases are respectively within 1 and 5%. The inorganic ions in the solids, such as sulfate, sulfide, sulfite, thiosulfate, carbonate and sodium were measured with a Dionex IC equipped with a conductivity and electrochemical detector. The reproducibility for sulfate, sulfite, thiosulfate, is within 1% and for sulfide, sodium and carbonate within 5%.

Sample Preparation and Experimental Procedures

Reagent grade Na₂SO₄ and Na₂CO₃ were dissolved in deionized water, dried and ground, and the powder sieved over a 500 mesh sieve. The catalyst powders (particle size < 25 μm) of Fe₃O₄ or TiO₂, were physically mixed with the reactant powder. All surfaces in contact with the sample during preparation were washed with deionized water to avoid contamination.

After adding 4 - 10 mg sample to the pan up to a bed height less than 0.5mm, the system is three times evacuated and refilled with N₂ or He. Then under a He or N₂ flow rate of 300 scc/min, the furnace temperature is raised from 20°C to a final reaction temperature at a rate of 25°C/min. When the temperature and sample weight are stabilized, CO and CO₂ are added to obtain the desired reduction atmosphere. The weight change of the sample is continuously recorded with accuracy better than 5 μg. The total weight loss during reduction is normally 0.5 to 2 mg. At the end of an experiment, the CO and CO₂ flows are stopped and the reactor is cooled to room temperature within two minutes. The sample is then immediately dissolved in deaired and deionized water with less than 10 seconds exposure to air to minimize oxidation. Within 5 minutes the sample is diluted with deaired and deionized water and injected for analysis of sulfide, sulfate, sulfite and thiosulfate.

Preliminary Experiments

Preliminary experiments were done to ensure that the measured weight loss rate is representative of the reaction between Na₂SO₄ and CO, and that gas phase heat and mass transfer limitations can be neglected. Shown in Table I are the maximum reaction rate, $-R_{max}$, the initial sulfate content (as mg S), $W_{SO_4}^o$, the final sulfate and sulfide content, respectively $W_{SO_4}^f$ (as mg S) and W_S^f , half the measured weight loss after CO addition, 0.5WL,

and the percentage difference in sulfur content of the sample before and after reaction, ΔW_s , for a number of experiments. The maximum reduction rate, $-R_{max}$, is normalized by the initial sulfate content. Sulfite and thiosulfate were normally not detected when the previously described analysis procedure was followed.

The following overall reactions may occur:



If the formation of COS can be neglected, the sulfur mass balance requires that

$$W_{\text{SO}_4}^o = W_{\text{SO}_4}^f + W_{\text{S}}^f \quad (5)$$

Also, if reaction (1) is the only significant reaction, then

$$0.5 \text{ WL} = W_{\text{S}}^f \quad (6)$$

Returning to Table I, it can be seen that the reactivities, $-R_{max}$, of duplicate experiments performed with a porcelain sample pan (resp. No. P1 and P2) differ considerably. It was observed that the porcelain pan was coated with carbon after a run, and that the CO_2 concentration in the exhaust was one to two orders of magnitude higher than could be produced by reduction of Na_2SO_4 . This indicates that reaction (4) takes place inside the reactor tube and on the surface of the sample pan. Soot formation on the surface of the pan was eliminated by using a high purity alumina (99.8%) pan. Duplicate experiments with the alumina pan (A1 and A2) in Table 1 show good agreement for $-R_{max}$. A picture of the pans before and after an experiment are shown in Figure 2. The measured CO_2 production was still one order of magnitude higher than that formed by reduction, because soot formation on the reactor tube surface is not eliminated.

It can also be noticed that equations (5) and (6) are reasonably satisfied for A1 and A2. All other experiments were subsequently done with the alumina pan.

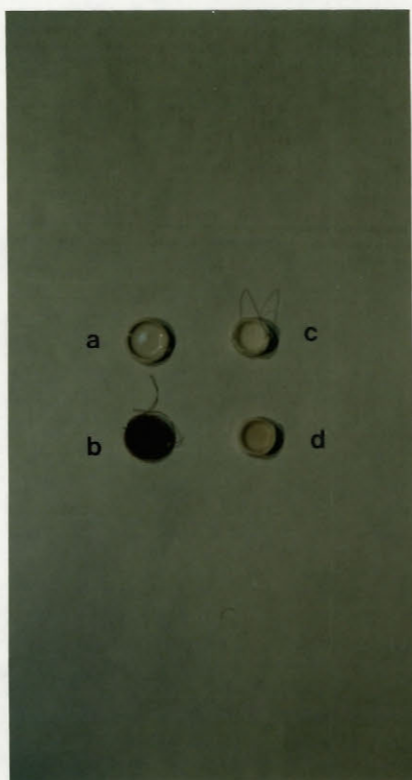


Figure 2, Sample pan before and after a reduction experiment.

- a, Porcelain pan, before a experiment;
- b, Porcelain pan, after a experiment;
- c, Alumina pan, before a experiment;
- d, Alumina pan, after a experiment.

TABLE I. EFFECT OF SAMPLE PAN, CARRIER GAS, TEMPERATURE
AND GAS COMPOSITION ON REACTIVITY AND SULFUR MASS BALANCE

No	T °C	[CO] %	[CO ₂] %	-R _{max} min ⁻¹	W _{SO₄} ^o mg	W _{SO₄} ^f mg	W _S ^f mg	0.5WL mg	ΔW _s %
P1	725	46	0	0.0082	1.28	1.10	0.15	0.18	-2.3
P2	725	46	0	0.0052	0.85	0.68	0.115	0.12	-6.5
A1	725	46	0	0.0051	0.62	0.513	0.06	0.06	-7.1
A2	725	46	0	0.0052	1.99	1.64	0.28	0.27	-3.5
H1	725	50	0	0.0061	1.69	1.35	0.22	0.23	-7.1
N1	725	50	0	0.0060	1.80	1.50	0.225	0.235	-4.2
a									
T1	725	50	0	0.0114	1.03	0.757	0.255	0.257	-1.7
T2	725	50	0	0.0117	1.79	1.43	0.44	0.42	+4.0
MB1	780	50	0	0.1305	0.77	0	0.79	1.65	+3.0
MB2	760	50	0	0.121	0.56	0.041	0.525	0.64	+1.0
MB3	750	50	0	0.0576	1.08	0.07	1.08	1.03	+6.0
MB4	800	50	1.5	0.151	0.53	0.01	0.501	0.55	-3.6
MB5	750	50	10	0.0038	1.03	0.72	0.06	0.195	-24.3
MB6	750	50	4	0.0025	0.81	0.392	0.37	0.385	-5.9

a: sample contains 1.3% Na₂CO₃ above this line, and 39.4% Na₂CO₃ below this line.

The most effective and simplest method to identify heat and mass transfer limitations for gas-solid reactions is to use different carrier gases, normally N₂ and He. Because of the large differences in thermal and molecular diffusivity any significant heat or mass transfer limitations associated with the gas-phase will result in different reaction rates. The runs H1 and N1 in Table 1 with respectively He and N₂, give almost the same reaction rate -R_{max}, indicating that gas phase related resistances are unimportant in the present system.

Sintering has been observed for many systems to reduce the reactivity of gas-solid reactions. To determine the importance of this effect in the

present system two runs (T1 and T2) were performed whereby in T1 the temperature was first raised to and held at 750°C for 12 minutes and then reduced to 725°C, while in T2 the temperature was raised directly to 725°C without over-heating. The close agreement of $-R_{max}$ for the two runs in Table 1 suggests that sintering is not important under the present reaction conditions.

As can be seen in Table I, in all cases the percentage deviation of the total sulfur mass, ΔW_s , according to equation (5) is less than or equal to 7% except for run MB5. The implication that reaction (2) is negligible was confirmed by the very low COS concentration (< 0.2 ppm) for all runs except MB5 where about 2 ppm COS was measured. The explanation for the different behavior of MB5 is an increased rate for reaction (2) and decreased reduction rate (reaction (1)) when the CO₂ concentration is increased as will be shown later.

Depending on temperature and gas composition equation (6) is also not always obeyed. Disregarding run MB5 for reasons given earlier, it is seen that large deviations of equation (6) occur for experiments MB1 and MB2, i.e. relative high temperatures and without the presence of CO₂. The reason is that reaction (3) is contributing to the weight loss by volatilization of Na₂CO₃. This is confirmed for MB1 by a measured sodium loss of 0.63 mg compared to a theoretical loss of 0.75 mg to obtain a balanced equation (6). It should be noticed however, that when CO₂ is added, reaction (3) is suppressed considerably even at 800°C as shown by the results of MB4.

An increased reactivity was obtained when Na₂CO₃ was increased from 1.3 to 39.4% (H1 versus T1) below line a. This effect will be discussed in more detail later. Unless specified otherwise, 39.4% Na₂CO₃ will be used. From the above results it is clear that great care is required to obtain good kinetic data from TGA experiments for the present reaction system.

Based on the above experimental results, it can be concluded that reliable kinetic data for Na₂SO₄ reduction by CO can be obtained between 760°C and 800°C when $1 < [CO_2] < 5\%$ and below 760°C when no CO₂ is added to the feed gas.

RESULTS AND DISCUSSION

Conversion-time data

When sulfur and sodium emission are not important, the conversion of sulfate reduction is calculated as

$$X (\%) = \frac{W_o - W_t}{W_{SO_4}^o} \times \frac{32}{64} \times 100 \% \quad (7)$$

where W_o and W_t are the sample weights respectively at the start and t seconds after introduction of CO. Some typical conversion vs time results with or without the presence of CO₂ are given in Figure 3. After an induction period the rate increases up to a maximum after which the rate decelerates until the end of the experiment. It can be seen from Figure 3 that the presence of CO₂ decreases the rate especially at higher conversions. The induction time also increases with presence of CO₂, and even more so when the CO concentration is reduced.

Microscopic pictures of samples reacted at 750°C in 50% CO at different conversions are shown in Figure 4. Picture (a) is after heating to 750°C without any reduction. Although the sample could be removed from the pan as one piece, the slightest pressure lead to disintegration into a fine powder, again showing that sintering was unimportant. Picture (b) is at about 30% conversion. At this stage, some localized fusion with a pink color of Na₂S was observed (picture (d)). The bulk structure of the sample is still intact and no significant sintering was observed. The localized fusion could be related to impurities or inhomogeneities which accelerate the reduction rate. At complete conversion, a thin pink film covers the complete inner surface of the pan including its 1 mm high rim, without obvious accumulation at the bottom of the pan. Some unmelted blocks remain in the pan and one is shown in picture (c).

The major decelerating part of the conversion curves without CO₂ addition is well described by

$$k (t - t_i) = 1 - (1 - X)^{1/3} \quad (8)$$

as can be seen in Figure 5 for different temperatures. The induction time, t_i , determined by setting $X=0$ in equation (8), is very small compared to the for complete reduction. Equation (8) is the theoretical expression for the conversion in the chemical reaction controlled shrinking core model for gas-solid reactions [11], as well as for the phase boundary reaction

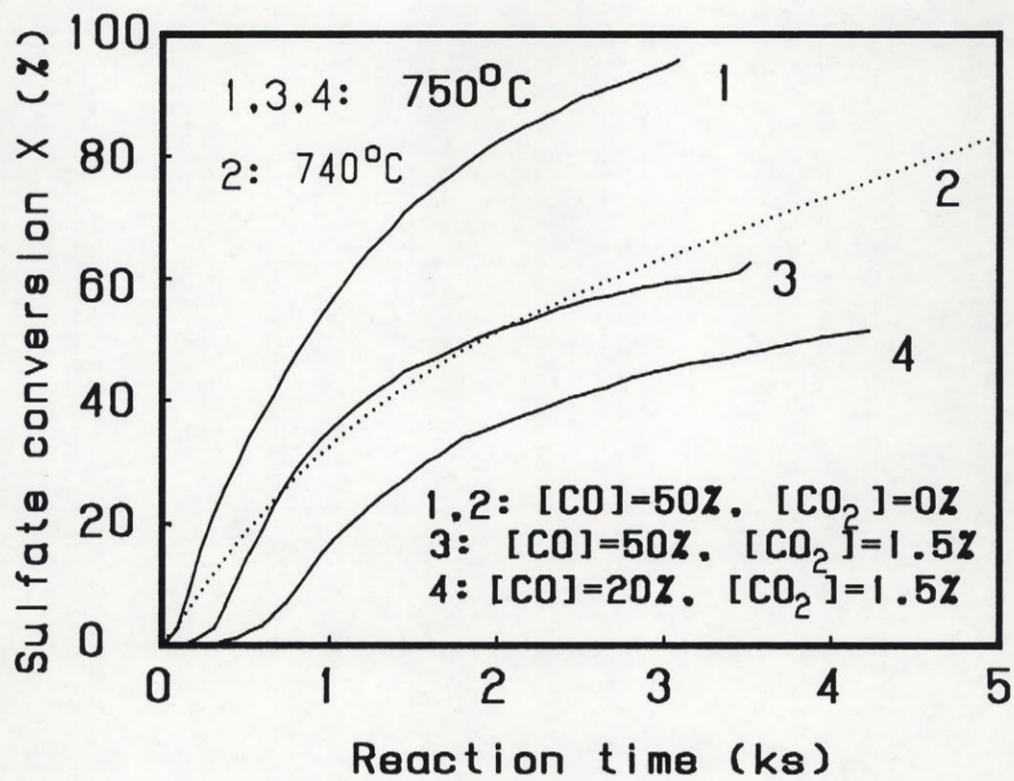
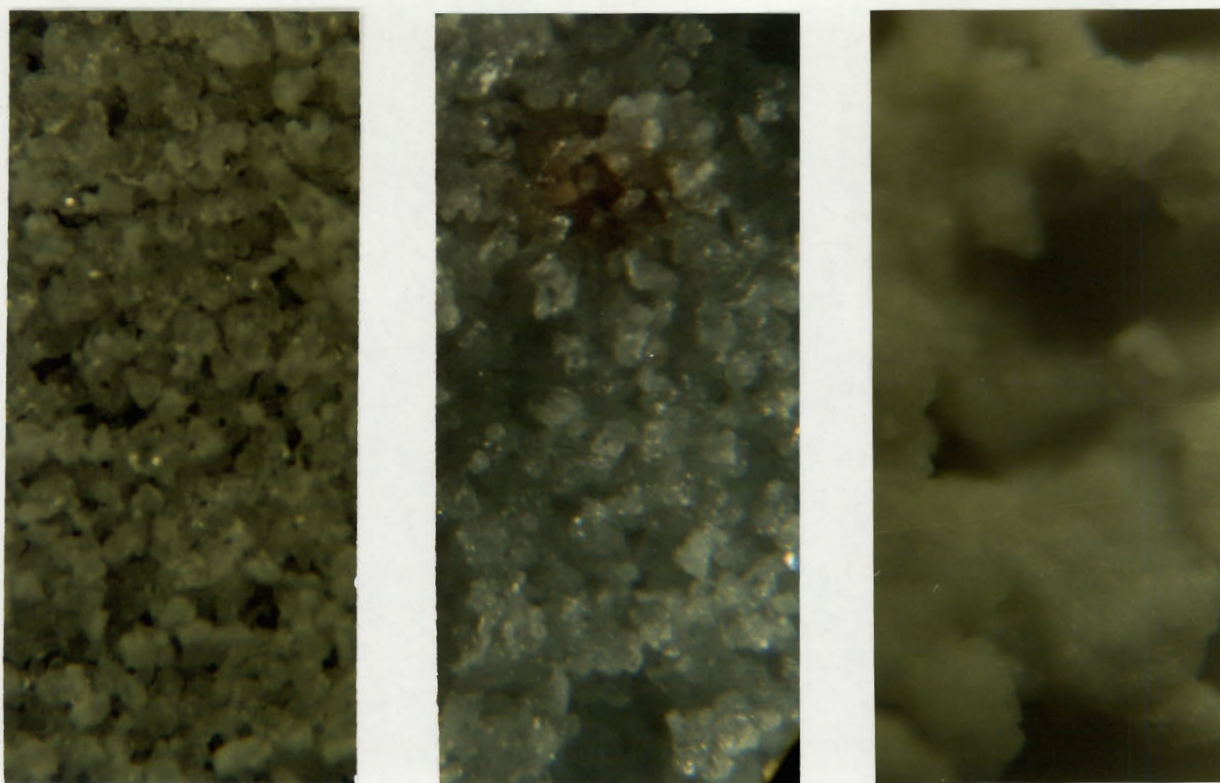


Figure 3, Typical Na₂SO₄ conversion as a function of time.



a)

b)

c)



d)

Figure 4, 60.6% Na_2SO_4 sample; a) just before reduction; b) at 30% conversion; c) at 100% conversion; d) localized fusion at 30% conversion.

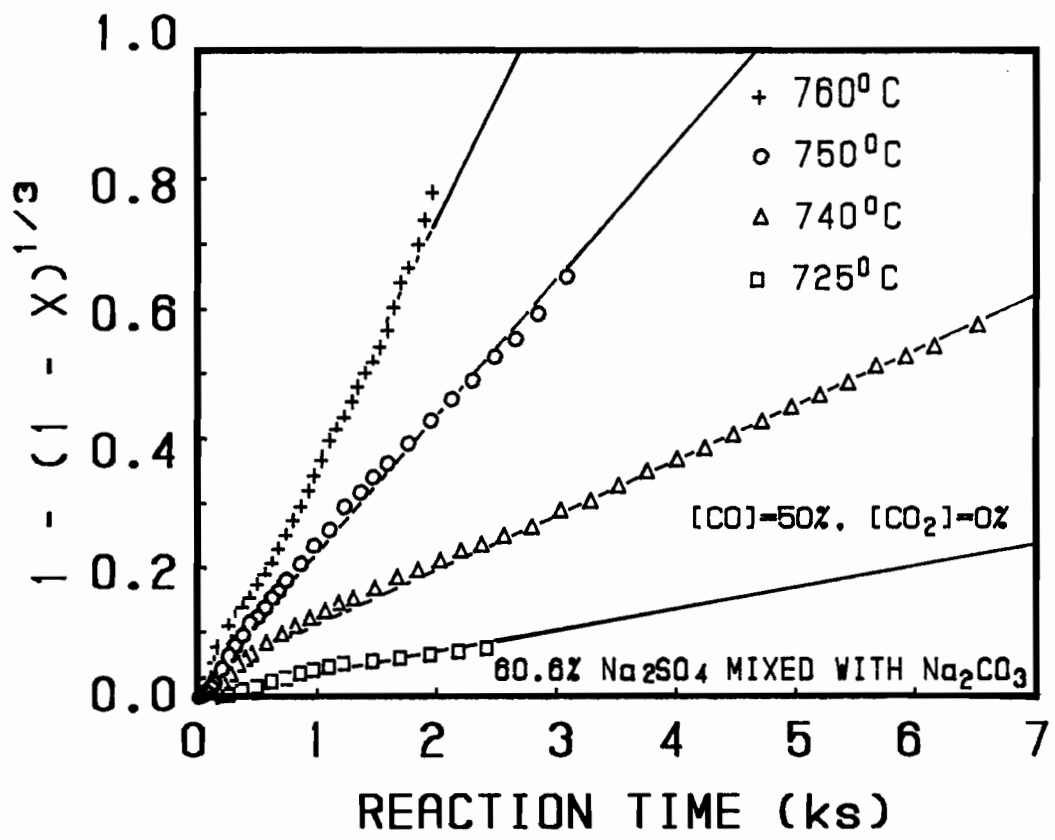


Figure 5, Reduction kinetics of Na₂SO₄ by CO.

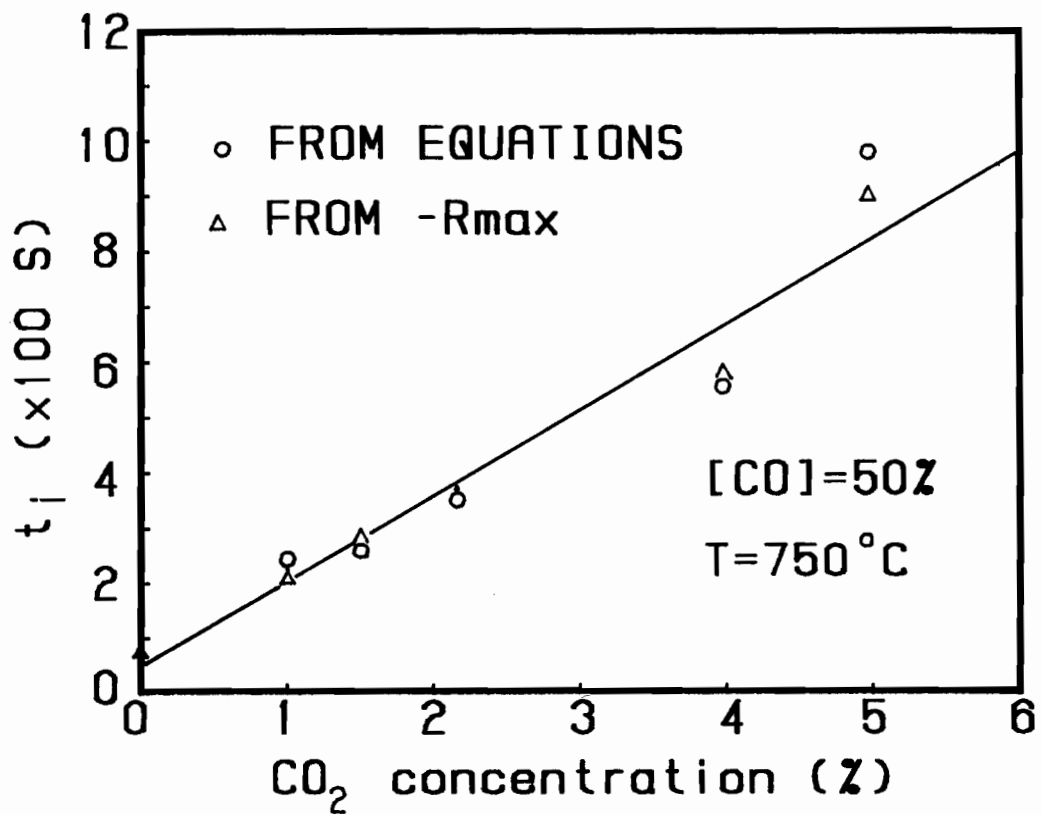


Figure 11, Influence of CO₂ concentration on initiation time.

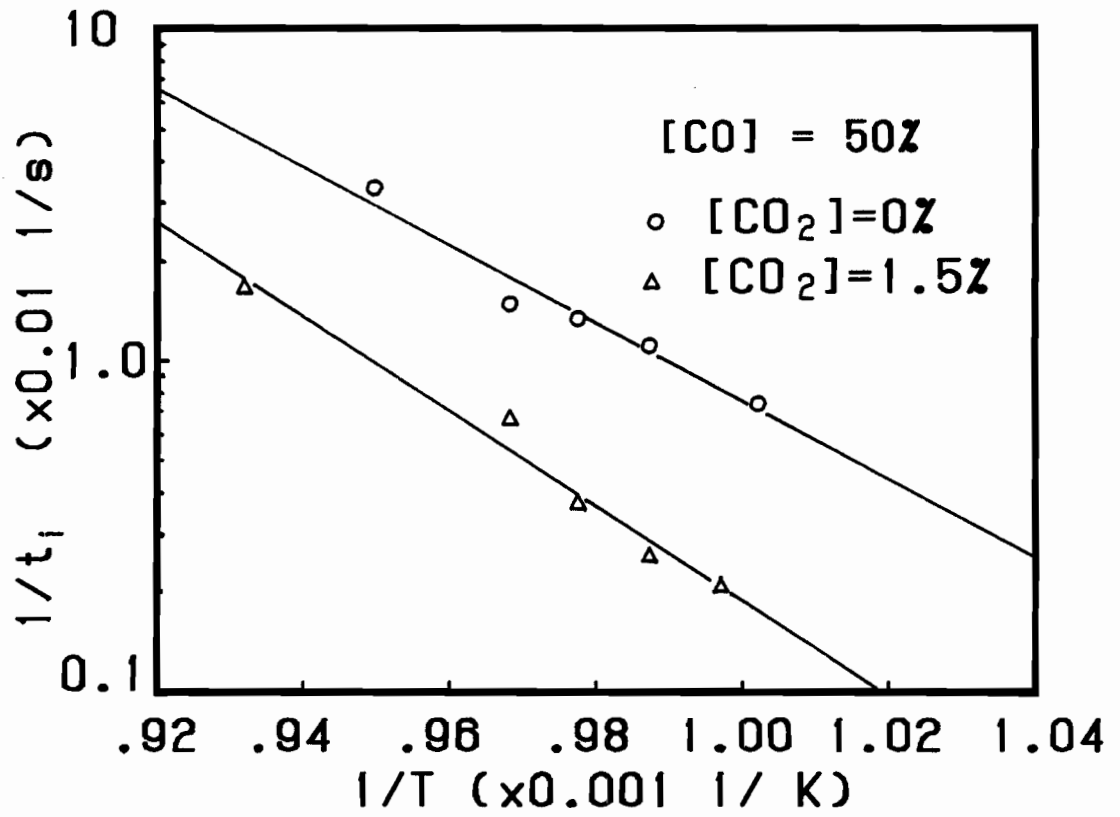


Figure 12, Influence of temperature on initiation time.

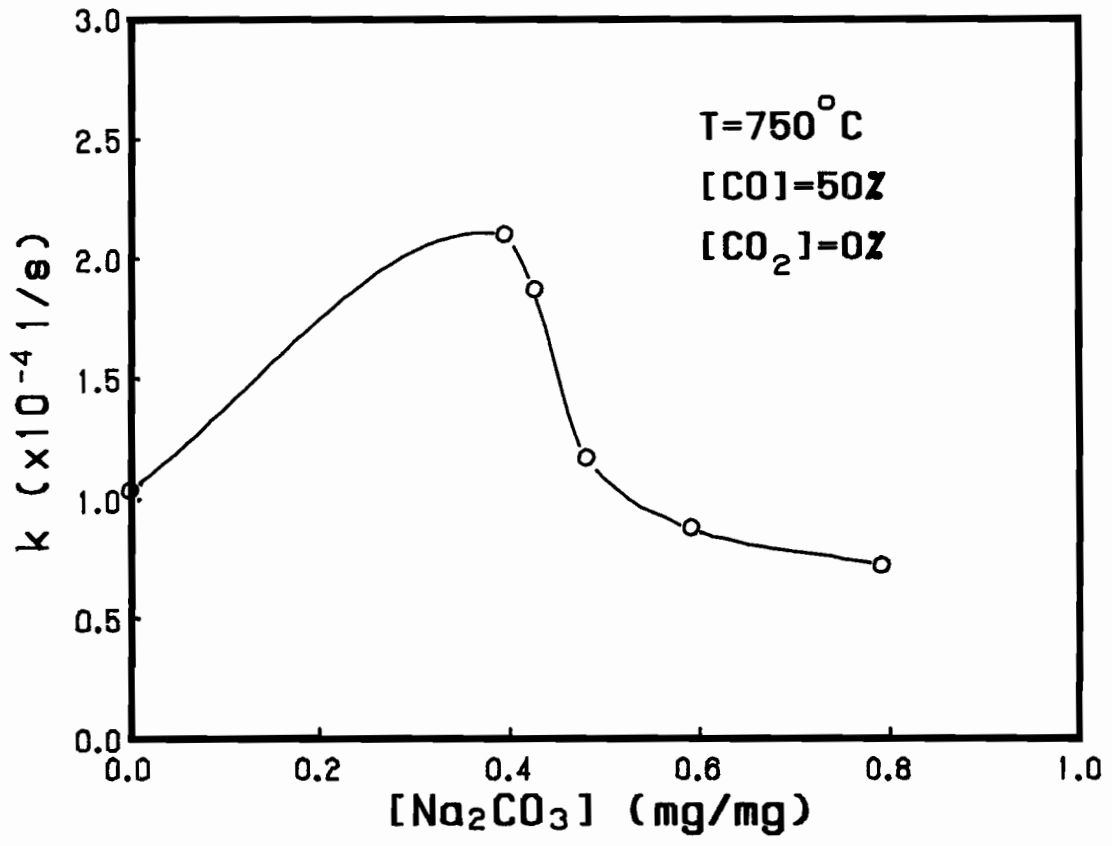


Figure 13, Influence of sodium carbonate on reduction rate.

[Na₂CO₃]. This behavior cannot be explained by either assuming that Na₂CO₃ is a catalyst or acts as an inert diluent. The change in reactivity with Na₂CO₃ concentration is more likely related to the melting behavior of the ternary system. Shown in Figure 14 is the phase diagram for Na₂CO₃-Na₂S-Na₂SO₄ reproduced from Andersson [16]. The results show that the lowest melting temperatures are obtained when the Na₂CO₃ mole fraction is less than about 55%. Since formation of a ternary melt at the reacting interface was assumed to be the most important step during reduction of Na₂SO₄, higher reactivity for mixtures which melt at a lower temperature is consistent with the proposed reaction mechanism. This would explain why the reactivity decreases with increasing [Na₂CO₃] when the [Na₂CO₃] is higher than the concentration at the eutectic melting point. With pure Na₂SO₄, the melting temperature would again be higher, leading to a reduced reactivity.

Effect of Molten Phase

Shown in Figure 15 is the sulfate conversion as function of time for 750, 760 and 800°C at 50% CO and 1.5% CO₂ for a salt mixture containing 39.4% of Na₂CO₃. At 760°C and 800°C the reaction rate remained constant over a wide range of conversion after an initial accelerating period. This behavior can be explained by a change of the system from gas-solid at 750°C or lower to gas-liquid at 760°C and higher. Evidence for the change in reaction system at 760°C and higher was that the final cold samples were transformed into solid flat disk. Although the minimum melting point of the ternary system of Na₂S, Na₂SO₄ and Na₂CO₃ is 715±5°C [16], the particle bed structure of the system remains intact during reduction below 750°C because the amount of melt formed at the reacting interface is still relatively small. This can be inferred from the narrow range of compositions in the ternary phase diagram in Figure 14, where the melting point is less than 750°C. A melt can only be present above about 760°C in the fully reduced product consisting of Na₂S and Na₂CO₃ because the eutectic melting point of this binary mixture is 762°C at 40 mol% Na₂S [16]. Consequently the bed structure will collapse to a uniform liquid melt in the pan when a sufficient amount of Na₂SO₄ is reduced above 760°C. The reaction rate will then be controlled by gas-liquid reaction laws, and a distinct change in reduction rate is expected. A sudden change in slope of conversion-time curve due to formation of a liquid phase has been reported earlier by Tran and Barham [19] for the reduction of sulfate by H₂.

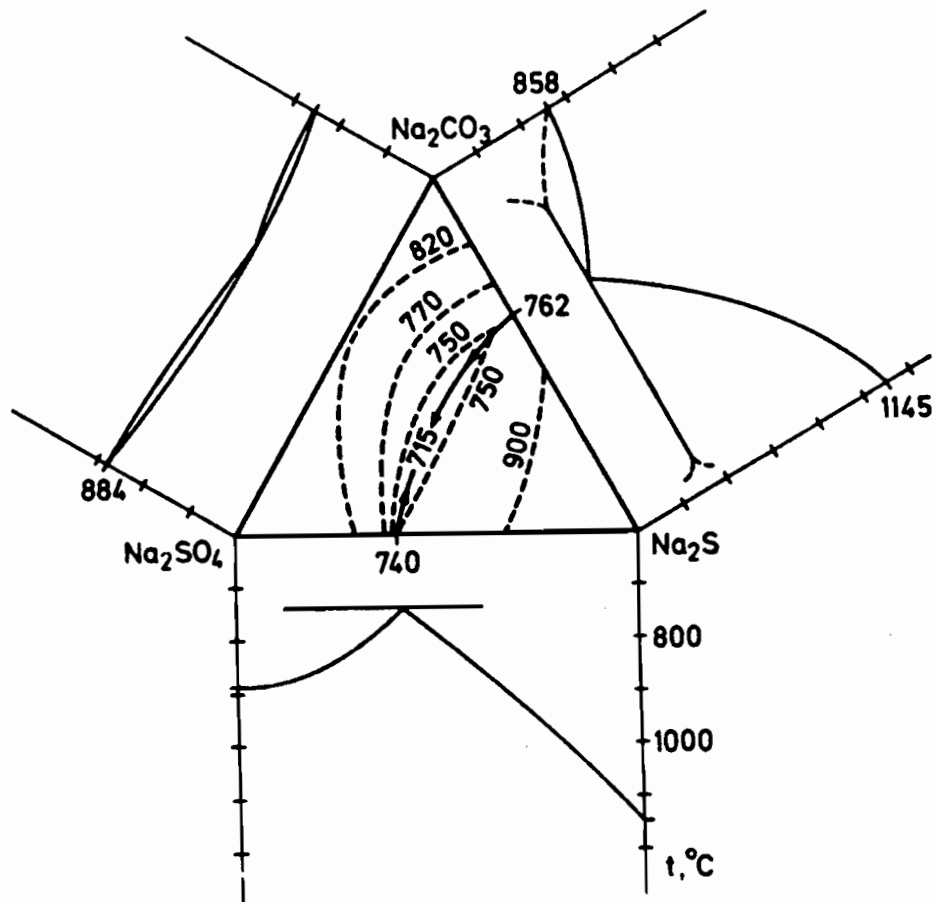


Figure 14 The phase diagram for Na_2CO_3 - Na_2S - Na_2SO_4 from Andersson [16].

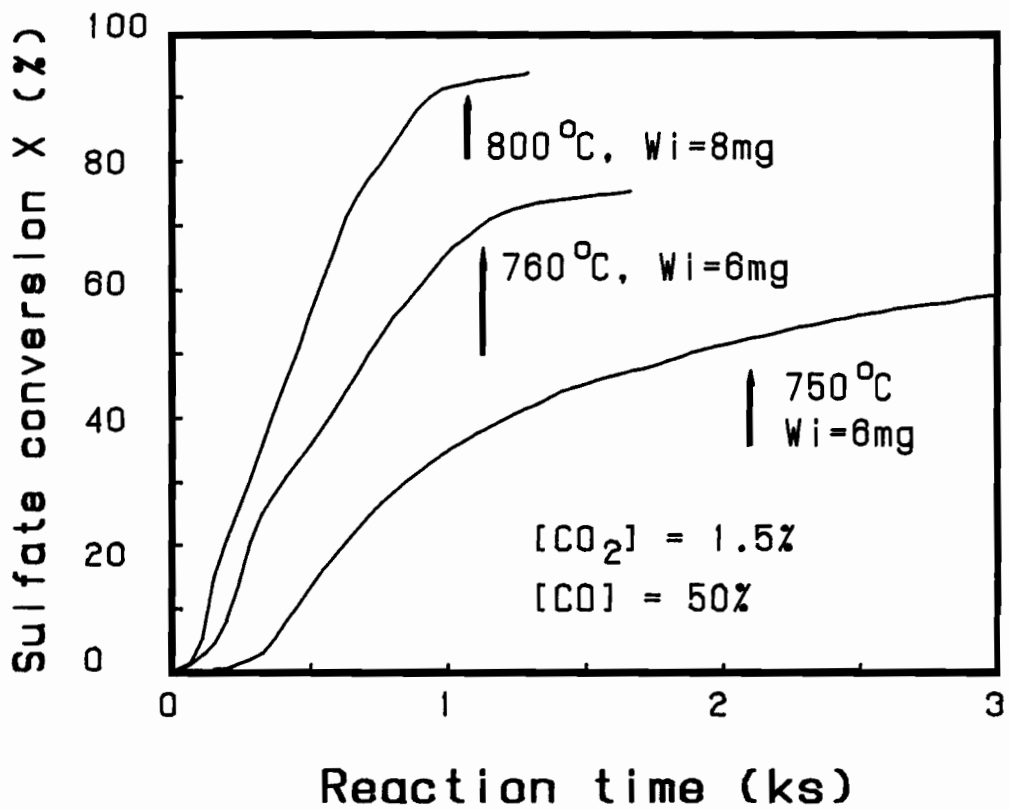


Figure 15 The sulfate conversion for 750, 760 and 800°C at 50% CO and 1.5% CO₂.

Finally, the transition of the linear reduction rate region to a much slower rate at high sulfate conversion is attributed to the formation of a solid crust of Na_2S in equilibrium with a ternary liquid phase [16].

Another point which should be addressed is why the reaction rate remains constant after formation of a liquid melt layer. Two different explanations are possible for such a behavior. First, the reduction rate is controlled by chemical kinetics and the reaction is zero order in sulfate concentration. Secondly, the rate can be controlled by mass transfer in the liquid film. To establish whether the reduction was mass transfer or chemical reaction controlled, the initial sample weight was varied. By increasing the sample weight the thickness of the melt layer will increase while the mass transfer surface area remains unchanged in the present sample pan. When mass transfer is rate controlling, an increase in sample weight will have no effect on the absolute reduction rate, but lead to a decrease in sulfate conversion rate because conversion is normalized with respect to initial sulfate weight. An increase in sample weight on the other hand will not have an effect on the sulfate conversion rate when chemical reaction is rate controlling, exactly because conversion is normalized with respect to initial sulfate weight. Shown in Figure 16 are the conversion-time results at 800°C for different initial sample weight. The conversion rate during the constant period are 0.108 and 0.071 min^{-1} with an initial sample weight of respectively 4 and 8 mg. This result suggests that the reduction rate for the present reaction system above 760°C is determined by mass transfer of CO in the thin top film of the melt layer. The reason that the rate is not exactly proportional to the sample weight is possibly because the surface areas of the melt in the two cases are not exactly equal.

Sjoberg and Cameron [4] reported that Na_2SO_4 reduction by CO in an alkali carbonate melt is zero order in Na_2SO_4 concentration and first order in CO concentration. The explanation for these results is that their reaction system is likely controlled by mass transfer of CO in the liquid phase. Evidence for this explanation is that the auto catalytic effect of Na_2S and the catalytic effect of iron species were also not found in their study, while this behavior has been reported by many others [9, 10]. No effect of reaction kinetics and catalyst will be found when the reaction rate is limited by mass transfer. Finally, an activation energy of 27.5 kcal/mol was obtained from their study. However, this value is not much higher than the activation energies related to diffusion in liquid metals, 1 to 16 kcal/mol , and in the range for diffusion slags, 10 to 95 kcal/mol

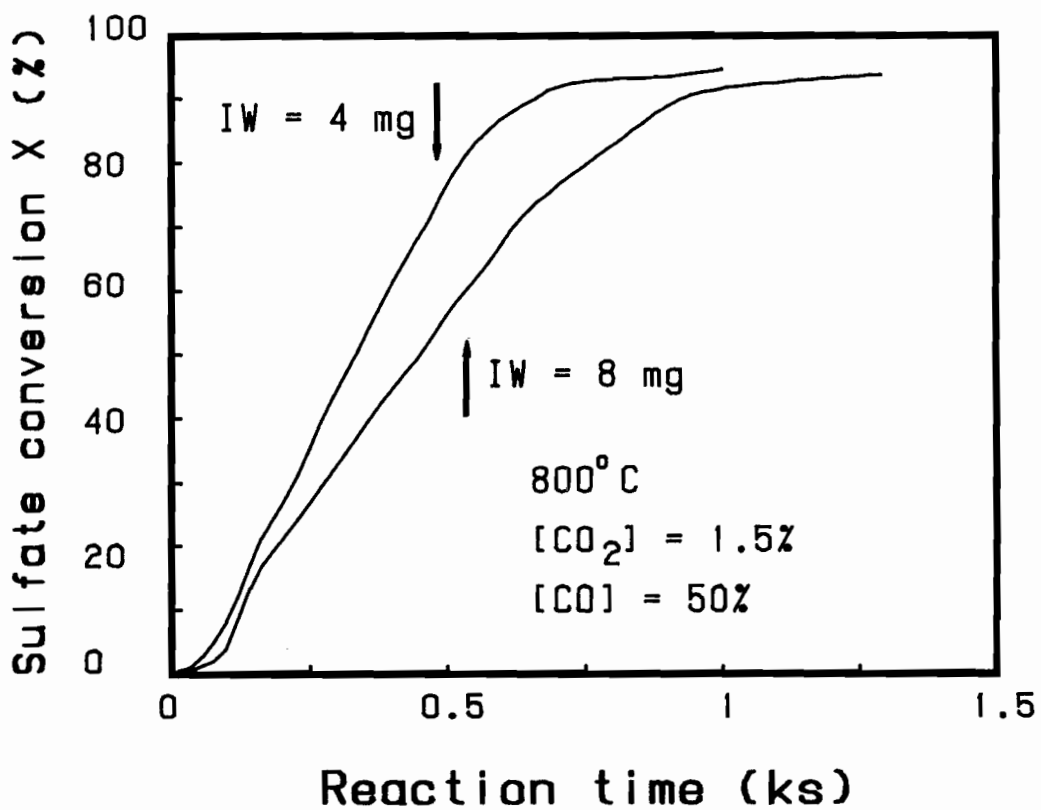


Figure 16, The conversion-time results at 800°C for different initial sample weight

[20]. So the increase of reaction rate measured with increasing temperature might be mainly due to an increase in diffusion coefficient. With the information given by Sjoberg and Cameron, a rate of 0.0075 min^{-1} can be calculated for reduction at 800°C , 50% CO and 0% CO_2 . This is more than 1 order of magnitude lower than the rate obtained in the present study for an initial weight of 4 mg and 800°C , 50% CO and 1.5% CO_2 .

The above interpretation of the present experimental data also can be verified by the following analysis based on theory for gas-liquid reaction systems. A simple but typical reaction system is that of a gas (component A) which undergoes an irreversible second-order reaction with a reactant (component B) dissolved in liquid. The stoichiometry of the reaction is represented by



The overall rate of the gas-liquid reaction, Φ , is normally described by

$$\Phi = r_A S = E k_L S C_A^* \quad (17)$$

where r_A is the average rate per unit interfacial area, E the enhancement factor over pure physical absorption, k_L the mass transfer coefficient, C_A^* the equilibrium concentration of A, and S the interfacial area. The complete analytical solution for this system was presented graphically by Coulson and Richardson [21], as E versus Hatta number, Ha , defined as

$$Ha = (D_A k C_{B0})^{1/2} / k_L \quad (18)$$

where D_A is the diffusion coefficient of gas A in the liquid, k the reaction constant, and C_{B0} the concentration of B in the liquid. It is found that for range of $0.02 < Ha < 0.3$ the enhancement factor E is equal to one. In this case the process is essentially one of physical absorption followed by reaction in the bulk liquid. However, the reaction is sufficiently fast so that C_A is close to zero in the bulk of the liquid. This means that the rate of reaction is complete determined by mass transport across the liquid film, and is proportional to k_L and the interface area S .

In many cases the equilibrium concentration of A, C_A^* , follows Henry's law

$$p_A = H C_A^* \quad (19)$$

where p_A is the partial pressure of A and H Henry's coefficient. From equations (17) and (19) follows that the rate of reaction is proportional to the partial pressure of A. Although the results discussed above are based on second-order reaction kinetics, it is also approximately valid for other type of kinetics [22] including auto catalytic reactions [23] for the same range of Ha.

By assuming that the reduction rate is controlled by mass transfer of CO in the melt, the rate can be estimated with equation (17) and compared with the present experimental results. The solubility of CO in alkali carbonate melt at 800°C is about $2 \times 10^{-7} \text{ mol} \cdot \text{cm}^{-3} \cdot \text{atm}$ [24]. k_L can be assumed to be $1 \times 10^{-2} \text{ cm}^{-2} \cdot \text{s}^{-1}$ [22]. The interfacial area is about 0.5 cm^2 . With $E=1$ and the above information, the reaction rate calculated with equation (17) for reduction at 50% CO and 800°C is about 0.5 mg/min, which is very close to 0.15 mg/min measured with a sample of 8 mg. This close agreement supports that the reduction at the constant rate period is controlled by mass transfer of CO in the melt.

Finally according to equations (17) and (19) the measured rate will be proportional to the bulk gas partial pressure when $E=1$. Shown in Figure 17 are the conversion-time results at 760°C for 30% and 50% CO. The reaction rates during the constant rate period are 0.022 and 0.038 min^{-1} respectively at 30 and 50% CO. i.e. directly proportional to the CO concentration. This further confirms that the reduction at the constant rate period is controlled by mass transfer of CO in the liquid melt.

Effect of Catalyst

Titanium and iron oxide are known for their auto causticizing properties [25]. If these metal oxides also act as catalyst during sulfate reduction, the viability of a low temperature, melt-free kraft recovery process will be greatly enhanced. Shown in Table II are the operating conditions and some key measurements obtained in 50% CO. All samples were prepared by physically mixing TiO_2 or Fe_3O_4 powder ($<25 \mu\text{m}$) with the 60.6% Na_2SO_4 powder used in most previous experiments. The relative large amount of sulfide formed within approximately 1 hr for the two experiments at 700°C, compared to virtually no reaction without TiO_2 or Fe_3O_4 , show that the two oxides catalyze the sulfate reduction. It can also be noticed that equation (5) is not satisfied for the experiment with Fe_3O_4 . The lack of a closed sulfur balance is confirmed by significant concentrations of COS in

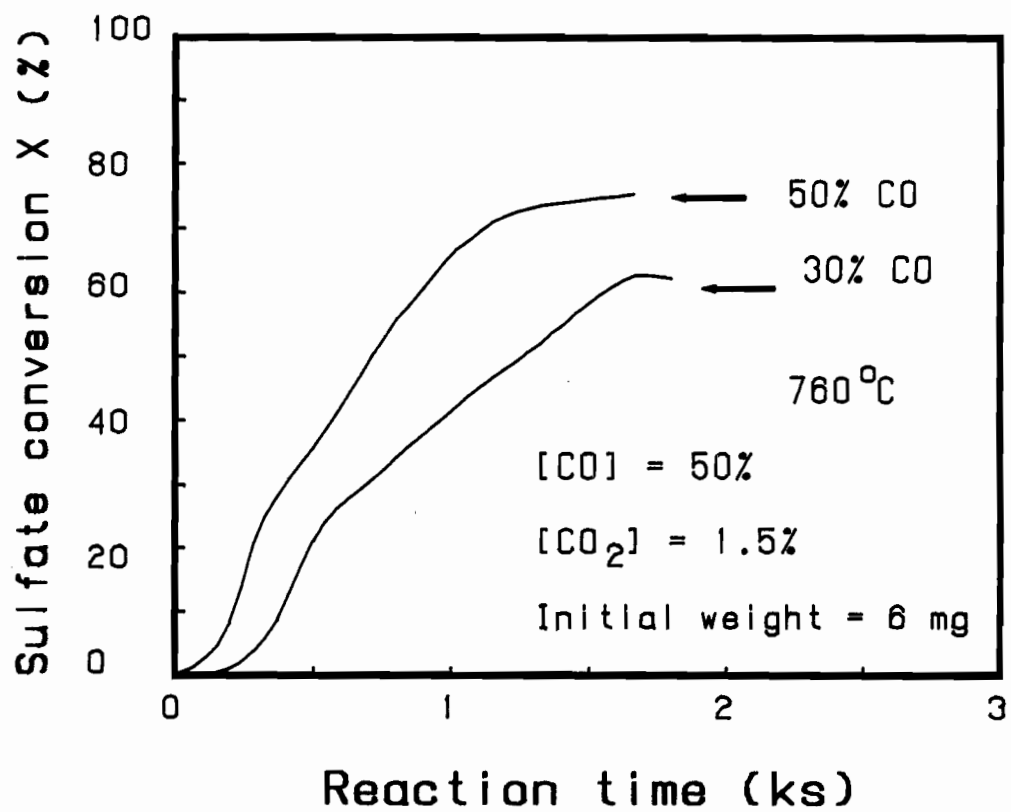


Figure 17, The conversion-time results at 760°C for 30% and 50% CO.

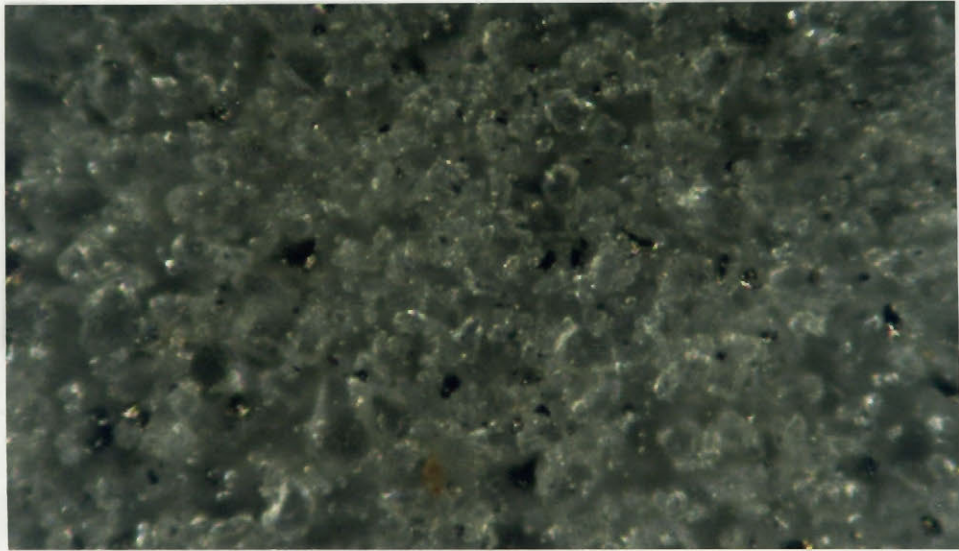
the exhaust. This suggests that Fe_3O_4 catalyzes the COS formation according to reaction (2). A microscopic picture of the final product obtained with Fe_3O_4 shows that heavy sintering occurred at 700°C . Considering the sulfur emission and sintering, Fe_3O_4 would seem unsuitable as a catalyst for low temperature reduction of sodium sulfate. The catalytic effect of other iron compounds, Fe and FeS, is also included in Table II. The results also indicate that those iron compounds are catalysts for sulfate reduction and COS formation. A microscopic picture of the sample before and after the reduction with Fe_3O_4 is shown in Figure 18.

With TiO_2 , a weight-loss accompanied by CO_2 production is measured at about 700°C before CO is added. This indicates that the auto causticizing reaction

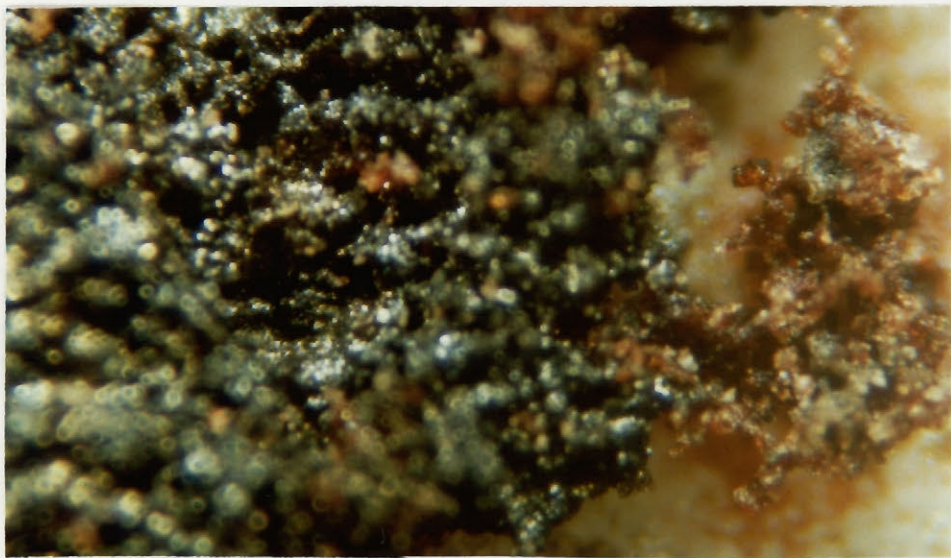


occurs before reduction is started. From the magnitude of the weight-loss it can be calculated that reaction (20) does not proceed to completion under the present conditions. Based on reaction (20), yields of 60% and 84% were obtained at 700 and 750°C respectively. However the results in Table II with TiO_2 show that equations (5) and (6) are satisfied. This proves that no sulfur is emitted and that sulfate reduction is the only significant reaction which occurs after CO is added. This makes TiO_2 a promising catalyst for reduction of sodium sulfate in an alternative low temperature kraft recovery process.

The kinetics of sulfate reduction of a mixture of 19% TiO_2 , 45% Na_2SO_4 and 36% Na_2CO_3 by 50% CO was studied at temperatures from 640 to 750°C . The conversion, X, versus time data is shown in Figure 19. The absence of an initiation and accelerating period in the conversion curve suggests that the reduction in the presence of TiO_2 is not catalyzed by Na_2S . Also included in Figure 19 are the same data fitted according to different gas-solid and solid-solid kinetic equations. It shows that the data are best described by equation (10) for an ash diffusion controlled gas-solid reaction [11] rather than equations (8) and (9) for solid-solid reactions. Most of the conversion-time data at other temperatures are also well described by equation (10) as can be seen in Figure 20. The linear correlations do not pass through the origin possibly because the reduction is reaction controlled at very low conversions [11]. The data for 730°C and 750°C deviate from equation (10) above conversions of respectively 80 and 60% (or kt of respectively 0.37 and 0.17) because fusion of the particles



a)



b)

Figure 18, The microscopic picture of the sample before a) and after b) the reduction with Fe_3O_4 .

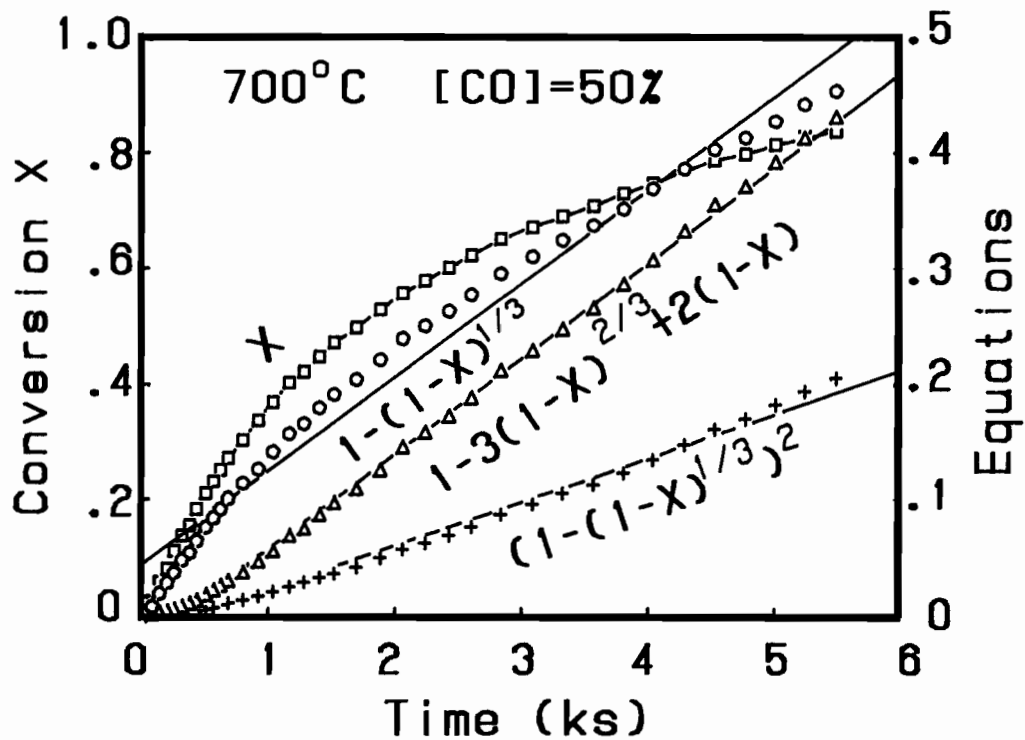


Figure 19, Reduction kinetics of Na_2SO_4 by CO in the presence of TiO_2 .

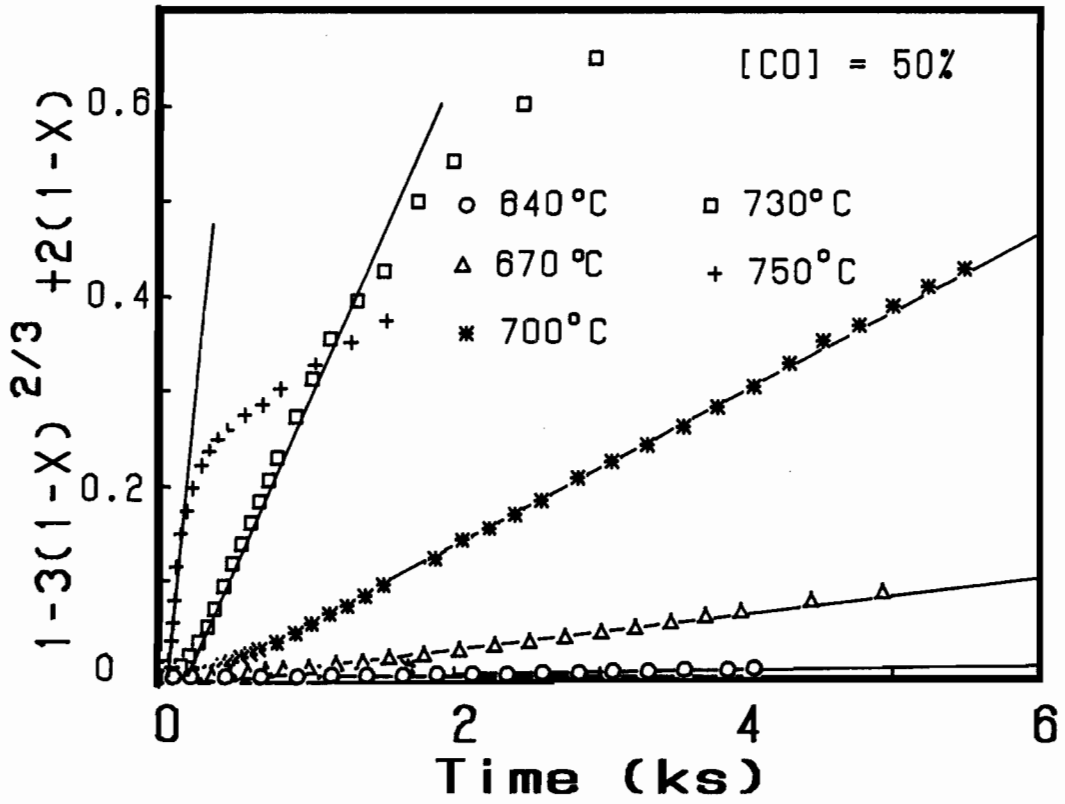


Figure 20, Influence of temperature on reduction kinetics in the presence of TiO_2 .

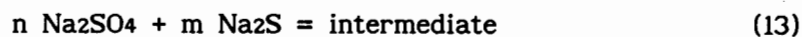
reduces the diffusion of CO. The slopes of the linear correlations in Figure 20 are plotted versus $1/T$ in Figure 21. The activation energy associated with the ash diffusion controlled reduction of sulfate in the presence of TiO_2 is 414 kJ/mol.

TABLE II. REDUCTION CATALYZED BY TITANIUM AND IRON OXIDE

Cat.	T °C	[CO] %	[CO ₂] %	TIME min	W _{SO₄} ^o mg	W _{SO₄} ^f mg	W _S ^f mg	0.5WL mg	ΔW _s %
-	725	50	0	56	1.79	1.43	0.40	0.43	+2
TiO ₂ 8%	700	50	1.5	64	0.86	0.40	0.45	0.45	-1.2
TiO ₂ 19%	730	50	0	55	0.58	0.007	0.57	0.56	-0.5
Fe ₃ O ₄ 8%	700	50	1.5	28	0.64	0.04	0.47	0.55	-21.3
Fe 7%	750	50	1.5	12	0.81	Neg.	0.55	0.62	-30
FeS 8%	700	50	1.5	16	1.48	0.16	0.45	0.84	-60

CONCLUSION

The reduction of sodium sulfate by CO is an auto catalytic reaction. After an initiation time, the conversion is well described by phase boundary reaction controlled kinetics for a solid-solid reaction. It is proposed that the rate determining solid-solid reaction is



followed by rapid reduction of the intermediate compound to Na_2S . The minor effect of CO concentration on the reduction is in agreement with this mechanism. The presence of CO_2 strongly reduces the reduction rate. For this case the major decelerating part of the conversion-time curve is best

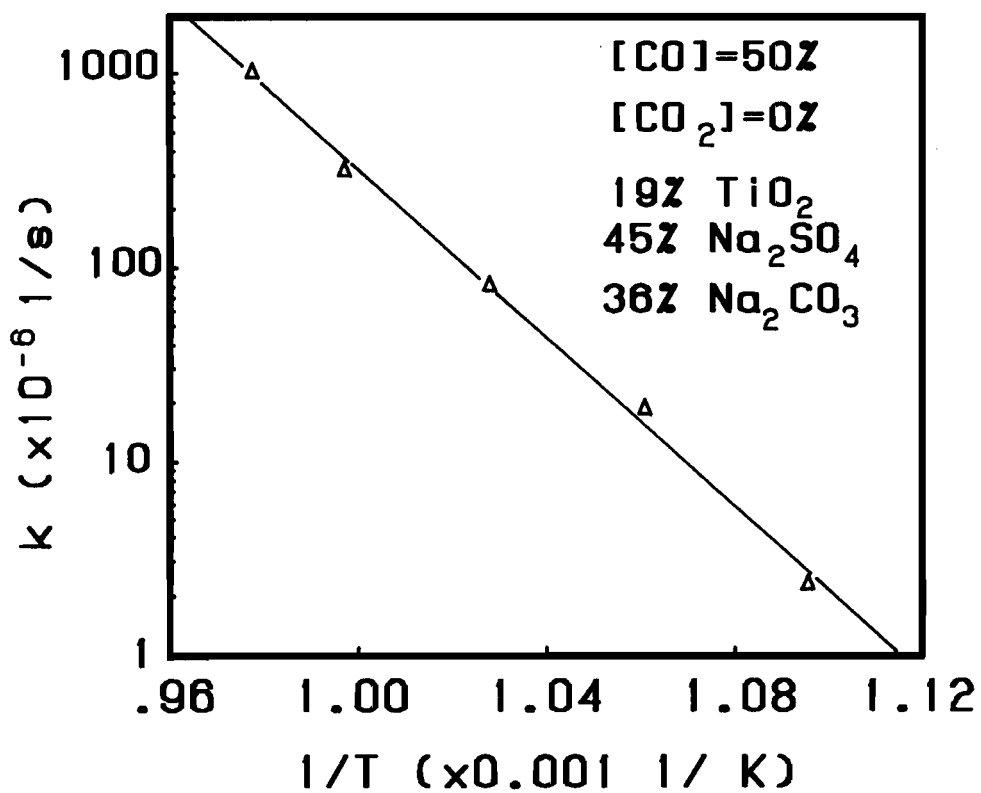


Figure 21, Arrhenius plot of the reaction constant of sulfate reduction by CO with presence of TiO₂.

described by product diffusion controlled kinetics for a solid-solid reaction. This indicates that diffusion of Na_2S to the reaction interface rather than the subsequent reaction (13) is determining the overall reduction rate. The gas-solid reaction between CO and Na_2SO_4 is identified as the initiation reaction. The reaction is first order in CO and has an activation energy of about 250 kJ/mol . The presence of Na_2CO_3 influences the reduction, due to its effect on melting temperature in the ternary system. When a uniform molten phase is formed, the reduction rate is controlled by mass transfer of CO in the liquid melt. The reduction of Na_2SO_4 by CO is catalyzed by titanium and iron oxide. However, iron oxide also catalyzes the formation of COS and its presence leads to sintering during reduction. Titanium dioxide does not suffer from these drawbacks and is a promising catalyst for an alternative low temperature kraft recovery process. The reduction is well described by the kinetic expression for ash diffusion controlled gas-solid reactions. No auto catalytic effect was observed. The activation energy over the temperature range of $640 - 750^\circ\text{C}$ is 414 kJ/mol .

NOMENCLATURE

C_A^*	= equilibrium concentration of A, $\text{mol}\cdot\text{m}^{-3}$
C_{B0}	= concentration of B in liquid, $\text{mol}\cdot\text{m}^{-3}$.
D_A	= diffusion coefficient of gas A in liquid, $\text{m}^2\cdot\text{s}^{-1}$
E	= enhancement factor over pure physical absorption.
H	= Henry's coefficient, $\text{m}^3\cdot\text{mol}^{-1}$.
Ha	= Hatta number.
k	= reaction rate constant, $1/\text{s}$.
k_L	= mass transfer coefficient, $\text{m}\cdot\text{s}^{-1}$.
K_1	= reaction rate constant for initial reaction, s^{-1} .
K_{1,CO_2}	= adsorption constant of CO_2 for initial reaction.
p_A	= partial pressure of A.
r_A	= average rate per unit interfacial area, $\text{mol}\cdot\text{s}^{-1}\cdot\text{m}^{-2}$.
$-R_{\text{max}}$	= maximum reaction rate, min^{-1} .
S	= interfacial area, m^2 .
t	= reaction time, s .
W_0	= sample weight at start of reaction, mg .
W_t	= sample weight at time t , mg .

- WL = weight-loss, mg.
- $W_{SO_4}^o$ = initial weight of sulfate, mg.
- W_S^f = final weight of sulfide, mg.
- $W_{SO_4}^f$ = final weight of sulfate, mg.
- ΔW_s = percentage difference in sulfur content of sample before and after reaction, %.
- X = sulfate conversion, mg/mg.

Greek symbols

- Φ = the overall rate of the gas-liquid reaction, $\text{mol}\cdot\text{s}^{-1}$.

REFERENCES

1. Nguyen, X.T., **Canadian Patent**, No. 1193406(1985).
2. Fallavollita, J., M.M. Avedesian and A.S. Mujumder, **Can. J. Chem. Eng.**, 65, 10, p.812(1987).
3. Birk, J.R., C.M.Larsen, W.G.Vaux and R.D.Oldenkamp, **IEC. Proc. Des. Dev.**, 10, 1, p.7(1971).
4. Sjoberg, M. and J.Cameron, **AIChE Symposium Series**, 76, 200, p.35(1981).
5. Cameron, J.H. and T.M. Grace, **IEC. Fundam.**, 22, 4, p.486(1983).
6. Cameron, J.H. and T.M. Grace, **IEC. Fundam.**, 24, 4, p.443(1985).
7. Budnikoff, P.B. and E. Shilov, **J. Soc. Chem. Ind.**, 6, 4, p.111T(1928).
8. White, J.F.M. and A.H. White, **Ind. Eng. Chem.**, 28, 2, p.244(1936).
9. Ahlgren, P. and et al **Acta. Chem. Scand.**, 21, p.1119(1967).
10. Oldenkamp, R.D. and E.D. Margolin, **Chem. Eng. Prog.**, 65(11), p.73(1969).
11. Levenspiel, O. **The Chemical Reactor Omnibook**, OUS Bookstore Inc., Corvallis, p 51.5 and p.55.2.
12. Jach, J. **Phys. Chem. Solids**, 24. p 63(1963).
13. Jander, W., **Z. Anorg. Allgem. Chem.**, 163, p 1(1927).
14. Park, J.Y. and O. Levenspiel, **Chem. Eng. Sci.**, 30, p.1207 (1975).

15. Dearnaley, R.I., D.H. Kerridge and D.J. Rogers, *Inorg. Chem.*, **22**, 22, p.3242(1983).
16. Andersson, S., *Chemica Scripta*, **20**, p.164(1982).
17. Tegman, R. and B. Warnqvist, *Acta Chem. Scand.*, **26**, 1, p. 413(1972).
18. Bergman, A.G., and A.K. Sementsova, *Zhur. Neorg. Khim.*, **3**, 2, p.388(1958).
19. Tran, H.N. and D. Barham, **1981 Intern. Recov. Conf. of Pulping Chem.**, p.67(1981).
20. Szekely, J., and N.J. Themelis, **Rate Phenomena in Process Metallurgy**, John Wiley & Son, Inc., N.Y., p.369(1976).
21. Coulson, J.M., and J.F. Richardson, **Chemical Engineering**, vol.3, Pergamon, NY, (1971).
22. Charpentier, J.C., **Advances in Chem. Eng.**, vol. 11, AP, p.1(1981).
23. Sim, M.T. and R.Mann, *Chem. Eng. Sci.*, **30**, p.1215 (1975).
24. Appleby, A.J., and C. van Drunen, *J of Electrochemical Soc.*, **127**(8), p.1655(1980).
25. Kiskila, E., **Paperi ja Puu-Papper och Tra**, **10**, p.639(1979).

CHAPTER 8

KINETICS OF SOLID STATE REDUCTION OF SODIUM SULFATE BY CARBON

ABSTRACT

The reduction rate of solid sodium sulfate in black liquor char was studied in a thermogravimetric analysis system. The char was obtained by pyrolysis of dry solids of oxidized black liquor mixed with additional sodium sulfate, and consists of a finely dispersed mixture of carbon, sodium carbonate and sodium sulfate. The reduction was performed with complete mass transfer limitation to the ambient by employing a reaction cup with a relatively large height-to-diameter ratio. It was found that sulfate reduction by carbon is auto catalytic. The reduction of sulfate is well described by second order nuclei growth controlled reaction kinetics over a wide range of conversions. An activation energy of 291 kJ/mol was determined from isothermal experiments at 680 to 780°C. The reduction rate increases with increasing carbon to sulfate ratio and amount of sodium carbonate. In the proposed reaction mechanism, Na₂S is initially formed on an active site by a slow reduction of sulfate to sulfite, followed by fast reduction of sulfite to sulfide with carbon or CO. The production of an intermediate, possibly liquid poly-sulfide from reaction between sodium sulfate and sodium sulfide, is proposed as rate determining step during the main reduction phase.

INTRODUCTION

The oldest method for commercial production of sodium sulfide is the reduction of Na_2SO_4 with powdered coal at 900-1000°C. Although this method is presently not in use any more [1], sodium sulfide, as one of the effective pulping chemicals, is produced under similar conditions in a kraft recovery furnace. In this furnace so-called black liquor is burned for energy generation and recovery of pulping chemicals. It is generally believed that the reduction of sulfate takes place in the char bed at the bottom of the recovery furnace at temperatures in excess of about 760°C [2]. The molten sulfate reacts in the presence of carbon to form sulfide, carbon monoxide and carbon dioxide.

A high char bed temperature is usually proposed [2] to achieve both a high reduction efficiency and a high rate of carbon consumption in the recovery furnace. Unfortunately the elevated char bed temperature leads to several technical and operational problems. For example, accidental contact between water and molten sodium salts after a steam pipe rupture can lead to a violent smelt-water explosion. Also, the emission rate of elemental sodium increases with increasing char bed temperature, causing fouling of the steam pipes. To solve these problems, and also to reduce the capital investment for the recovery operation, a number of kraft recovery alternatives have been proposed [3]. A fluidized bed recovery process is an attractive alternative from an investment point of view because the high heat and mass transfer characteristics of fluidized beds leads to a more compact process. However, to prevent agglomeration of the char particles, a fluidized bed has to be operated below the melting point of the sodium salts. This simultaneously eliminates the hazard of smelt-water explosions and reduces the sodium emission and corrosive nature of the sodium salts in the char. Important questions are, however, whether a high reduction efficiency can be obtained at temperatures below the melting point of the sodium salts and what are the important controlling parameters for this reaction.

Very little is known about the kinetics and mechanism of solid state reduction of Na_2SO_4 by carbon, despite the fact that reduction of Na_2SO_4 by H_2 , CO or carbon has been the subject of investigation of many studies [4-11]. A number of studies of Na_2SO_4 reduction by carbon in the solid

state were reported many years ago [4-6]. Budnikoff [4] stated that Na_2SO_4 could not be reduced by graphite below 850°C . White and White [5] reported that reduction of Na_2SO_4 by bituminous coal starts at about 650°C . Kubelka and Hojnos [6] found that the reduction of sulfate starts at a temperature between 600 and 630°C for a mixture of fine powdered activated carbon and sodium sulfate. With the addition of powdered sodium carbonate, reduction efficiencies of about 90% are obtained when the mixture is kept at 650°C for 30 minutes. Other relevant studies are those by Cameron and Grace [9-10] concerning Na_2SO_4 reduction by carbon in sodium carbonate melts. They found that the reduction rate was zero order at low sulfate concentrations, proportional to carbon surface area, and slower in a NaCl melt.

The objectives of this study are to develop kinetic equations for solid state reduction of Na_2SO_4 by carbon in black liquor char. The results of this study will aid the development of a melt-free reduction reactor as part of an alternative low temperature kraft recovery process.

BACKGROUND OF REACTOR DESIGN

It was first reported by Budnikoff and Shilov [4] that Na_2SO_4 reduction by carbon was much faster with CO present than by carbon or CO alone. Based on their experimental results, Cameron and Grace [9] proposed a mechanism for sulfate reduction by carbon in a carbonate melt. They proposed that sulfate in the carbonate melt adsorbs on a carbon surface active site and then reacts with the site forming CO_2 and a reduced sulfur compound. The active sites were postulated to be CO molecules adsorbed on the carbon surface. The produced CO_2 could in turn react with carbon forming more CO which would adsorb on the carbon surface, etc. These two studies suggest that the reduction may proceed via gas intermediates, CO and CO_2 .

It has been found that many high temperature solid-solid reactions proceed via liquid or gas intermediates [12]. Probably the most common and important examples of this type of reaction are the reduction of metal oxides by carbon in the metallurgical field. Because of its industrial importance, this type of reaction has been studied by many researchers both theoretically and experimentally [13-16]. It was pointed out by Sohn and Szekey [14] that in order to study the chemical kinetics of this type of reaction, the system has to be mass transfer limited to the ambient so that the gas phase composition surrounding the solids is only determined by

product gases. A criteria was proposed to test this condition. In general, a high reaction rate and a low ratio of exposed surface area to solids volume are required to obtain this condition. Based on this requirement, a special micro-reactor crucible with a relatively large height-to-diameter ratio was used in the present study.

It was found by the present author [17-18] that emission of CO and CO₂ and sodium vapor from black liquor char due to reaction of sodium carbonate with carbon can be very significant under an inert atmosphere at temperatures above 700°C. However, it was also found that the decomposition of sodium carbonate can be suppressed when a few percent of CO is present in the gas phase. Since the product gas of Na₂SO₄ reduction will contain CO and CO₂ it is expected that decomposition of sodium carbonate is insignificant.

It was found during preliminary experiments that the CO/CO₂ ratio in the product gas changed with type of char, experimental conditions and progress of reduction. Since the reduction can be described by the following two overall reactions,



the weight-loss curve obtained with the TGA system cannot be used to obtain the reduction rate. However, the oxygen removed with CO and CO₂ as function of time can be used to obtain the reduction kinetics.

EXPERIMENTAL

Experimental Apparatus

A schematic picture of the Cahn TGA 113-DC system with auxiliary gas preparation system is shown in Figure 1. N₂ (99.998%) and He (99.995%) are zero grade quality and CO₂ is anaerobe grade (99.99%). An oxygen trap is used for each gas. The temperature inside the reactor tube is measured by two thermocouples, K and E type. The reproducibility of the temperature setting is better than ± 1°C, and the accuracy is better than ± 5°C.

of watch glasses below 120°C. This drying method was used to prevent enrichment of inorganic salts in the mother liquor. After scraping from the glass surface, the solids were pyrolysed for 30 minutes under nitrogen in a tube furnace preheated to 580°C. Swelling occurred during pyrolysis of untreated black liquor or samples with a small addition of chemicals. The pyrolysis yield depends on the amount of chemical added. The composition and pyrolysis yield of the char and modified chars are given in Table II. The chars were subsequently ground and the fractions passing a near 400 mesh (<30 µm) sieve were used.

In order to get a better understanding of the reaction mechanism, a reference sample was made from porous graphite powder (made by G.L.C.) mixed with a saturated Na₂SO₄ solution. The dry solids were ground and the powder with particle size below 25µm was used.

Experimental Procedure

With a full crucible containing 30-50 mg sample, the TGA system is flushed with 500 scc/min of N₂ or He for over 40 minutes. Then under the same He or N₂ flow rate, the furnace temperature is raised from 20°C to 550°C at a rate of 25°C/min. After holding at 550°C for 15 minutes, the furnace temperature was raised to the reduction temperature at a maximum rate of 35°C/min. Shown in Figure 2 are the temperature, weight-loss and CO and CO₂ concentrations recorded by the computer for a typical run. Some weight-loss and some generation of CO and CO₂ occur during the heat-up period. The reason for keeping the sample at 550°C is to remove all CO and CO₂ from the char at a temperature where reduction of Na₂SO₄ does not yet take place. When the furnace temperature reached the reduction temperature, large amounts of CO and CO₂ were produced and a continuous sample weight decrease was recorded. At end of the experiments the reaction was quenched by cooling the reactor below 500°C within a half minute. When the furnace was at room temperature, the sample was immediately dissolved in deaired and deionized water with less than 10 seconds exposure to air to minimize oxidation. Within 5 minutes the sample was diluted with deaired and deionized water and injected into the IC for analysis of sulfide, sulfate, sulfite and thiosulfate. A small amount of H₂O₂ was then added to a part of the solution, whereby all sulfur containing species were oxidized into sulfate. Subsequently, total sulfur in the sample was determined by analysis of sulfate in the oxidized solution with the IC.

RESULTS

Mass Balance

The following chemical reactions may take place simultaneously:

1) Na₂SO₄ reduction



2) Na₂CO₃ decomposition



3) Desorption of oxygen



Since the sodium carbonate decomposition is negligible under the present conditions, the weight-loss is only due to formation of CO and CO₂. Therefore, the weight-loss recorded by the balance, ΔW_{tg} , should be equal to the total weight, ΔW_{gas} , of CO and CO₂ removed with the off gas as

$$\Delta W_{\text{gas}} = \int_t^0 \frac{Q}{R T} \left[M_1 p_1(t) + M_2 p_2(t) \right] dt \quad (7)$$

where Q is the gas flow rate, R the gas constant, T the temperature, M₁ and M₂ the molecular weight of CO and CO₂ respectively, and p₁ and p₂ the partial pressures of CO and CO₂ respectively. The starting time for integration is when the temperature is raised from 550°C.

If there is no oxygen desorbed from the char surface (reaction (6)), the weight of sulfide produced, ΔW_{S} , should be equal to half the oxygen weight, ΔW_{oxy} , in CO and CO₂ calculated as

$$\Delta W_{\text{oxy}} = \int_t^0 \frac{M_3 Q}{R T} \left[p_1(t) + p_2(t) \right] dt \quad (8)$$

where M₃ is the molecular weight of oxygen. Shown in Table III are the

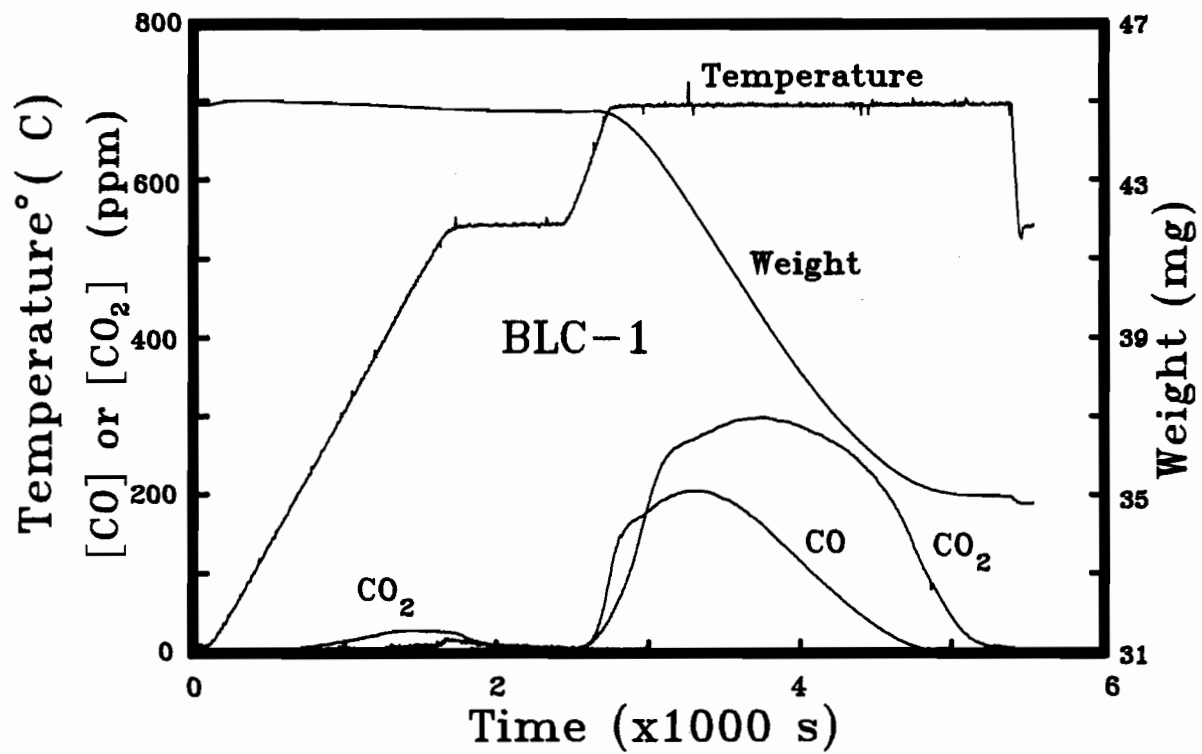


Figure 2, A typical computerized printout of an experiment.

total weight and oxygen versus sulfide mass balances for some typical runs.

TABLE III MASS BALANCE

Run No	Sample No	T (°C)	ΔW_{tg} (mg)	ΔW_{gas} (mg)	$\frac{1}{2}\Delta W_{oxy}$ (mg)	$\Delta W_{S=}$ (mg)	$\Delta W_{SO_4=}$ (mg)	ΔW_{St} (mg)	ϵ (%)
2	BLC-1	700	9.95	10.5	4.0	3.66	5.23	8.98	-8.5
3	BLC-2	700	11.5	11.7	3.85	3.44	1.13	4.95	-10
4	BLC-2	720	15.0	14.9	4.7	4.20	0.40	4.94	-10
5	BLC-2	740	16.1	16.3	5.47	5.44	0.11	5.93	-0.5
6	BLC-3	700	12.9	13.0	4.2	4.37	0.05	4.59	+4.0

Also listed in Table III are $\Delta W_{SO_4=}$ and ΔW_{St} , respectively the weight of sulfate and total sulfur in the final sample, and ϵ , the difference between $0.5\Delta W_{oxy}$ and $\Delta W_{S=}$ in percent.

As can be seen from Table III, the maximum difference between ΔW_{tg} and ΔW_{gas} is about 5% and mostly within 2%, confirming that sodium carbonate is stable. The maximum absolute value for ϵ is about 10%. This value is mainly the result of some sulfide being oxidized to other sulfurous species like sulfite, thiosulfate and poly-sulfides in the aqueous solution during analysis. Even with the stringent precautions used here, it was not possible to avoid oxidation of sulfide, and a very small amount of sulfite and thiosulfate accounting for up to 5% to 10% of sulfide formed was always detected. Therefore, the actual difference between sulfide in the solid sample, $\Delta W_{S=}$, and $0.5\Delta W_{oxy}$ is much less than 10%. This is confirmed when comparing the difference between ΔW_{St} and $\Delta W_{SO_4=}$ with $0.5\Delta W_{oxy}$, which shows a closer agreement. Based on the results in Table III, one can conclude that CO and CO₂ are only originating from the reduction of sulfate by carbon.

The accuracy of the data is accentuated in Figure 3 which shows the weight-loss curve obtained from the balance and that calculated with equation (7) for two typical runs. It shows that the two weight-loss curves for each experiment almost overlap each other. The slightly lower values obtained by equation (7) at the beginning of reduction can be explained by a transport delay of about 10 seconds between production of CO and CO₂ in the sample pan and detection by the analyzers. The slightly lower weight loss obtained by TGA at almost complete reduction can be explained by the

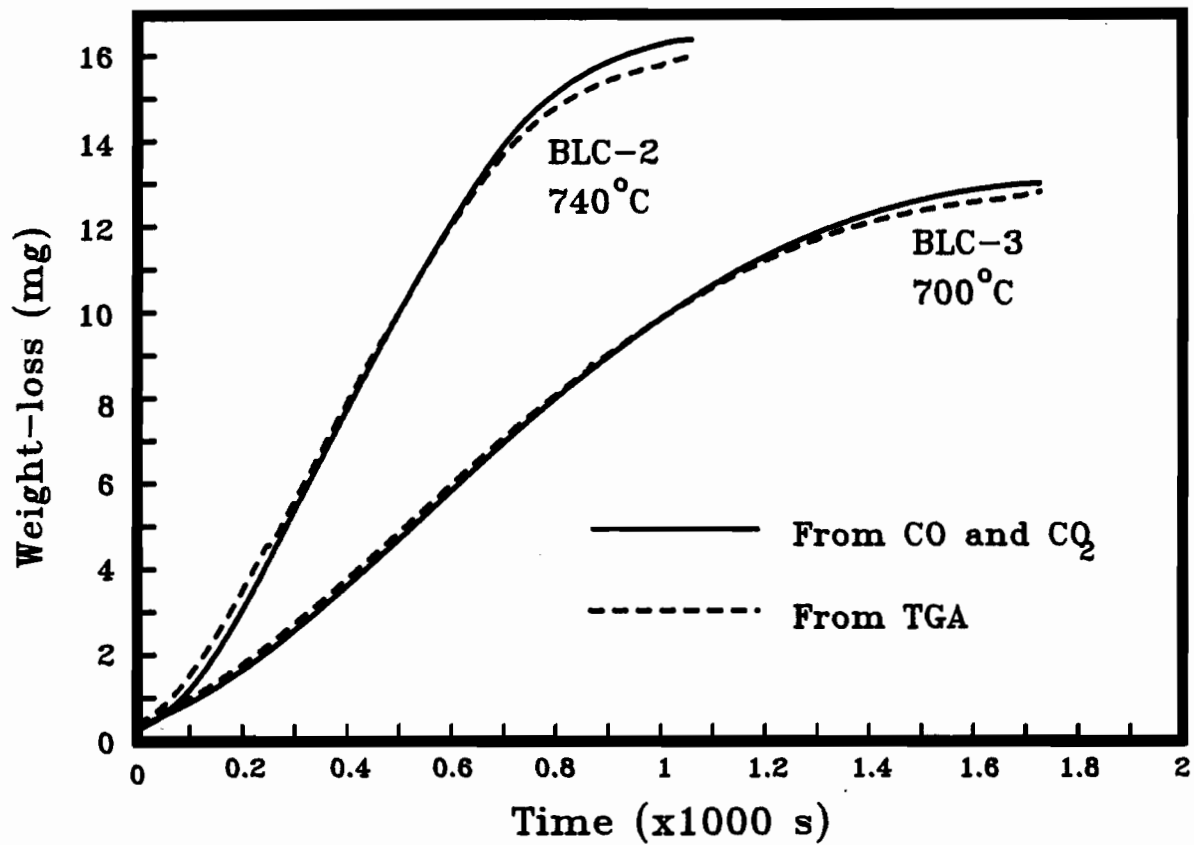


Figure 3, Weight-loss measured by TGA and calculated from CO and CO₂.

somewhat higher drag experienced by the pan at the higher reduction temperature compared to 550°C due to gas expansion and thus higher gas velocity.

Data Reduction

The sulfate conversion is calculated as:

$$x(t) = \frac{0.5 \Delta W_{oxy}}{\Delta W_{St}} \quad (9)$$

Shown in Figure 4 are the sulfate conversion-time curves obtained for sample No BLC-2 at different temperatures. As was stated before, the time when the furnace temperature was raised from 550°C was chosen as the starting point for integration of the CO and CO₂ data. However, the time when the constant reduction temperature was reached was taken as the starting time for analysis of the conversion versus time data. In most experiments, the amount of sulfate reduced during the heating up period accounted for less than 2% of total conversion. Only at temperatures above 760°C, this increased to 5 - 8% of total conversion, as can be seen in Figure 4.

Solid State Kinetics

Like many solid-solid reactions, the conversion-time curves in Figure 4 have a sigmoidal shape with an induction, acceleration and deceleration period. The induction period is not always clearly seen because it starts during the heating up period. The major part of the curve, 5 to 90% of conversion, was analyzed and tested for different kinetic expressions listed in Table IV.

It was found that the results obtained with sample BLC-0, BLC-2, BLC-3 and BL-N2 are well described by the nuclei growth controlled model or the well-known Avrami-Erofe'ev equation [19] for the case of n=2 (equation (19) in Table IV). This is shown in Figure 5 for BLC-3 at 700°C, where equation (19) is tested for n=1, 2 and 3. Besides 1, 2 and 3, other values of n tested were 2.5 and 5/3. In general, equation (19) with n=2 best fits the data for conversions of 0.05 to 0.90.

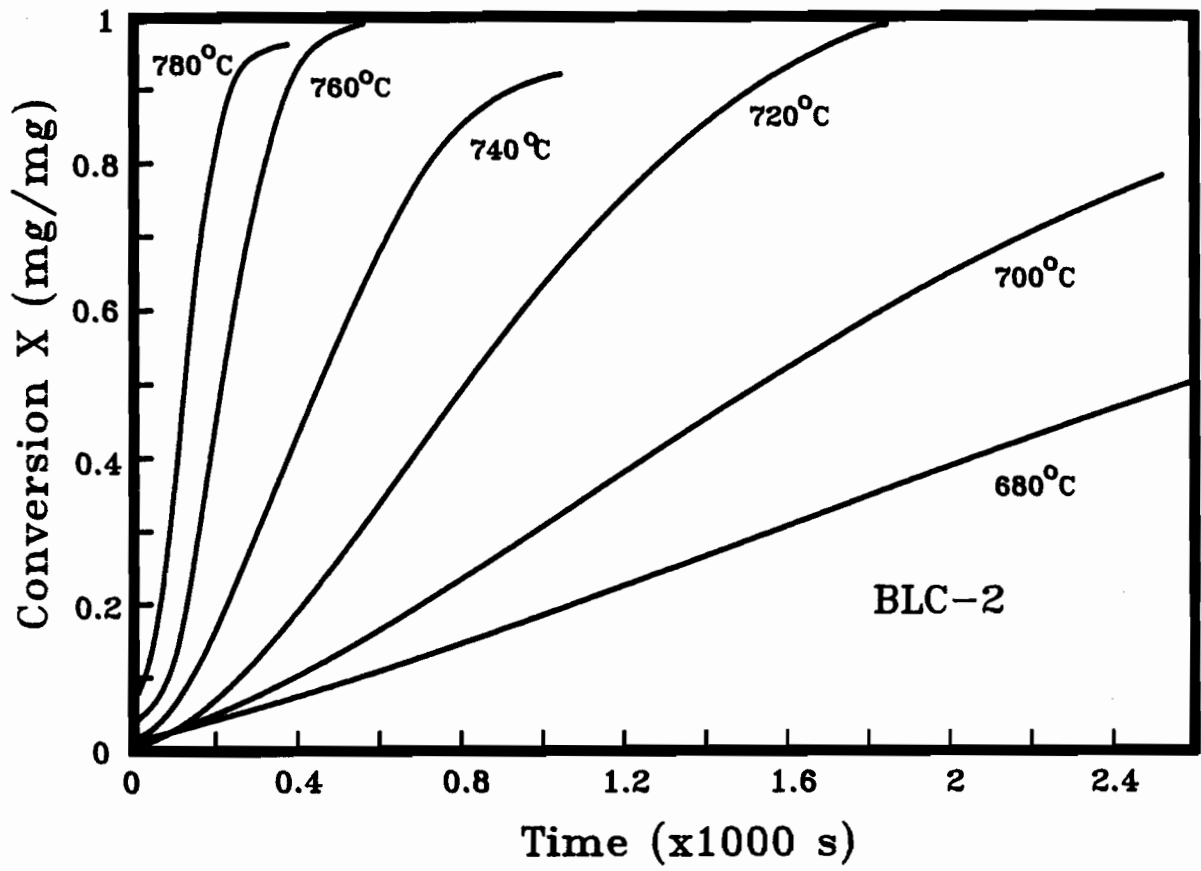


Figure 4, Sulfate conversion as function of temperature.

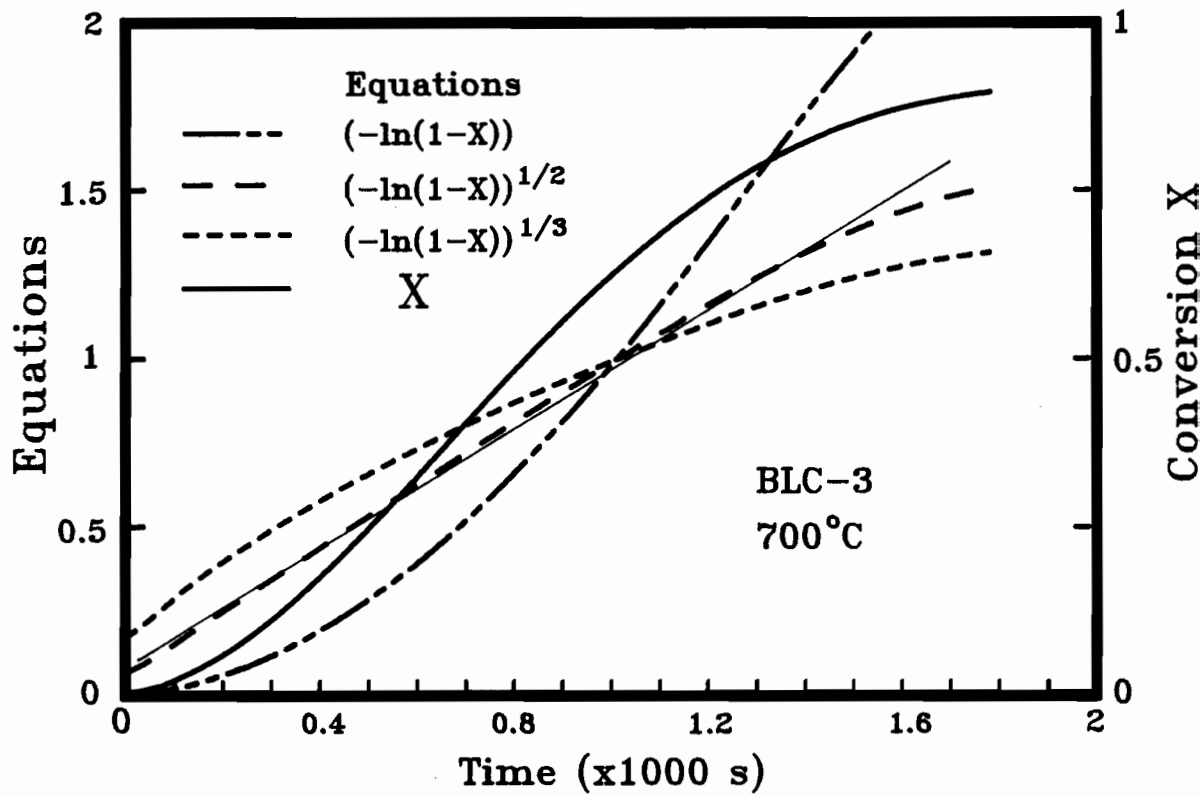


Figure 5, Reaction kinetics of sulfate reduction by carbon in black liquor char.

TABLE IV. KINETIC MODELS FOR SOLID STATE REACTIONS

Models	Mathematical Expression	Eq. No.	Ref. No.
<i>Product layer</i>			
<i>Diffusion:</i>			
One-Dimensional	$x^2 = kt$	(10)	[20]
Two-Dimensional	$(1-x) \ln(1-x) + x = kt$	(11)	[20]
Three-D	$[1 - (1-x)^{1/3}]^2 = kt$	(12)	[21]
Ginstlin-Brounstein	$1 - 2x/3 - (1-x)^{2/3} = kt$	(13)	[20]
<i>Phase Boundary</i>			
<i>Reaction:</i>			
Disk & cylinder	$1 - (1-x)^{1/2} = kt$	(14)	[22]
Sphere	$1 - (1-x)^{1/3} = kt$	(15)	[22]
<i>Based on order of reaction:</i>			
First order	$-\ln(1-x) = kt$	(16)	[20]
Second order	$(1-x)^{-1} = kt$	(17)	[20]
Third order	$(1-x)^{-2} = kt$	(18)	[20]
<i>Nuclei growth control:</i>	$[-\ln(1-x)]^{1/n} = kt$	(19)	[19]
<i>Acceleration equations:</i>			
Power law	$x^{1/n} = kt$	(20)	[20]
Exponential law	$\ln x = kt$	(21)	[20]
<i>Prout-Tompkins</i>	$\ln[x/(1-x)] = kt$	(22)	[23]

Effect of Temperature

Shown in Figure 6 are the data in Figure 4 fitted to equation (19) with $n=2$. As can be seen, the curves are linear over a wide range, indicating the validity of nuclei growth controlled kinetics for sulfate reduction by carbon in black liquor char. The reaction constant k was determined from the slope of the linear part of the curves. Shown in Figure 7 is the Arrhenius plot of the reaction constants. From the slope of the least

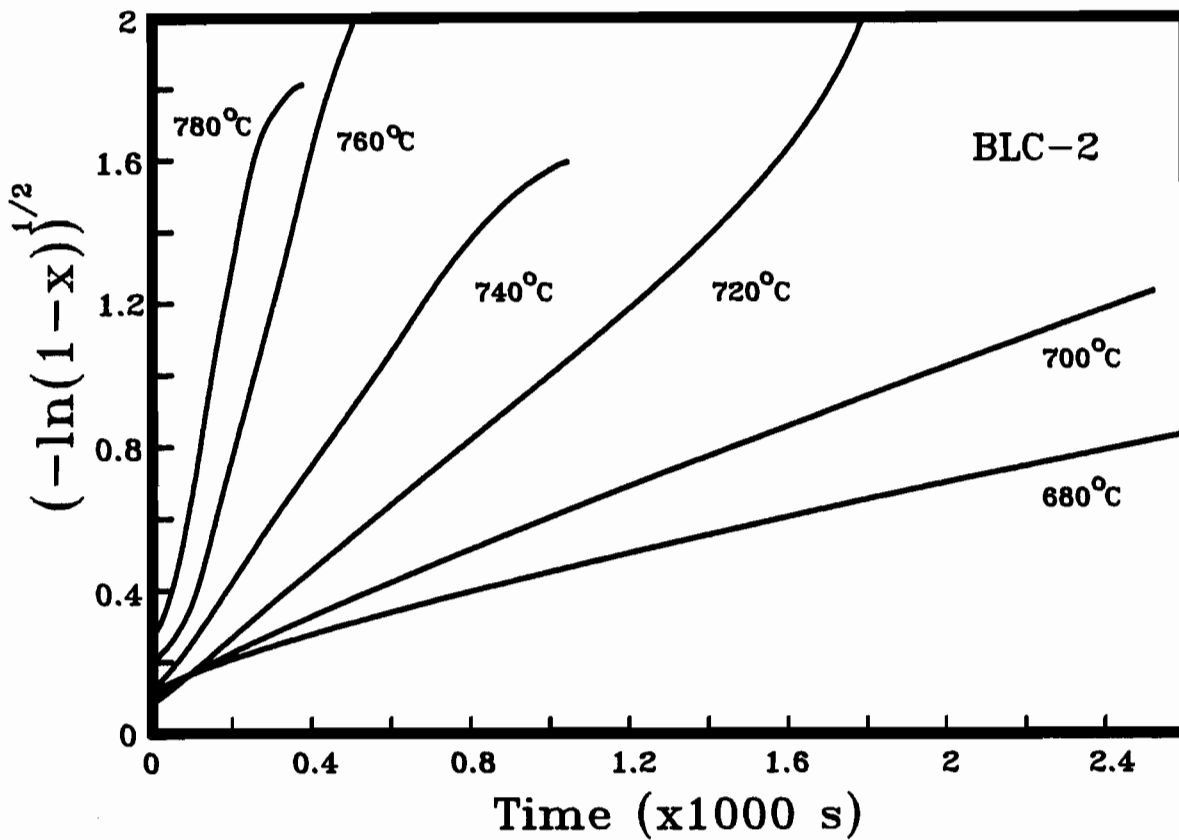


Figure 6, Effect of temperature on reaction rate.

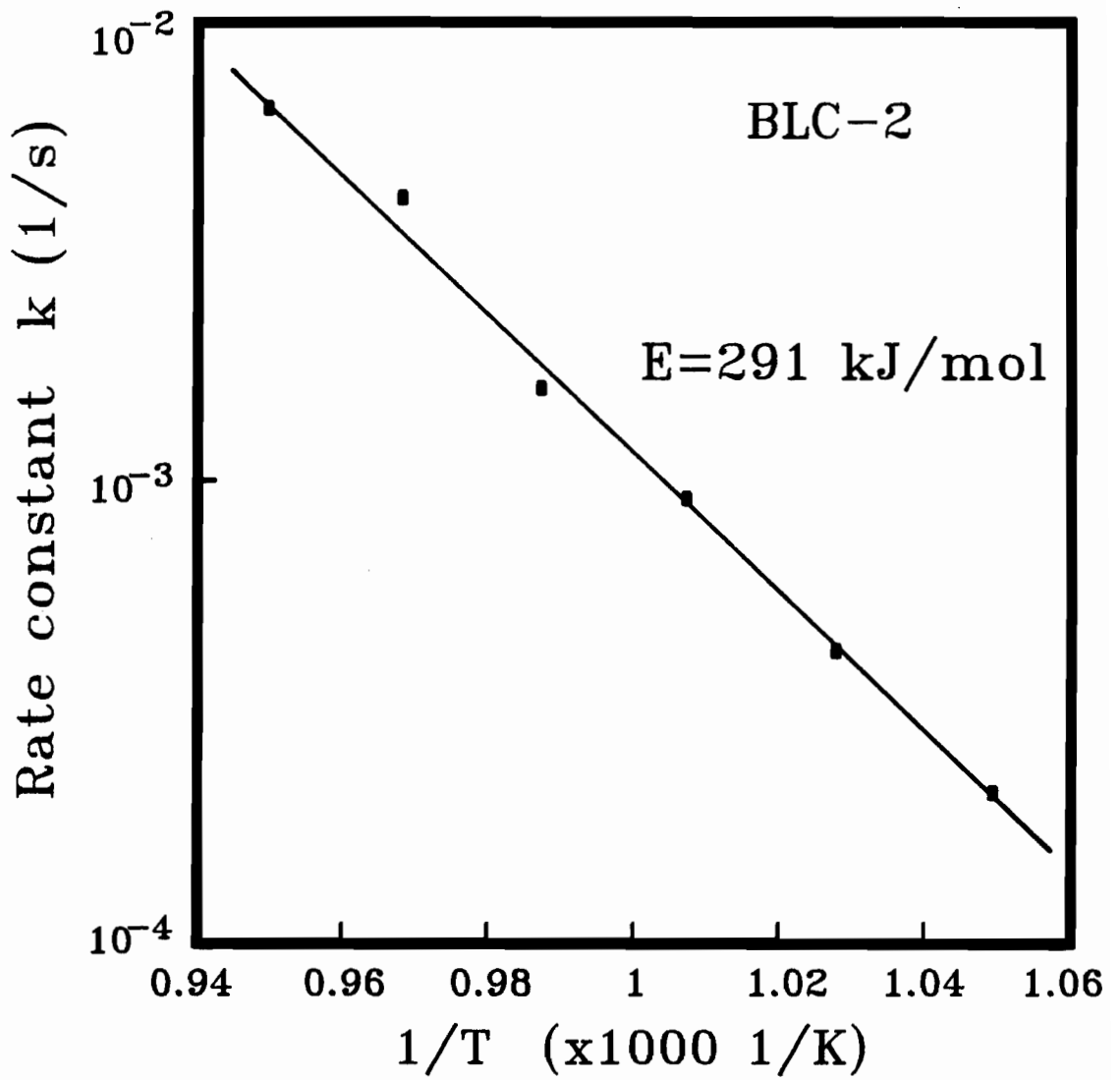


Figure 7, Arrhenius plot of reaction constant for sulfate reduction by carbon.

square fitted straight line, an activation energy of 291 kJ/mol is obtained for BLC-2.

Effect of Sodium Sulfate Addition

The effect of sodium sulfate addition to black liquor was studied by comparing the conversion data obtained with sample No. BLC-0, BLC-1, BLC-2 and BLC-3. The carbon to sulfate ratio of in these chars is given in Table II and Figure 8. Shown in Figure 8 is the sulfate conversion vs. time for these four chars at 700°C. It shows that with increasing Na₂SO₄ addition the reduction rate decreases. The lowest rate was obtained for sample BLC-1 in which the carbon to sulfate molar ratio is approximately equal to one. By fitting the data shown in Figure 8, it is found that only the results obtained for BLC-1 cannot be described by equation (19) and n=2.

Effect of Sodium Carbonate

In order to study the influence of sodium carbonate on Na₂SO₄ reduction by carbon, sodium carbonate in the original black liquor was converted into sodium sulfate to varying degrees according to reaction equation (3). The results of sulfate reduction obtained for samples BL-N1, BL-N2 and BLC-2 at 740°C are shown in Figure 9. As can be seen from the figure, the rate for BL-N2 is higher than that of BLC-2 although the latter has a larger sodium carbonate content. The higher rate of BL-N2 compared to BLC-2 is possibly caused by the higher C/SO₄ molar ratio of 6.5 for BL-N2 versus 2.8 for BLC-2. However the results for BL-N1 indicate that the reduction rate decreases significantly when almost all sodium carbonate is converted into sodium sulfate. Another important finding is that the conversion-time data for BL-N1 no longer can be described by nuclei growth controlled kinetics (Equations (19)). This means that the rate determining step in the reduction without sodium carbonate is different from that with sodium carbonate. As a matter of fact the reduction results for BL-N1 could not be described by any of the equations listed in Table IV.

Sulfate Reduction with Graphite

In order to get more insight in the mechanism, Na₂SO₄ reduction by graphite (sample G-S1) was studied. Plotted in Figure 10 are the results

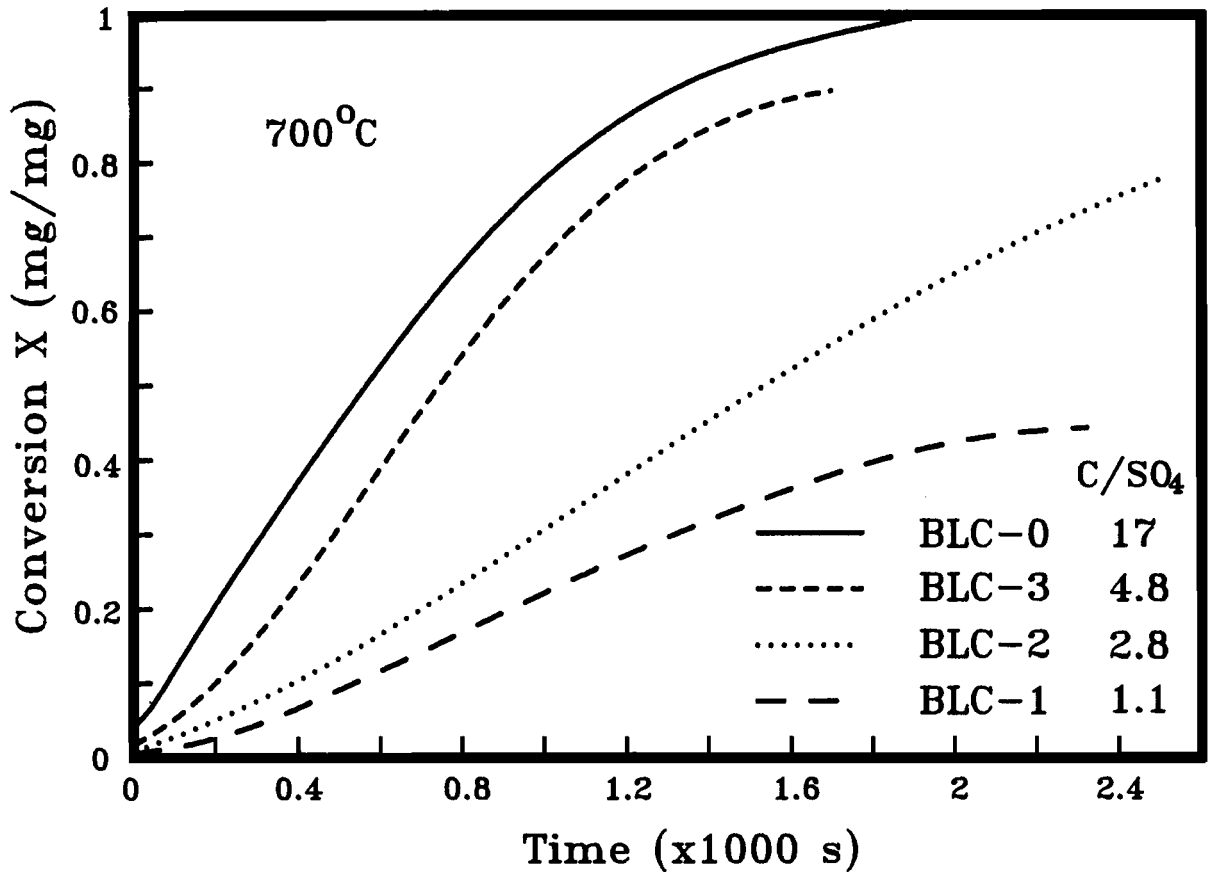


Figure 8, Effect of sodium sulfate addition on reduction rate.

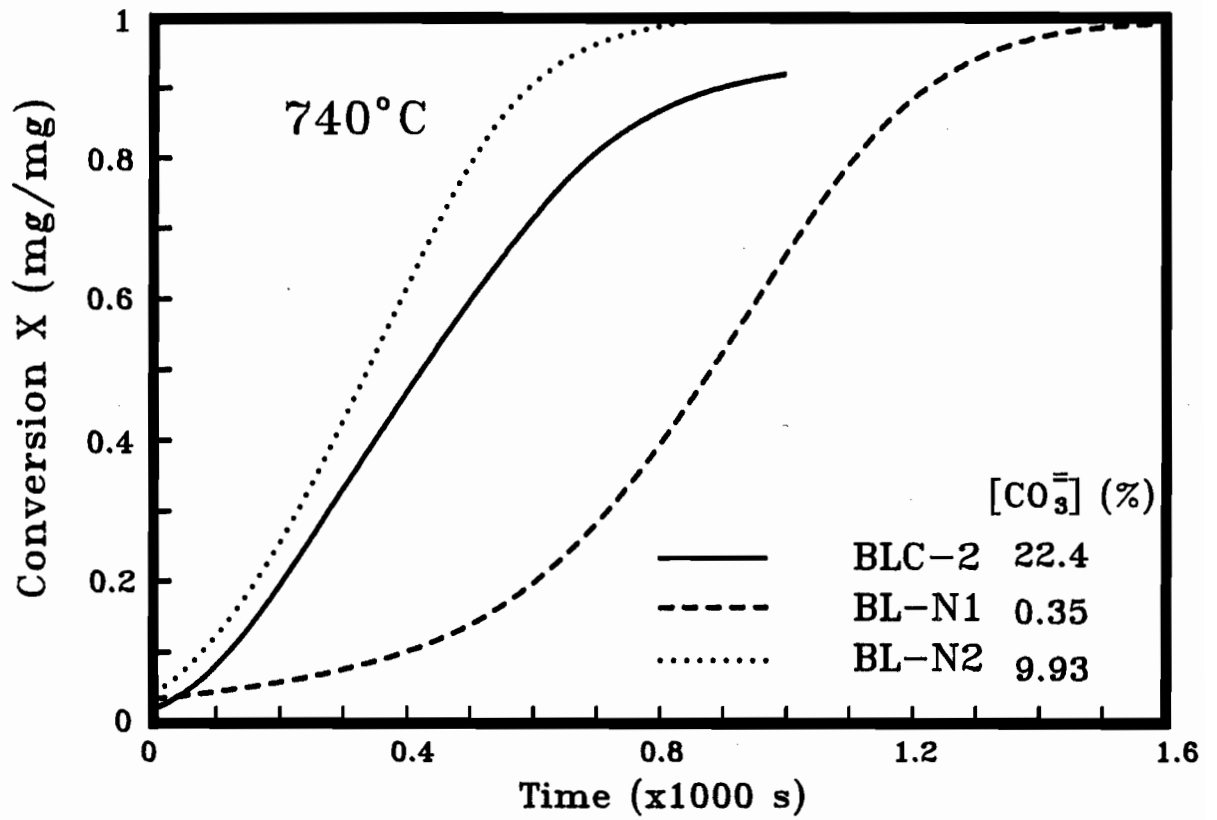


Figure 9, Effect of sodium carbonate on reduction rate.

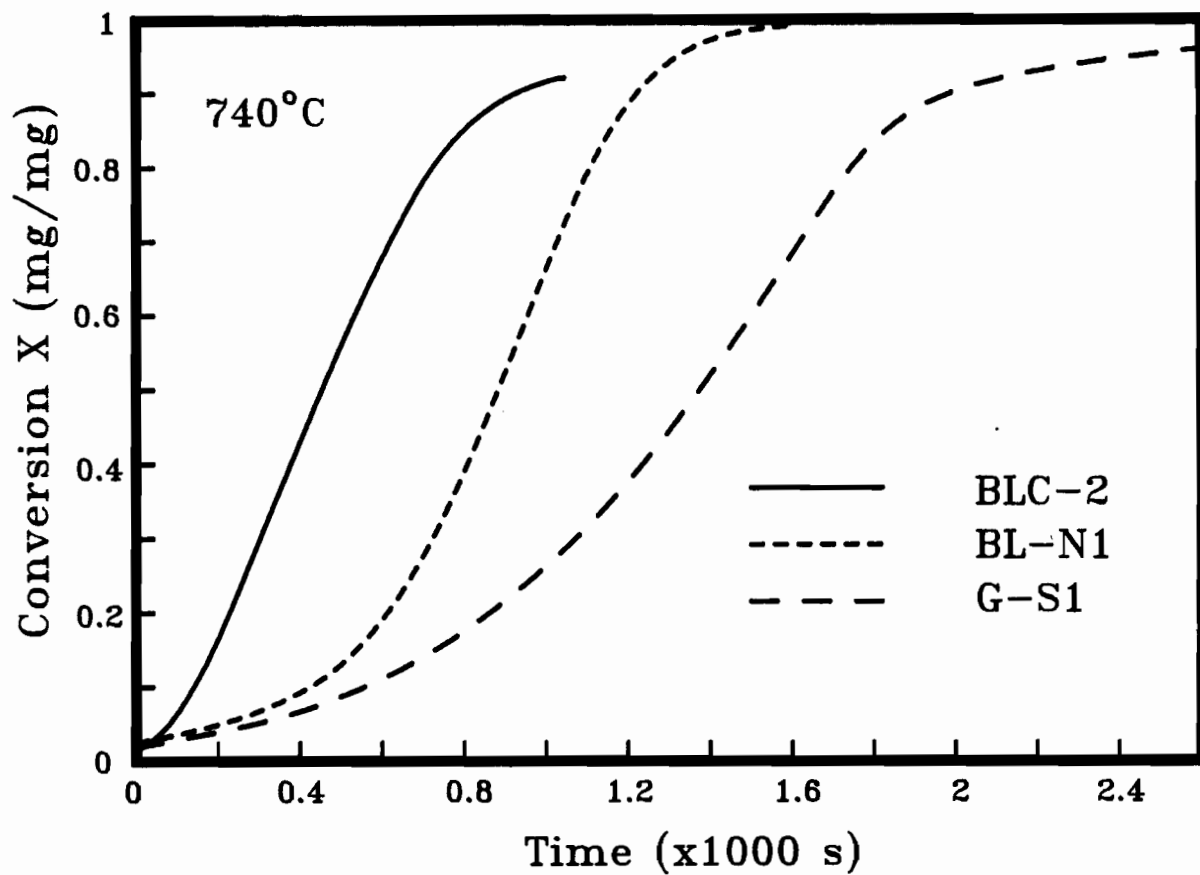


Figure 10, Comparison of sulfate reduction by black liquor char and graphite.

obtained at 740°C for samples G-S1, BLC-2 and BL-N1. The time to obtain 95% conversion for G-S1 is about twice that of BL-N1 although the latter has a slightly smaller carbon/sulfate molar ratio. As can be seen from the figure, the shape of the conversion-time for graphite is very different from that of the BLC samples, with an accelerating period extending up to 75% conversion. It was found that the accelerating period can only be well described by a power law reaction kinetic expression with $n=4$ (equation 18).

Effect of Particle Size

The effect of particle size was studied for sample BLC-2. Only two fractions were used: $> 30\mu\text{m}$ and $< 30\mu\text{m}$. The reduction was performed at 700°C and the results are shown in Figure 11. The results show that the reduction rate is not significantly affected by particle size for conversions below 40%. Above 40% conversion, the reduction rate for larger particles is slightly smaller. The conversion-time curve for the larger particles can be described by equation (19), but with $n=5/3$ rather than $n=2$ for $0.05 < x < 0.9$.

Effect of Sample Pan

In order to study the effect of external mass transfer limitation of ambient gas on reduction rate, an experiment was performed using the shallow dish-shaped pan and helium as carrier gas. Because most black liquor char samples contain large amounts of Na_2CO_3 and reaction (3) cannot be suppressed under these conditions, sample BL-N1 was used for its very low content of Na_2CO_3 and close similarity in physical structure to the BLC samples. The reduction was performed at 740°C, and the results are presented in Figure 12. The shape of the conversion curve obtained with the shallow pan is quite different from that of the deep sample pan. As can be seen from the figure, the duration and shape of the accelerating period is respectively shorter and steeper with the shallow pan, resulting initially higher conversions. However, because the decelerating period starts earlier with the shallow pan, the time to achieve over 95% conversion is double that of the deep pan. It was found that the decelerating part of the conversion-time data for the shallow pan is well described by the kinetic expression for a three dimensional product layer controlled solid-solid reaction (equation (12) in Table IV) as is shown in Figure 12.

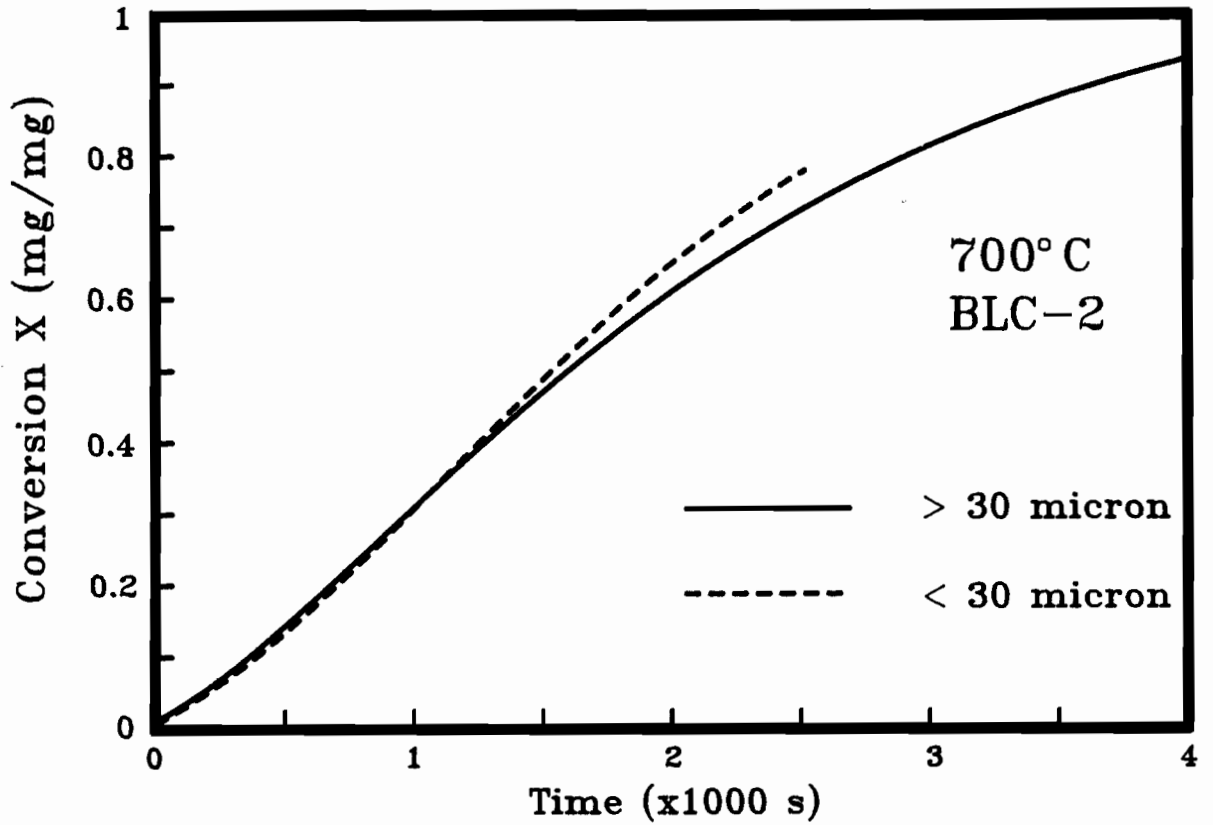


Figure 11, Effect of particle size on sulfate reduction rate.

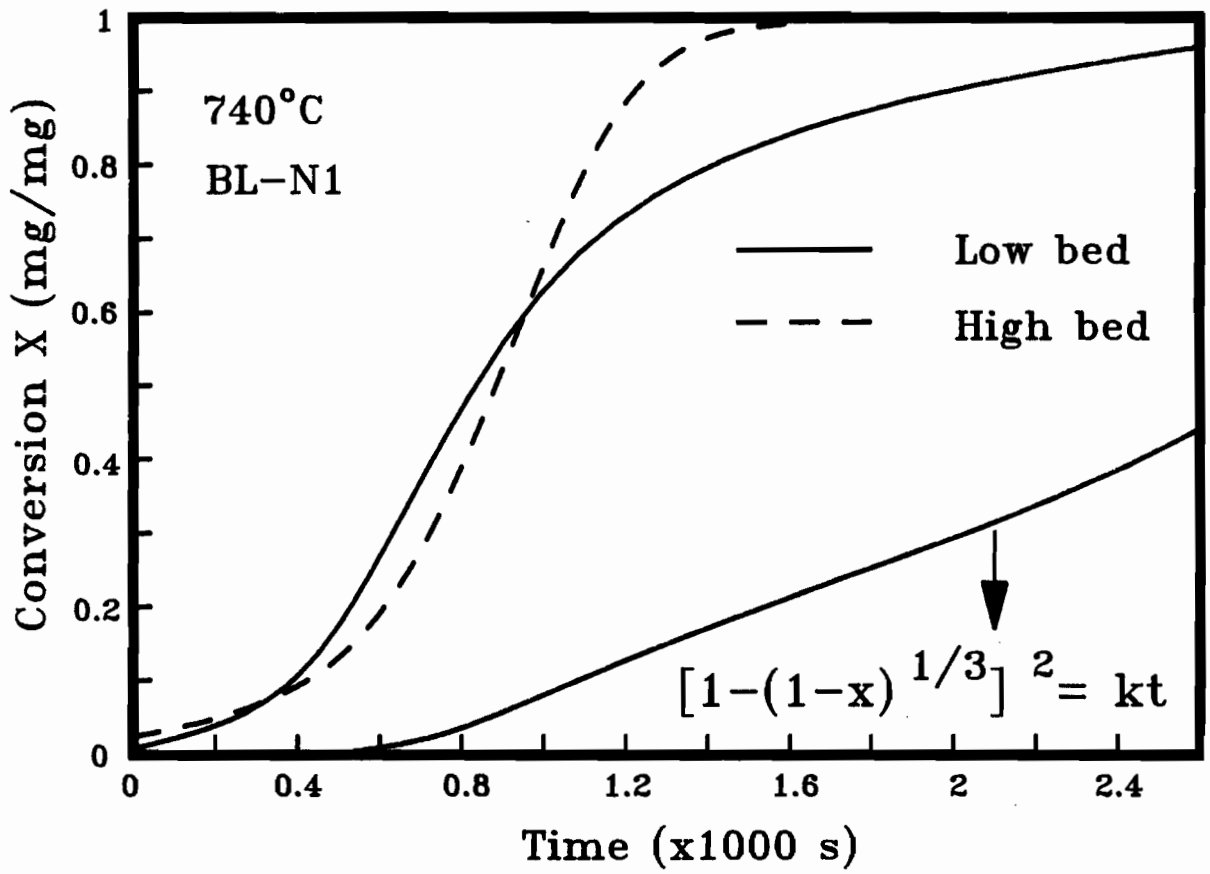


Figure 12, Effect of ambient gas on sulfate reduction rate.

DISCUSSIONS

Reduction Mechanism

System Analysis

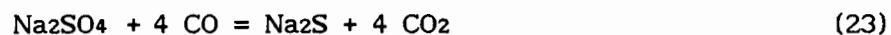
The previous results show that the conversion-time curves for sulfate reduction have a sigmoidal shape like many solid-solid reactions [12, 20]. The accelerating period starts during heating up and continues long after isothermal conditions are achieved. The decelerating period starts generally at relative high sulfate conversion.

Like the reduction of many metal oxides by carbon, the following reactions may be taking place simultaneously in the present reaction system:

a) direct reduction by carbon:



b) reduction by CO:



and

c) production of CO by gasification of carbon:



Reactions of type (1) and (2) proceed with difficulty for many metal oxides [16]. Reactions (23) and (24) form a closed cycle, and this type of reaction has been referred to as solid-solid reaction via a gas intermediate. The following analysis is to determine whether or not the present reaction system is controlled by this type of reaction mechanism.

For black liquor char if the sulfate reduction proceeds via a gas intermediate, the over-all reaction rate will be controlled by reaction (23), or reaction (24) or both. However, the reduction rate cannot be controlled by carbon gasification (reaction (24)) because of the following reasons. a). The CO₂ gasification of black liquor char [Chapter 3] or graphite [24] is first order in carbon and described by Langmuir-Hinshelwood type kinetics, while the reduction with its sigmoidal conversion-time behavior must be described by quite different kinetics. It has been pointed

out by several researchers [14-16] that the conversion-time curve will only be sigmoidal in shape, if the conversion-time curve of any of the rate determining reactions is sigmoidal. b). If the rate is controlled by reaction (24), CO₂ will be the major gas product. Shown in Figure 13 is the CO/CO₂ ratio in the product gas plotted as function of sulfate conversion for the experiments shown in Figure 4. It shows that the CO and CO₂ concentrations are of the same order of magnitude, indicating that the reduction rate is not limited by gasification. c) The activation energy of gasification by CO₂ [Chapter 3] is about 250 kJ/mol which is lower than 291 kJ/mol obtained for sulfate reduction.

TABLE V. CARBON GASIFICATION RATE
(Sample: BLC-2)

T (°C)	P ₁ / P ₂	P ₁ (atm)	P ₂ (atm)	-r _{c,c} (min ⁻¹)	-r _{c,m} (min ⁻¹)
680	1.38	0.42	0.58	0.0094	0.017
700	1.26	0.442	0.558	0.019	0.030
720	1.32	0.43	0.57	0.034	0.057
740	0.85	0.54	0.46	0.089	0.12
760	0.736	0.576	0.424	0.18	0.29

It has been shown in Chapter 7 that Na₂SO₄ reduction by CO (reaction (23)) is auto-catalytic and described by a sigmoidal conversion-time curve. Therefore, when the overall rate of reaction (3) is controlled by reaction (23), a sigmoidal type of conversion-time curve will be obtained. However, the following must be valid: a) a high CO/CO₂ ratio in the product gas, which increases with temperature because the gas composition is determined by the equilibrium of reaction (24); b) the gasification rate by CO₂ must be much faster than the carbon consumption rate for Na₂SO₄ reduction. The results in Figure 13 show that requirement a) is not true. Requirement b) can be tested by estimating the carbon gasification rate, -r_{c,c}, from kinetic data in chapter 3, assuming that only CO and CO₂ gas are present inside the char bed at a CO/CO₂ ratio shown in Figure 13. Another assumption is that the gasification rate is not significantly influenced by the presence of sodium sulfate or sulfide. The calculated gasification rates at about 30% sulfate conversion for the runs shown in Figure 4 are

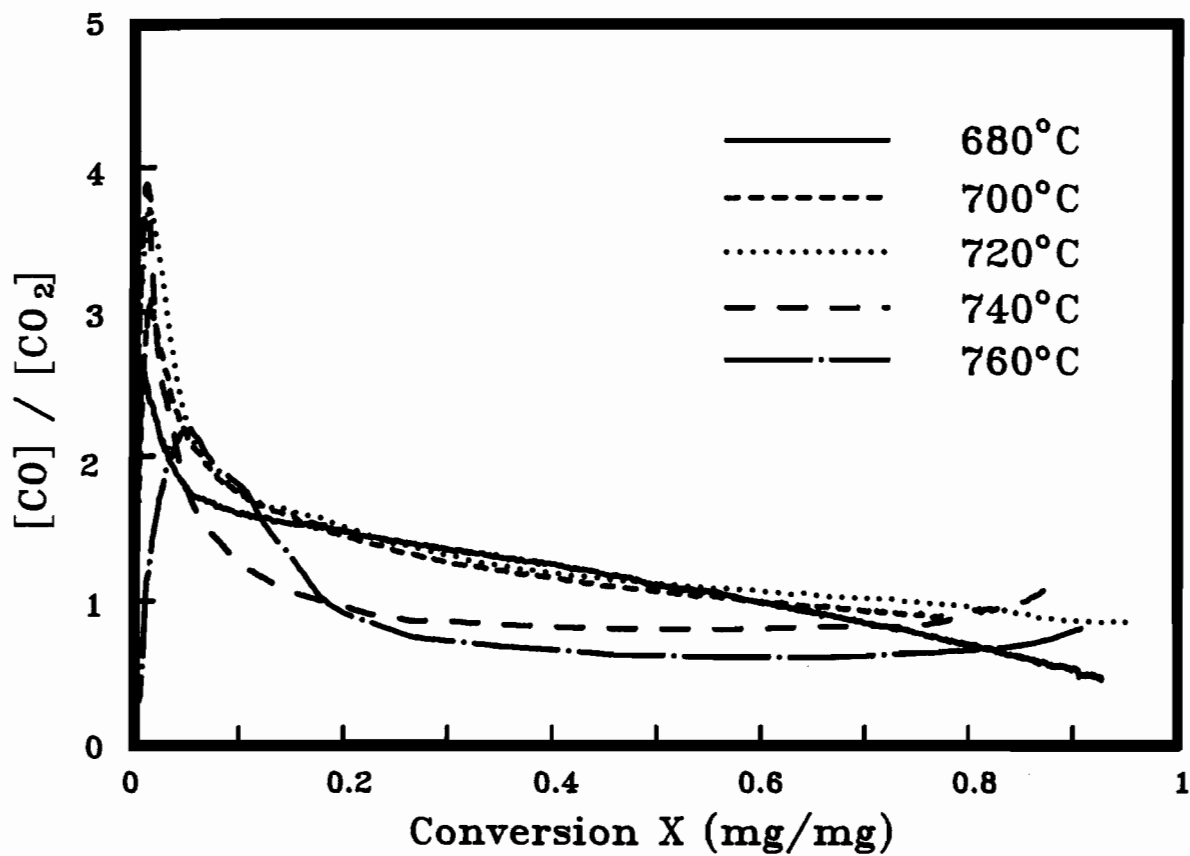


Figure 13, Effect of temperature on CO/CO₂ ratio.

listed in Table V. Also listed in Table V is the measured carbon consumption rate during reduction, $-r_{c,m}$, obtained from the CO and CO₂ production rates at about 30% of sulfate conversion. The results show that the rates of carbon gasification measured during reduction and calculated from CO₂ gasification kinetics are comparable, indicating that requirement b) is also not met. Therefore it appears that the reaction (24) is also not rate controlling and that it is unlikely that the reduction of sulfate by carbon proceeds via a gas intermediate for the present reaction system.

Proposed Mechanism

The above analysis then suggests that the kinetics of black liquor char reduction by carbon are determined by reactions (1) and (2). Based on the reaction mechanisms presented in chapter 3 and 7 for respectively carbon gasification by CO₂ and sulfate reduction by CO, the following reaction mechanism for sodium sulfate reduction by carbon is proposed. In black liquor char, sodium carbonate can be reduced by carbon whereby active sites, C* and C(O), are formed [Chapter 3]. During the initial period, sodium sulfate reacts with these active sites and forms sodium sulfite



and



It will be shown that sodium sulfite is extremely reactive and is rapidly reduced by carbon and CO into sodium sulfide

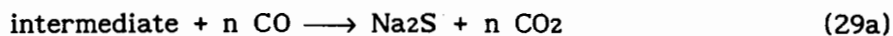


so that reactions (25) and (26) are the rate controlling steps during the initial period. Analogous to the mechanism for sulfate reduction by CO it is now proposed that Na₂S reacts with Na₂SO₄ to form an intermediate as



The nature of the intermediate is unknown, although poly-sulfide compounds have been proposed by others [7, 25] in sulfate reduction studies. The reduction of the intermediate is assumed to be much faster than the

reduction of Na_2SO_4 via reactions (25) and (26) and takes place via two parallel reactions



According to this proposed mechanism the sulfate reduction would be auto catalytic in Na_2S and accelerate until reaction (28) becomes limited by the amount of Na_2SO_4 available or by laws of solid-solid reaction kinetics as will be discussed later.

Sodium Sulphite Reduction

In order to support the proposed mechanism, some additional TGA experiments were performed with Na_2SO_3 in the shallow dish-shaped pan.

TABLE VI. DISPROPORTIONATION OF Na_2SO_3

T (°C)	Time (min)	$\Delta W_{\text{SO}_3}^i$ (mg)	ΔW_{S}^f (mg)	$\Delta W_{\text{SO}_4}^f$ (mg)	$\Delta W_{\text{SO}_3}^f$ (mg)	ΔW_{St}^f (mg)	Y (%)	δ (%)
700	14	0.305	0.022	0.069	0.208	0.299	32	1.8
750	6	0.311	0.071	0.228	0.012	0.306	96	1.5

Shown in Table VI are the test results obtained for disproportionation of pure Na_2SO_3 at 700 and 750°C in an inert atmosphere of nitrogen,



In the table, $\Delta W_{\text{SO}_3}^i$ is the initial sulfite weight as sulfur, while ΔW_{S}^f , $\Delta W_{\text{SO}_4}^f$, $\Delta W_{\text{SO}_3}^f$ are respectively the amount of sulfide, sulfate and sulfite in the final sample as sulfur, ΔW_{St}^f the sum of ΔW_{S}^f , $\Delta W_{\text{SO}_4}^f$ and $\Delta W_{\text{SO}_3}^f$, and δ the difference between initial sulfur $\Delta W_{\text{SO}_3}^i$ and final sulfur ΔW_{St}^f , divided by $\Delta W_{\text{SO}_3}^i$. The small values for δ prove that Na_2SO_3 disproportionates only in Na_2SO_4 and Na_2S . The results show that under inert atmosphere Na_2SO_3 is not stable at temperatures above 700°C, and a sulfite conversion, Y, of 32 and 96% is obtained in 14 and 6 minutes at 700 and 750°C respectively.

In the second set of experiments Na_2SO_3 is reduced by CO and graphite.

The first experiment shown in Table VII is the reduction of pure Na_2SO_3 powder with a particle size of $<30 \mu\text{m}$ by 100% CO at 600°C . It shows that reduction of Na_2SO_3 already starts at 600°C with 11% sulfide formed after 35 minutes. Comparison of $\Delta W_{\text{SO}_3}^i$ with ΔW_{St}^f shows that about 25% of the sulfur is not accounted for, and probably emitted as a sulfurous gas. The second run is the reduction of pure Na_2SO_3 by 100% CO when the sample is heated at a rate of $25^\circ\text{C}/\text{min}$. It was found that at about 700°C the weight loss was completed within half a minute. The last experiment was performed with a mixture of Na_2SO_3 and graphite powder under 10% CO in N_2 carrier gas and a heating rate of $5^\circ\text{C}/\text{min}$. In this case the weight loss was completed at a much lower temperature of 600°C within half a minute. The sulfur mass balance for the last two runs indicates that a large amount of sulfur was lost during the thermal treatment. A large amount of SO_2 and some COS were found in the exhaust gas during the rapid weight-loss period. The small values of $\Delta W_{\text{SO}_3}^f$ for the last two runs indicate that almost complete conversion of Na_2SO_3 was obtained. The large number of products and their unusual stoichiometric ratios in Table VII indicate that a number of complex reactions take place during conversion of Na_2SO_3 .

TABLE VII. REDUCTION OF Na_2SO_3 BY CO AND GRAPHITE

Sample Type	[CO] (%)	T ($^\circ\text{C}$)	Time (min)	$\Delta W_{\text{SO}_3}^i$ (mg)	ΔW_{S}^f (mg)	$\Delta W_{\text{SO}_4}^f$ (mg)	$\Delta W_{\text{SO}_3}^f$ (mg)	ΔW_{St}^f (mg)
Na_2SO_3	100	600	35	0.350	0.04	0.011	0.215	0.266
Na_2SO_3	100	700	<0.5	0.476	0.165	0.116	0.01	0.291
Na_2SO_3 +Graphite	10	600	<0.5	0.648	0.400	0.057	0.018	0.475

These results confirm that the reduction of sulfite by carbon and CO according to reactions (27) and (27a) is fast compared to reduction of Na_2SO_4 .

Solid State Kinetics

A relationship between the Na_2SO_4 reduction mechanism and the solid-solid reaction nucleation kinetics for black liquor char must be made. The generation of a small amount of Na_2S in the form of a large number of nuclei uniformly distributed throughout the bulk of the char via reactions

(25), (26) and (27) can be considered as the initial or induction period. Subsequent growth of these nuclei via rate limiting reaction (28) leads to the nuclei growth controlled kinetics until other limitations such as availability of Na_2SO_4 take over.

The nuclei growth controlled kinetics are found to be applicable for many homogeneous solid systems, while only a modified form is applicable for some reactions between solids [20]. The reason that sulfate reduction by carbon in black liquor char, a typical solid-solid reaction, can be described by nuclei growth controlled kinetics may be related to its fine and three dimensional distribution of Na_2SO_4 and Na_2CO_3 in the carbon matrix. These unique properties are obtained because black liquor char is produced from a liquid in which Na_2SO_4 and Na_2CO_3 are mixed with the char precursor on a molecular scale [Chapter 3]. The fine dispersion of Na_2SO_4 in black liquor char leads to a kinetic behavior similar to that of a transformation in a homogeneous solid. It is also significant that the reduction kinetics of Na_2SO_4 impregnated graphite, a more standard solid-solid system, could not be described by nucleation controlled kinetics.

Based on theory [20], the exponent n in equation (19) for nuclei growth controlled kinetics is equal to $\beta + \lambda$, where β represents the number of steps involved in nucleus formation (frequently $\beta=1$ or 0 , the latter corresponding to instantaneous nucleation) and λ is the number of dimensions in which the nuclei grows ($\lambda=3$ for spheres or hemispheres, 2 for discs or cylinders and 1 for linear development). With the large number of active sites in black liquor char generated by reduction of sodium carbonate with carbon, the nuclei formation would be instantaneous so that $\beta=0$. This requires $\lambda=2$, corresponding to two-dimensional growth of the nuclei. The two dimensional development might be related to the fact that the present sample is obtained by film drying which may lead to formation of two dimensional micro-crystals (discs or cylinders) in the dry solids..

Effect of Temperature

There is no published data on the activation energy for solid state sulfate reduction by carbon. The activation energies obtained by Cameron and Grace [9] for sulfate reduction by graphite rods in an alkali carbonate melt vary from 205 to 297 kJ/mol, depending on melt composition. With kraft black liquor char in alkali carbonate melt they obtained an activation

energy of 122 kJ/mol [10]. The latter value is much smaller than the present activation energy of 291 kJ/mol. However, no conclusion can be drawn because of the differences in reaction system. However, the present activation energy is within range found for most solid-solid reactions [20].

The effect of temperature on product distribution is shown in Figure 13. At temperatures below 720°C, temperature has no significant influence on the CO/CO₂ concentration ratio. This result agrees well with the proposed reduction mechanism in which the rate of gasification has no influence on reduction. Above 740°C, the CO/CO₂ ratio decreases slightly. This may be due to a larger fraction of the intermediate reduced by CO (equation (29a)) than by carbon (equation (29)) at higher temperature.

Effect of Sodium Sulfate Addition

The influence of carbon to sulfate ratio on reduction rate is shown in Figure 8. The results show that the reduction rate decreases with decreasing carbon to sulfate ratio. This may be because the nuclei growth rate not only depends on formation of the intermediate (equation (28)) but is also influenced by the reduction of the intermediate (equation (29)). Shown in Figure 14 is the CO/CO₂ ratio as function of sulfate conversion. The CO/CO₂ ratio decreases with decreasing carbon to sulfate ratio, indicating that the rate of reduction of the intermediate by carbon (equation (29)) decreases compared to reduction by CO (equation (29a)). However, the overall reduction rate increases with increasing carbon to sulfate ratio, suggesting that the reduction of the intermediate by carbon is faster than by CO.

The kinetics of BLC-1 cannot be described by equation (19). The molar carbon to sulfate ratio in this sample is lower than two, i.e. lower than required for complete conversion of sulfate via reaction (2). As can be seen from Figure 14, the CO to CO₂ ratio decreases with decreasing carbon to sulfate ratio, indicating that reduction of the intermediate by CO becomes more and more important relative to reduction by carbon. For BLC-1 the CO/CO₂ ratio approaches zero, suggesting that all CO produced by gasification is used for sulfate reduction.

Effect of Sodium Carbonate

The effect of sodium carbonate on reduction rate was shown in Figure 9.

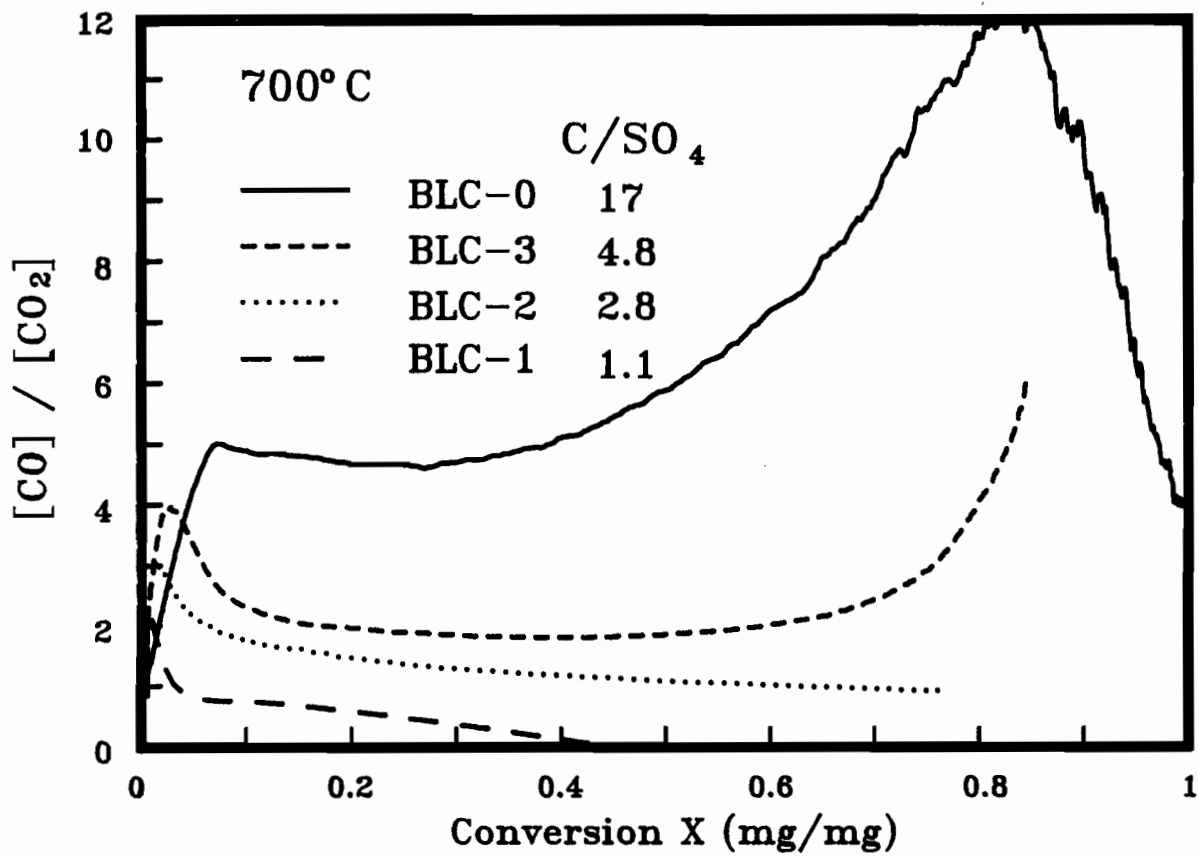


Figure 14, Effect of carbon to sulfate ratio on CO/CO₂ ratio.

The results indicate that carbon/sulfate molar ratio has a stronger influence on reduction rate than the sodium carbonate concentration because the carbonate concentration and carbon/sulfate ratio in sample BL-N2 are respectively lower and higher than those of BLC-2. However, when all sodium carbonate is converted into sodium sulfate in sample BL-N1, the reduction rate is strongly reduced, indicating that the reduction rate is enhanced by presence of sodium carbonate. Comparing the conversion-time curves of BLC-2 and BL-N1, it can be seen that the initial accelerating period for BL-N1 lasts much longer than BLC-2. However, at conversion above 20%, the reduction rate of BL-N1 becomes similar to the rate of BLC-2, which indicates that sodium carbonate influences the reduction rate only during the initial and accelerating periods. This behavior would suggest that the presence of sodium carbonate accelerates nucleation and nuclei growth.

Shown in Figure 15 is the CO/CO₂ ratio obtained for the reduction experiments shown in Figure 9. Similar to Figure 14, the CO/CO₂ ratio increases with increasing C/SO₄ ratio.

Reduction by Graphite

It was shown (Figure 10) that the conversion-time curve obtained for Na₂SO₄ impregnated graphite (G-S1) is described by a power law kinetic expression rather than nucleation controlled kinetics. This suggests that the rate determining step of sulfate reduction by graphite is different from that in black liquor char. The sigmoid shape of the graphite conversion curve confirms that Na₂SO₄ reduction by graphite is also auto catalytic. The lower reduction rate might be due to both the absence of Na₂CO₃ and reduced contact between sulfate and carbon in G-S1 compared to black liquor char. The long initial and accelerating period in G-S1 may be because sodium carbonate is absent and the Na₂SO₄ crystals are larger.

The CO/CO₂ ratio as function of conversion for the runs in Figure 10 is shown in Figure 16. The CO/CO₂ ratio for G-S1 remains constant at about 0.5 over a wide range conversions and is considerably lower than that for BLC-2 and BL-N1. This CO/CO₂ ratio suggests that the relative importance of reaction (29a) compared to reaction (29) is larger for Na₂SO₄ impregnated graphite than for black liquor char.

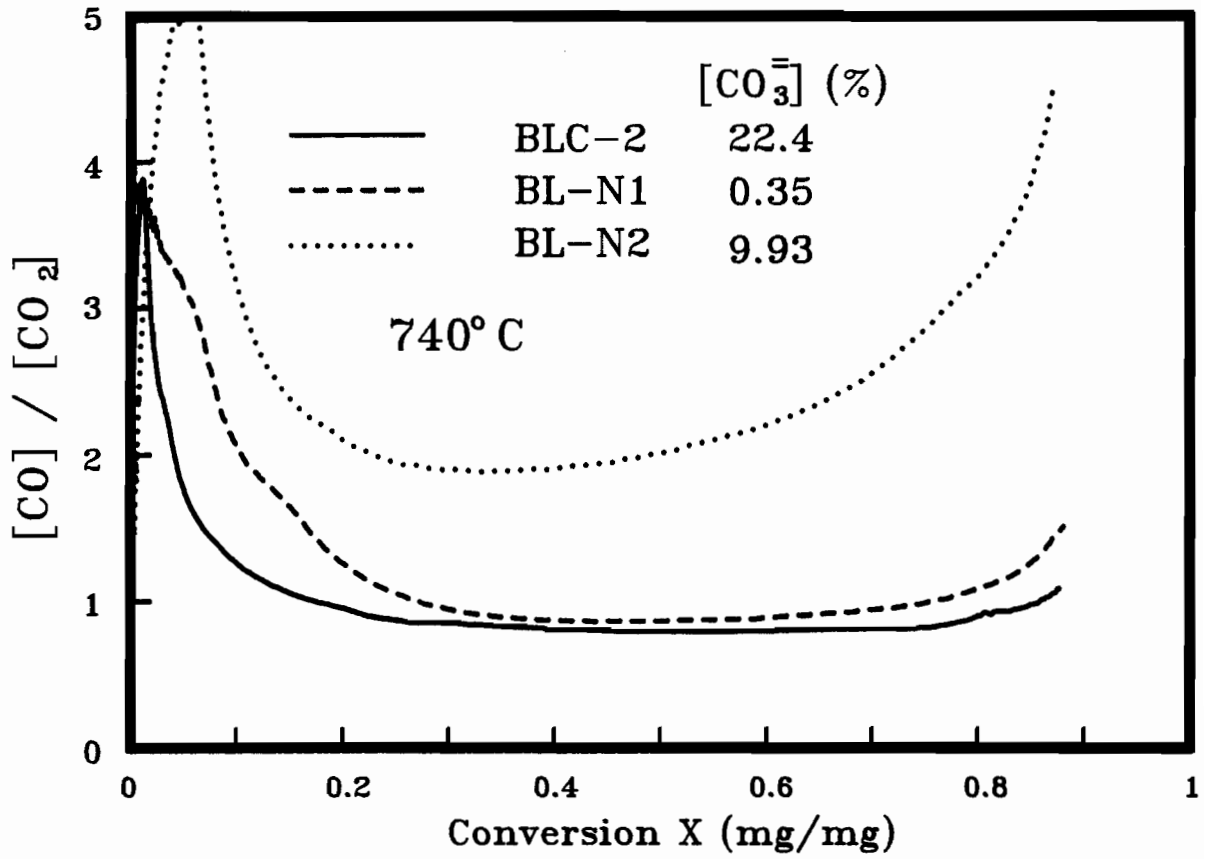


Figure 15, Effect of carbonate on CO/CO₂ ratio.

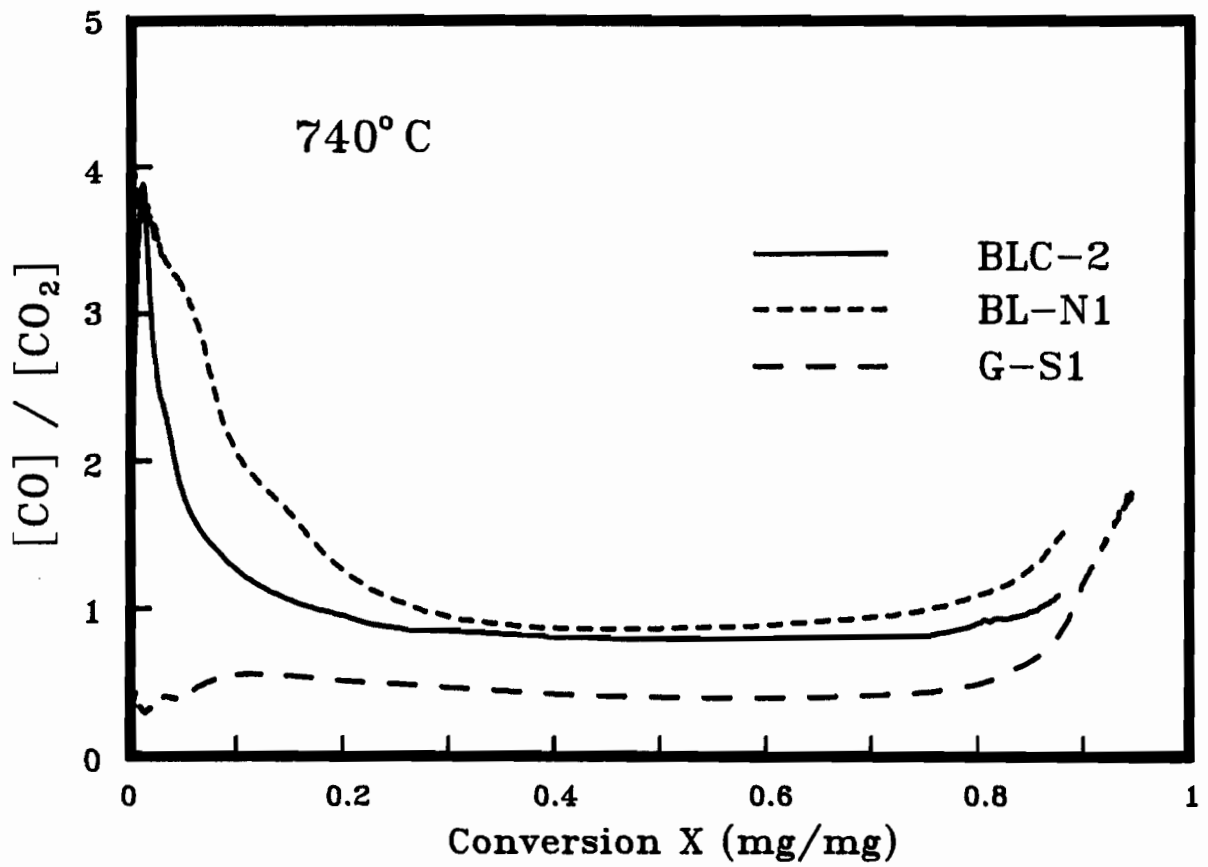


Figure 16, Effect of type of carbon on CO/CO₂ ratio.

Effect of Type of Pan

The conversion-time curve obtained with black liquor char in the shallow pan is also sigmoidal in shape. The initial accelerating period indicates again the auto catalytic character of the reaction, however, the major decelerating period suggests that a different step is rate controlling during this period compared to reduction in the deep pan. It was confirmed by calculation of the criteria developed by Sohn and Szekely [14] that the gas atmosphere in the deep pan is complete made up of gases produced by reduction of Na_2SO_4 by carbon. However, when reduction is conducted in the shallow pan with He as carrier gas, the reaction is free of gas phase mass transfer limitation and over 99% of the gas inside the bed is He. The reason for a shorter initial and accelerating with the shallow pan might be that the low CO and CO_2 concentration facilitates the progress of the rate determining initiation reactions (25) and (26). However, the major decelerating period should be related to a change in the rate determining step controlling the growth of the Na_2S nuclei. In the proposed mechanism, nuclei growth depends on both formation of the intermediate (equation (28) and the reduction of the intermediate (equations (29) and (29a)). With the deep bed the reduction of the intermediates by CO (equation (29a)) will not be rate limiting, because of the very high concentration of CO (30 to 80%) inside the pan. In the shallow pan, on the other hand, the reduction of the intermediate will be mostly by carbon (reaction (29)). Since the decelerating part of the conversion data in Figure 12 is well described by equation (12) for a product layer diffusion limited process, the rate determining step might be diffusion of the intermediate through the product layer to the carbon surface. It is important to point out that poly-sulfide as that the intermediate is very mobile, because all sodium poly-sulfides are in liquid form above 600°C and mostly stable up to 1300°C .

Shown in Figure 17 is the CO/ CO_2 ratio for the experiments shown in Figure 12. The CO/ CO_2 ratio for the shallow pan is much lower than that for the deep pan. This is explained by the much lower carbon gasification rate in the shallow pan, because the concentration of CO_2 in the shallow pan (<1%) is two orders of magnitude lower than that in the deep pan (20 to 70%).

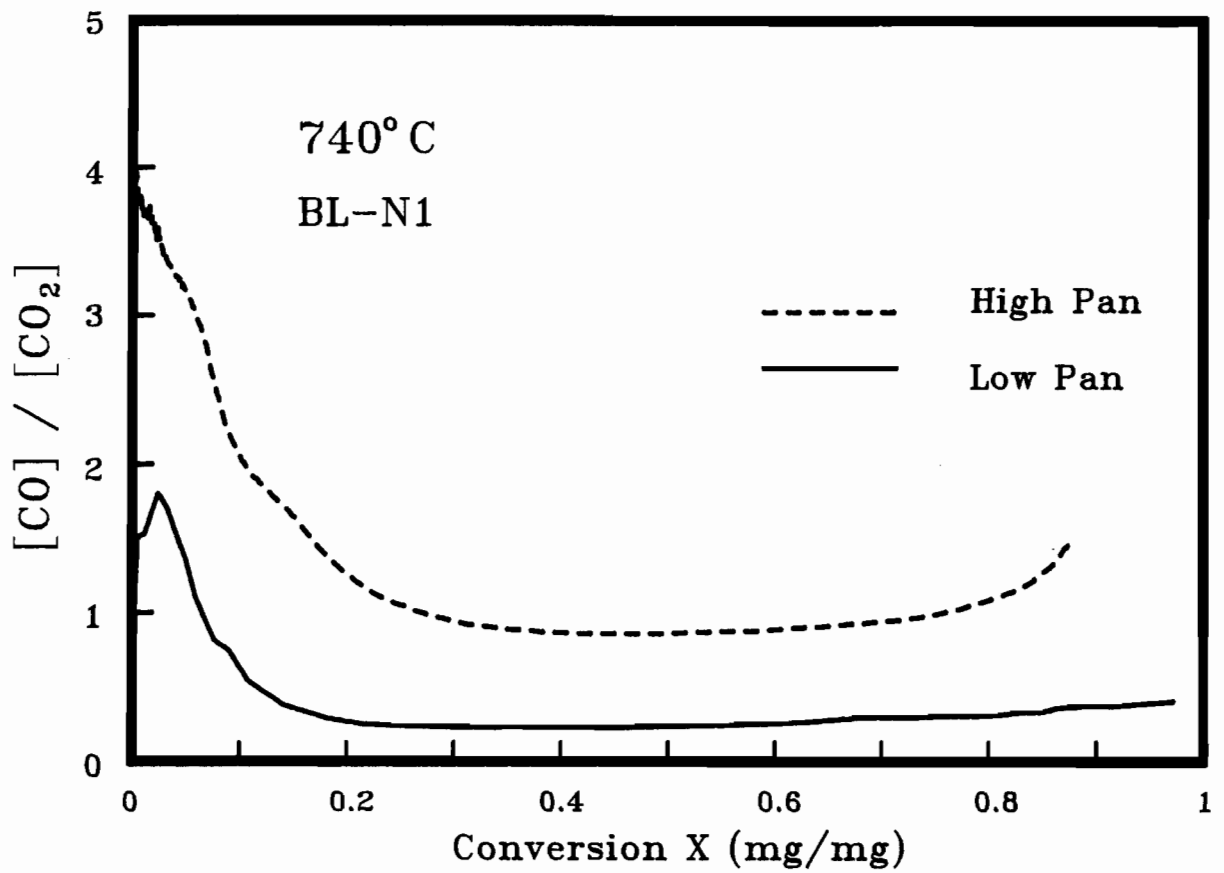


Figure 17, Effect of type of pan on CO/CO₂ ratio.

CONCLUSIONS

The sulfate reduction by carbon is auto catalyzed by the product Na₂S. The conversion of sulfate in black liquor char is well described by the second order nuclei growth controlled reaction kinetics

$$(-\ln(1-x))^{1/2} = k t \quad (19)$$

over a wide range of conversions. An activation energy of 290 kJ/mol was determined from isothermal experiments at 680 to 780°C. The reduction rate increases with increasing carbon to sulfate ratio and the amount of sodium carbonate. In the proposed reaction mechanism, Na₂S is initially formed via a slow reduction of sulfate to sulfite at active sites on the carbon surface, followed by fast reduction of sulfite to sulfide by carbon and CO. An intermediate, possibly liquid poly-sulfide, is formed from sulfate and sulfide and this reaction explains the auto catalytic behavior. The intermediate is much more mobile and easier reduced to Na₂S by carbon and CO than sodium sulfate. The reduction rate is controlled by formation and reduction of the intermediate.

IMPLICATION

Application of the present results to the proposed low temperature recovery process suggests that reduction of sodium sulfate by carbon in black liquor char can be achieved at temperatures below the melting point of the sodium salts. A reactor whereby flow through the black liquor char bed is minimized, such as in a rotary furnace, should be used because the build up of high concentrations of product gases not only eliminates sodium emission but also reduces the reduction time significantly.

NOMENCLATURE

E	= activation energy, kJ/mol.
k	= reaction rate constant, 1/s.
M_1	= molecular weight of CO.
M_2	= molecular weight of CO ₂ .
M_3	= molecular weight of O ₂ .
n	= order of reaction equation.
p_1	= partial pressure of CO.
p_2	= partial pressure of CO ₂ .
Q	= gas flow rate, cm ³ /min.
$-r_{c,c}$	= carbon gasification rate, 1/min.
$-r_{c,m}$	= consumption rate by sulfate reduction, 1/min.
R	= gas constant.
t	= time, s.
T	= temperature, K.
ΔW_{gas}	= total weight calculated from CO and CO ₂ production, mg.
ΔW_{oxy}	= weight of oxygen., mg.
$\Delta W_{S^=}$	= weight of sulfide, mg.
$\Delta W_{SO_4^=}$	= weight of sulfate, mg.
ΔW_{St}	= weight of total sulfur, mg.
$\Delta W_{SO_3^=}^i$	= initial weight of sulfite, mg.
$\Delta W_{S^=}^f$	= final weight of sulfide, mg.
$\Delta W_{SO_3^=}^f$	= final weight of sulfite, mg.
$\Delta W_{SO_4^=}^f$	= final weight of sulfate, mg.
ΔW_{St}^f	= final weight of total sulfur, mg.
ΔW_{tg}	= weight-loss recorded by balance, mg.
x	= sulfate conversion, mg/mg.

Greek symbols

β	= number of steps involved in nucleus formation.
δ	= error in mass balance, (%).
ϵ	= error in mass balance, (%).
λ	= number of dimensions of nuclei growth.

REFERENCES

1. Standen, A., **Kirk-Othmer Encyclopedia of Chemical Technology**, vol. 18, John Wiley & Sons, Inc., p.511 (1969).
2. Cameron, J.H. and T.M. Grace, **Tappi**, 65(7), p.84(1982).
3. **Forum on Kraft Recovery Alternatives**, Institute of Paper Chemistry, Appleton, US, (1976).
4. Budnikoff, P.B., and E. Shilov, **J. Soc. Chem. Ind.**, 6(4), p.111T(1928).
5. White, J.R.M., and A.H. White, **Ind. Eng. Chem.**, 28(2), p.244(1936).
6. Kubelka, V., Jr., and J. Hojnos, **Collection Czech. Pulp & Paper Ind. Res. Works**, 1:113-31 (1956).
7. Birk, J.R., C.M. Larsen, W.G. Vaux and R.D. Oldenkamp, **IEC. Proc. Des. Dev.**, 10(1), p.7(1971).
8. Sjoberg, M. and J. Cameron, **AIChE Symposium Series**, 76(200), p.35(1981).
9. Cameron, J. H., and T.M. Grace, **IEC Fundam.**, 22(4), p.486(1983).
10. Cameron, J.H. and T.M. Grace, **IEC. Fundam.**, 24(4), p.443(1985).
11. Li, J. and A.R.P. van Heiningen, **Chem. Eng. Sci.**, 43(8), p.2079(1988).
12. Doraiswamy, L.K. and M.M. Sharma, **Heterogeneous Reactions: Analysis, Examples, and Reactor Design**, vol. 1, John Wiley and Sons, N.Y., p.511(1984).
13. Rao, Y.K., **Metallurgical Transactions**, 2(May), p.1439(1971).
14. Sohn, H.Y., and J. Szekely, **Chem. Eng. Sci.**, 28, p.1789(1973).
15. Rao, Y.K., and Y.K. Chuang, **Chem. Eng. Sci.**, 29, p.1933(1974).
16. Wynnyckyj, J.R., and W.J. Rsukin, **Metallurgical Trans. B**, 19B(2), p.73(1988).
17. Li, J., and A.R.P. van Heiningen, **Can. J. Chem. Eng.**, 67(4), p.693(1989).
18. Li, J., **Master Thesis**, McGill University, (1986).
19. Avrami, M., **J. Chem. Phys.**, 7, p.1103(1939); 8, p.212(1940); 9, p.177(1941).
20. Bamford, C.H., and C.F.H. Tipper, **Comprehensive Chemical Kinetics; vol 22: Reactions in the solid state**, Elsevier Co., Amsterdam, (1980).
21. Jander, W., **Z. Anorg. Allgem. Chem.**, 163, p.1(1927).
22. Jach, J., **J. Phys. Chem. Solids**, 24, p.63(1963).
23. Prout, E.G., and F.C. Tompkins, **Trans. Faraday Soc.**, 40, p.488(1946).
24. Austin, L.G., and P.L. Walker, Jr., **AIChE J**, 9(3), p.303(1963).
25. Dearnaley, R.I., and et al, **Inorg. Chem.**, vol.22, No.22, p.3243(1983).

CHAPTER 9

GENERAL CONCLUSIONS

GENERAL SUMMARY

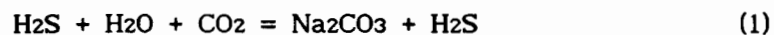
Kraft black liquor is the spent liquid formed during pulp production by digestion of wood in an aqueous solution of sodium hydroxide and sodium sulfide at elevated temperature and pressure. Recovery of the inorganic chemicals and generation of steam, by burning the liquor, has been an integral part of alkaline pulping almost from the outset for economical and environmental reasons. Although the objective of chemical recovery is adequately achieved, there are major drawbacks associated with the present commercial recovery furnace. Potential safer, cleaner and less capital intensive alternatives are processes using fluidized beds operating at or near the melting point of the inorganics. However, for its development as well as for better understanding of the operation of the conventional furnace, fundamental knowledge is needed of the chemical and physical processes taking place during recovery.

This thesis is concerned with the rate processes occurring during gasification and reduction of kraft black liquor char (BLC) below or near the melting point of the inorganics. A thermogravimetric analysis (TGA) system was the main experiment equipment used to determine the kinetics and mechanism of these rate processes. Other supporting techniques include gas analysis by IR and gas chromatography, and analysis of the solids by ion chromatography and SEM-EDS. Fully oxidized kraft black liquor, i.e. all inorganic sulfur in the form of sulfate, made from Black Spruce was used. In most experiments the char was prepared by "fast pyrolysis" of dried black liquor solids. Model mixtures or modified black liquor chars were used to obtain supporting evidence for the mechanisms of BLC gasification and reduction.

CONTRIBUTIONS TO KNOWLEDGE

1. The heat and mass transfer characteristics of a common hanging basket type thermobalance are determined. A simple method of performing experiments with respectively He or N₂ as carrier gas is suggested for detection of gas phase heat and mass transfer limitations. A "dilution factor" is defined, which allows determination of the product gas concentration in the sample bed from the measured concentrations in the exhaust and the mass transfer characteristics of the TGA system. Knowledge of the "dilution factor" removes the major operational drawback of a TGA system for kinetic studies compared to investigation with a fixed bed.
2. The kinetics of CO₂ and steam gasification of "fast pyrolysis" black liquor char have been determined. The rate of both reactions is well described by Langmuir-Hinshelwood type kinetics, and is at least one order of magnitude higher than that of activated carbon impregnated with alkali metal carbonates.
3. The high gasification reactivity of black liquor char compared to other carbonaceous materials, is explained by the three dimensional and extremely fine dispersion of sodium salts in the carbon matrix. These unique properties of black liquor char are confirmed by SEM-EDS and mapping and line scan techniques.
4. The present data suggests that internal surface area measurements rather than swelling tests might be more appropriate to characterize combustion properties of black liquors.
5. The CO₂ concentration in the product gas during steam gasification is higher than predicted by assuming that the water-shift reaction is at equilibrium. A mechanism is proposed which explains this effect by assuming that CO₂ is a primary gasification product.
6. The COS concentration inside a char bed during CO₂ gasification of reduced black liquor char at low CO₂ concentration and high temperature is determined by thermodynamics. The COS emission rate under these conditions is controlled by external mass transfer to the bed. COS production is promoted by both CO and CO₂. The effect of CO on COS formation is much smaller than that of CO₂ and can be explained by reaction between CO and S₂ in the gas phase.
7. The H₂S concentration inside a char bed during steam gasification of reduced black liquor char is in thermodynamic equilibrium with steam and CO₂, the latter being produced by carbon gasification. Therefore, the H₂S

emission rate is governed by thermodynamic equilibrium of reaction (1)



,carbon gasification kinetics and the gasification product gas distribution.

8. The reduction of Na_2SO_4 in a mixture of Na_2SO_4 and Na_2CO_3 by CO is auto catalytic and the conversion-time behavior can be described by an initiation, acceleration and deceleration period. The major deceleration period is described by phase boundary reaction controlled or product layer diffusion controlled solid-solid kinetics for respectively reduction with or without the presence of CO_2 . The gas-solid reaction between CO and Na_2SO_4 is identified as the initiation reaction. Na_2CO_3 does not have a catalytic effect on the reduction, but may influence the reduction rate due to formation of a ternary melt system. When a uniform molten phase is formed, the reduction rate is controlled by mass transfer of CO in the liquid melt. Na_2SO_4 reduction by CO is catalyzed by TiO_2 and Fe_3O_4 . The reduction in the presence of TiO_2 is not auto catalytic and well described by ash diffusion controlled kinetics for gas-solid reactions.

9. The sulfate reduction by carbon in black liquor char is auto catalytic and well described by second order nuclei growth controlled reaction kinetics over a wide range of conversions. The reduction rate increases with increasing carbon to sulfate ratio and the amount of sodium carbonate. In the proposed reaction mechanism, Na_2S is initially formed via a slow reduction of sulfate to sulfite at active sites on the carbon surface, followed by fast reduction of sulfite to sulfide by carbon and CO. An intermediate, possibly liquid poly-sulfide, is formed from sulfate and sulfide and this reaction explains the auto catalytic behavior. This intermediate is mobile and easier reduced to Na_2S by carbon and CO than sodium sulfate. The reduction rate is controlled by formation and reduction of the intermediate.

RECOMMENDATIONS AND SUGGESTIONS FOR FUTURE WORK

1. To study the effect of total surface area on BLC gasification rate, with a reactor system capable of measuring the gasification rate and char surface area, and relate this knowledge to combustion properties of black liquors if possible.

2. To further study the reaction mechanism of BLC gasification and reduction, using isotope labeled chemicals for identification of reaction intermediates and products.
3. To study the kinetics of combustion of black liquor char as function of temperature and gas composition.
4. To study the relation between char reactivity and pyrolysis history in terms of char porosity, surface area and pore size distribution.
5. To study the kinetics of sulfate reduction in combusted black liquor by H_2 with or without catalyst in the solid state, in order to determine the most suitable reducing conditions and catalyst for a low temperature recovery process.
6. To study the effect of the presence of a melt on the gasification and reduction kinetics of BLC and apply this information to the conventional recovery furnace.
7. To develop a mathematic model for combustion of a black liquor droplet.
8. To develop a mathematic model for char bed burning in a recovery furnace.
9. To study the absorption kinetics of a mixture of H_2S and CO_2 in a solution of Na_2CO_3 .